

**Phenotypic variations and chemosensitivity in  
small cell lung cancer**

**Emeline Furon**

Department of Pathology  
School of medicine  
Cardiff University  
UK

A thesis submitted to the School of medicine, Cardiff University  
For the degree of Doctor of Philosophy  
December 2008

UMI Number: U584592

All rights reserved

INFORMATION TO ALL USERS

The quality of this reproduction is dependent upon the quality of the copy submitted.

In the unlikely event that the author did not send a complete manuscript and there are missing pages, these will be noted. Also, if material had to be removed, a note will indicate the deletion.



UMI U584592

Published by ProQuest LLC 2013. Copyright in the Dissertation held by the Author.  
Microform Edition © ProQuest LLC.

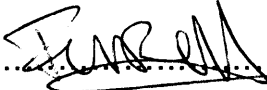
All rights reserved. This work is protected against  
unauthorized copying under Title 17, United States Code.



ProQuest LLC  
789 East Eisenhower Parkway  
P.O. Box 1346  
Ann Arbor, MI 48106-1346

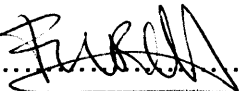
## Declaration

This work has not previously been accepted in substance for any degree and is not concurrently submitted in candidature for any degree.

Signed.......... (candidate)      Date ....2/6/9.....


### STATEMENT 1

This thesis is being submitted in partial fulfillment of the requirements for the degree of PhD.

Signed.......... (candidate)      Date ....2/6/9.....


### STATEMENT 2

This thesis is the result of my own independent work/investigation, except where otherwise stated. Other sources are acknowledged by explicit references.

Signed.......... (candidate)      Date ....2/6/9.....

### STATEMENT 3

I hereby give consent for my thesis, if accepted, to be available for photocopying and for inter-library loan, and for the title and summary to be made available to outside organisations.

Signed.......... (candidate)      Date ....2/6/9.....

## Acknowledgments

I would like to express my gratitude to all those who gave me the possibility to complete this thesis.

First and foremost, I would like to specially thank my supervisors, Professor Paul Smith and Doctor Rachel Errington for their inspiring dedication and enthusiasm in the field, their full support, invaluable advice and unbelievable patience throughout this study. I am also indebted to my third supervisor Doctor Simon Reed for his stimulating suggestions and encouragement.

I wish to acknowledge and thank EPSRC and particularly Stefan Ogrodzinski and Biostatistics for funding this project.

I am grateful to Professor Laurence Patterson and Doctor Robert Falconer, from the Institute of Cancer Therapeutics at Bradford, for their collaboration, providing carbohydrate-based probes agents, helpful discussions and suggestions addressing the experimental therapeutics theme of the study.

I would also like to give thanks to the staff from the Department of Pathology at Cardiff University for their technical help and advices. Especially I am obliged to Janet, Kerensa, Marie, Oscar and Sally for their expertise and time. I would like to acknowledge Agurtzane, Shirong, Yachuan and Yumin for their expertise on molecular biology and biochemistry along with Dr Peter Giles for his expertise on microarray analysis and Dr J.M. Morgan for his help with the paraffin sections.

Last but not least, je tiens à exprimer toute ma gratitude aux Docteurs Christophe Fleury, Mathieu Hauwel et Philippe Gasque pour m'avoir offert l'opportunité de venir travailler à Cardiff. Merci à tous mes proches pour leur soutien, en particulier Emilie, Jean-Baptiste, Nicolas et Magali.

*Je dédie ce travail à mes parents et à mon frère qui m'ont encouragée, soutenue et surtout supportée tout au long de mes années d'études.*



## Summary

Many complex properties of cancer cells are effectively under selection within the *in vivo* microenvironment or following therapeutic insult. This critical combination of instability and shifting selection drives the heterogeneity of tumour cell populations in terms of many critical features.

Small cell lung cancer (SCLC) is an aggressive, rapidly metastasizing neoplasm with an ability to develop resistance against chemotherapeutic agents. New SCLC therapeutic strategies are urgently needed that contain spreading disease without further compromising tumour chemosensitivity.

Variants for attachment to tissue culture plastic of the NCI-H69 cell line, which grows in suspension but generates low frequency appearance of adhesion variants, were enriched, without prejudice for any specific extracellular matrix directed advantage, and then allowed for any proliferation/survival advantage *in vitro* to impact on the evolution of variation. Two sub-lines were generated representing two stages in variant enrichment.

The developed SCLC model, which encompasses elements of variation and heterogeneity, provides opportunities to link *in vitro* behaviour of SCLC with *in vivo* characteristics with particular reference to the challenges faced in the management of SCLC such as the accrual of drug resistance.

The variant model was characterized using microscopy, flow cytometry and microarray analysis, revealing variation in adherence and morphology impacting on SCLC behaviour, proliferative rate and polysialylation of the neural cell adhesion molecule. The microarray analysis has also revealed new cancer biomarkers that can be explored in clinic studies.

This unique SCLC model was used to gain insights into links with chemoresistance. The studies revealed that the variant selection did not result in expansion of a drug resistant clone. Moreover, evidence of clonal evolution/selection was uncovered together with the finding of the absence of CSCs, even in enriched variants, as defined by the classical side population phenotype.

The defined PSA expression patterns of the variants allowed for screening of carbohydrates-based agents for polysialylation knock-down.

## Table of contents

<b>Title</b> .....	<b>I</b>
<b>Declaration</b> .....	<b>II</b>
<b>Acknowledgements</b> .....	<b>III</b>
<b>Summary</b> .....	<b>IV</b>
<b>Table of contents</b> .....	<b>IV</b>
<b>List of figures</b> .....	<b>IX</b>
<b>List of tables</b> .....	<b>XII</b>
<b>Abbreviations</b> .....	<b>XIII</b>
<b>I. Introduction</b> .....	<b>- 1 -</b>
I.1. Cancer progression and origins of cellular heterogeneity .....	<b>- 2 -</b>
I.2. Phenotypic plasticity.....	<b>- 5 -</b>
I.2.1. Definition and implications .....	<b>- 5 -</b>
I.2.2. EMT/MET: an example of cell plasticity .....	<b>- 6 -</b>
I.2.3. The cancer stem cells plasticity and therapeutic challenges .....	<b>- 8 -</b>
I.3. Metastasis .....	<b>- 11 -</b>
I.3.1. Metastasis: a multi-step cascade inviting early intervention.....	<b>- 11 -</b>
I.3.2. Metastasis and phenotypic plasticity .....	<b>- 14 -</b>
I.4. Chemoresistance .....	<b>- 16 -</b>
I.4.1. Apoptosis modulation.....	<b>- 17 -</b>
I.4.2. Cell cycle modulation: kinetic resistance .....	<b>- 18 -</b>
I.4.3. Multidrug resistance: innate and acquired.....	<b>- 19 -</b>
I.5. Environment and cell adhesion.....	<b>- 23 -</b>
I.5.1. Cell adhesion mechanisms .....	<b>- 23 -</b>
I.5.2. Cell adhesion and drug resistance .....	<b>- 26 -</b>
I.6. Plasticity of the phenotype and genotype of SCLC .....	<b>- 28 -</b>
I.6.1. Molecular characteristics.....	<b>- 29 -</b>
I.6.2. Chemoresistance and early invasion: therapeutic challenge .....	<b>- 31 -</b>
I.7. NCAM biology .....	<b>- 32 -</b>
I.7.1. Structure .....	<b>- 32 -</b>
I.7.2. Role in development and CNS .....	<b>- 35 -</b>
I.7.3. Polysialic acid and links with metastatic behaviour.....	<b>- 35 -</b>
I.7.4. PSA-NCAM and the therapeutic challenge.....	<b>- 37 -</b>
I.8. Aims of the thesis .....	<b>- 38 -</b>
<b>II. Materials and methods</b> .....	<b>- 40 -</b>
II.1. Materials .....	<b>- 40 -</b>
II.1.1. Drug and molecular probes table .....	<b>- 40 -</b>
II.1.2. Antibodies and sources tables .....	<b>- 41 -</b>
II.2. Cell lines and culture conditions .....	<b>- 42 -</b>
II.2.1. Cell lines.....	<b>- 42 -</b>
II.2.2. Suspension and adherent cell culture .....	<b>- 42 -</b>
II.3. cDNA microarray .....	<b>- 43 -</b>
II.3.1. Drug treatment .....	<b>- 43 -</b>

II.3.2. RNA extraction .....	- 43 -
II.3.3. RNA quality controls .....	- 44 -
II.3.4. Data acquisition.....	- 44 -
II.3.5. Data analysis .....	- 46 -
II.3.5.1. Arrays quality assessment.....	- 47 -
II.3.5.2. Raw data processing and normalization.....	- 47 -
II.3.5.3. Quantification of differential expression .....	- 48 -
II.3.5.4. Functional analysis and representation .....	- 49 -
II.4. Flow cytometry .....	- 50 -
II.4.1. Cytometers .....	- 50 -
II.4.2. Cell cycle analysis.....	- 51 -
II.4.3. Immunofluorescence analysis .....	- 52 -
II.4.4. Cellular integrity assays .....	- 52 -
II.5. Imaging .....	- 52 -
II.5.1. Microscopes .....	- 52 -
II.5.2. Transmission imaging .....	- 53 -
II.5.3. Immunofluorescence labelling .....	- 53 -
II.5.4. Fluorescence imaging.....	- 54 -
II.5.5. Timelapse imaging .....	- 54 -
II.6. SDS-PAGE/Immunoblotting .....	- 54 -
II.7. Statistical analyses .....	- 55 -
<b>III. Characterization of an <i>in vitro</i> SCLC model system .....</b>	<b>- 56 -</b>
III.1. Introduction .....	- 56 -
III.2. Specific material and methods .....	- 60 -
III.2.1. Cell lines, cell culture and cell proliferation estimation .....	- 60 -
III.2.2. Plastic substrate-adherent sub-population enrichment .....	- 61 -
III.2.3. Attachment assay .....	- 62 -
III.2.4. Cell size measurement .....	- 62 -
III.2.5. DNA content measurement.....	- 63 -
III.2.6. Neuraminidase digestion of PSA.....	- 63 -
III.2.7. Cell adhesion assay: MSA .....	- 63 -
III.2.8. Paraffin cell aggregates section preparation and staining.....	- 65 -
III.2.9. Invasion assay .....	- 66 -
III.3. Results .....	- 67 -
III.3.1. SCLC cell lines <i>in vitro</i> phenotype and variants selection .....	- 67 -
III.3.2. NCI-H69 model phenotype characteristic .....	- 72 -
III.3.2.1. Variants enrichment.....	- 72 -
III.3.2.2. Attachment properties.....	- 73 -
III.3.2.3. Cell size and DNA content .....	- 75 -
III.3.2.4. PSA-NCAM.....	- 77 -
III.3.3. NCI-H69 model: gene expression changes.....	- 82 -
III.3.3.1. Arrays quality assessment.....	- 82 -
III.3.3.2. Statistical analyses .....	- 82 -
III.3.3.3. Overview of the ontology analysis .....	- 86 -
III.3.4. NCI-H69 model: SCLC phenotype.....	- 88 -
III.3.5. NCI-H69 model: growth characteristics .....	- 92 -
III.3.6. NCI-H69 model: cell adhesion .....	- 94 -
III.3.6.1. Cell-ECM adhesion: MSA.....	- 96 -
III.3.6.2. Cell-cell adhesion .....	- 99 -

III.3.7. NCI-H69 model: cell motility and invasiveness.....	- 104 -
III.4. Discussion .....	- 106 -
IV. Chemosensitivity and heterogeneity of the NCI-H69 variants...	- 114 -
IV.1. Introduction and aims .....	- 114 -
IV.2. Specific Material and Methods.....	- 121 -
IV.2.1. Drugs and inhibitor .....	- 121 -
IV.2.2. Cell lines.....	- 121 -
IV.2.3. ABCG2 immunodetection .....	- 121 -
IV.2.4. Hoechst side population assay .....	- 121 -
IV.2.5. TPT uptakes.....	- 122 -
IV.2.6. alamarBlue assay .....	- 123 -
IV.2.6.1. Method design: continuous exposure vs. end-point assay...	- 123 -
IV.2.6.2. Chemosensitivity testing.....	- 124 -
IV.2.6.3. % reduction calculation .....	- 124 -
IV.3. Results.....	- 125 -
IV.3.1. ABC transporters expression.....	- 125 -
IV.3.2. ABCG2 profiling and function .....	- 126 -
IV.3.3. Identification and analysis of the side population phenotype.....	- 129 -
IV.3.4. TPT Pharmacokinetics.....	- 136 -
IV.3.5. TPT pharmacodynamics – the overall response to topotecan .....	- 139 -
IV.3.5.1. Topoisomerase expression.....	- 139 -
IV.3.5.2. alamarBlue method implementation and optimisation.....	- 140 -
IV.3.5.3. Chemosensitivity to TPT .....	- 144 -
IV.3.5.4. Effect of the variant phenotype on TPT chemosensitivity ..	- 144 -
IV.4. Discussion.....	- 148 -
V. Focus on PSA-NCAM .....	- 153 -
V.1. Introduction and aims.....	- 153 -
V.2. Specific materials and methods .....	- 156 -
V.2.1. Inhibitors and treatment .....	- 156 -
V.2.2. Cell lines .....	- 156 -
V.2.3. RT-PCR.....	- 156 -
V.2.4. Time lapse imaging.....	- 158 -
V.3. Results .....	- 160 -
V.3.1. Surface glycoalyx modulation.....	- 160 -
V.3.1.1. Major glycosylation pathways .....	- 160 -
V.3.1.2. Sialic acid pathway in the variants.....	- 161 -
V.3.2. Chemical-biology approach to intervention on PSA synthesis.....	- 164 -
V.3.2.1. First generation compound: R1108.....	- 165 -
V.3.2.2. Other compounds. ....	- 166 -
V.3.3. Effect on NCAM decoration.....	- 166 -
V.3.3.1. R1108.....	- 166 -
V.3.3.2. ICT compounds.....	- 167 -
V.3.4. Cytotoxicity.....	- 168 -
V.3.4.1. R1108: dose-dependant cytotoxicity.....	- 168 -
V.3.4.2. A role for R1108 metabolic products in cytotoxicity?.....	- 172 -
V.3.4.3. A role for purification regimen of R1108 compound? .....	- 173 -
V.3.4.4. ICT compounds.....	- 174 -
V.3.5. R1108 toxicity: microarray study .....	- 176 -

V.3.5.1. Induction of stress-related genes.....	- 178 -
V.3.5.2. MT induction validation .....	- 180 -
V.3.5.2.1. MT induction upon R1108/2006 treatment.....	- 180 -
V.3.5.2.2. ICT compounds.....	- 180 -
V.3.6. Metallothionein.....	- 181 -
V.3.6.1. Inhibition of CHO growth by R1108.....	- 182 -
V.3.6.2. Effect on mitosis .....	- 184 -
V.4. Discussion .....	- 188 -
<b>VI. Discussion .....</b>	<b>- 195 -</b>
<b>Appendix I: Reagents and suppliers.....</b>	<b>- 207 -</b>
<b>Appendix II: Western blotting solutions.....</b>	<b>-208 -</b>
<b>Appendix III: RT-PCR solutions.....</b>	<b>- 210 -</b>
<b>Appendix IV: SCLC cell lines panel PSA-NCAM expression... </b>	<b>- 211 -</b>
<b>Appendix V: 2008 arrays quality assessment.....</b>	<b>- 212 -</b>
<b>Appendix VI: SCLC characteristics .....</b>	<b>- 214 -</b>
<b>Appendix VII: Cell cycle and growth.....</b>	<b>- 216 -</b>
<b>Appendix VIII: Cell adhesion .....</b>	<b>- 219 -</b>
<b>Appendix IX: MSA.....</b>	<b>- 227 -</b>
<b>Appendix X: Cell motility.....</b>	<b>- 232 -</b>
<b>Appendix XI: Glycosylation.....</b>	<b>- 234 -</b>
<b>Appendix XII: 2005 arrays quality assessment.....</b>	<b>- 235 -</b>
<b>References.....</b>	<b>- 238 -</b>

## List of figures

### I. Introduction

Figure I.1: Cellular plasticity: the EMT / MET transition.....	- 7 -
Figure I.2: The tumour metastatic process.....	- 12 -
Figure I.3: Chemoresistance mechanisms overview .....	- 17 -
Figure I.4: ABC transporters protein arrangements.....	- 20 -
Figure I.5: Major classes of cell adhesion molecules .....	- 25 -
Figure I.6: Proposed mechanisms for integrin-mediated protection from genotoxic therapy .....	- 27 -
Figure I.7: NCAM isoforms structure and polysialylation pattern.....	- 33 -

### II. Materials and methods

Figure II.1: DNA microarray processing.....	- 45 -
Figure II.2: DNA microarray analysis process .....	- 46 -

### III. Characterization of an *in vitro* SCLC model system

Figure III.1: Summary of the SCLC model system characterization objectives ...	- 59 -
Figure III.2: MSA slides layout.....	- 65 -
Figure III.3: <i>In vitro</i> characteristics of the panel of SCLC cell lines .....	- 68 -
Figure III.4: SCLC cell lines and adherent variants .....	- 70 -
Figure III.5: SCLC cell lines and variants NCAM and PSA-NCAM expression ..	- 71 -
Figure III.6: <i>In vitro</i> appearance of the NCI-H69 variants over increasing Passage.....	- 72 -
Figure III.7: Attachment properties of the different adhesion variants of the NCI-H69 cell line.....	- 74 -
Figure III.8: NCI-H69 variants cell and nuclei diameters.....	- 76 -
Figure III.9: Flow cytometry determination of NCI-H69 variants DNA content.....	- 77 -
Figure III.10: PSA and NCAM expression in the NCI-H69 variants .....	- 78 -
Figure III.11: PSA-NCAM and NCAM expression in the NCI-H69 variants.....	- 79 -
Figure III.12: Immunoblotting detection of NCAM and PSA-NCAM.....	- 80 -
Figure III.13: Fluorescence detection of NCAM and PSA-NCAM in NCI-H69 SP cells .....	- 81 -
Figure III.14: Microarray statistical analysis .....	- 85 -
Figure III.15: SCLC and NSCLC markers (Kraus et al., 2002) expression in the NCI-H69 variants .....	- 89 -
Figure III.16: SCLC markers .....	- 91 -
Figure III.17: Growth properties of the different variants of the NCI-H69 cell Line.....	- 92 -
Figure III.18: Cell cycle and growth-related gene expression .....	- 94 -
Figure III.19: Cell adhesion and cytoskeleton .....	- 95 -
Figure III.20: Adhesion profile of the NCI-H69 variants on ECM proteins.....	- 97 -
Figure III.21: Cell morphology on MSA ECM proteins spot.....	- 98 -
Figure III.22: Reversibility of the attached phenotype .....	- 100 -
Figure III.23: Growth properties of the NCI-H69 model cultured on hydrophobic substrate .....	- 102 -
Figure III.24: Expression and localization of NCAM and PSA-NCAM in the NCI-H69 variants grown on hydrophobic surfaces .....	- 103 -
Figure III.25: Determination of the invasion potential of the NCI-H69 variants.....	- 105 -

### IV. Chemosensitivity and heterogeneity of the NCI-H69 variants

Figure IV.1: Topotecan — a camptothecin derivative .....	- 117 -
Figure IV.2: ABC transporters expression in NCI-H69 variants .....	- 125 -

Figure IV.3: ABCG2 immunofluorescence detection .....	- 126 -
Figure IV.4: Hoechst 33342 uptake profiles in the A549 and each of the NCI-H69 variants .....	- 128 -
Figure IV.5: A549 Hoechst 33342 uptake profiles .....	- 130 -
Figure IV.6: NCI-H69 SP Hoechst 33342 uptake profiles .....	- 133 -
Figure IV.7: NCI-H69 AP3 Hoechst uptake profiles .....	- 134 -
Figure IV.8: NCI-H69 AP78 Hoechst uptake profiles .....	- 135 -
Figure IV.9: Modulation of TPT uptake with the ABCG2 inhibitor FTC .....	- 136 -
Figure IV.10: Differences of TPT uptake for the NCI-H69 variants .....	- 137 -
Figure IV.11: Profiles of TPT uptake for variant NCI-H69 cells .....	- 138 -
Figure IV.12: FL4 signal of TPT uptakes with or without FTC .....	- 139 -
Figure IV.13: Topoisomerase expression across all NCI-H69 variants .....	- 140 -
Figure IV.14: Continuous alamarBlue exposure is toxic for all NCI-H69 variants .....	- 141 -
Figure IV.15: AlamarBlue method optimization .....	- 143 -
Figure IV.16: Dose response to continuous TPT treatment .....	- 144 -
Figure IV.17: TPT treatment of all NCI-H69 variants as single cell suspension ...	- 146 -
Figure IV.18: TPT treatment of all NCI-H69 variants pre-seeded into wells .....	- 147 -
Figure IV.19: Solid tumours cancer stem cell markers .....	- 152 -
<b>V. Focus on PSA-NCAM</b>	
Figure V.1: Time-lapse imaging analysis .....	- 159 -
Figure V.2: Venn-diagram representation of glycosylation-related genes expression modulation in the NCI-H69 variants .....	- 161 -
Figure V.3: Sialic acid biosynthesis pathway and sialylation of glyconjugates ..	- 163 -
Figure V.4: ST8SIA4 and ST8SIA2 expression .....	- 164 -
Figure V.5: Effect of R1108 treatment on PSA levels .....	- 167 -
Figure V.6: Effect of 24h ICT compounds treatment on NCAM decoration .....	- 168 -
Figure V.7: Effect of a 48h R1108 treatment on NCI-H69 variants cell lines .....	- 169 -
Figure V.8: R1108 toxicity.....	- 171 -
Figure V.9: Benzyl alcohol effect on cells.....	- 173 -
Figure V.10: R1108 purification batches .....	- 174 -
Figure V.11: Induction of cell death by candidate PST inhibitors .....	- 175 -
Figure V.12: Transcriptional responses to R1108 .....	- 177 -
Figure V.13: Immunoblotting detection of metallothionein induction .....	- 180 -
Figure V.14: Immunoblotting detection of metallothionein induction after 24 h treatment .....	- 181 -
Figure V.15: mouse Metallothionein-1 overexpressing CHO .....	- 182 -
Figure V.16: Effect of a range of R1108/2006 concentrations on the growth of the population of CHO-K1 and mMT-CHO-K1 .....	- 183 -
Figure V.17: Effect of various concentrations of R1108 on cell growth .....	- 184 -
Figure V.18: Effect of increasing concentrations of R1108 on the mitotic outcome of the CHO cell lines over three generation .....	- 186 -
Figure V.19: Effect of various concentrations of R1108 on the mitotic duration and the intermitotic time (IMT) .....	- 187 -
<b>VI. Discussion</b>	
Figure VI.1: Overview of the thesis highlights addressing the stated aims of the Study .....	- 196 -
Figure VI.2: NCI-H69 variant model .....	- 198 -
Figure VI.3: SCLC .....	- 206 -

<b>Appendix IV: SCLC cell lines panel PSA-NCAM expression.</b>	
Figure 1: SCLC cell lines panel PSA-NCAM expression .....	- 211 -
<b>Appendix V: 2008 arrays quality assessment.</b>	
Figure 1: 2008 arrays — MAS5 computed quality control report .....	- 212 -
Figure 2: 2008 arrays — AffyPLM package for Bioconductor quality assessment — RLE and NUSE plots .....	- 213 -
<b>Appendix IX: MSA.</b>	
Figure 1: MSA adhesion profile after PSA digestion .....	- 227 -
Figure 2: Cell morphology on MSA ECM proteins spot after endoN digestion ..	- 228 -
Figure 3: Reassembled full MSA array — NCI-H69 SP .....	- 229 -
Figure 4: Reassembled full MSA array — NCI-H69 AP3 .....	- 230 -
Figure 5: Reassembled full MSA array — NCI-H69 AP78 .....	- 231 -
<b>Appendix XII: 2005 arrays quality assessment.</b>	
Figure 1: 2005 arrays — MAS5 computed quality control report .....	- 235 -
Figure 2: 2008 arrays. AffyPLM package for Bioconductor quality assessment — RLE and NUSE plots .....	- 236 -
Figure 3: Microarray analysis accounting for failed quality control array .....	- 237 -



## List of tables

### I. Introduction

Table I.1: Metastasis-related genes .....	- 14 -
Table I.2: ABC transporters known to be involved in MDR .....	- 21 -
Table I.3: SCLC molecular characteristics .....	- 29 -

### II. Materials and methods

Table II.1 drug and molecular probes used .....	- 40 -
Table II.2 primary antibodies used .....	- 41 -
Table II.3 secondary antibodies used .....	- 41 -
Table II.4 Cell lines routine culture description .....	- 42 -
Table II.5: Flow cytometry fluorescence optics .....	- 51 -
Table II.6: CBS camera fluorescence filters .....	- 54 -

### III. Characterization of an *in vitro* SCLC model system

Table III.1: SCLC cell lines description .....	- 60 -
Table III.2: Distribution and enrichment amongst the GO SLIM categories of the 1004 probes .....	- 87 -

### VI. Focus on PSA-NCAM

Table V.1: RT-PCR primers .....	- 157 -
Table V.2: R1108 batches .....	- 166 -
Table V.3: ICT compounds .....	- 166 -
Table V.4: Effect of R1108 different batches on PSA decoration of NCAM ....	- 167 -
Table V.5: R1108 batches — toxicity profile .....	- 172 -
Table V.6: Transcriptional responses to R1108 .....	- 179 -

### Appendix VI: SCLC characteristics.

Table 1: SCLC and NSCLC markers expression in the NCI-H69 variants .....	- 214 -
Table 2: SCLC markers expression in the NCI-H69 variants .....	- 215 -

### Appendix VII: Cell cycle and growth.

Table 1: Overlap between 1189 gene list and GO: 7049 cell cycle .....	- 216 -
Table 2: Cell growth. Overlap between 1189 gene list and GO: 40007 growth ..	- 218 -

### Appendix VIII: Cell adhesion.

Table 1: Overlap between 1189 gene list and GO: 7155: cell adhesion .....	- 219 -
Table 2: Overlap between 1189 gene list and GO: 5856: cytoskeleton and GO: 7010: cytoskeleton organisation and biogenesis .....	- 222 -
Table 3: Overlap between 1189 gene list and GO: 30054: cell junction .....	- 225 -
Table 4: Integrins expression .....	- 226 -

### Appendix X: Cell motility.

Table 1: Overlap between GO 6928 cell motility and 1189 gene list .....	- 232 -
---	---------

### Appendix XI: Glycosylation.

Table 1: Glycans structure and biosynthesis (KEGG 1.7) .....	- 234 -
--	---------

### Appendix XII: 2005 arrays quality assessment.

Table 1: Microarray analysis accounting for failed quality control array .....	- 237 -
--	---------

## Abbreviations

A	absorbance
AB	alamarBlue
ANOVA	Analysis of variance
AP	Adherent phenotype
ATP	adenosine triphosphate
BSA	Bovine Serum Albumin
CAM	Cell Adhesion Molecule
CAM-DR	Cell Adhesion-Mediated Drug resistance
CDS	Cell Dissociation Solution
CHO	Chinese Hamster Ovary cells
CSC	Cancer stem cell
DMEM	Dulbecco's Modified Eagle Medium
DMSO	Dimethyl sulfoxide
DTT	Dithiotreitol
ECM	Extracellular Matrix
EDTA	ethylene diaminetetraacetic acid
EGTA	ethylene glycol tetraacetic acid
EMEM	Eagle's Minimum Essential Medium
EMT	epithelial to mesenchymal transition
FCS	Fetal Calf Serum
FDR	False discovery rate
Fn	Fibronectin
FTC	Fumitremorgin C
GAPDH	Glyceraldehyde-3-phosphate dehydrogenase
GO	Gene ontology
h	hours
HOP	hydrophobic bacteriological Petri dishes
HPLC	high performance liquid chromatography
HRP	HorseRadish Peroxidase
HSPG	heparan sulfate proteoglycan
ICC	Immunocytochemistry
Ig	Immunoglobulin
IgSf	Immunoglobulin SuperFamily
kDa	kiloDalton
L	Litre
m	milli
m	meter
μ	micro
M	Molar concentration

<b>MET</b>	<b>mesenchymal to epithelial transition</b>
<b>min</b>	<b>minutes</b>
<b>MSA</b>	<b>Multiple Substrate Array</b>
<b>MT</b>	<b>Metallothionein</b>
<b>n</b>	<b>nano</b>
<b>NaCl</b>	<b>Sodium Chloride</b>
<b>NCAM</b>	<b>Neural Cell Adhesion Molecule</b>
<b>NE</b>	<b>Neuroendocrine</b>
<b>Neu5Ac</b>	<b>Sialic acid</b>
<b>PBS</b>	<b>Phosphate Buffered Saline</b>
<b>PCR</b>	<b>Polymerase chain reaction</b>
<b>PI</b>	<b>Propidium Iodide</b>
<b>PI3K</b>	<b>phosphatidylinositol 3- kinase</b>
<b>PMSF</b>	<b>PhenylMethylSulphonyl fluoride</b>
<b>PSA</b>	<b>Polysialic acid</b>
<b>PVDF</b>	<b>PolyVinylidene Fluoride</b>
<b>QC</b>	<b>Quality controls</b>
<b>RMA</b>	<b>Robust multiarray average</b>
<b>RNA</b>	<b>Ribonucleic acid</b>
<b>rpm</b>	<b>rotation per minute</b>
<b>RPMI</b>	<b>Roswell Park Memorial Institute</b>
<b>RT</b>	<b>room temperature</b>
<b>RT</b>	<b>reverse transcription</b>
<b>Sec</b>	<b>seconds</b>
<b>SCLC</b>	<b>Small Cell Lung Cancer</b>
<b>SD</b>	<b>Standard Deviation</b>
<b>SDS-PAGE</b>	<b>sodium dodecyl sulfate-polyacrylamide gel electrophoresis</b>
<b>Sia</b>	<b>Sialic acid</b>
<b>SP</b>	<b>suspension phenotype</b>
<b>TCP</b>	<b>tissue culture plastic</b>
<b>TPT</b>	<b>Topotecan</b>
<b>U</b>	<b>Units</b>
<b>W</b>	<b>Watt</b>
<b>WT</b>	<b>wild type</b>

## I. Introduction

The loss of genomic stability and resulting gene alterations are key molecular pathogenic steps that occur early in tumourigenesis. However, many complex properties of cancer cells are effectively under selection within the *in vivo* microenvironment or following therapeutic insult. This critical combination of instability and varying selection drives the heterogeneity of tumour cell populations in terms of many critical features including: cell growth characteristics, invasion behaviour, metastatic potential and the forms of innate or acquired resistance to therapy. The current study addresses the development of a small-cell lung cancer (SCLC) model, which encompasses elements of variation and heterogeneity, to provide opportunities to link *in vitro* behaviour of SCLC with *in vivo* characteristics with particular reference to the challenges faced in the management of SCLC such as the accrual of drug resistance. SCLC is an aggressive, rapidly metastasizing neoplasm with a high propensity for bone marrow involvement. The striking ability of SCLC to develop resistance against chemotherapeutic agents has led to the proposal that changes in cytokine receptor expression and cell adhesion properties within the tumour microenvironment contribute both to metastatic potential and to the laying of the foundations of chemoresistance. Difficulty arises when attempting to link the steady-state phenotype of SCLC cells *in vitro* with opportunities for therapeutic design and validation. *In vitro* cultures may present a coherent model, accessible to analysis but these and their linked signalling pathways are not challenged by the *in vivo* environment. *However, in vitro models that disassemble the components of variation within a tumour cell population provide a starting position to understand the plasticity or heterogeneity of phenotypes within a dynamic tumour system.* Here the aim was to use such a SCLC model to address the specific origins of resistance to a relevant cytotoxic agent or indeed to novel therapies based on the targeting of cellular processes that control cellular interactions and are relevant to behaviour within microenvironments.

## **I.1. Cancer progression and origins of cellular heterogeneity**

The importance of genetic changes in neoplastic progression is well recognized, with the alteration of three general groups of genes — oncogenes, tumour-suppressor genes and genome stability genes — all contributing in complex combinations to tumourigenesis. Mutations in oncogenes and tumour suppressor genes (TSGs) enhance the net reproductive rates of a cell, while mutations in genetic stability genes increase the rate of mutational processes such as point mutations, insertions, deletions, gene amplification, chromosome rearrangements and gain or loss of whole chromosomes (Vogelstein and Kinzler, 2004). According to Vogelstein (Vogelstein and Kinzler, 2004), there are three major challenges in understanding origins and progression in cancer: the discovery of new genes that have a causal role in neoplasia; the delineation of the pathways through which these genes act and the basis for the varying actions in specific cell types; the exploitation of this knowledge for the target validation and drug discovery to improve treatment in the clinic.

Cancer progression is recognized as involving significantly more complexity and multi-functionality than mutation driven clonal expansion. Indeed, recent advances have showed that cancer is as much an epigenetic disease as it is a genetic disease, and epigenetic alterations in cancer often serve as potent surrogates for genetic mutations (Jones and Baylin, 2007). Epigenetics is defined as modifications of DNA or associated factors that have information content and are heritable (aside from the DNA sequence itself). Normal epigenetic modifications of DNA encompass three types of changes, all of which are interrelated: chromatin modifications, DNA methylation, and genomic imprinting (see for review Bernstein *et al.*, 2007). A common theme to disease epigenetics is the disruption of phenotypic plasticity (Feinberg, 2007). Epigenetic or 'transcriptional' targeted therapies can involve attempts to modify DNA methylation-linked epigenetic mechanisms used by the cancer cells for long-term silencing of gene expression. However, the problem remains that it cannot be assumed that molecular targets are equally and optimally present by all neoplastic cells. Pragmatically, our understanding of the consequences of molecular defects and identification of therapeutic opportunities must address

the added complexity of intra-tumour variation when viewed at specific point in time during diagnostic or therapeutic processes.

A readily observable form of genetic instability is chromosomal instability (CIN) leading to abnormally structured chromosomes and changes in chromosome numbers (Rajagopalan *et al.*, 2003; Sieber *et al.*, 2003) putatively arising from abnormalities in chromatin dynamics and a reduced fidelity of the surveillance of cell cycle events. One end result of chromosomal instability is aneuploidy. Aneuploidy is observed in most cancers and is in its own right a driver of chromosomal instability (Duesberg and Li, 2003). It is still unclear whether genetic instability is an early event and therefore a driving force of cancer progression or a late stage consequence of the somatic evolution that leads to cancer (Rajagopalan *et al.*, 2003; Sieber *et al.*, 2003) but can have the impact of driving clonal elements in a progressing tumour. Although it is accepted that most cancers are clonal in origin (Nowell, 1976), tumour cells may have different karyotypes and phenotypes. Indeed, individual cells of a given cancer often differ widely from each other in phenotypic properties such as metastatic capacity, drug sensitivity, growth rates, metabolism, and morphology (Fialkow, 1979; Konemann *et al.*, 2000). Co-existing with such variation in tumour cell systems is the operation, in some cancers at least, of a process by which cancer stem cells (CSCs) may sustain tumourigenesis, generating cellular hierarchies and heterogeneity through the 'stem-like' properties of self-renewal and differentiation (Visvader and Lindeman, 2008). CSCs may also contribute to chemoresistant subfractions or sub-populations with extended recovery potential in a variety of malignancies, including brain tumours, leukemias, and breast carcinomas (Hart and El-Deiry, 2008; Reya *et al.*, 2001) leading to a search for targets for the specific elimination of CSCs (Beier *et al.*, 2008).

Thus, tumour cell heterogeneity arising by different routes, not least through the innate plasticity or stochastic nature of cellular processes, provides a wide range of cellular repertoires. Within this state there can be bias associated with the selective pressure of the local environment from which different repertoires can provide selective advantage. Indeed, cancer development is recognized to be an evolutionary process and tumour progression has been compared to Darwinian evolution (Nowell, 1976;

Tomlinson and Bodmer, 1999). Cancer genes (used in the broadest sense to include oncogenes and tumour suppressor genes) mediate the evolution of cancer cells, so cancer genes can be envisaged to function by increasing “cellular fitness.” The term “cellular fitness” is useful because it appeals to a common-sense understanding of Darwinian evolution, and it correctly implies a broad range of mechanisms. Increased “cellular fitness” means that a heritable event has allowed clonal expansion under selection. The comment by Prof. Mel Greaves (Institute of Cancer Research, UK) that, “The only fitness test of natural selectability in evolution is survival and reproductive success” (Greaves, 2007) could apply equally to the *in vitro* and *in vivo* situations.

Clearly, tumour growth is a complex process ultimately dependent on proliferation and cell dynamics and the potential for nurture in the spread to new microniches. A common view of tumour growth kinetics is based on the general assumption that tumour cells grow exponentially (Bru *et al.*, 2003). Such kinetics agrees with the unlimited proliferative activity of tumour cells recorded in early, mainly *in vitro*, studies. However, a number of poorly explained issues remain in disagreement with a simple exponential regime of cell proliferation even when modified for apoptotic / cell death events. For example, there is a clear discrepancy between the exponential tumour growth theory and experimental data obtained from tumour cells growing *in vivo*: tumour doubling times have been found to greatly exceed cell cycle times. Lower-than-expected activity of tumour cells and greater-than-expected aneuploidy has also consistently been found. These issues are of importance since conventional chemotherapy is largely limited by tissue kinetics (Bru *et al.*, 2003), while failure and relapse can arise from *phenotypic plasticity that impacts on selectability* – in the context of this thesis, the undesirable potential to maximise Darwinian fitness for the selection of metastatic and drug-resistant variants that can drive new phases of tumour growth.

## **I.2. Phenotypic plasticity**

### **I.2.1. Definition and implications**

In ecological terms, phenotypic plasticity “is the ability of an organism to express different phenotypes depending on the biotic or abiotic environment” (Agrawal, 2001). The term “plasticity” has been used in a variety of biological contexts from epigenetics to stem cell biology (Wagers and Weissman, 2004). In the case of the latter, the classical definition of stem cell plasticity implies the ability of stem cells to provide progenitors that differentiate into various cell lineages, although the possibility that stem cells may be capable of differentiation across tissue lineage boundaries has recently emerged (Wagers and Weissman, 2004). This apparent greater potency of adult stem cells has been termed stem cell plasticity, with true stem cell plasticity being defined as dedifferentiation and redifferentiation or even transdifferentiation (Lakshminpathy and Verfaillie, 2005). The situation is even less certain in the case of putative solid tumour CSC sub-populations in which phenotypic heterogeneity is likely to operate (Visvader and Lindeman, 2008) and co-exist with clonal expansion processes. It appears likely that CSCs are distinct from the cell of origin that receives the ‘first oncogenic hit(s)’ and that they do not necessarily originate from the transformation of normal stem cells. The term of plasticity has also been applied to epigenetics. Indeed, Feinberg (2006) defined genetic and epigenetic plasticity as “*an enhanced ability to stably evolve its phenotype, with both a genetic and epigenetic basis*”.

Although normal and tumour cell plasticity, have been widely used to describe differentiation and particularly epithelial-mesenchymal transitions (Prindull and Zipori, 2004), recently, phenotypic plasticity has taken on another dimension in cancer biology with the notion that cancer is indeed not only a genetic disease but an epigenomic disease (Jones and Baylin, 2007), presumably with the implication that if parts of the disease process demonstrate plasticity, then they may be reversible by therapeutic targeting. The acceptance of the importance of heterogeneity at the tumour cell level (Konemann *et al.*, 2000) combined with increasing consideration given to the integration of cancer stem cell theory into clonal expansion models (Visvader and Lindeman, 2008),



the description of oncogene-induced plasticity (Rapp *et al.*, 2008) and the epigenetics influences in cancer biology (Feinberg, 2007), all raise attention to the notion of disassembling tumour cell heterogeneity, within experimentally accessible systems, before investigating phenotypic plasticity *per se*.

A stringent definition of phenotypic plasticity of a tumour cell would describe the ability to reciprocally dedifferentiate, redifferentiate, and/or transdifferentiate in response to specific stimulation (Yaccoby, 2005). Feinberg (2007) has provided a refinement of his definition of phenotypic plasticity as “*the ability of cells to change their behaviour in response to internal or external environmental cues*”. This is a pragmatic view of plasticity and it is this latter operational definition of phenotypic plasticity that has been adopted in the current study.

### **I.2.2. EMT/MET: an example of cell plasticity**

Behavioral transformations of cells, reflecting phenotypic plasticity, characterize embryogenesis, wound healing, physiological adaptation and neoplasia (Eyden, 2004; Grunert *et al.*, 2003; Jechlinger *et al.*, 2003). The plasticity of solid tumour cells has been extensively studied for epithelial-to-mesenchymal transition (EMT) and mesenchymal-to-epithelial reverse transition (MET). Plasticity is indisputable for both EMT and MET, as they have been observed at a single cell level and moreover they both appear to be reversible phenomenon. Both transitions entail drastic phenotypic and functional changes. Indeed, an immobile epithelial cell tightly bound to adjacent cells loses its cell-cell contact (i.e. tight- and adherens-junctions) and becomes a mobile fibroblast-like mesenchymal cell (Prindull and Zipori, 2004). EMT occurs widely under both normal and pathologic conditions. EMT occurs at diverse steps during embryo development. While MET occurs during somitogenesis, kidney development and coelomic-cavity formation (Thiery and Sleeman, 2006).

Figure I.1 shows the different stages occurring during EMT and MET. EMT induces the loss of polarized phenotype accompanied by transcriptional loss of epithelial markers, such E-cadherin an important caretaker of the epithelial polarised phenotype, and upregulation of mesenchymal markers, such as fibronectin and vimentin. While MET is the reverse process (Prindull and

Zipori, 2004; Thiery and Sleeman, 2006). The term EMT has been applied to a variety of epithelial plasticity scenarios where epithelial cells become fibroblastoid in shape and lose their epithelial phenotype but never fully transition to mesenchymal cells (Grunert *et al.*, 2003).

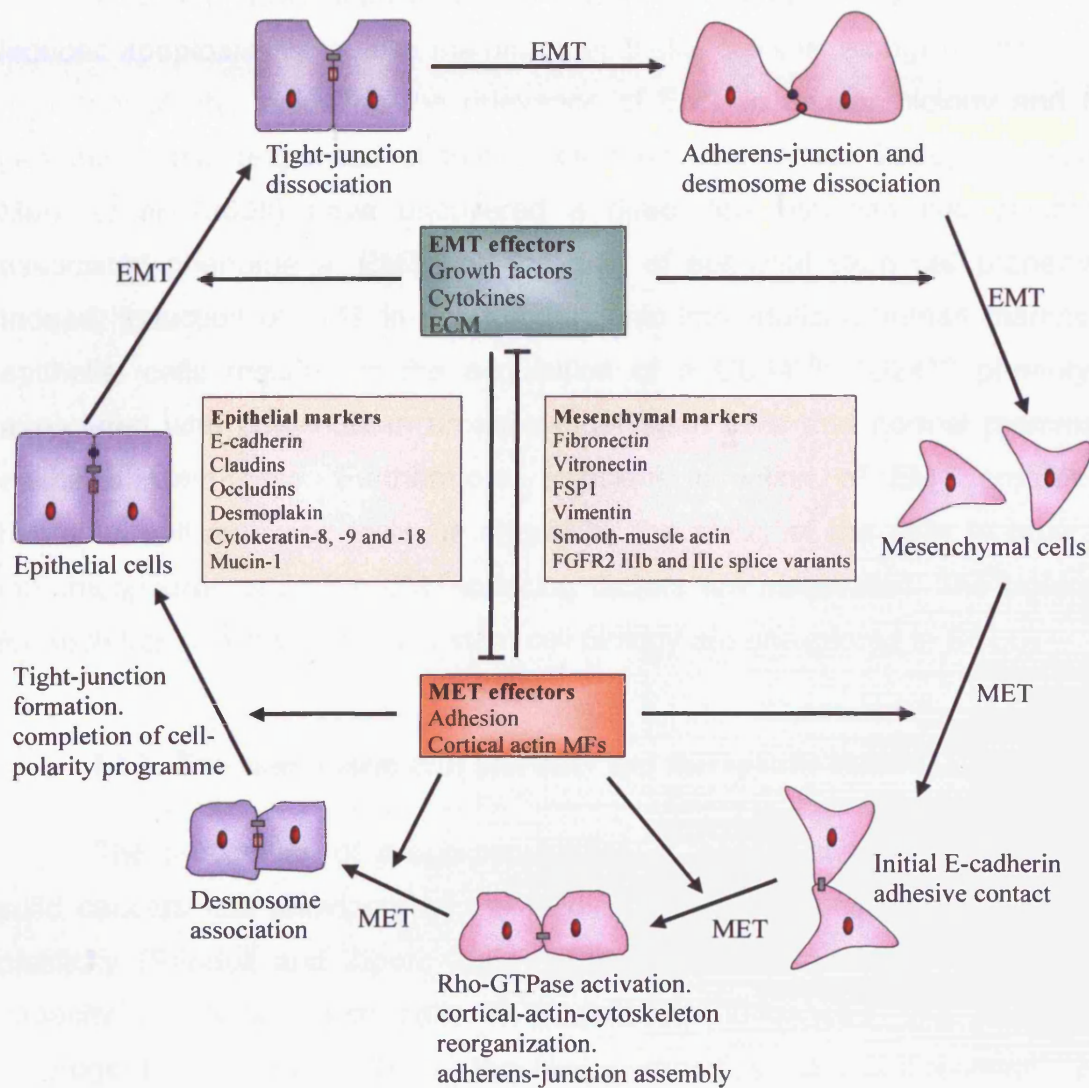


**Figure I.1:** Cellular plasticity: the EMT / MET transition (from Thiery and Sleeman, 2006).

EMT is a developmental program that is often activated during cancer invasion and metastasis. Due to its importance in development and pathology, EMT has been extensively studied, helped by the development of *in vitro* 3-D cultures (O'Brien *et al.*, 2002). EMT is also a process highly responsive to the

environment and is guided by a functional interplay of multiple signal transduction pathways (e.g. TGF- $\beta$ , Notch and Wnt) coordinating the action of transcription factors (such as Snail), triggering gene responses such as the transcriptional repression of E-cadherin - essential for the maintenance of the epithelial phenotype (Derynck and Akhurst, 2007; Moustakas and Heldin, 2007).

Recently, EMT induction was shown to increase resistance to UV-induced apoptosis in a mouse mammary epithelial cell line, alongside increased migratory ability, indicating the relevance of EMT in cancer biology and the genomic stress responses of tumour cells (Robson *et al.*, 2006). Moreover, Mani *et al.* (2008) have uncovered a direct link between two plasticity-associated phenomena, EMT and the gain of epithelial stem cell properties. Indeed, induction of EMT in non-tumourigenic immortalized human mammary epithelial cells resulted in the acquisition of a CD44<sup>high</sup>/CD24<sup>low</sup> phenotype associated with both human breast cancer stem cells and normal mammary epithelial stem cells. Furthermore, transient induction of EMT creates a heritable, self-renewing state as shown by the ability of the cells to grow as mammospheres once the EMT-inducing factors are inactivated. The potential for such transitions with links to stem cell biology are unexplored in SCLC.

### **1.2.3. The cancer stem cells plasticity and therapeutic challenges**

The recognition of a sub-populations of 'cancer stem cells' (CSCs) in solid cancers has reinvigorated the field including the concept of cancer cell plasticity (Prindull and Zipori, 2004). The description reflects the functional capacity of cancer stem cells to sustain tumourigenesis and population heterogeneity through the 'stem-like' properties of self-renewal and differentiation capacity (Visvader and Lindeman, 2008). CSCs cells have the potential to give rise to more differentiated cell forms (Reya *et al.*, 2001). The existence of CSCs implicates a pluripotent stem cell as the cell of origin for cancer, although this is not certain. A current line of investigation in cancer biology is to link tumourigenesis and stem cell biology. Despite being different entities normal tissue stem cells and CSCs share similar properties: drug resistance, differentiation and increased mitotic capacity (Hirschmann-Jax *et al.*, 2004). Furthermore, there is a continuing drive to identify functional markers of

neoplastic cells with stem-like properties (Visvader and Lindeman, 2008). Searching for such markers in SCLC is problematic given the inherent heterogeneity observed.

CSCs may contribute to tumourigenic and chemoresistant sub-fractions in a variety of malignancies, including brain tumours, leukaemias, and breast carcinomas (Hart and El-Deiry, 2008; Reya *et al.*, 2001) leading to a search for targets for the specific elimination of CSCs (Beier *et al.*, 2008) or the mechanisms by which CSCs evade cytotoxic therapies (Visvader and Lindeman, 2008). Enhanced drug efflux mediated by ATP-binding cassette transporters is one of several mechanisms of multi-drug resistance potentially linked with the chemoresistance failure of human cancers. For example the ABCB5 novel drug transporter (Huang *et al.*, 2004) is a chemoresistance mediator in human malignant melanoma (Frank *et al.*, 2005). ABCB5 has been recognized as a CSC marker (Visvader and Lindeman, 2008) given that ABCB5+ tumour cells detected in human melanoma patients show a primitive molecular phenotype and *in vivo* genetic lineage tracking can demonstrate a specific capacity of ABCB5+ sub-populations for self-renewal and differentiation (Schatton *et al.*, 2008).

Some DNA interactive drugs are preferably subject to adenosine triphosphate (ATP)-dependent efflux by the breast cancer resistance protein (BCRP) - a 655 amino-acid polypeptide designated as ABCG2 (MXR/BCRP/ABCP1 / Doyle and Ross, 2003; Ee *et al.*, 2004). ABCG2 also shows an intriguing linkage with the CSC phenotype (Visvader and Lindeman, 2008), given that enhanced ABCG2 transporter expression contributes to the defining ability of pluri-potential "side population" of cells to exclude the DNA minor groove-binding dye Hoechst 33342 (Goodell, 2002; Goodell *et al.*, 2005; Hirschmann-Jax *et al.*, 2005; Hirschmann-Jax *et al.*, 2004; Storms *et al.*, 2000) and enforced expression of the ABCG2 cDNA directly confers the side population phenotype to bone-marrow cells (Zhou *et al.*, 2001). It is likely that the physiological function of ABCG2/Bcrp1 expression in hematopoietic stem cells is to provide protection from cytotoxic xenobiotics (Zhou *et al.*, 2002). Interestingly, the ABCG2 transporter is functional for TPT and the related agents 9-aminocamptothecin, Irinotecan and SN-38 (Polgar *et al.*, 2008; Robey *et al.*, 2007). The ABCG2 half-transporter is sensitive to inhibitors (eg

Fumitremorgin C / FTC), such inhibition resulting in resistance reversal (Rabindran *et al.*, 2000) and has therefore been of therapeutic interest. However, ABCG2 is yet to have a fully defined role in drug resistance in human cancers due to complex substrate specificity patterns, co-expression of other ATP-binding cassette transporters, the effects of mutation on the spectrum of molecules transported and uncertainty over the impact of only moderate increases in transporter function (Doyle and Ross, 2003; Nakanishi *et al.*, 2003; Rabindran *et al.*, 2000; Ross and Doyle, 2004).

Considering the *in vitro* potential for clonal evolution (Visvader and Lindeman, 2008), it is remarkable that CSCs can be identified in sub-fractions of established cell lines (Blazek *et al.*, 2007; Fan *et al.*, 2006; Fukuda *et al.*, 2004; Kondo *et al.*, 2004; Setoguchi *et al.*, 2004) although the link between stem cell marker expression and clonogenicity may be weak (Srivastava and Nalbantoglu, 2008). According to the CSC theory, significant ABCG2 function may be restricted to cell sub-populations that may vary considerably in frequency in human tumours and may have uncertain representation in established cell lines from solid tumours. The existence of side population phenotypes in SCLC biopsies or *in vitro* cell lines remains to be investigated.

### **I.3. Metastasis**

Metastasis is considered to be a critical and often defining phase in solid tumour progression and its outcome a leading cause for cancer-related death rather than the local impact of the primary tumour. Due to difficulties in study, with until recently only end-point metastasis information being accessible much remains to be discovered about the basic metastatic process. However, *in vivo* video imaging has opened new ways to study the metastatic cascade (Wyckoff *et al.*, 2000). Mathematical models of the early phases of metastasis dynamics, using modified Gompertzian models, have previously been used to inform a rationale for screening and treatment (Clare *et al.*, 2000). Despite obvious limitations for prediction it appears that metastatic initiation could occur at a tumour volume of a primary lesion that is only slightly smaller than that at the time of tumour diagnosis (Koscielny *et al.*, 1985).

#### **I.3.1. Metastasis: a multi-step cascade inviting early intervention**

The metastatic process is a multi-step cascade (figure I.2), and all these steps are essential (reviewed in Steeg, 2006) but may differ considerably in their kinetics and probability. The first step in the metastatic process is invasion, the penetration of the basement membrane and stroma surrounding the primary tumour, this requiring changes in cell adhesion to the extracellular matrix (ECM) and proteolytic degradation of surroundings (Friedl and Wolf, 2003). For the cell to disseminate into the body, they need to enter the circulation — a blood vessel or the lymphatic system — phenomenon called intravasation (Wong and Hynes, 2006). Time spent in circulation for disseminated tumour cells is believed to be short. However the bloodstream is a difficult environment to survive in due to shear pressure, presence of immune cells and lack of attachment, indeed anoikis — death upon detachment — is thought to contribute to metastasis inefficiency (Steeg, 2006). Capture in the bloodstream is generally thought to be due to size restriction of capillary structures or binding to coagulation factors (Steeg, 2006). Tumour cells must then escape from the vasculature (extravasation) in order to form a metastasis — although growth at



the secondary site without crossing the vascular wall has been observed (Weidner, 2002).

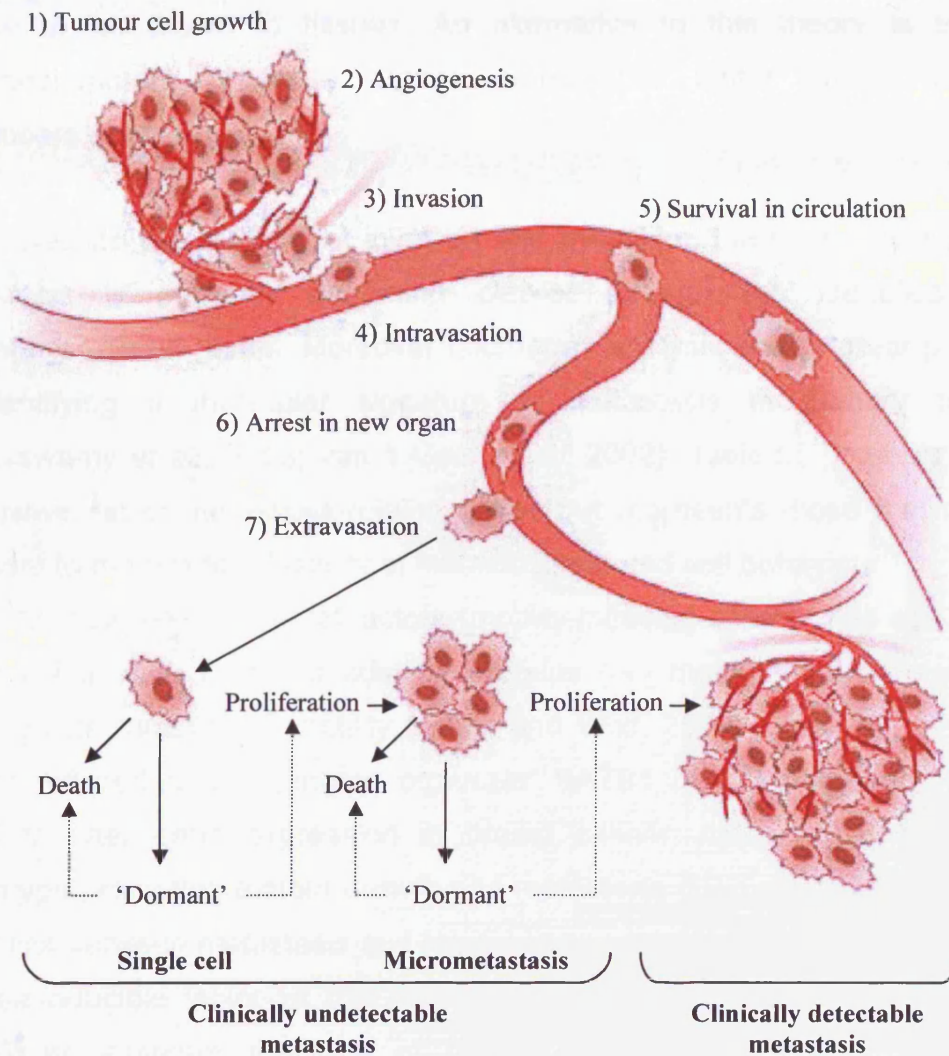


**Figure I.2:** *The tumour metastatic process* (from McGee *et al.*, 2006).

With only very few cells in the circulation forming metastasis, growth at metastatic sites is considered to be the limiting factor of the metastatic cascade. The host molecular influence is believed to play a major role in colonization efficiency — the theory of “seed” and “soil” compatibility (Steege, 2006). Cells at the new site can undergo proliferation, apoptosis or dormancy. Indeed, it is thought that within 24h of intravasation most cells undergo apoptosis (Wong and Hynes, 2006). Dormancy can also occur at the later stage of

micrometastasis and is thought to be the result of apoptosis balancing proliferation (Townson and Chambers, 2006). It is a frequent occurrence for certain types of cancer to metastasize to specific organs and it is said that “homing” could not be explained by blood flow patterns, rather cancer cells appear to be drawn to tissues. An alternative to this theory is that the microenvironment of those organs could offer better growth potential (Chambers *et al.*, 2002).

Despite the diversity of invasion and migration, the multi-step nature of metastasis is currently becoming clearer through the identification of metastasis-related genes. Moreover microarray analysis shows great promises in identifying a molecular signature of metastasis in primary tumours (Ramaswamy *et al.*, 2003; van 't Veer *et al.*, 2002). Table I.1 presents a non-exhaustive list of metastasis-related genes but represents those that may be pertinent to models for plasticity of metastasis-related cell behaviour.

Multiple environmental factors (motility-inducing chemokines and growth factors) alongside ECM remodelling proteins (*i.e.* matrix metalloproteinases) can regulate tumour cell motility (Friedl and Wolf, 2003). Recently, a nuclear protein referred to as ‘genome organizer’ SATB1 (SATB homeobox 1) was found to alter gene expression in breast cancer, inducing an aggressive phenotype promoting tumour growth and metastasis (Han *et al.*, 2008). Also, a direct link between metastasis and hypoxia was recently uncovered. Indeed the hypoxia-inducible factor-1 $\alpha$  (HIF-1 $\alpha$ ) was found to regulate the expression of TWIST an essential mediator of cancer metastasis (Yang *et al.*, 2008). Comparison of tumourigenic non-metastatic cells with metastatic tumour cells has identified genes potentially involved in metastasis repression (loss of function in metastasis) named metastasis suppressor genes (MSG). Those genes represent attractive potential biomarkers candidates as well as therapeutics targets (Shevde and Welch, 2003; Steeg, 2003).



Table I.1: *Metastasis-related genes.****pro-migratory factors (Friedl and Wolf, 2003)***


---

Phosphoglucose isomerase (GPI / AMF)  
 Stromal-cell-derived factor-1/CX-chemokine receptor-4 (SDF1 / CXCR4)  
 Epithelial growth factor (EGF)  
 lysophosphatidic acid (LPA)  
 Insulin-like growth factor-1 (IGF1)  
 Matrix metalloproteinase 1, 2 and 13 (MMP1, 2 and 13)  
 membrane-type 1 matrix metalloproteinase (MT1-MMP)

***Metastasis suppressor genes (Shevde and Welch, 2003; Steeg, 2003)***


---

non-metastatic cells 1, protein (NM23A) expressed in (NME1 / NM23)  
 mitogen-activated protein kinase kinase 4 (MAP2K4 / MKK4)  
 CD82 molecule (CD82 / KAI1)  
 breast cancer metastasis suppressor 1 (BRMS1)  
 KiSS-1 metastasis-suppressor (KISS1)  
 Rho GDP dissociation inhibitor (GDI) beta (ARHGDI2 / RHOGDI2)  
 mediator complex subunit 23 (MED23 / CRSP3)  
 thioredoxin interacting protein (TXNIP / VDUP1)  
 TIMP metalloproteinase inhibitors (TIMPs)  
 cadherins  
 Src-suppressed C kinase substrate (SSeCKS)  
 N-myc downstream regulated 1 (NDRG1 / Drg-1 / CAP43 / RTP)

**I.3.2. Metastasis and phenotypic plasticity**

Traditional models for metastasis propose that secondary tumours result from rare cells with migratory potential, appearing at later stages of tumour progression. Those models have been challenged, especially with insights provided by microarray analysis. Indeed, using microarray analysis Ramaswamy *et al.* (2003) have suggested that metastatic potential of human tumours could be encoded in the primary tumour and that gene expression signature could be common for many tumour types. Moreover, van't Veer *et al.* (2002) have been able to predict tumour dissemination, with a 90% accuracy using gene expression profile of primary tumours. This has led to the suggestion that genetic alterations responsible for carcinogenesis were also

responsible for metastasis (Bernards and Weinberg, 2002), and that tumour progression and metastasis may be underpinned by the behaviour of migrating and phenotypically plastic cancer stem cells (Brabletz *et al.*, 2005).

It has been suggested that reversible transitions may not only enable the development of embryonic stem cells to adult stem but also, through the fundamental property of plasticity, facilitate metastatic spread and the progression of micrometastases. As suggested by the loss of epithelial differentiation and acquisition of migratory phenotype, reflecting EMT / MET transitions, are thought to play an important role in metastasis (Friedl and Wolf, 2003). In the present study there is therefore a rationale for an expectation of overlap of plasticity-related genes with those potentially permissive for metastasis and those recruited in the expression of stem-like properties – an unexplored area for SCLC heterogeneity.

#### **I.4. Chemoresistance**

The concept of drug resistance has been partly based on the work of Luria and Delbruck (1943) on spontaneous mutations in bacteria producing variants resistant to bacteriophages. Applying that concept to tumour cells, the Goldie-Coldman model (Goldie and Coldman, 1979) proposed that the probability for a tumour to contain resistant cells is a function of the mutation rate and that even with a low mutation rate of 1 in  $10^6$  mitoses, resistant cells would be found in a clinically detectable tumour ( $1 \text{ cm}^3 / 10^9$  tumour cells). This has informed the attempts of chemotherapeutic approaches to combination therapy and the development of several model for drugs administration to prevent the appearance of clonal resistance (DeVita *et al.*, 1975; Norton, 1997; Panetta, 1998). Disappointingly, it is the general experience that tumours that respond rapidly to cytotoxic drugs also relapse. It is likely that optimal adjuvant drug therapy must include both induction ('cytotoxic') and maintenance components *e.g.* metastasis-suppressive maintenance drugs (Epstein, 2005).

Cancer cells can develop several mechanisms of resistance impeding the activity of agents (figure I.3). The following overview will focus on the 3 drug resistance mechanisms relevant for the thesis aims.

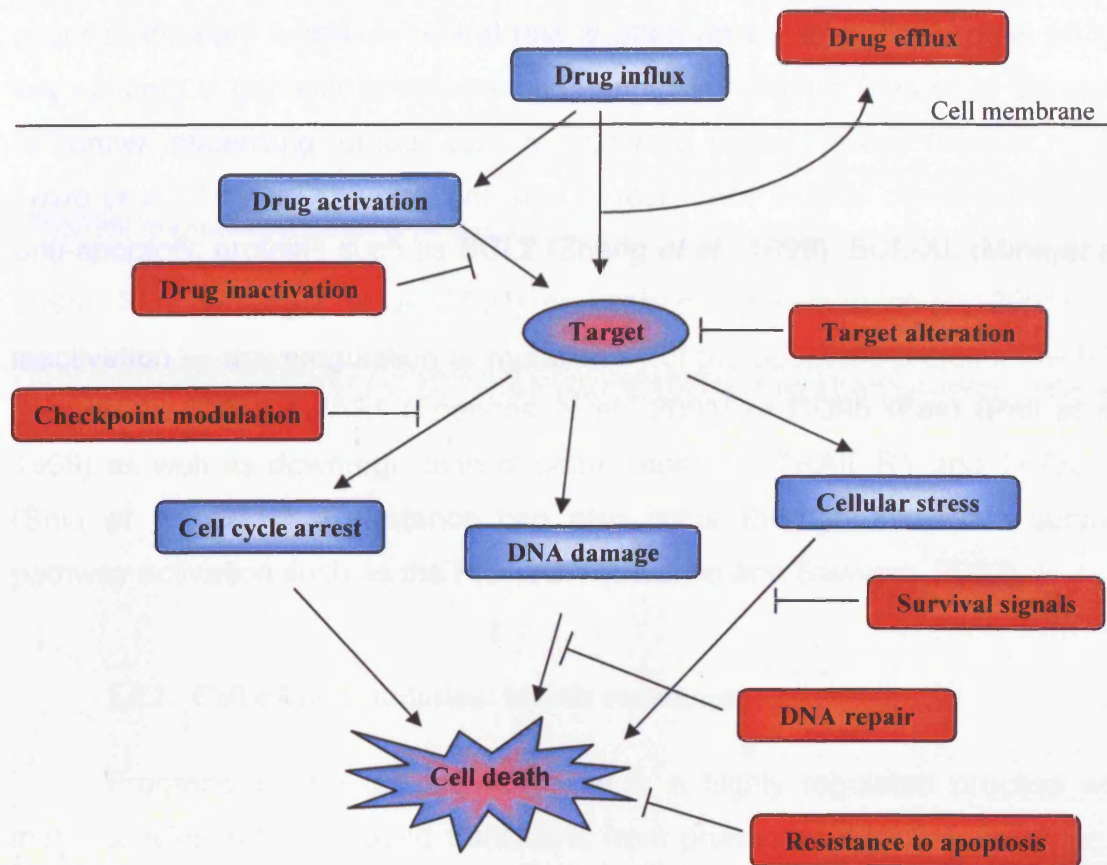


Figure I.3: Chemoresistance mechanisms overview (adapted from Wilson *et al.*, 2006).

#### I.4.1. Apoptosis modulation

For tissue homeostasis to be maintained there is a need for a balance between proliferation and programmed cell death, or apoptosis. Apoptosis is an active multi-step multi pathway cell death program regulated by a complex balance between numerous anti-apoptotic and pro-apoptotic molecules. Apoptosis can be initiated via two pathways: the intrinsic pathway — regulated by the mitochondria — or the extrinsic pathway — involving death receptors (Letai, 2008). Proliferation alone is not sufficient for tumour progression, indeed oncogene activation and genetic instability ought to induce apoptosis, therefore resistance to apoptosis is essential to tumour growth. As irradiation treatments and conventional agents often act (*e.g.* cytotoxicity) through apoptosis induction, deficiency in this pathway can induce resistance to therapy (Igney and Krammer, 2002). Apoptosis is a multi-pathway program and resistance can

occur at different levels. A central role is often attributed to the protein p53, a key element in genomic stress-induced apoptosis, which is frequently disrupted in cancer influencing tumour cells response to chemotherapy (Kastan, 2007; Lowe *et al.*, 1994). Other mechanisms of resistance include overexpression of anti-apoptotic proteins such as BCL2 (Zhang *et al.*, 1999), BCL-XL (Minn *et al.*, 1995), FLIP (Krueger *et al.*, 2001) or survivin (Grossman *et al.*, 2001) and inactivation — downregulation or mutation — of pro-apoptotic proteins like BAX (Yin *et al.*, 1997), APAF1 (Soengas *et al.*, 2001) or CD95 (Fas) (Peli *et al.*, 1999) as well as downregulation of death receptors TRAIL-R1 and TRAIL-R2 (Shin *et al.*, 2001). Resistance can also occur through excessive survival pathway activation such as the PI3K/AKT (Vivanco and Sawyers, 2002).

#### **I.4.2. Cell cycle modulation: kinetic resistance**

Progression through the cell cycle is a highly regulated process with many checkpoints, regulating transitions from phases of the cycle in order to prevent replication of DNA damages driving genomic instability (Nurse, 2000). Major cell cycle transitions are driven by cyclin-dependent kinase (CDK) regulated by cyclins and cyclin-dependent kinase inhibitors (CDKI). Those regulators function to permit the cell to maintain the timing of both the onset and the fidelity of DNA replication and mitosis (Georgi *et al.*, 2002). The emergence of neoplasia with the loss of spatial control of growth and temporal control of proliferation invariably reflects a dysregulation of the cell cycle. It is clear that many cell cycle regulatory proteins can act as oncogenes or tumour suppressor genes, or are closely associated with the transformation process (Smith *et al.*, 2006). Cell cycle-derived resistance has been attributed to the cause of drug resistance to agents, essentially arising from the position of the cell in the cell cycle (Shah and Schwartz, 2001), hence highlighting the importance of combination chemotherapy.

### I.4.3. Multidrug resistance: innate and acquired

Multidrug resistance (MDR) describes resistance (innate or acquired) to a combination of agents structurally and functionally unrelated. MDR was first described when cell lines selected for resistance to a drug demonstrated cross-resistance to chemically unrelated drugs (Biedler and Riehm, 1970). This was soon interpreted as a reduced plasma membrane permeability due to the expression of a cell surface glycoprotein (Juliano and Ling, 1976; Ling and Thompson, 1974). One of the most studied MDR mechanisms is drug efflux and is frequently due to enhanced expression of members of the ATP binding cassette (ABC) family of transporters. ABC transporters are ATP (adenosine triphosphate) binders involved in mostly unidirectional energy-dependent transport across all cell membranes. They transport a wide variety of substrates across extra- and intracellular membranes, including metabolic products, lipids and sterols, in addition to xenobiotics. The ABC genes code for a large family, 49 members, of transmembrane proteins constituted of 7 classes according to sequence homologies, A to G (see for review Dean *et al.*, 2001; Huang and Sadee, 2006; Scotto, 2003).

ABC transporters share 30 to 50% sequence homologies. Typically, ABC transporters are composed of 2 transmembrane domains (composed of 6  $\alpha$  helices) and 2 nucleotides (ATP) binding domains (figure I.4a). However some members of the ABCC (MRP) family (MRP1, 2, 3, 6 and 7) have five extra transmembrane regions forming a third transmembrane domain (figure I.4b). The ABCE and ABCF families contain genes with an ATP-binding domain but no transmembrane domain and are not known to be involved in any membrane transport function. Finally, some ABC family members, such as ABCG2 (figure I.4c), are half-transporters containing only one transmembrane domain and one ATP binding domain (Couture *et al.*, 2006) and must combine with another half transporter to gain functionality.

The nucleotide binding domain (NBD) is more conserved across ABC transporters than the transmembrane domains (TMD), suggesting that in transporters of different functions and substrates, the NBDs are powering the transports, while the TMDs are thought to contain the substrate binding site (Hollenstein *et al.*, 2007; Kerr, 2002). ABC transporters are active transporters

and can pump substrate against a concentration gradient requiring energy *i.e.* binding and hydrolysis of ATP (Higgins and Linton, 2004).

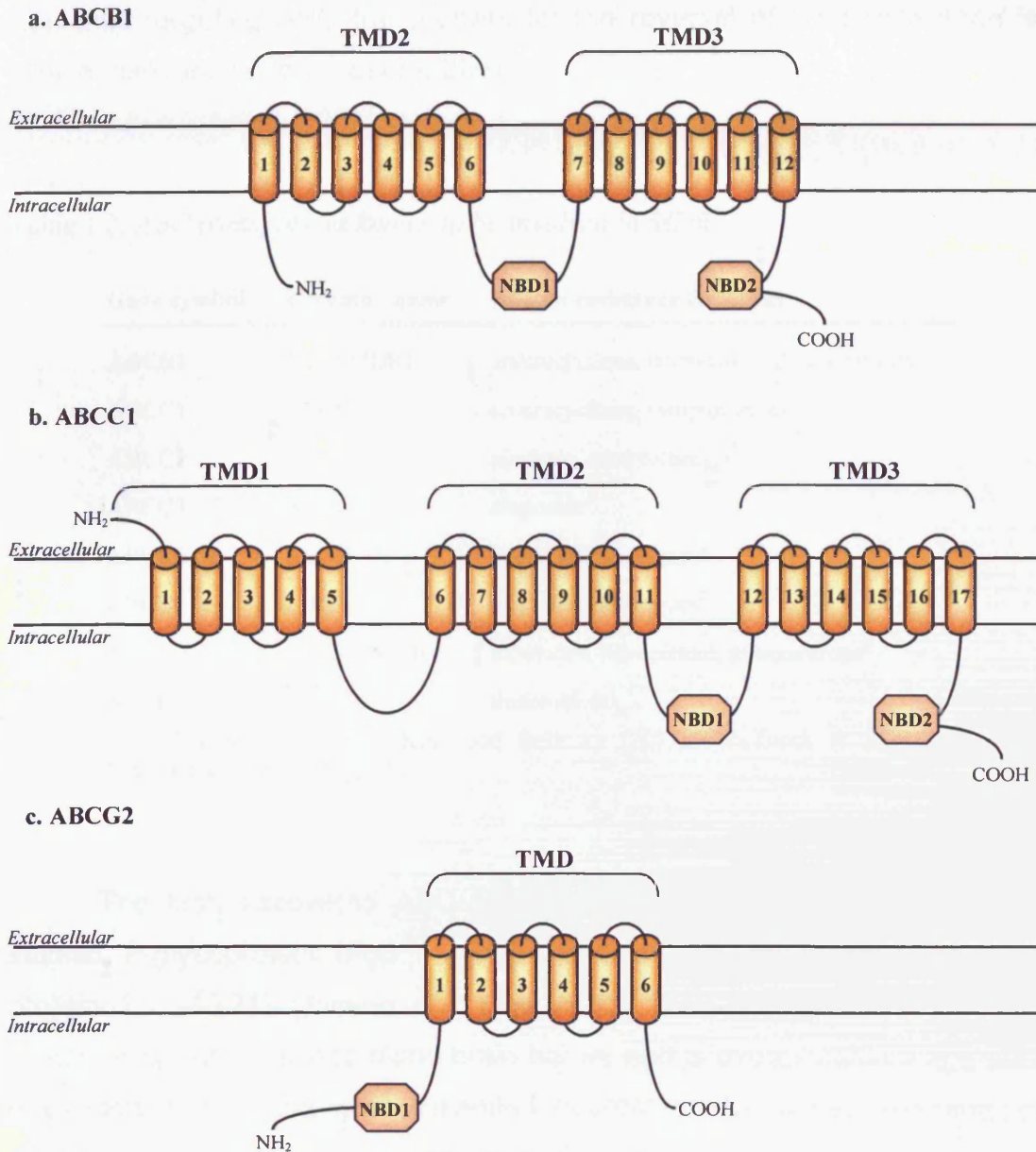


Figure I.4: ABC transporters protein arrangements (adapted from Couture *et al.*, 2006). Representative structures of the three different ABC proteins arrangements. **a.** full transporters. **b.** Transporters containing an extra transmembrane domain. **c.** half transporters containing only one transmembrane domain and one nucleotide binding domain.

ABC transporters are responsible for uptake and efflux of a multitude of substances involved in diverse physiological process. Furthermore, ABC function is one of the major causes of drug resistance and chemotherapeutic failure in cancer. Several notorious ABC transporters are involved in MDR (table I.2), thus targeting ABC transporters for the reversal of drug resistance is of clinical relevance (Ponte-Sucre, 2007).

Table I.2: ABC transporters known to be involved in MDR.

Gene symbol	Common name	Known resistance factor for
ABCB1	Pgp / MDR1	anthracyclines, etoposide, Vinca alkaloids <sup>1</sup>
ABCC1	MRP1	anthracyclines, camptothecins <sup>2</sup>
ABCC2	MRP2	cisplatin, camptothecins <sup>2</sup>
ABCC3	MRP3	etoposide <sup>2</sup>
ABCC4	MRP4	nucleotide analogues <sup>2</sup>
ABCC5	MRP5	nucleotide analogues <sup>2</sup>
ABCG2	BCRP / MXR	topotecan, flavopiridol, mitoxantrone <sup>3</sup>
ABCG5	/	doxorubicin <sup>4</sup>

<sup>1</sup>Ambudkar *et al.* (2003), <sup>2</sup>Kruh and Belinsky (2003), <sup>3</sup>Hardwick *et al.* (2007), <sup>4</sup>Visvader and Lindeman (2008)

The first discovered ABC transporter involved in MDR is the widely studied P-glycoprotein (Pgp / ABCB1 also known as multidrug resistance protein 1 / MDR1) (Juliano and Ling, 1976). ABCB1 normally functions in kidney, intestine, liver and blood-brain barrier and is overexpressed in a variety of cancers (e.g. lymphomas, leukemias, neuroblastoma, kidney, liver and colon cancer) contributing to resistance to various agents including actinomycin D, paclitaxel, anthracyclines and etoposide (Ambudkar *et al.*, 2003). The second frequently studied ABC transporters is the breast cancer resistant protein (BCRP / ABCG2 also known as mitoxantrone resistant protein / MXR). ABCG2 was first discovered in the breast cell line MCF7, selected for resistance to mitoxantrone (Nakagawa *et al.*, 1992) or doxorubicin (Chen *et al.*, 1990). ABCG2 is endogenously expressed at apical membranes of polarised cells



such as hepatocytes, enterocytes and endothelial cells suggesting a role in protection against environmental substances. Its expression in numerous cancers (e.g. leukemias, SCLC, and melanoma) confers resistance to drugs such as topotecan, mitoxantrone and flavopiridol (Hardwick *et al.*, 2007; Mao and Unadkat, 2005). Recently, a role of ABC transporters as phenotypic markers of stem cells has been uncovered (Alison, 2003; Bunting, 2002). Furthermore, the stem cells marker ABCG2 has been shown to be a molecular determinant for the Hoechst 33342 side population phenotype (Zhou *et al.*, 2001). These intriguing roles of ABCG2 in stem cell biology have been discussed in previous sections.

## **I.5. Environment and cell adhesion**

The microenvironments of tumours introduce level of inherent complexity in defining cellular phenotypes with implications for tumour suppression and progression (Bissell and Radisky, 2001). Many resistance models (particularly *in vitro*) lack relevance for host-tumour interactions and hence the unknown impact and role of tumour cell adhesion properties (Joyce, 2005). For instance, integrin-associated signalling can render tumour cells more resistant to anti-cancer agents, a phenomenon termed cell-adhesion-mediated drug resistance (CAM-DR) in SCLC (Buttery *et al.*, 2004). However, the search for anti-adhesion molecules offers promising and possibly low-toxicity strategies that may be broadly applicable cancer treatment (Schmidmaier and Baumann, 2008).

The following brief overview of the major cell adhesion mechanisms encompasses the role of the glycocalyx and the implications for cancer biology and drug resistance. In the case of mammalian cell systems, the term *glycocalyx* was initially applied to the polysaccharide matrix excreted by epithelial cells forming a coating on the surface of epithelial tissue – imparting passive protection. Here the term is used to refer conveniently to the specific decoration of cell surface molecules – a feature that can impact on cancer cell behaviour. Accordingly, malignant transformation is associated with changes in glycosylation, resulting in ‘abnormal’ glycosylations patterns in tumour cells. Indeed, it is recognized that carbohydrate-mediated adhesion in cancer plays a role in metastasis and angiogenesis (Kannagi *et al.*, 2004).

### **I.5.1. Cell adhesion mechanisms**

Cell adhesion to other cells or the surrounding substrate (extracellular matrix) mediated by cell adhesion molecules (CAM), is an important component of tissue architecture enabling the association of cells into a 3D structure providing additional multi-level spatial, mechanical and gradient properties. In addition to cell-cell and cell-matrix interactions, CAMs have recognized roles in influencing cell shape and polarity, cytoskeletal organization, cell motility, proliferation, survival and differentiation (Hynes, 1999). A crucial role has been

attributed to the cytoskeleton — a network of actin filaments, microtubules and intermediate filaments — in mediating cell organization and cell motility (Hynes, 1999). Cell junctions can be divided in 2 types, cell-cell adhesion — principally mediated by desmosomes, tight junctions, gap junctions and adherens junctions (Cavallaro and Christofori, 2004) — and cell-matrix adhesion — mainly focal adhesions and hemi-desmosomes. There are 4 major superfamilies of CAMs (figure I.5):

*Cadherins* — are the principal components of desmosomes and adherens junction. The cadherin superfamily consists in classical cadherins involved in  $\text{Ca}^{2+}$  dependent homophilic binding and non-classical cadherins including protocadherins. Cadherin superfamily includes cadherins, protocadherins, desmogleins, and desmocollins, and more (Cavallaro and Christofori, 2004). Nearly all cadherins have a single transmembrane domain (figure I.5a), the extracellular domain is composed of repeated blocks (cadherin repeats) variable in number (Stemmler, 2008).

*The immunoglobulin superfamily cell adhesion molecule (IG-CAM)* — members are expressed in many different cell types and involved in many biological processes. They are characterized by the presence of 1 or more immunoglobulin-like (Ig-like) domain and various number of fibronectin type III (Fn III) domain (figure I.5b). Ig-CAM is a very diverse group of proteins, typically they have a large extracellular domain, a single transmembrane domain and a cytoplasmic tail (Juliano, 2002). They are involved in both homophilic and heterophilic interactions (Cavallaro and Christofori, 2004).

*Selectins* — are a family of 3 glycoproteins (E-, L- and P-selectin) with an extracellular domain highly conserved among them and between species. Selectins are membrane proteins (figure I.5c) containing a N-terminal sugar binding lectin domain followed by an epidermal growth factor (EGF)-like motif, a series of short consensus repeat, a transmembrane domain and a cytoplasmic tail (Ley, 2003). Selectins bind heavily glycosylated proteoglycans such as selectin P ligand (SELPLG / P-selectin glycoprotein ligand 1 precursor / PSGL-1), or the carbohydrates sialyl Lewis a and sialyl Lewis x (Witz, 2008).

*Integrins* — are heterodimeric transmembrane proteins composed of 2 subunits  $\alpha$  and  $\beta$  non-covalently linked. In mammals there are 18  $\alpha$  and 8  $\beta$  subunits forming 24 distinct integrins. Integrins act primarily as extracellular

matrix receptor and are the principal receptors for cell-matrix interactions (Berrier and Yamada, 2007). Integrins function as dimers (figure I.5d), with the ligand-binding site formed by the  $\alpha$ - and  $\beta$ -subunits extracellular domains. Cytoplasmic tails are usually short (van der Flier and Sonnenberg, 2001). Integrins are capable of transmitting information in either direction across the membrane, cytoplasmic interactions trigger conformational changes of the extracellular domain while matrix interactions trigger changes in cytoplasmic regions and further downstream signalling (Wegener and Campbell, 2008).

*Other CAMs* — includes syndecans, disintegrin family.

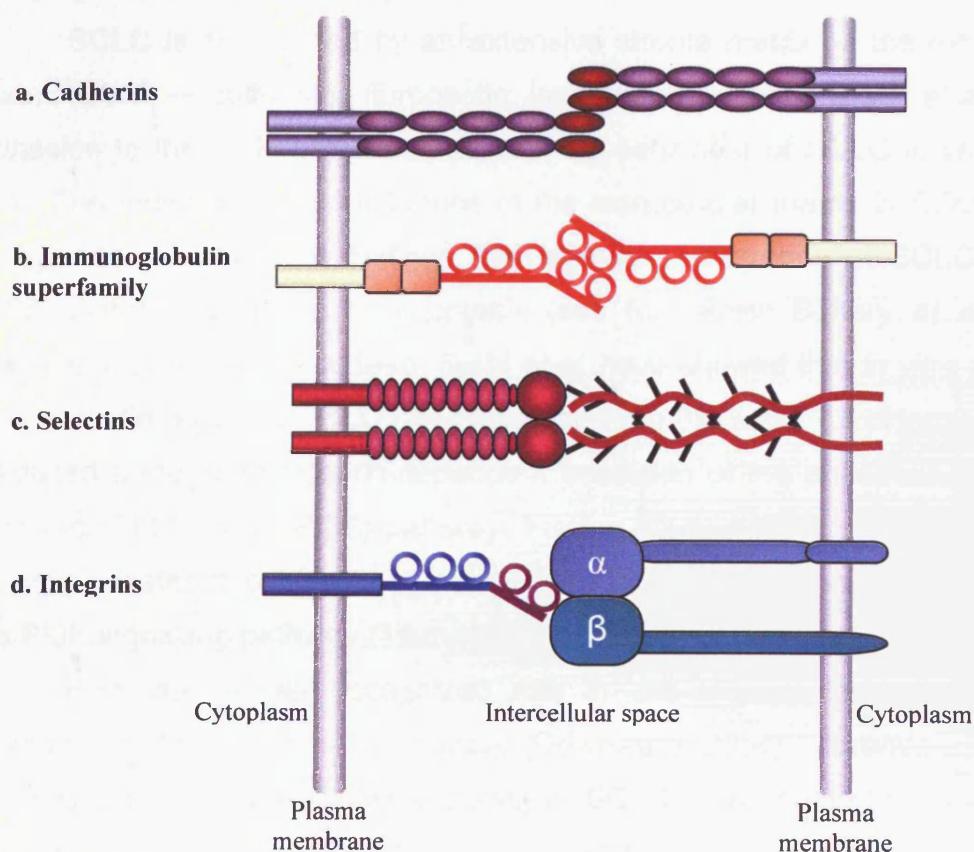


**Figure I.5:** Major classes of cell adhesion molecules (adapted from Hynes, 1999). The figure shows: **a.** a classic cadherin engaged in homophilic binding, **b.** a member of the immunoglobulin superfamily, NCAM engage in homophilic binding, **c.** a selectin, P-selectin (left) bound to a heavily glycosylated proteoglycan (PSGL-1) and **d.** an integrin bound to a member of the Ig-SF (ICAM-1).

### I.5.2. Cell adhesion and drug resistance

A role for cell-cell contact in drug resistance was first suggested when CHO cells grown in spheroid systems were found to be more resistant to radiation damage than individual cells (Durand and Sutherland, 1972). Since then, cell adhesion-mediated drug resistance (CAM-DR) mechanisms have been uncovered in a number a tumours, such as breast cancer (Aoudjit and Vuori, 2001), colon cancer (Kouniavsky *et al.*, 2002), glioma (Uhm *et al.*, 1999) and myeloma (Hazlehurst *et al.*, 2000). Recent studies have proposed CAM-DR as a *de novo* drug resistance process, allowing the cells to evade cytotoxic effects and favour the accrual of multi-drug resistance (Hodkinson *et al.*, 2007), implying mechanisms for adaptation.

SCLC is surrounded by an extensive stroma matrix — the extracellular matrix (ECM) — containing fibronectin, laminin and tenascin (Sethi *et al.*, 1999). Adhesion to the ECM profoundly affects the behaviour of SCLC *in vivo* and *in vitro*. The importance and influence of the extracellular matrix in SCLC is well recognized including the findings that selective adherence of SCLC cells to ECM confers resistance to apoptosis (see for review Buttery *et al.*, 2004; Hodkinson *et al.*, 2007). Indeed, Sethi *et al.* have showed that *in vitro* adhesion to fibronectin provides SCLC cell protection from the action of cytotoxic agents mediated through  $\beta$ 1 integrin-dependent activation of the phosphatidyl inositol 3-kinase (PI3-kinase / PI3K) pathway. Further studies provide similar evidence for drug resistance conferred by adhesion to laminin, also shown to act through the PI3K signalling pathway (Tsurutani *et al.*, 2005).

PI3K has a well recognized role in cell survival through the direct regulation of the apoptosis machinery (Downward, 2004). Moreover, PI3K has been found to be constitutively active in SCLC cells, promoting anchorage-independent growth (Moore *et al.*, 1998) and to be an essential survival signal in SCLC as well as a key regulator of cell cycle progression (Krystal *et al.*, 2002). Moreover,  $\beta$ 1 integrin expression has been linked with a poor prognosis for patients with SCLC (Oshita *et al.*, 2002). Recently, a role was also suggested for the chemokine receptor CXCR4 (C-X-C chemokine receptor type 4) in mediating the  $\beta$ 1 integrin-dependent adhesion of SCLC cells to surrounding ECM (Hartmann *et al.*, 2005) – relevant to a role in SCLC ‘homing’

in tumour spread. The  $\beta 1$ -integrin-dependent resistance pathway has been further elucidated (figure I.6). In SCLC cells  $\beta 1$  integrin-mediated activation of PI3K activation, via phosphorylation of downstream targets Akt (AKT1 / v-akt murine thymoma viral oncogene homolog 1 / Protein kinase B / PKB) and GSK3 $\beta$  (glycogen synthase kinase 3 beta), was found to lead to an override of G2/M checkpoint mechanisms and arrest, induced by etoposide and ionizing radiation treatment, hence promoting progression through the cell cycle and progression to mitosis (Hodkinson *et al.*, 2006). SCLC cells also differentially activate Akt post-adhesion to ECM substrates. For instance, SCLC adhesion to laminin, fibronectin, collagen I and collagen IV leads to activation of the Akt pathway, however, it is clear that Akt activation appears to be dependent on the cell line derivation as well as the ECM component (Tsurutani *et al.*, 2005). Therefore it is clear that cell-ECM interactions impact on the underlying properties of tumour heterogeneity.

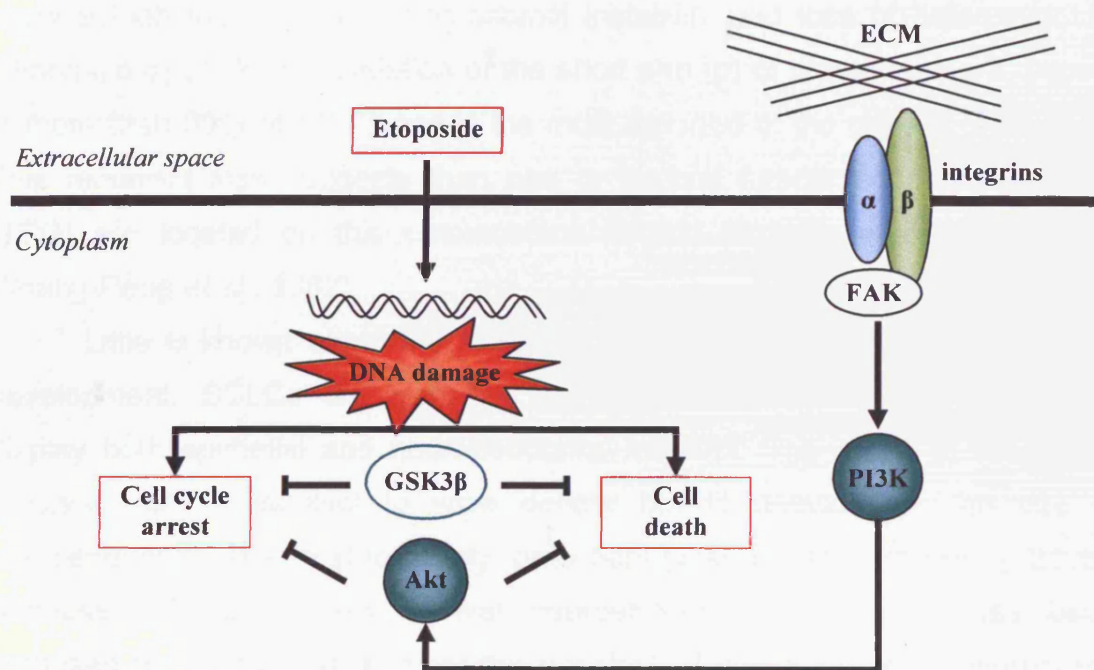


Figure I.6: Proposed mechanisms for integrin-mediated protection from genotoxic therapy (adapted from Hodkinson *et al.*, 2007).



## 1.6. Plasticity of the phenotype and genotype of SCLC

Lung cancer is the most common form of cancer usually diagnosed when patients present symptoms. There are 4 major histologic types of lung cancer: SCLC and three NSCLC, undifferentiated (large cell carcinoma), adenocarcinoma and squamous cell carcinoma (Minna *et al.*, 2002). SCLC is an aggressive disease with a poor prognosis accounting for approximately 20% of all lung cancer. SCLC is a particularly fast growing cancer characterized by frequent and early metastasis and the development of chemoresistance (Beadsmoore and Screatton, 2003). Chemotherapy is the main form of treatment but despite an initial good response to therapy, the patient almost always relapses with recurring disease (Hoffman *et al.*, 2000).

As for other solid tumours, many genetic changes are suspected of involvement in the full pathogenesis of SCLC (reviewed in Balsara and Testa, 2002). SCLC demonstrates genetic instability – ranging from gene mutation to chromosomal deletion, aberrations and changes in ploidy – SCLC tumours show a high incidence of chromosomal instability and loss of heterozygosity (Ninomiya *et al.*, 2006). Deletion of the short arm (p) of chromosome 3, occurs in more than 90% of SCLC and is the most reported of the genetic anomalies. This recurrent loss suggests that one or several tumour suppressor genes (TSG) are located on this chromosomal region (Balsara and Testa, 2002; Whang-Peng *et al.*, 1982).

Little is known about the molecular alterations that occur during SCLC development. SCLCs are classified as neuroendocrine (NE) tumours and display both epithelial and neuroendocrine markers. The origin of the SCLC precursor cell is subject to wide debate but is relevant for the use of neuroendocrine markers for early detection (Warren and Hammar, 2006). Because SCLCs express several neuroendocrine markers, it has been proposed that it could arise from the neoplastic transformation of neurocrest-derived neuroendocrine lung cells. An alternative hypothesis suggests that neoplasm would arise from pluripotent cells of endodermal origin and undergo early neuroendocrine differentiation, although the cell type receiving the first oncogenic hit remains unclear (Gudermann and Roelle, 2006).

### I.6.1. Molecular characteristics

Several molecular alterations are characteristics to SCLC tumours and frequently displayed by SCLC derived cell lines (Table I.3). These molecular characteristics are frequently used as markers and can be related to SCLC profiling, including neuroendocrine phenotype, metastasis and chemoresistance (reviewed in Iyengar and Tsao, 2002; reviewed in Sattler and Salgia, 2003; Taneja and Sharma, 2004; Wistuba *et al.*, 2001).

Table I.3: *SCLC molecular characteristics.*

<b>'Classical markers'</b>	
MYC family	oncogene
BCL2	antiapoptotic
SCF / c-kit	growth factor
c-Met	growth factor
CXCR4	
p53	tumour suppressor
Retinoblastoma (Rb)	tumour suppressor
<b>'Neuroendocrine markers'</b>	
Gastrin-releasing peptide (GRP)	growth factor
Neural cell adhesion molecule (NCAM)	cell adhesion and migration
Achaete scute homologous protein (ASCL1)	transcription factor in neuronal differentiation
Chromogranin A (CgA)	neuroendocrine secretory protein
L-dopa decarboxylase	
Neuron-restricted silencer factor (NRSF/REST)	transcription repression of neuronal genes
Neuron-specific enolase (NSE)	

*The neuroendocrine phenotype:* Ectopic expression of NE genes is essential to SCLC pathogenesis. The transcription factor Achaete-scute homologue-1 (ASCL1) known to be involved in neuronal commitment in vertebrates is expressed by 'classic' SCLC cell lines. Its depletion leads to downregulation of some neuroendocrine features in SCLC cell line underlying its role in maintenance of NE phenotype (Borges *et al.*, 1997). In addition, deficient activity of the neuron restrictive silencer factor (NRSF) has been observed in SCLC. NRSF is expressed in non-neuronal tissue and has role in repression of neuronal genes (Gurrola-Diaz *et al.*, 2003). Additionally, several



neuronal proteins including chromogranin A (CgA), neuronal cell adhesion molecule (NCAM) and neuron-specific enolase (NSE) are expressed by SCLC tumour and are widely used as NE differentiation markers.

*Tumour suppressor, oncogenes and apoptosis:* Although SCLC tumour development remains to be elucidated, some insight was provided by the development of a mouse model of SCLC. Somatic inactivation of p53 and Retinoblastoma 1 (Rb1) was necessary and sufficient to generate SCLC-like tumours with histopathologic characteristics and metastasizing capacity strikingly similar to SCLC (Meuwissen *et al.*, 2003). Alteration in p53 and Rb alteration occurs in over 90% of cases of SCLC (Wistuba *et al.*, 2001). Abnormal expression of MYC family of oncogenes is common in SCLC tumour and cell lines (Kim *et al.*, 2006; Takahashi *et al.*, 1989). MYC oncogenes are DNA binding proteins known to be involved in transcription regulation, cellular proliferation and apoptosis (Sattler and Salgia, 2003). Aberrant expression of the negative regulator of cell death BCL2 has been observed in most SCLC and inhibition induces cytotoxicity in SCLC xenografts (Oltersdorf *et al.*, 2005)

*Autocrine growth stimulation:* Autocrine growth stimulation has long been recognized in SCLC and is well documented. SCLC tumours and cell lines express several receptors tyrosine kinase (RTK). Among them is c-kit receptor to the Stem Cell Factor (SCF). SCF and c-kit are coexpressed in a majority of SCLC cell lines resulting in autocrine growth stimulation (Krystal *et al.*, 1996). Functional c-Met/Hepatocyte Growth Factor (HGF) pathway can also be found in SCLC influencing cell proliferation and motility (Jagadeeswaran *et al.*, 2007; Maulik *et al.*, 2002). Moreover, an extensive array of neuropeptides and their receptor expression has been implicated in driving the growth of SCLC tumour in autocrine and paracrine fashions (for a review, see Heasley, 2001).

*Metastasis and homing:* SCLC often metastasise to the bone marrow and bone marrow metastases are an important negative prognostic in SCLC (Beadsmoore and Screatton, 2003). It is thought to be due to the SDF1 / CXCR4 axis (CX-chemokine receptor-4 and ligand CXCL12 / CXC chemokines ligand 12, also known as stromal derived factor 1 / SDF-1) known to be involved in bone marrow homing (Hartmann *et al.*, 2004). Indeed, high amount of SDF1 are constitutively secreted by marrow stromal cells and SCLC cells express

functional CXCR4 mediating migration, integrin activation and adhesion to stromal cells (Burger *et al.*, 2003).

### **I.6.2. Chemoresistance and early invasion: therapeutic challenge**

Due to its propensity for metastasis, the SCLC tumour is often metastatic at the time of diagnosis. Thus SCLC is rarely treated by surgical resection. Staging — limited or extensive disease — alongside the extent of metastasis both dictate the treatment regiment. Chemotherapy is the standard care, radiotherapy is only used in limited disease (Beadsmoore and Screatton, 2003). Combination chemotherapy regimens include a platinum agent (cisplatin or carboplatin) combined with etoposide, are the standard of care for most SCLCs. Currently, new drugs and combinations are undergoing clinical trials, including topotecan, iritonecan, paclitaxel and amrubicin (Ferraldeschi *et al.*, 2007; Murray and Turrisi, 2006; Rosti *et al.*, 2006). Novel approaches employing targeted therapies are currently undergoing investigation, including BCL2 and receptors tyrosine kinase targeting (Fischer *et al.*, 2007). After the completion of first line therapy, 80% of patients with limited disease and almost all patients with extensive disease relapse, underlying the need for second line therapy. The main second treatments include a combination of cyclophosphamide, doxorubicin and vincristine or the use of topotecan as single agent treatment (Tiseo and Ardizzoni, 2007).

Despite initial advances in treatment, the development of chemoresistance remains a problem. Chemotherapy improves the survival of patients with limited-stage or extensive-stage SCLC, but it is curative in only a minority of patients. Trials have demonstrated some survival advantage for patients, with a call for a better understanding of the underlying SCLC biology to progress further. As discussed previously, there is a need to understand the classical SCLC chemoresistance mechanisms and their co-existence for cell adhesion mediated resistance processes and active roles for the neuronal protein marker PSA-NCAM in SCLC metastasis (Lantuejoul *et al.*, 1998).

## I.7. NCAM biology

The neural cell adhesion molecule (NCAM, also denominated NCAM1 or CD56) belongs to the immunoglobulin superfamily of cell adhesion molecule (IgCAM). NCAM was first detected in the chick brain and retina (Rutishauser *et al.*, 1976; Thiery *et al.*, 1977) and is present on neural cells and various neuroendocrine tumours, almost all SCLC tumour cells show NCAM expression detected at the plasma membrane (Lantuejoul *et al.*, 1998).

### I.7.1. Structure

NCAM is a group of glycoproteins emanating from a single gene located on band q23 of chromosome 11 (Nguyen *et al.*, 1986). NCAM is composed of 5 immunoglobulin (Ig) domains and 2 fibronectin (Fn) domains and 4 isoforms exist (figure I.7a). Of these isoforms, 3 are produced by alternative splicing and a secreted form can be generated by either expression of the SEC exon or proteolytic cleavage (Walmod *et al.*, 2004). The two large isoforms, 140 and 180 kDa, contain intracellular domains of different length, while the 120 kDa form is attached to the membrane via a GPI-anchor. In addition to these forms, further heterogeneity can occur; the first is the presence of a differentially expressed 10 amino acid extra sequence —called VASE— situated in the IgIV domain (Small and Akeson, 1990). Although the role and expression pattern of the different NCAM isoforms is not yet clear, a shift from NCAM 120 in normal to NCAM 140 and 180 expression has been observed in pancreatic tumour progression in mice (Perl *et al.*, 1999) and isoforms expression seems to correlate with neuroblastoma differentiation status (Winter *et al.*, 2008).

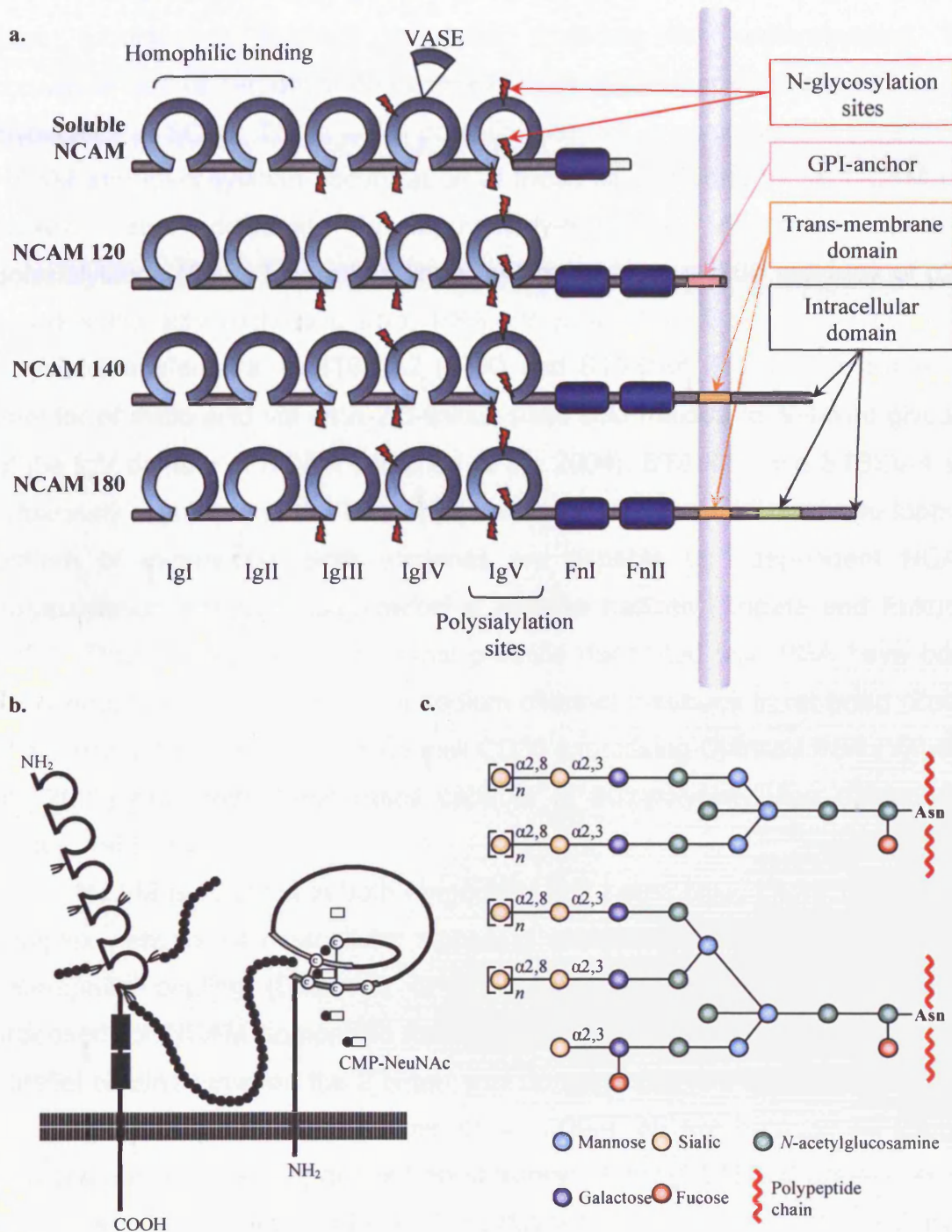


**Figure I.7:** NCAM isoforms structure and polysialylation pattern. **a.** NCAM isoforms (adapted from Walmod *et al.*, 2004). **b.** Scheme representing a polysialyltransferase (ST8SIA4) transferring sialic acid to NCAM (Angata and Fukuda, 2003). **c.** Diagram representing PSA found on bi- or tri-antennary N-glycan chains attached to the fifth Ig-like domain of all isoforms of NCAM (Kleene and Schachner, 2004).

NCAM can be highly glycosylated shifting its molecular weight – and as such provides a relevant exemplar molecule for understanding the consequences of carbohydrate decoration and roles of specific aspects of the glycocalyx in SCLC. There are 6 potential sites for *N*-glycosylation present on NCAM and glycosylation occurs at all of these sites. Furthermore, NCAM can present an additional developmentally-regulated decoration pattern, polysialylation (figure I.7b and c): linear polymers of up to 200 residues of  $\alpha$ -2-8 linked sialic acid (polysialic acid, PSA, PolySia). Two Golgi-associated  $\alpha$ -2-8 polysialyltransferases — ST8SIA2 (STX) and ST8SIA4 (PST) — facilitate the transfer of sialic acid via an  $\alpha$ -2,3-linked sialic acid residue to *N*-linked glycans of the IgV domain of NCAM (Walmod *et al.*, 2004). ST8SIA2 and ST8SIA4 are separately regulated at the transcriptional level and have different overlapping pattern of expression. Both enzymes are capable of independent NCAM polysialylation although cooperation is likely to happen (Angata and Fukuda, 2003). Thus far only a few mammal proteins decorated with PSA have been described: the voltage-dependent sodium channel  $\alpha$ -subunit in rat brain (Zuber *et al.*, 1992), the human and mice milk CD36 expressing O-linked PSA (Yabe *et al.*, 2003) and both transferases capable of autopolsialylation (Close and Colley, 1998).

NCAM is involved in both homophilic and heterophilic interactions and a complex network of intracellular signalling is activated upon homophilic and heterophilic binding (Ditlevsen *et al.*, 2008). Several models have been proposed for NCAM homophilic trans-interaction between opposite cells: anti-parallel binding between the 2 N-terminal domains (Igl and IgII) or interactions involving all 5 Ig domains (Kasper *et al.*, 2000). NCAM heterophilic ligands includes the glial cell line-derived neurotrophic factor (GDNF) (Paratcha *et al.*, 2003), another neural CAM (L1) (Ditlevsen *et al.*, 2003), brain-derived neurotrophic factor (BDNF), platelet-derived growth factor (PDGF) (Ditlevsen *et al.*, 2008). NCAM is also known to interact with several ECM components, including the glycosaminoglycan heparin, collagen I to IV and a number of chondroitin sulfate proteoglycans (CSPG) and heparan sulfate proteoglycans (HSPG) (Walmod *et al.*, 2004). NCAM does not possess catalytic activities and signalling is mediated by intracellular and extracellular partners, one central

partner is the fibroblast growth factor receptor (FGFR) activated upon NCAM homophilic binding (Kiselyov *et al.*, 2005). Recently, a role was suggested for the PI3K/Akt pathway in NCAM-mediated neuronal cell survival (Ditlevsen *et al.*, 2003)

### **I.7.2. Role in development and CNS**

NCAM is highly expressed during development and expression is subsequently isolated to parts of the central nervous system in the adult. While the amount of PSA decoration decreases with development and VASE expression correspondingly increases and therefore the level of PSA decoration, in simple terms, could be seen to be correlated with the need to a switch from a dynamic phase requiring tissue plasticity into a stable or differentiated state. Indeed, PSA decoration of NCAM regulation and NCAM regulation seem to be independent and in the adult PSA-NCAM is only expressed in areas showing high degree of plasticity, such as the lateral ventricle and hippocampus where PSA plays a role in regulating several steps of adult neurogenesis (Kiss *et al.*, 2001; Walmod *et al.*, 2004). In the central nervous system, PSA-NCAM plays a pivotal role in neuronal development and synaptic plasticity linked to memory and learning as well as in axon guidance and neurite outgrowth (Rutishauser, 2008). NCAM knock-out mice show a smaller olfactory bulb and reduced body weight and display an impairment of their learning faculties (Cremer *et al.*, 1994). However, dramatic effects can be shown as a result of PSA knock-out mice, indeed the absence of PSA by deletion of the two polysialyltransferases leads to a lethal phenotype rescued by a simultaneous NCAM deletion (Weinhold *et al.*, 2005).

### **I.7.3. Polysialic acid and links with metastatic behaviour**

NCAM has been described as having tumour suppressor function. Indeed, reduced NCAM expression is associated with poor prognosis in a number of cancers, for instance, loss of NCAM expression has been linked to metastasis dissemination in pancreatic tumours (Crnic *et al.*, 2004; Perl *et al.*, 1999). However, in neuroblastoma and neuroendocrine tumours NCAM

expression concomitant with high polysialylation is associated with a poor prognosis (Lantuejoul *et al.*, 1998). The carbohydrate PSA provides a polyanionic cell surface decoration of NCAM affecting function and membrane-membrane apposition. Indeed, PSA has been shown to increase the amount of intercellular space affecting membrane-membrane closeness (Yang *et al.*, 1992). And recently, Johnson *et al.* (2005) have provided direct evidence that NCAM polysialylation increases inter-membrane repulsion and abrogates NCAM homophilic adhesion and C-cadherin-mediated inter-membrane adhesion. Numerous studies show increase in adhesion after PSA removal by endoneuraminidase — an enzyme specific to the  $\alpha 2,8$  linkage of sialic acid — however adhesion to specific member of the ECM seems to be dependant on the cell type. Indeed PSA removal was shown to increase cell-cell aggregation (Rutishauser *et al.*, 1985), cell adhesion to laminin (Acheson *et al.*, 1991), cadherin and fibronectin (Fujimoto *et al.*, 2001), fibronectin and collagen IV but not laminin (Dennis *et al.*, 1982). PSA is therefore considered an anti-adhesive molecule reducing cell interactions with implications for cell motility and metastasis. PSA has been shown to be a requirement for O-2A brain progenitor migration (Wang *et al.*, 1994) and aberrant expression of PSA-NCAM is associated with tumour malignancy and metastasis. Indeed generation of SCLC cell line variant sublines with high levels of PSA expression correlate with reduced cell-cell adherence, greater clonogenic ability in semisolid media, and a significantly higher incidence of intracutaneous metastases in nude mice (Scheidegger *et al.*, 1994). Suzuki *et al.* (2005) showed that mice inoculated with glioma cells transfected with ST8SIA2 harboured extensive tumour spreading properties compared to the controls expressing only NCAM. *In vivo* injection of endoneuraminidase reduced lung metastases in animals inoculated with rhabdomyosarcoma cell line expressing PSA (Daniel *et al.*, 2001). PSA decoration has also been linked to tumour proliferation with PSA removal inducing tumour growth inhibition by affecting NCAM signalling (Seidenfaden *et al.*, 2003).

#### I.7.4. PSA-NCAM and the therapeutic challenge

Over the past few years, glycoscience has become a growing field of research with recognition that glycans play an important role in essential cell biology processes (Merry and Merry, 2005). Interest has been increased with the availability of analytical tools and the discovery that aberrant glycosylations occurs in all types of cancer (Hakomori, 2002). Such insights provide for new therapeutics opportunities (Shriver *et al.*, 2004). An important component of the glycocalyx in some tumour cells is the decoration of NCAM known to assist the metastatic spread. The control of changes in NCAM decoration is therefore an attractive proposition. An early model (Acheson *et al.*, 1991) of glycocalyx dynamics makes the striking prediction that PSA could affect not only NCAM function, but also other ligands not directly involved in NCAM-mediated adhesion – widening the possible functional impact of PSA targeted agents – suggesting that PSA modulation in cancer may be necessary at specific stages but not sufficient. Importantly, in normal adult cells PSA-NCAM is virtually non-existent, only occurring at limited defined sites in the brain, increasing the attractiveness for selective targeting. A recent attempt to capitalise on this selective PSA expression has involved vaccination of SCLC patients with polysialic acid or *N*-propionylated polysialic acid conjugated to keyhole limpet hemocyanin in an attempt to eradicate chemoresistant micrometastatic disease (Krug *et al.*, 2004).

A therapeutic concept — relevant to SCLC and forming a backdrop to the direct of the present study — would be to limit PSA decoration of NCAM, by post-translational small molecule targeting prior to or during cell-shedding by a tumour, to increase the adhesive properties of cells and therefore reduce or prevent their detachment. Clearly, this simple concept uncovers issues of the recruitment of aberrant cell behaviour and concomitant resistance, underlining the need for new SCLC experimental systems to test concepts and to provide possible validation/screening opportunities for candidate agents.



## I.8. Aims of the thesis

The overall aim of the thesis was to disassemble the complexity of the cellular *in vitro* phenotypes associated with SCLC and to understand how phenotypic variation might impact on aspects of SCLC biology. The conservation of gene expression patterns and biomarkers from tumour to cell line (noted above) provide some confidence that *in vitro* studies can progress a fundamental of SCLC biology. The classification of SCLC cell lines (reviewed in the subsequent sections) suggests a clear potential for variation and plasticity with implications for clinical and therapeutic challenges. Furthermore, any disassembly of complexity should proved cellular systems that can be progressed into more complex analytical situations – not least microenvironment manipulation and *in vivo* assessment.

Thus a study was undertaken to enrich cultures for SCLC ‘adhesion’ variants, without prejudice for any specific ECM directed advantage, and then to allow for any proliferation/survival advantage *in vitro* to impact on the evolution of variation. The aim was to establish and characterize the new SCLC sub-lines that represent the nature and consequence of variant enrichment and to undertake an assessment of this defined *in vitro* SCLC for heterogeneity and plasticity. The working hypothesis is that phenotypic plasticity of a tumour mass acts as a driver for metastasis and the accrual of chemoresistance through an enhancement of Darwinian fitness. Therefore in order to understand the implications of phenotypic heterogeneity *in vitro*, the aim was to use such a unique SCLC model to gain insights into:

- 1) How changes in cell-cell and cell-substrate interactions might impact on the molecular signatures of SCLC and cellular phenotypic behaviours such as *in vitro* growth, cell survival, cell motility and cell adhesion. In particular to understand the down stream implications on the proliferative advantage within SCLC heterogeneity and clonal selection.

- 2) How phenotypic or variant heterogeneity can affect critical pathways for drug resistance to an exemplar cytotoxic anticancer agent with a known mechanism of action that offers opportunities to assess different modes of resistance using both gene expression and functional assays.

3) The use the SCLC model to explore the possible impact of variation and plasticity on an as yet undetermined role for cancer stem cell origins in SCLC drug resistance.

4) How differences in polysialylation of NCAM map to the heterogeneity of SCLC populations, with reference to expression patterns of glycosylation pathways, and therefore offer the ability for cells to express PSA-NCAM plasticity or offers opportunities for therapeutic target of the glycocalyx.

The subsequent thesis chapters encompass these general aims, provide pertinent overviews to frame the context of more detailed experimental aims and provide details of the specific methodologies employed. The overall synthesis is contained within the Main Discussion chapter with directions for future research and exploitation of the study's findings.

## II. Materials and methods

All reagents were stored, handled and disposed of according to Cardiff University Health and Safety regulations, informed by the Material Safety Data Sheets, provided by the suppliers. Information about specific methodologies and reagents, linked with a focus area of investigation, are provided within the results chapters.

### II.1. Materials

All chemical reagents used are listed in Appendix I, together with their sources.

#### II.1.1. Drug and molecular probes table

Drugs and fluorescent dyes were prepared, stored and disposed of according to the supplier instructions.

Table II.1: Drug and molecular probes used.

Name	Carrier	Source	Storage	Concentration used
Topotecan	H <sub>2</sub> O	GlaxoSmithKline (Brentford, UK)	- 80°C	10 µM
Fumitremorgin C	DMSO	Sigma (St Louis, MO, USA)	4°C	10 µM
R1108/2	methanol	Institute of cancer therapeutics (Bradford, UK)	- 20°C	0.03 to 0.3 µM
DRAQ5	/	Biostatus (Shepshed, UK)	4°C	20 µM
Propidium Iodide	/	Invitrogen Molecular Probes (Carlsbad, CA, USA)	4°C	3 µM
Hoechst 33342	/	Invitrogen Molecular Probes (Carlsbad, CA, USA)	4°C	5 µM

## II.1.2. Antibodies and sources tables

**Table II.2: Primary antibodies used.** WB/western blot, IF/immunofluorescence and FC/flow cytometry.

antigen	isotype	clone name	source	concentration used (µg/mL) or dilution		
				FC	IF	WB
PSA-NCAM	rat IgM	12F8	BD Bioscience Pharmingen (San Diego, CA, USA)	—	1.25	0.5
PSA	mouse IgM	2-2B	AbCys (Paris, France)	1:400	1:400	1:4000
NCAM	mouse IgG <sub>1</sub>	B159	BD Bioscience Pharmingen (San Diego, CA, USA)	1.25	1.25	0.16
MT	mouse IgG <sub>1</sub>	E9	DakoCytomation (Ely, UK)	—	—	0.46
ABCG2	mouse IgG2	5D3	Chemicon international (Millipore, Temecula, CA, USA)	—	5	—
GAPDH	mouse IgG <sub>2b</sub>		Abcam (Cambridge, UK)	—	—	1:1000

**Table II.3: Secondary antibodies used.** WB/western blot, IF/immunofluorescence and FC/flow cytometry.

antigen	host	conjugate	source	concentration used (µg/mL)		
				FC	IF	WB
Mouse Igs	rabbit	HRP	DakoCytomation (Ely, UK)	—	—	0.1
Rabbit Igs	swine	HRP	DakoCytomation (Ely, UK)	—	—	0.1
Rat IgG+IgM	goat	HRP	Jackson ImmunoResearch (West Baltimore Pike, PA, USA)	—	—	0.33
Rat IgM	goat	Alexa 488	Invitrogen Molecular Probes (Carlsbad, CA, USA)	—	2	—
Mouse IgG	goat	Alexa 568	Invitrogen Molecular Probes (Carlsbad, CA, USA)	2	2	—

## II.2. Cell lines and culture conditions

### II.2.1. Cell lines

**Table II.4:** Cell lines routine culture description.

name	description	medium	split ratio	growth type	source
NCI-H69 <sup>1</sup>	<i>Homo sapiens</i> , SCLC	RPMI-1640*	1:6	suspension	American Type Culture Collection <sup>I</sup>
COR-L47 <sup>2</sup>	<i>Homo sapiens</i> , SCLC	RPMI-1640	1:6	suspension	Dr P. Twentyman <sup>II</sup>
COR-L88 <sup>2</sup>	<i>Homo sapiens</i> , SCLC	RPMI-1640	1:2	suspension	Dr P. Twentyman <sup>II</sup>
COR-L279 <sup>3</sup>	<i>Homo sapiens</i> , SCLC	RPMI-1640	1:6	suspension	Dr P. Twentyman <sup>II</sup>
SHP-77 <sup>4</sup>	<i>Homo sapiens</i> , SCLC	RPMI-1640	1:6	suspension	American Type Culture Collection <sup>I</sup>
COR-L51 <sup>2</sup>	<i>Homo sapiens</i> , SCLC	RPMI-1640	1:3	suspension	Dr P. Twentyman <sup>II</sup>
COR-L23 <sup>2</sup>	<i>Homo sapiens</i> , lung large cell carcinoma	RPMI-1640	1:10	adherent	Dr P. Twentyman <sup>II</sup>
A549 <sup>5</sup>	<i>Homo sapiens</i> , lung alveolar cell carcinoma	DMEM*	1:20	adherent	American Type Culture Collection <sup>I</sup>
SU-DHL-4 <sup>6</sup>	<i>Homo sapiens</i> , B cells lymphoma	RPMI-1640	1:30	suspension	Prof. F. E. Cotter <sup>III</sup>
CHO-K1 <sup>7</sup>	<i>Cricetulus griseus</i> , ovary	EMEM**	1:20	adherent	Dr J. H. Beattie <sup>IV</sup>
mMTCHO-K1 <sup>8</sup>	<i>Cricetulus griseus</i> , ovary	EMEM**	1:20	adherent	Dr J. H. Beattie <sup>IV</sup>

<sup>1</sup>Gazdar *et al.* (1980), <sup>2</sup>Baillie-Johnson *et al.* (1985), <sup>3</sup>Twentyman *et al.* (1992), <sup>4</sup>Fisher and Paulson (1978), <sup>5</sup>Lieber *et al.* (1976), <sup>6</sup>Epstein *et al.* (1976), <sup>7</sup>Kao and Puck (1968), <sup>8</sup>Beattie *et al.* (2005), \*Gibco (Invitrogen, Carlsbad, CA, USA), \*\*Sigma (St Louis, MO, USA), <sup>I</sup>Manassas, VA, USA, <sup>II</sup>MRC Clinical Oncology & Radiotherapeutics Unit, MRC Centre, Cambridge, UK, <sup>III</sup>Institute of Child Health, London, UK, <sup>IV</sup>Rowett Research Institute, Aberdeen, UK.

### II.2.2. Suspension and adherent cell culture

Cell lines (see table II.4) were routinely cultured twice a week. All media were supplemented with 10% fetal calf serum (FCS) (Autogen Bioclear, Calne, UK), 0.5 mM glutamine (Sigma, St Louis, MO, USA), 10 U/mL penicillin (Sigma, St Louis, MO, USA) and 0.1 mg/mL streptomycin (Sigma, St Louis, MO, USA). Cultures were maintained at 37°C under standard culture conditions in a humidified incubator with 5% CO<sub>2</sub>. All adherent SCLC cell lines were detached using cell dissociation solution (CDS / Sigma, St Louis, MO, USA), a non-enzymatic solution prepared in PBS and containing ethylene diaminetetraacetic

acid (EDTA). Other adherent cell lines were detached using trypsin / EDTA (Gibco Invitrogen Carlsbad, CA, USA).

### **II.3. High-density oligonucleotide microarray**

Two sets of microarray analyses were performed during the study. The first, termed '2005 arrays', was done early in the thesis and tested the effect of a potential ST8SIA4 inhibitor (R1108) on the NCI-H69 parental cell line and a variant (NCI-H69 AP55). The second, termed '2008 arrays', was performed to characterize the established three-line NCI-H69 model: NCI-H69 SP vs. NCI-H69 AP3 vs. NCI-H69 AP78.

#### **II.3.1. Drug treatment**

For the 2005 arrays, NCI-H69 SP and NCI-H69 AP55 were seeded in triplicate at a concentration of  $3 \times 10^6$  cells per T75 flasks and allowed to establish for 48h under normal culture conditions. Cells were then treated with R1108 (0.3 mM) for 6 h and then cells were washed with phosphate buffered saline (PBS) prior to RNA extraction.

For the 2008 arrays NCI-H69 cultures were seeded at  $3 \times 10^6$  cells in a standard culture dish in triplicate. After 72h, adherent cells were washed once with PBS before adding 1.5 mL of TRIZOL to the flask prior to RNA extraction

#### **II.3.2. RNA extraction**

Total RNA were isolated using TRIZOL (Invitrogen, Carlsbad, CA, USA) — a modified protocol to the single-step RNA isolation developed by Chomczynski and Sacchi (1987) — according to the manufacturer's instruction. PBS washed adherent cell cultures received 1.5 mL of TRIZOL, while suspension cell cultures were spun down (10 min, 100 g) washed once with PBS and then resuspended in 1.5 mL of TRIZOL. Homogenised samples were let to stand for 10 min at room temperature (RT). After addition of 300  $\mu$ L of chloroform, each sample was thoroughly shaken and the mixture was added to Phase lock gel Heavy (Eppendorf, Hamburg, Germany) and spin down for 2 min

at 12000 x g (Murphy and Hellwig, 1996). RNA from the upper aqueous phase was then precipitated by adding 500 µL of isopropanol. After 10 min at RT, samples were centrifuged at 12000 x g and 4°C for 10 min. After pellets were washed with 75% ethanol, centrifuged at 7500 x g / 4°C for 5min and dried at RT for 10 min, RNAs were dissolved in 200 µL of H<sub>2</sub>O. Samples were precipitated overnight at -20°C with 0.1 volume of 3M sodium acetate and 2.5 volume of 100% ethanol and centrifuged at 12000 x g / 4°C for 30 min. Finally, pellets were washed with 80% ethanol and centrifuged at 12000 x g/4°C for 10 min and RNAs were resuspended in H<sub>2</sub>O. RNA samples were kept at -80°C until further use.

### **II.3.3. RNA quality controls**

RNA quantities and quality controls (QC) were assessed by measuring the absorbance (A) of the RNA solution at 260 nm and 280 nm on a spectrophotometer (DU® 800 UV/visible Spectrophotometer; Beckman Coulter, Fullerton, CA, USA). RNAs were then given to the Affymetrix GeneChip expression profiling service (CBS, School of medicine, Cardiff) for further quality assessment on Agilent RNA Chip (Agilent, Santa Clara, CA).

### **II.3.4. Data acquisition**

The microarray processing steps were performed by Affymetrix GeneChip expression profiling service (CBS Cardiff) and are described in figure II.1. The Human genome U133A array (HG\_U133A) was chosen for hybridization of the 2005 arrays, while the 2008 arrays were hybridized onto the Human genome U133A\_2.0 array (HG\_U133A\_2.0). All probes sets represented on the genechip HG\_U133A are identically replicated on HG\_U133A\_2.0; however the HG\_U133A\_2.0 has a reduced size compared to HG\_U133A allowing smaller sample volumes. Both arrays represent 14500 well-characterized human genes.

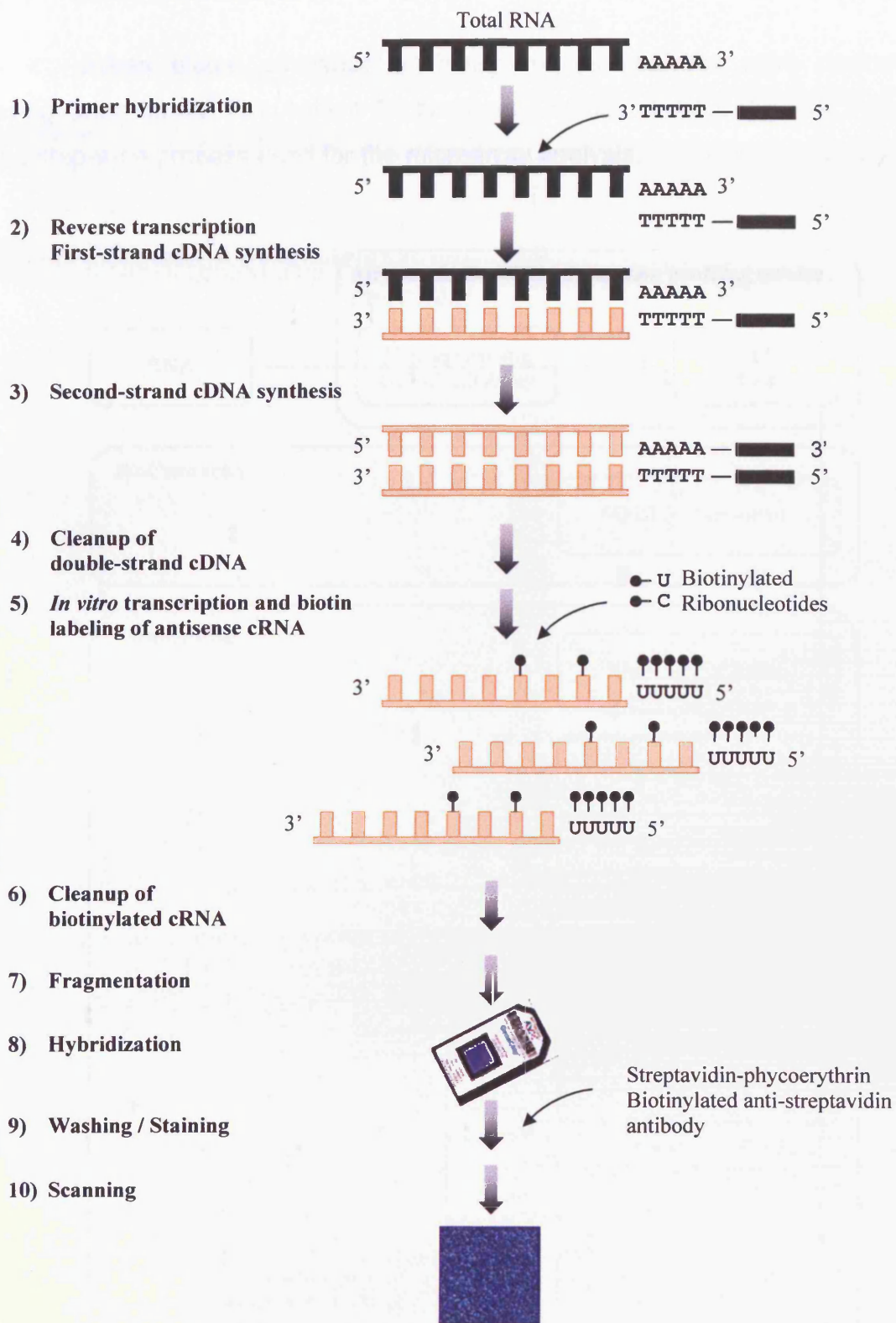
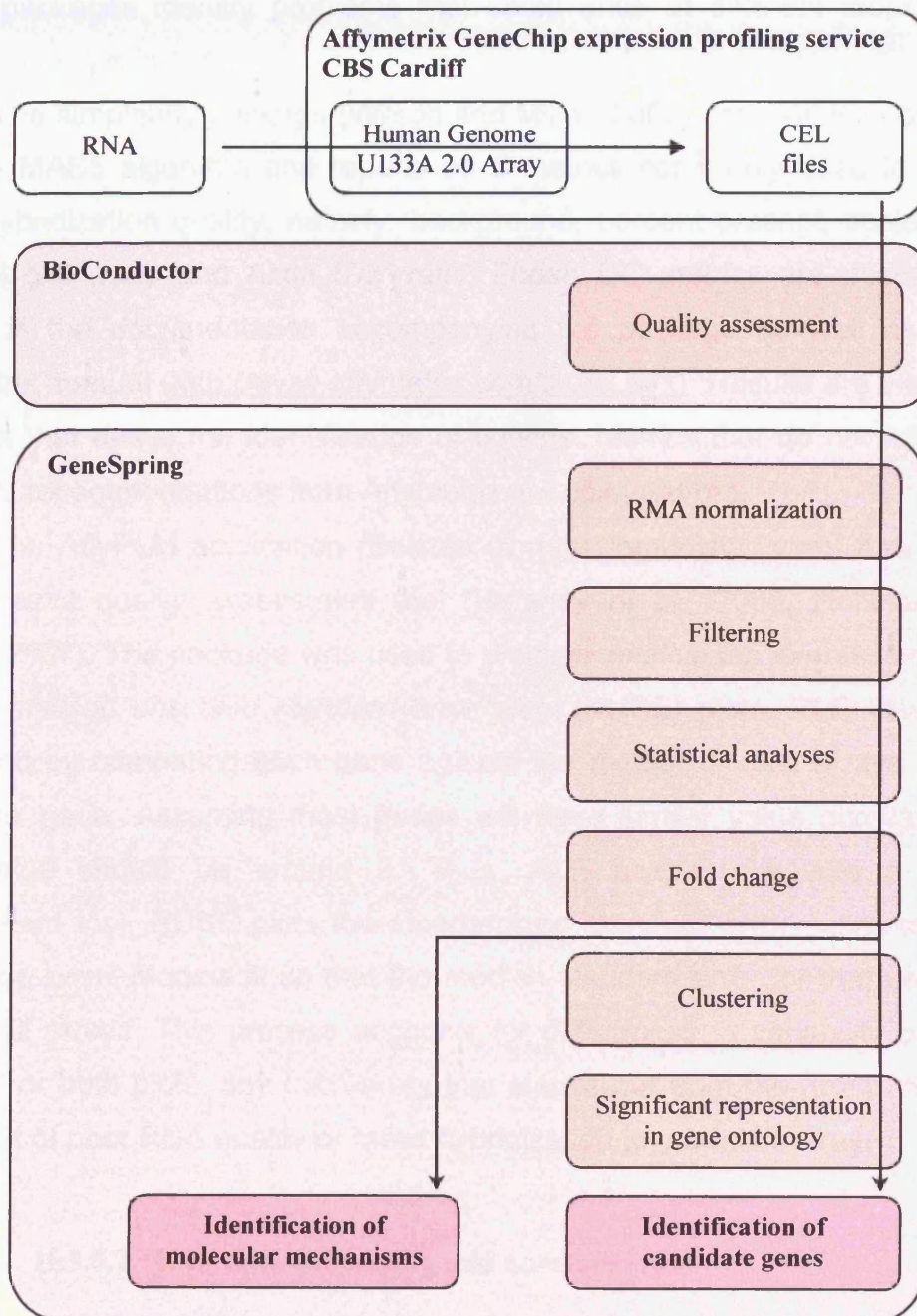


Figure II.1: DNA microarray processing. Diagram representing the steps involved in microarray RNA processing (from Affymetrix Expression Analysis Technical Manual).



### II.3.5. Data analysis

Unless stated otherwise all bioinformatics analyses were performed using GeneSpring<sup>®</sup> 7.3 (Agilent Technologies, Stockport, UK). Figure II.2 shows the step-wise process used for the microarray analysis.



**Figure II.2:** DNA microarray analysis process. Flow diagram representing the steps involved in microarray analysis of the 2008 arrays.

### II.3.5.1. Arrays quality assessment

Quality assessment for the arrays hybridization were performed using the open source software framework BioConductor (Gentleman *et al.*, 2004) run in R (<http://cran.r-project.org/>). Two packages from the BioConductor project were used to control the quality of the raw data (CEL files): AffyPLM and simpleaffy. Those packages identify problems that could arise at different steps of the microarray experiment.

The simpleaffy package (Wilson and Miller, 2005) uses values computed for/from MAS5 algorithm and reports on 5 metrics commonly used to assess array hybridization quality, namely: background, percent present, scale factor, GAPDH 5'/3' ratio and Actin 5'/3' ratio. Those QC metrics are described in details in the documentation accompanying the package as well as in the Affymetrix manual (<http://www.affymetrix.com/index.affx>). Results are visualised in a plot that eases the identification of outliers. Metrics that do not follow the standard recommendations from Affymetrix are coloured red.

The AffyPLM application (Bolstad, B; <http://bmbolstad.com>) has proven to be useful quality assessment tool (Hershey *et al.*, 2008; Robinson and Speed, 2007). The package was used to produce *relative log expression* (RLE) and *normalised unscaled standard error plots* (NUSE) plots. RLE values are computed by comparing each gene against the median across arrays for that particular gene. Assuming most genes will have similar value across arrays RLE value should be around 0. Thus, RLE boxplots provide a quality assessment tool. NUSE plots the standardized standard error estimates from the Probe Level Models fit so that the median standard error for that gene is 1 across all arrays. This process accounts for differences in variability between genes. For both plots, any microarray that stands out from the group could be the result of poor RNA quality or failed hybridization to the microarray.

### II.3.5.2. Raw data processing and normalization

Microarray raw data needs processing in order to calculate gene expression and normalization, to remove chip-to-chip variations, in order to optimize the signal-to-noise ratio. The identification of up- or down-regulated

genes depend on the normalization method used (Millenaar *et al.*, 2006), underlying the need to choose the right normalization method depending on the biology.

*Processing and per-chip normalisation* — The robust multiarray average (RMA) preprocessing and normalisation method (Irizarry *et al.*, 2003) was chosen because it yields the most reproducible results and performs well with low confounding noise projects (Seo *et al.*, 2004), such as the microarray analysis of established cell lines. RMA normalisation was performed in GeneSpring 7.3 (Agilent Technologies, Stockport, UK). RMA corrects arrays for background using a quantile normalization, based on the complete data set, with a fitted model to detect abnormally behaving probes and exclude them for calculating gene expression, such that the intensities across each chip are adjusted to produce identical distributions (Irizarry *et al.*, 2003). RMA normalization is a per-Chip normalization applied on a single sample,

*Per-gene normalisation* — “The normalised to median” per-gene normalization was performed in GeneSpring 7.3 (Agilent Technologies, Stockport, UK) as advised by Agilent (<http://www.chem.agilent.com/>). Each gene was normalised to the median measurement for that gene across all the arrays in the data set. Per gene normalization centres normalised expression values around 1 (“normal” expression around 1, downregulation from 0 to 0.9 and upregulation from 1.1).

### II.3.5.3. Quantification of differential expression

*Detection call* — Normalised data were first filtered based on Affymetrix detection call information (<http://www.Affymetrix.com>) determined with the MAS 5 algorithm (microarray suite version 5 software, Affymetrix). MAS5 assigns a p-value based on detection level, this p-value is subsequently used to generate a ‘detection call’ indicating whether a transcript is reliably expressed. This detection call flags transcripts as Absent, Marginal or Present (Pepper *et al.*, 2007). Data were filtered so that genes not flagged Present in at least 1 in 9 arrays were excluded from further analysis.

*T-Test* — Pair-wise comparison of conditions was performed in GeneSpring 7.3 (Agilent Technologies, Stockport, UK) using T-test statistical

analysis, followed by the Benjamini and Hochberg correction for multiple testing (Benjamini and Hochberg, 1995) with a p-value cut-off of 0.05.

*Analysis of variance (ANOVA)* — Analysis of Variance followed by the Benjamini and Hochberg correction for multiple testing (Benjamini and Hochberg, 1995) with a p-value cut-off of 0.05, was performed in GeneSpring 7.3 (Agilent Technologies, Stockport, UK).

*Significance analysis of microarrays (SAM)* — SAM (Tusher *et al.*, 2001) was performed using the Microsoft Excel addin v3.0. The analysis was performed using a SAM-FDR (false discovery rate) cut-off of 0.

*Filter on fold change* — Finally, only genes with their expression altered by more than two fold were selected for further analysis.

#### **II.3.5.4. Functional analysis and representation**

Functional analyses were performed in GeneSpring 7.3 (Agilent Technologies, Stockport, UK) using resources from IHOP (information protein hyperlinked / <http://www.ihop-net.org/UniPub/iHOP> / Hoffmann and Valencia, 2004), KEGG pathways (Kyoto encyclopedia of genes and genomes / <http://www.genome.ad.jp/kegg/pathway.html> / Kanehisa *et al.*, 2004) and gene ontology (GO / <http://www.geneontology.org> / Ashburner *et al.*, 2000). When possible, gene nomenclature were chosen according to the human genome organization (HUGO / <http://www.hugo-international.org> / Eyre *et al.*, 2006).

*Ontologies used* — Gene ontologies (<http://www.geneontology.org/>) are vocabularies that describe the attributes of genes (for example, their biological functions). Each term in the vocabularies is called a GO term which represents a possible attribute value possessed by one or more genes. Gene ontologies are relational in the sense that GO terms are related and form a directed acyclic graph. The Gene Ontology Consortium (Ashburner *et al.*, 2000) is creating three standard gene ontologies that describe the associated biological processes, cellular components and molecular functions for genes and their products (RNA or protein products encoded by genes). GO annotations are made to associate each gene or gene product with its related GO terms. Those GO terms reflect the normal function, process, and localization (component) of the gene or gene product. KEGG pathways (<http://www.genome.ad.jp/kegg/pathway.html>) are a

collection of manually drawn pathway maps representing knowledge on the molecular interaction and reaction networks for biological processes (Kanehisa *et al.*, 2004).

*Gene ontology enrichment analysis* — Gene ontology enrichment analysis was performed in GeneSpring 7.3 using the Gene Ontology Browser feature (Agilent Technologies, Stockport, UK). A p-value, using a hypergeometric test without multiple testing correction, is assigned based on whether the number of selected genes within each category is greater than expected by random sampling given the subset of the total number of genes within that GO annotation.

*Clustering* — Hierarchical clusterings were performed in GeneSpring 7.3 (Agilent Technologies, Stockport, UK). Similarity measures were calculated using Pearson correlation and average linkage as the clustering algorithm. The resulting gene trees group together the genes with similar expression pattern (see for review D'Haeseleer, 2005).

*Results representation* — Microarray results were represented using GeneSpring 7.3 (Agilent Technologies, Stockport, UK) as gene trees or bar graph. Bar graphs represent partially normalised data without per-gene normalisation. Indeed, although ratios, given by per-gene normalisation, help to reveal pattern of expression they remove information about gene expression level. In bar graph representation probes are sorted according to the control value for each probe (median value across all chips). All microarray representations show the average value of the three triplicates.

All microarray data (except bar graph) are coloured according to the expression value of the first condition (NCI-H69 SP), yellow indicates overexpression, black average expression and blue underexpression.

## **II.4. Flow cytometry**

### **II.4.1. Cytometers**

Analyses were carried out on one of two different cytometers:

1) **FACScan system** (Becton-Dickinson Immunocytometry Systems, San Jose, CA, USA) incorporating an argon ion laser (15 mW output) used to the 488-nm line.

2) **FACS Vantage** flow cytometer (Becton-Dickinson Immunocytometry Systems, San Jose, CA, USA) equipped with a Coherent Enterprise II laser (Coherent, Inc., Santa Clara, CA, USA) simultaneously emitting at multiline UV (351–355 nm range) and 488-nm wavelengths with the beams made noncolinear using dichroic separators. The laser power was regulated at 30 mW (monitored on the multiline UV output).

All parameters were collected using CellQuest software (Beckton-Dickinson Immunocytometry Systems, San Jose, CA, USA). Forward and 90° light scatter were analyzed to exclude any cell debris. Unless stated otherwise data were collected for  $1 \times 10^4$  cells using the FSC parameter as the master signal. Optics used for both systems are listed in Table II.5.

Data analyses were performed using CellQuest software (Beckton-Dickinson Immunocytometry Systems, San Jose, CA, USA) or FlowJo (Tree Star, San Carlos, CA, USA).

**Table II.5:** *Flow cytometry fluorescence optics.*

Probe / drug	FACScan		FACS Vantage	
	excitation (nm)	Parameter & emission filter (nm)	excitation (nm)	Parameter & emission filter (nm)
alexa 448	488	FL1 530 / 30	488	FL1 530 / 30
DRAQ5	488	FL3 650 LP	488	FL3 695 LP
PI	—	—	488	FL2 585 / 42
TPT	—	—	488	FL1 530 / 30
Hoechst 33342	—	—	UV	FL4 530 / 30
	—	—	UV	FL5 424 / 44
	—	—	UV	FL4 620 LP

#### II.4.2. Cell cycle analysis

DNA measurements were made using the preparation described previously (Njoh *et al.*, 2006; Smith *et al.*, 2000). Cells were removed from the

substrate spun down (100 x g), washed once with PBS and fixed with 100% methanol for 20 min at -20°C. After centrifugation (200 x g / 10 min), cells were resuspended in 200 µL of PBS and 20 µM DRAQ5 was added and held at room temperature 5 min before acquisition.

#### **II.4.3. Immunofluorescence analysis**

The general flow cytometric method has been previously described (Smith *et al.*, 2007). Attached cells and suspension cells were harvested spun down at 100 x g for 10 min, washed once with PBS and fixed with 100% methanol at -20°C for 20 min. After one wash with PBS and spin (200 x g / 5 min), cells were incubated overnight with 10% goat serum in PBS. Following centrifugation (200 x g / 5 min), the cell pellet was resuspended with the suitable primary antibody in 200 µL of 1% goat serum in PBS and incubated at room temperature for 1 h. Cell suspensions were washed with PBS, spun down (200 x g / 5 min) and the pellet was resuspended with the suitable secondary antibody in 200µL of 1% goat serum in PBS and incubated for 45 min at room temperature. Finally, cells were washed with PBS and resuspended with 200 µL of PBS

#### **II.4.4. Cellular integrity assays**

Cells were harvested and resuspended in full RPMI medium to a concentration of  $2 \times 10^5$  cells / mL. Viability was assessed by adding propidium iodide (PI), as a non-permanent dye for cells with intact membranes, to a final concentration of 3 µM to the cells and incubating for 10 min at 37°C prior to acquisition on the FACS Vantage.

### **II.5. Imaging**

#### **II.5.1. Microscopes**

All camera, shutter and stage were initially controlled by AQM 2000 software (Kinetic Imaging Ltd, Wirral, UK) before all systems were moved to

MetaMorph version 7.5 (Molecular Devices, Downingtown, PA, USA). All image analyses were conducted using MetaMorph Offline starting at version 6.3 to version 7.5 (Molecular Devices, Downingtown, PA, USA). Several microscopy systems have been used:

1) Fluorescence microscope CBS camera system (CBS Cardiff) consisting of an inverted Axiovert S100 TV microscope (Carl Zeiss, Inc., Welwyn Garden City, UK) with Hamamatsu camera (model C4742-95-12, Hamamatsu Photonics, Welwyn Garden City, UK), fluorescent lamp (model ebx75 isolated, Carl Zeiss, Inc., Welwyn Garden City, UK) and shutter lambda 10-2 (Kinetic Imaging Ltd, Wirral, UK).

2) Timelapse microscope system (CBS Cardiff) composed of a HAL100 microscope (Zeiss, Welwyn Garden City, UK) fitted with temperature (37°C) regulating incubator system and CO<sub>2</sub> (5%) supply (Solent Scientific, Segensworth, UK). Illumination was controlled by a shutter (Prior Scientific, Cambridge, UK) placed in front of the transmission lamp and a motorized xyz stage (Prior Scientific, Cambridge, UK) permitted multi-field acquisition. Phase transmission images (x10 objective lens) were acquired with a cooled CCD camera (model 4920 COHU, San Diego, CA, USA).

### **II.5.2. Transmission imaging**

Bright field images from live cells in full culture media were captured on the CBS camera system.

### **II.5.3. Immunofluorescence labelling**

Cells were harvested and cell suspensions (100 µL of approximately 1x10<sup>5</sup> cells per mL) were cytopspun (Cytospin 2, Shandon Scientific, Runcorn, UK) onto microscope slides for 5 min at 30 x g. Cells were washed once in PBS, before fixation with 100% cold methanol for 20 min at RT. Cells were washed once with PBS, then blocked by 200 µl of 1% bovine serum albumin (BSA) in PBS for 30 minutes, at RT. Blocking solution was then replaced with 200 µL of the suitable primary antibody in 1% BSA / PBS and incubated 2h at RT. After 3 washes with PBS, 200 µL of the suitable secondary antibody and



Hoechst in 1% BSA / PBS was added to the slides followed by incubation at RT for 2h. Finally after 3 washes with PBS, slides were mounted with coverslips using Hydromount (National Diagnostics, Atlanta, GA, USA) mounting media.

#### II.5.4. Fluorescence imaging

Images from fluorescently-stained slides were captured on the CBS camera system using the suitable filters block (see Table II.6).

Table II.6: CBS camera fluorescence filters.

	excitation (nm)	DCLP (nm)	emission (nm)
alexa 488	480 / 30	505	535 / 40
alexa 568	560 / 40	595	630 / 60
Hoechst 33342	340	455	480 / 40

#### II.5.5. Timelapse imaging

For live cell imaging of different cell types or treatments over short or long period of time, time-lapse imaging was used. A standard multi-well culture dish containing the cells was incubated on a stage of a time-lapse instrument as previously described (Errington *et al.*, 2005; Marquez *et al.*, 2003). Conditions (drug treatment, cell type, field numbers, time delay...) are described in each chapter specific material and methods.

### II.6. SDS-PAGE/Immunoblotting

Adherent cells were detached using CDS for 2 min. Suspension cells were centrifuged and treated with CDS for 2 min. Cells were then washed twice with cold PBS and incubated with 100  $\mu$ L of lysis buffer per  $10^6$  cells (see Appendix II) for 30 min on ice. After centrifugation at 15000 x g and 4°C for 15 min, samples were quantified using Bio-Rad DC Protein Assay (Bio-Rad, Hemel Hempstead, UK) according to the manufacturer instructions with BSA as standard. Briefly, dilution of cell extracts were incubated 15 min with Bio-Rad

DC Protein Assay solution (Bio-Rad, Hemel Hempstead, UK) and absorbance at 750 nm was measured with a plate reader POLARStar OPTIMA (BMG Labtech, Offenburg, Germany) using a 750-12 nm emission filter.

Sample aliquots containing the same amount of protein were heated (15 min at 70°C) in 0.5 volume of sample loading buffer and separated by 7.5 or 12% SDS-PAGE (Bio-Rad, Hemel Hempstead, UK). Samples were run alongside molecular weight marker (Rainbow marker RPN800 / GE Healthcare, Little Chalfont, UK). Proteins were transferred onto Hybond-P PVDF membrane (GE Healthcare, Little Chalfont, UK) for 15 min or 1 h at 15 Volts using a Semi-dry blotter (GE Healthcare, Little Chalfont, UK). After blocking with blocking solution (see Appendix II) for 1 h at RT, membranes were incubated with anti-PSA-NCAM or anti-MT (0.5 µg / mL or 0.46 µg / mL, respectively, in blocking solution) for 2 h at RT. Membranes were then washed 3 times with wash solution and incubated for 1 hour at room temperature with secondary antibodies-HRP conjugated: rabbit anti-mouse (0.1 µg / mL) or Goat anti-rat (0.33 µg / mL). After 3 washes proteins were detected using enhanced chemiluminescent (ECL) Advance Detection Kit (GE Healthcare, Little Chalfont, UK). Images were captured with AutoChemi System (UVP, Upland, CA, USA).

## **II.7. Statistical analyses.**

All additional statistical analyses were carried out using GraphPad Prism software version 3.00 for windows (GraphPad Software, San Diego, CA, USA).

### III. Characterisation of an *in vitro* SCLC model system

#### III.1. Introduction

The events leading to drug resistance acquisition and metastasis in SCLC remain unclear. Several *in vitro* SCLC cell lines have been derived from patients over the past two decades in order to elucidate the sequence and nature of the steps involved. These *in vitro* models of SCLC display a range of phenotypic characteristics while frequently retaining the NE properties of the tumours. An early study by Carney *et al.* (1985) described 4 major categories of morphology for SCLC *in vitro* culture: type 1- tight floating aggregates with frequent central necrosis, type 2- irregular, dense aggregates without central necrosis, type 3- very loose aggregates and type 4- attached growth with non-SCLC appearance. Most SCLC cell lines grow *in vitro* as floating aggregates type 1 and 2 (Carney *et al.*, 1985). Alongside this classification regarding their cell-cell interactions and adhesion properties *in vitro*, SCLC cell lines can also be divided into 2 classes: 'classic' and 'variant' (Carney *et al.*, 1985). SCLC variants (v-SCLC), with resemblance to NSCLC and a loss of the NE phenotype, can be more aggressive (Shtivelman and Namikawa, 1995). SCLC cultures can differentiate spontaneously to variant forms with enhanced metastasis (v-SCLC) generating sublines with diminished sensitivity to etoposide, cyclophosphamide and gamma radiation (Kraus *et al.*, 2002) attributed to a reversible Akt suppression of cell death.

A central difficulty has been the *in vitro* growth patterns of SCLC cell lines – involving slow growth rates, propensity for cell aggregation in suspension and variable expression of adherent growth. Thus assays for growth inhibition often lack dynamic range or readouts that can be readily compared with those of other tumour cell lines. Such difficulties have resulted in the exclusion or withdrawal of SCLC cell lines from wider screens for chemosensitivity such as those carried out by the Developmental Therapeutics Program of the US NCI. However this complexity associated with the SCLC phenotype is likely to be intrinsic to the inherent plasticity expressed by SCLC biology. Despite the difficulties, several *in vitro* SCLC plasticity models based on variant selection or enrichment have been developed: drug resistant variant

(Mirski *et al.*, 1987), chemical induction of differentiation (Gilchrist *et al.*, 2002; Khan *et al.*, 1993), v-ras / c-myc induction of NSCLC phenotype (Falco *et al.*, 1990; Risse-Hackl *et al.*, 1998), changes of morphology upon alteration of culture conditions (Terasaki *et al.*, 1986), selection on the basis of biochemical markers (PSA expression) (Scheidegger *et al.*, 1994) or standard tissue culture plastic substrate (Doyle *et al.*, 1990; Salge *et al.*, 2001; Seddon *et al.*, 1998).

A frequently used SCLC cell line is the NCI-H69 cell line — an established, clonable cell line with a classic phenotype and the potential to form proliferating tumours as xenografts. Under standard suspension culture conditions, the NCI-H69 cell line grows as floating aggregates (type 2 morphology). Previous studies have demonstrated the ability to derive plastic-adherent variants from the NCI-H69 cell line possibly associated with a putative stem cell-like sub-population generating small cell and non-small cell-like populations. The transition from suspension to adherent growth was accompanied by tissue factor and metalloproteinase expression, biochemical characteristics more compatible with aggressive growth and high metastatic potential observed in SCLC patient (Salge *et al.*, 2001). Bromodeoxyuridine (BrdU) induction of differentiation also led to NCI-H69 morphological transformation to an epithelial phenotype (Gilchrist *et al.*, 2002) with a decrease in NCAM expression, integrin expression upregulation and loss of tumourigenicity in mice. The capacity for 'transformation' suggests that NCI-H69 might provide a suitable system for the stated objectives of the current study. It was therefore decided that there was a need to assess the suitability of NCI-H69 against a range of SCLC cell lines. The strategy was to first affirm the suitability of NCI-H69 by undertaking a review of the characteristics of a reference SCLC cell line panel (Baillie-Johnson *et al.*, 1985; Carney *et al.*, 1985; Koros *et al.*, 1985). The aim was to permit a reference classification of the SCLC characteristics with respect to the culture conditions employed.

Direct observation of classical suspension cultures of SCLC cell lines reveals the presence of sub-populations attempting to attach to a standard cell / tissue culture plastic (TCP) substrate, but never becoming dominant under normal culture passaging due to constant dilution of the cultures. This property exemplifies the problem with maintaining SCLC cell lines in culture without

effectively applying a degree of selection for a given phenotype with proliferative advantage. Here, this propensity to attempt substrate attachment was used to develop a phenotypically reversible cell system based on the suspension phenotype of NCI-H69, in which cultures were progressively enriched over a period of >50 passages for sub-populations growing with an attached phenotype (AP) on a standard plastic cell culture substrate. This was achieved by the gentle mechanical removal of suspension or loosely attached cells from the culture at each passage, and the EDTA harvesting of attached cells for further culture.

The overall aim of the thesis was to disassemble the complexity of the cellular phenotypes associated with SCLC and to understand how phenotypic variation might impact on aspects of SCLC biology. Thus this chapter describes: the scoping of the NCI-H69 characteristics with respect to a wider SCLC panel; the selection / enrichment procedure for adhesion variants; the establishment and characterisation of new SCLC sublines and an assessment of the defined *in vitro* system to study SCLC plasticity. The major characterisations carried out are summarised in figure III.1 using both whole population and single cell analysis approaches, the latter to address the important issue of heterogeneity.

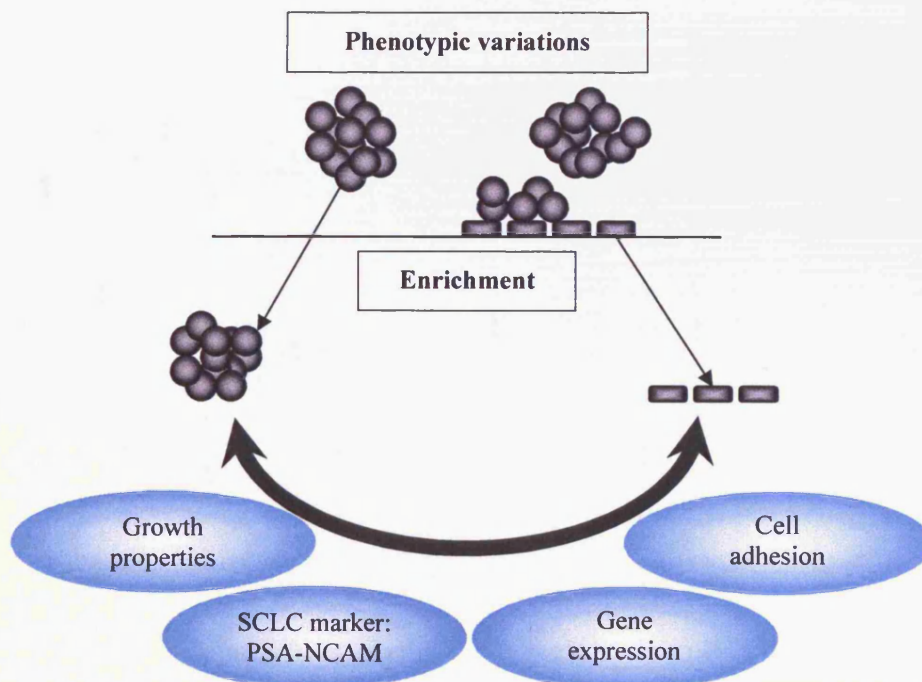


Figure III.1: Summary of the SCLC model system characterization objectives.

In summary, the experimental objectives of this chapter are to first review the overall morphological properties and PSA-NCAM expression profile of a small cell lung cancer panel. Then to develop a SCLC model system to investigate and address phenotypic variation; to isolate adherent variants and thus investigate:

- Growth properties and DNA content of each variant
- Cell-cell and cell-substrate properties of each variant
- Microarray expression profiling for direct comparisons and to determine unique biomarkers.
- PSA-NCAM expression, turnover and impact on variants and patterns during substrate reversal.

## III.2. Specific material and methods

### III.2.1. Cell lines, cell culture and cell proliferation estimation

**Cell lines:** a panel of 6 SCLC cell lines and 1 reference NSCLC was used in this study. All lines were maintained as previously described (see Material and methods). Table III.1 describes the sources of the cell lines. This panel includes 4 cell lines described as classic SCLC cell lines: NCI-H69, COR-L47, COR-L51 and COR-L88 (Baillie-Johnson *et al.*, 1985; Carney *et al.*, 1985). The morphological characteristics of the SCLC cell line COR-L279 were never described. The SHP-77 cell line has the morphology of a variant but the biochemical properties of classical SCLC cell lines (Koros *et al.*, 1985). The NSCLC cell line COR-L23 was used as a control.

Table III.1: SCLC cell lines description.

Cell line	source	patient	previous chemotherapy
NCI-H69 <sup>1</sup>	pleural effusion	male	yes
SHP-77 <sup>2,5</sup>	primary tumour	male	no
COR-L47 <sup>3,4</sup>	lymph node	male	no
COR-L51 <sup>3,4</sup>	pleural effusion	male	yes
COR-L88 <sup>3,4</sup>	pleural effusion	male	yes
COR-L279 <sup>4</sup>	lymph node	male	no
COR-L23 <sup>3</sup> (large cells)	pleural effusion	male	unknown

<sup>1</sup>Gazdar *et al.* (1980), <sup>2</sup>Fisher and Paulson (1978), <sup>3</sup>Baillie-Johnson *et al.* (1985), <sup>4</sup>Twentyman *et al.* (1992), <sup>5</sup>Campling *et al.* (1997).

**Cell culture:** all SCLC and NSCLC cell lines were cultured as previously described (see Materials and methods) in RPMI (Gibco, Invitrogen, Carlsbad, CA, USA). Unless stated otherwise, cells were grown on tissue culture treated substrate.

**In vitro cell proliferation estimation:**  $1 \times 10^5$  cells in 3 mL were set up in triplicate in a standard 6 well-dish and incubated under standard culture

conditions. Cells were counted using Z1 Coulter particle counter (Beckman Coulter, Fulton, California) at 24, 48, 96 and 144 h. Mean values and standard deviations were calculated from triplicate wells.

Growth on hydrophobic or tissue culture substrates: cells were grown on hydrophobic (HOP) bacteriological Petri dishes (Fisher Scientific, Loughborough, UK) or tissue culture (TCP) tissue culture treated Petri dishes (Corning, Fisher Scientific, Loughborough, UK). Cells in TCP were cultured as normal while cells in HOP were refed without disturbing the cell aggregates. To estimate the *in vitro* cell proliferation on hydrophobic substrates:  $5 \times 10^5$  cells in 10 mL were seeded in 9 cm diameter dishes in triplicate. Cells were detached, dissociated and counted at 24h intervals and cell numbers of triplicates were averaged, standard deviations were calculated and results were plotted with GraphPad Prism (GraphPad Software, San Diego, CA, USA).

### **III.2.2. Plastic substrate-adherent sub-population enrichment**

Routine culture enrichment work was primarily carried out through the acknowledged technical support of Ms Marie Wiltshire, providing a consistent methodology and schedule for culture maintenance.

Initial enrichment: to obtain the plastic substrate-adherent populations of COR-L88, COR-L279, SHP-77 and NCI-H69, biweekly, flasks were lightly tapped to remove any loosely adherent cells. Floating cells were, then, removed from the culture flasks and plastic-adherent cells were fed with fresh medium. This process was repeated until sufficient number of plastic adherent cells (detachable from the substrate only by application of an EDTA solution) was obtained.

NCI-H69 model development: the enrichment approach was extended in the case of NCI-H69 SP to establish independent variant cell lines, termed NCI-H69 AP3 and NCI-H69 AP78 (attached phenotype enriched at passage 3 and passage 78). The variant cell lines were subsequently subcultured as two separate cell lines. NCI-H69 AP3 was cultured under constant enrichment



process, while NCI-H69 AP78 was subcultured as an attached cell line under standard culture conditions.

### **III.2.3. Attachment assay**

Cells were detached, dissociated and counted as previously described (see Materials and methods). Cells were set up in triplicate at  $4 \times 10^6$  cells per T25 flasks and cultured under standard cell culture conditions. At 6, 24 and 48 h post seeding, cells in suspension and attached cells (after removal with cell dissociation fluid, Sigma, St Louis, MO, USA) in each flask were counted separately using Z1 Coulter particle counter (Beckman Coulter, Fulton, California). Mean values and standard deviations were calculated from triplicate. Statistical differences were calculated with GraphPad Prism (GraphPad Software, San Diego, CA, USA) using one-way ANOVA followed by Bonferroni's Multiple Comparison Test to compare pairs.

### **III.2.4. Cell size measurement**

Attached cells were detached and left to dissociate in CDS for 2 min in the incubator. Suspension cells were spun down, resuspended in CDS and left to dissociate for 2 min in incubator. After centrifugation, cells were resuspended in full medium and seeded onto glass dishes (Lab-Tek II chambered coverglass, Nalge Nunc International, Rochester, NY, USA). The DNA dye DRAQ5 was added to the medium to a final concentration of 20  $\mu$ M. Bright field and DRAQ5 pictures of 10 random fields on the dishes were taken on the CBS camera (X20 magnification). Analysis was carried out in Metamorph (Molecular Devices, Downingtown, PA, USA) on 101 single cells randomly selected. The diameter of the entire cell (bright field image) and the nucleus of the same cell (DRAQ5 image) were determined by drawing a line across the cell and the nucleus. Statistical analyses were performed in GraphPad Prism (GraphPad Software, San Diego, CA, USA), using a non-parametric test comparing 3 groups (Kruskal-Wallis test) followed by Dunn's multiple comparison test for each pair.

### **III.2.5. DNA content measurement**

Cells were detached, dissociated, spun down, washed in cold PBS and resuspended in 100% methanol. After 20 min incubation at -20°C, cells were spun down, resuspended in PBS supplemented with DRAQ5 to a final concentration of 20 µM. Stained cells were then analyzed by flow cytometry (see Materials and methods) using a FACS scan (Becton-Dickinson Immunocytometry Systems, San Jose, CA, USA) with cell quest software (Becton-Dickinson Immunocytometry Systems, San Jose, CA, USA) and the results were analyzed using FlowJo software (Tree Star, San Carlos, CA, USA) as previously described (Smith *et al.*, 2000).

### **III.2.6. Neuraminidase digestion of PSA**

Endoneuraminidase (endoN) was purchased from AbCys S.A. (Paris, France). This non-toxic bacteriophage enzyme specifically cleaves PSA and is active in culture medium (Rutishauser *et al.*, 1985; Wang *et al.*, 1994). PSA cleavage was performed on live cells by adding the enzyme directly to the culture medium. Cells ( $2 \times 10^6$ ) were seeded in T25 flasks with 5 mL of complete culture medium and allowed to settle down for 24h. Then, 0.7 units of endoN or heat-inactivated endoN (80°C for 15 min) were added to the flasks and cells were incubated overnight (12h-15h). To ensure complete removal of PSA, western blot detection of NCAM and PSA was performed on an aliquot of cells after each digestion.

### **III.2.7. Cell adhesion assay: MSA**

The adhesion potential of the variants with or without PSA removal (see III.2.7) to ECM components was measured using MSA technology (Kuschel *et al.*, 2006) according to manufacturer's instruction. Briefly, MSA slides (figure III.2) were adjusted to room temperature (1 h), mounted in a ProPlate multi-array slide module (Grace BIO-LABS, Bend, Oregon) which provides individual chambers for each array and the wells were rinsed twice with PBS. Single cell suspensions were prepared in serum-free medium as follows, adherent cells

were detached with CDS and suspension cells were centrifuged at 1000rpm for 5 min and resuspended in CDS. All cells were then centrifuged and resuspended in serum-free medium at the desired density. Cells were passed gently three times through a 19 gauge needle to dissociate aggregates and  $5 \times 10^5$  cells were put aside for western blot analyses of PSA expression. Cells ( $3 \times 10^4$  in 200  $\mu$ L) were then added to the wells and incubated at 37°C under standard culture condition. During the incubation time, slides were rigorously agitated by hand for 4 sec every 10 min. After 2h, the slides were dismounted, washed with PBS<sup>++</sup> (PBS supplemented with Ca<sup>2+</sup> 0.1mM and Mg<sup>2+</sup> 1mM), incubated for 10 min with the fixation and staining solution (50% methanol, 10% acetic acid, 40% H<sub>2</sub>O and 0.05% (w/v) Coomassie blue), rinsed in PBS, stained with 5 $\mu$ M Hoechst 33342 in PBS for 10 min. Finally, the slides were left to dry at room temperature and mounted using Hydromount (National Diagnostics, Atlanta, GA, USA). Arrays were imaged using fluorescence and bright field microscopy (CBS camera objective x10 see Materials and methods). Images were analyzed using MetaMorph Offline version 6.3 (Molecular Devices, Downingtown, Pennsylvania).

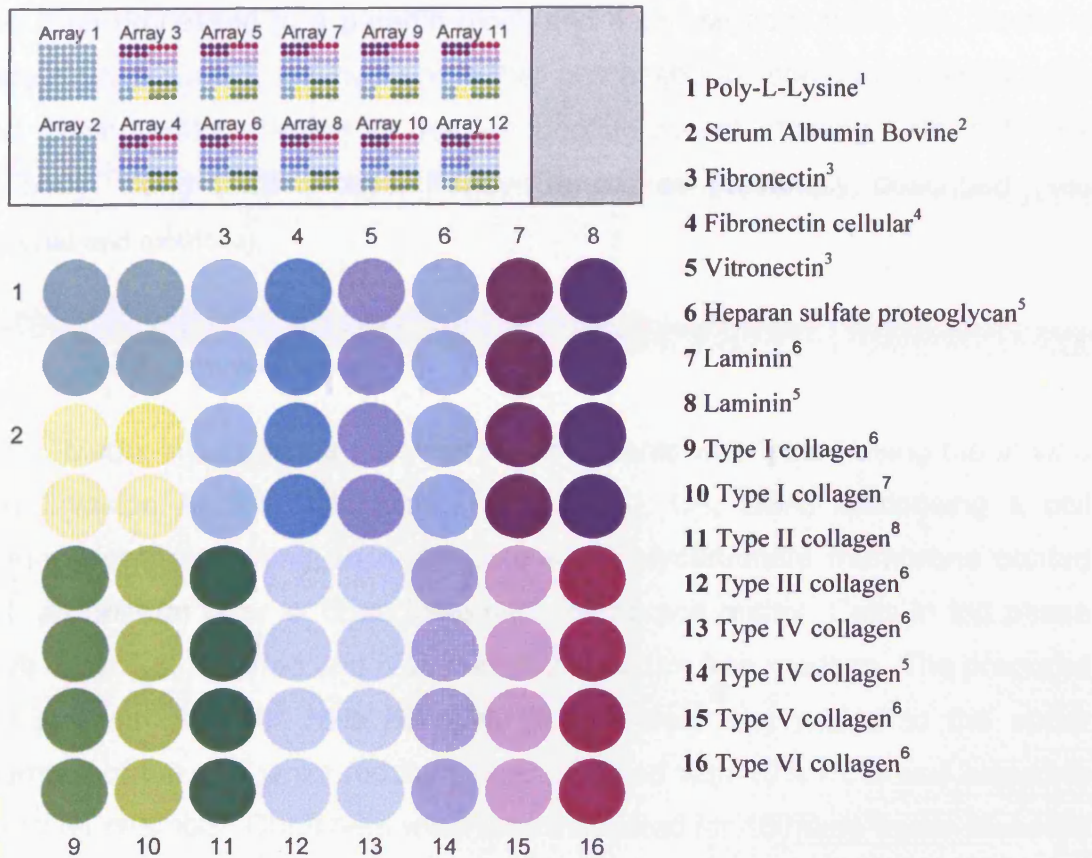


Figure III.2: *MSA slides layout*. Overview of the MSA array (adapted from the MSA protocol) indicating the arrangement of the 14 ECM proteins along with their sources. <sup>1</sup>synthetic, <sup>2</sup>serum, <sup>3</sup>human plasma, <sup>4</sup>human fibroblast, <sup>5</sup>basement membrane of Englebreth-Holm-Swarm murine sarcoma, <sup>6</sup>human placenta, <sup>7</sup>rat tail, <sup>8</sup>chicken cartilage.

### III.2.8. Paraffin cell aggregates section preparation and staining

Paraffin embedding, sectioning, haematoxylin-eosin and dewaxing were performed in collaboration with Dr J.M. Morgan (Clinical scientist, Department of Histopathology, University Hospital of Wales). Cells were grown on hydrophobic surfaces for 7 days, then centrifuged, washed with cold PBS once and fixed overnight in 10% formalin in isotonic PBS at pH 7.0 to 7.2. After fixation at room temperature for 12 - 16 h the cells were allowed to settle out from suspension and the cell pellet was transferred to a 1.5 ml microcentrifuge tube. The pellet was then washed twice in PBS, before adding 50µL of 4% agar at 60°C. When set, the agar containing the cells was then processed for paraffin embedding by sequential dehydration, of 1 hour in each, in ethanol series, 10% to 100%, followed by immersion in xylene, 4 washes of 1 h each. The agar / cell pellet

was then processed to a paraffin block and 4 µm sections were cut. Sections were then dewaxed, washed and either processed for standard haematoxylin and eosin (H&E) staining or for immunofluorescent staining with anti-PSA antibody, clone 2-2B (Abcys, Paris, France) as previously described (see Material and methods).

### **III.2.9. Invasion assay**

Matrix invasiveness potential of the variants was tested using the *in vitro* Cell Invasion Assay (Calbiochem, San Diego, CA, USA) comprising a cell culture insert containing an 8 µm pore size polycarbonate membrane coated with an uniform layer of dried basement membrane matrix. Cells in log phase were detached, washed and resuspended in serum free medium. The prepared cell solution ( $3 \times 10^5$  cells per well in triplicates) was added to the upper chamber of the well while medium supplemented with 10% FCS was added to the lower chamber. Chambers were then incubated for 48 hours under standard culture conditions. Dissociation and labelling of invaded cells are performed in one step using the cell detachment solution containing calcein-AM (dilution 1:300). After transfer in duplicate of the solution containing the cells to a 96-well plate (Greiner Bio-One Ltd, Stonehouse, UK), calcein-AM fluorescence was measured using a Fluostar Optima multi-well plate reader (BMG Labtechnologies, Durham, NC, USA) along with a 485/10 excitation filter and a 520/10 emission filter.

### III.3. Results

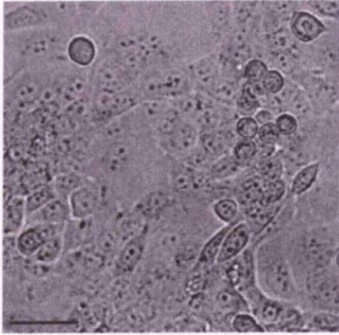
#### III.3.1. SCLC cell lines *in vitro* phenotype and variants selection

The panel of SCLC cell lines used in this study displays a range of phenotype. Figure III.3 shows bright field images of the SCLC cell lines as grown under local laboratory conditions. The large cell lung carcinoma, COR-L23 cells grow as tightly substrate-adherent culture with an epithelioid morphology. The morphologies of the SCLC cell lines (apart from COR-L279) have been previously described in the literature and, with the exception of the COR-L47, no significant changes in morphology were apparent when culturing the cells in our laboratory. The panel of SCLC cell lines offers a selection of almost all types of SCLC *in vitro* morphology. The COR-L51 cell line grows as tightly packed cell aggregates as previously described. Three of the cell lines, COR-L47, SHP-77 and NCI-H69, grow as type 2 morphology (irregular relatively dense aggregates). However, COR-L47 was previously classified as a type 1 morphology (tight floating aggregates with frequent central necrosis), while the SHP-77 cell line has been previously described as a difficult cell line to classify and has been designated as mixed type 2 and 4 SCLC cell line (Fisher and Paulson, 1978; Koros *et al.*, 1985). Moreover, NCI-H69 and SHP-77 display very few cells lightly attached to the substrate and not displaying an epithelial phenotype. The last two cell lines, COR-L88 and COR-L279, displayed loose aggregates with a large proportion of cells attached to the substrate.



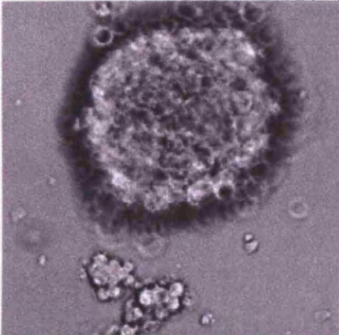
NSCLC

COR-L23



Type 1

COR-L51 [type 1<sup>1</sup>]



**SCLC *in vitro* cell lines morphological classification<sup>2</sup>**

Type 1- tight floating aggregates with frequent central necrosis

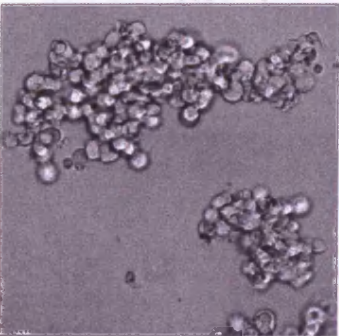
Type 2- irregular, relatively dense aggregates without central necrosis

Type 3- very loose aggregates growing in small clumps

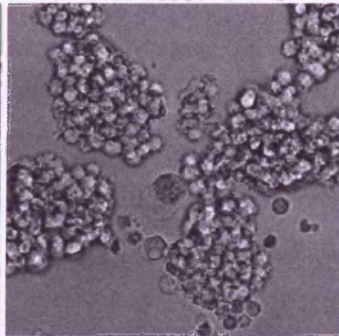
Type 4- substrate-attached growth

Type 2

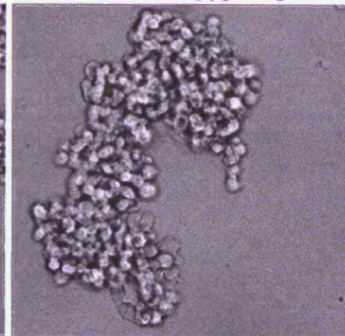
NCI-H69 [type 2<sup>2</sup>]



SHP-77 [type 2-4<sup>3,4</sup>]

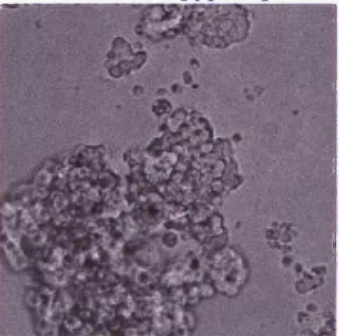


COR-L47 [type 1<sup>1</sup>]



Type 2 + 4

COR-L88 [type 4<sup>1</sup>]



COR-L279

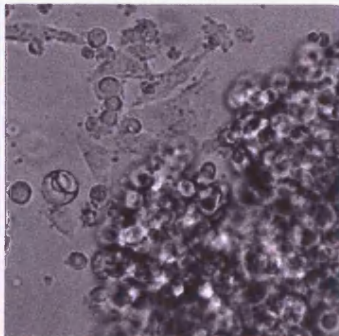


**Figure III.3:** *In vitro* characteristics of the panel of SCLC cell lines. Bright field images of SCLC cell lines classified according to their morphology types (classification of Carney *et al.* (1985). Previously published typing of those cell lines, when available, is indicated in bracket. <sup>1</sup>Bailie-Johnson *et al.* (1985), <sup>2</sup>Carney *et al.* (1985) and <sup>3</sup>Fisher and Paulson (1978) and <sup>4</sup>Koros *et al.* (1985). Calibration bar represents 50  $\mu$ m.

As described above, all SCLC cell lines in the panel, with the exception of COR-L51 and COR-L47, show a sub-population of cells that undergo spontaneous non-specific binding to standard tissue culture substrate. Adherence variants were obtained from minimal selection (1-2 month) for the attached phenotype. Bi-weekly, floating aggregates were removed from the culture dish and the attached cells were fed with fresh medium until a confluent flask of attached cells — that could only be detached with CDS — was obtained. Figure III.4 shows bright field images of the original cell lines and their phenotypic variants. All selected variants presented mixed populations of cells attached to the substrate and cells attached to each other. However, enrichment greatly increased the proportion of cell attached to the substrate.

All variants showed morphological changes toward an epithelial-like phenotype. Indeed variants cell showed a rounded shape and flattened morphology. Cells also appeared tightly aggregated and grew in cluster apparently retaining their cell-cell adhesion capacity. Moreover, monolayer growth was increased upon enrichment. However a few cells in NCI-H69 and COR-L279 adherent variants showed an elongated shape similar to a fibroblast-like morphology (Vaughan and Trinkaus, 1966; Wiggan *et al.*, 2002).



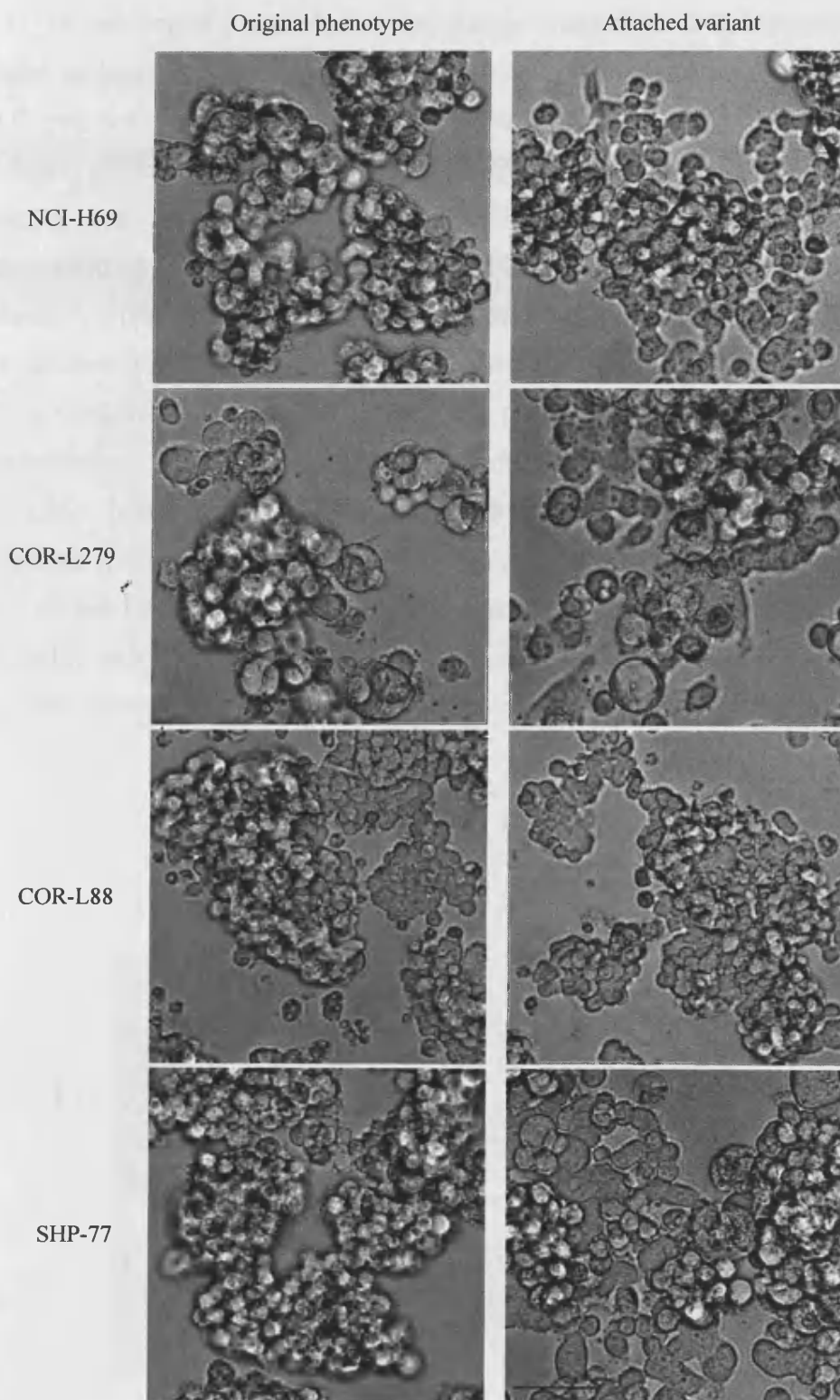


**Figure III.4:** *SCLC cell lines and adherent variants.* Bright field images of the panel cell lines and their respective attached variants after 1 month of continuous culture (or 2 months for NCI-H69 adherent). The calibration bar represents 50  $\mu\text{m}$ .

To determine the profile of the chosen marker for SCLC plasticity — the surface antigen PSA-NCAM — western blotting was performed on the panel of SCLC cell lines and their adherent variants (see figure III.5). All original SCLC cell lines expressed PSA-NCAM, while PSA-NCAM or NCAM could not be detected for the large cells lung carcinoma, COR-L23, providing an immunoblotting biological control. COR-L51 appeared to be the higher expresser, while SHP-77 was the lowest expresser in agreement with previous intra-laboratory PSA detection analyses (see Appendix IV). All original cell lines had a relatively high proportion of non-polysialylated NCAM or low polysialylation, shown by a strong band detected around 140kDa, except for COR-L51. Interestingly both COR-L279 and SHP-77 adherent variants expressed more PSA than their respective original cell line, characterised by most of the NCAM being highly polysialylated. While a decrease in PSA expression was observed in NCI-H69 adherent cell line. Thus PSA expression cannot be directly correlated, across the panel, with the adherent phenotype *per se*.

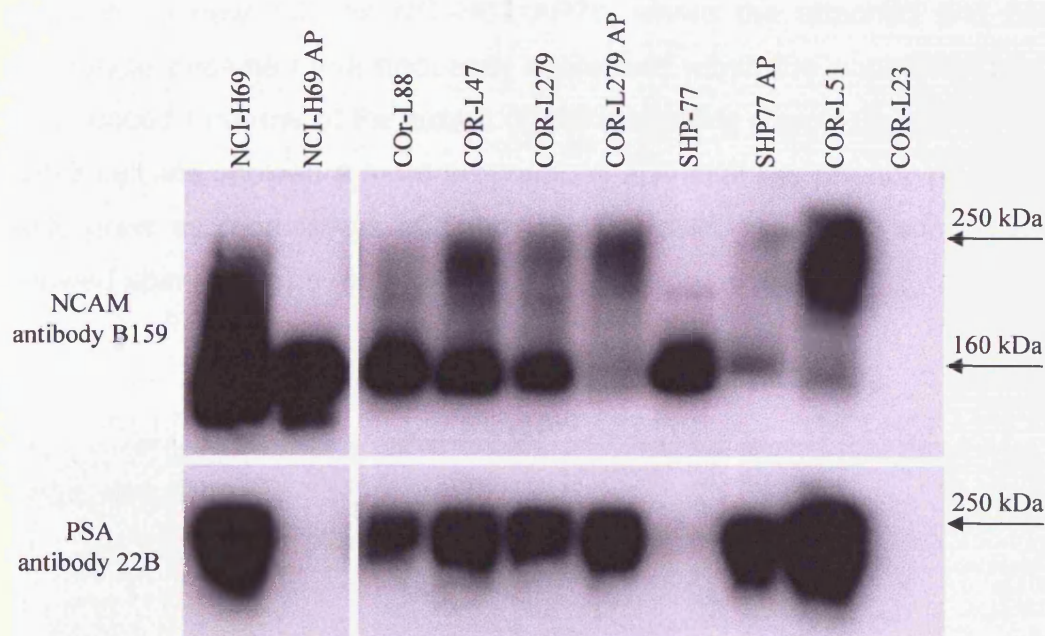


**Figure III.5:** SCLC cell lines and variants NCAM and PSA-NCAM expression. NCAM and PSA-NCAM detection by western blotting, the western blot is representative of two independent experiments.

The interesting linked characteristic of the NCI-H69 adherent cell line retaining NCAM expression, while down-regulating polysialylation, provides an

opportunity to investigate the impact of PSA changes rather than loss of NCAM *per se*. Moreover, the observed phenotypic changes toward an epithelioid phenotype, combined with a relatively homogeneous parental cell line fitted the initial characteristic required for the plasticity model. Thus NCI-H69 and its attached variants were selected for further enrichment and model development.

### III.3.2. NCI-H69 model phenotype characteristic

#### III.3.2.1. Variants enrichment

The NCI-H69 cells — hereafter referred to as NCI-H69 SP (to indicate suspension phenotype) — can be sub-cultured to enrich for the growth of cells with attached phenotype (AP) to the bottom of a standard cell culture substrate. This enrichment eventually produced after 3 passages (6 months of continuous culture) a new cell line, termed NCI-H69 AP3, capable of growth on its own and which could only be detached using an EDTA solution. Further passaging of the cell line for growth with an attached phenotype, over a period of >70 passages, produced a new sub-line NCI-H69 AP78, where the attached and flattened phenotype became more frequently expressed within the population and more pronounced in terms of the extent of cell spreading (figure III.6). The NCI-H69 AP78 cell line showed a more pronounced epithelial-like phenotype, in that the cells grew as monolayers of tightly packed cells. However, some cells also showed spindle-shape morphology.

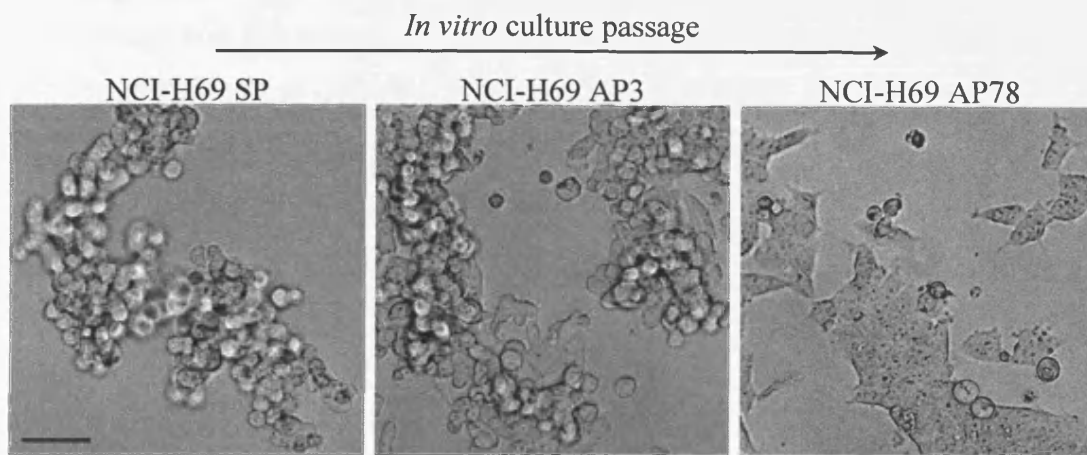


Figure III.6: *In vitro* appearance of the NCI-H69 variants over increasing passage. The calibration bar represents 50  $\mu\text{m}$ .

These 3 cell lines were chosen for further characterisation. They represent the SCLC model variants referred to throughout the thesis. To avoid the complication of phenotypic drift, cells were frozen down at those stages to create a pool of passage 3 and 78 cultures. Cells were kept in culture for no more than 20-30 passages, before going back to cells from stock. Phenotype was confirmed each time after defrosting before proceeding with experiments.

### **III.3.2.2. Attachment properties**

Attachment properties of the variants for standard plastic culture dish — the primary means of enrichment — were examined and quantified (figure III.7). Cells floating or cells attached to the substrate were imaged and counted at 6, 24 and 48h. At 6h after seeding, NCI-H69 AP3 presented a similar phenotype as NCI-H69 SP (figure III.7a), while flattened cells could already be observed for the latest stage of selection, NCI-H69 AP78. From 24h, for both adherent cell lines, the adherent phenotype with an epithelioid morphology became predominant. NCI-H69 SP presented a side population of attached cells (3 to 4%) present as early as 6h and that proportion was stable for the rest of the experiment (figure III.7b). After 6h, 66 % of the NCI-H69 AP3 cells were still in suspension. While, for NCI-H69 AP78, 67 % of the cells were already adherent to the substrate at 6h. Differences in number of cells floating and cells in suspension at 6h for all cell types were statistically tested for significance using one-way ANOVA ( $p$ -value  $< 0.0001$ ) followed by Bonferonni's multiple comparison test (all paired comparison  $p$ -values  $< 0.001$ ). However, at 24h and 48h the proportion of attached cells became equivalent (respectively 76 % and 78 % at 24h and 92 % and 94 % at 48h).



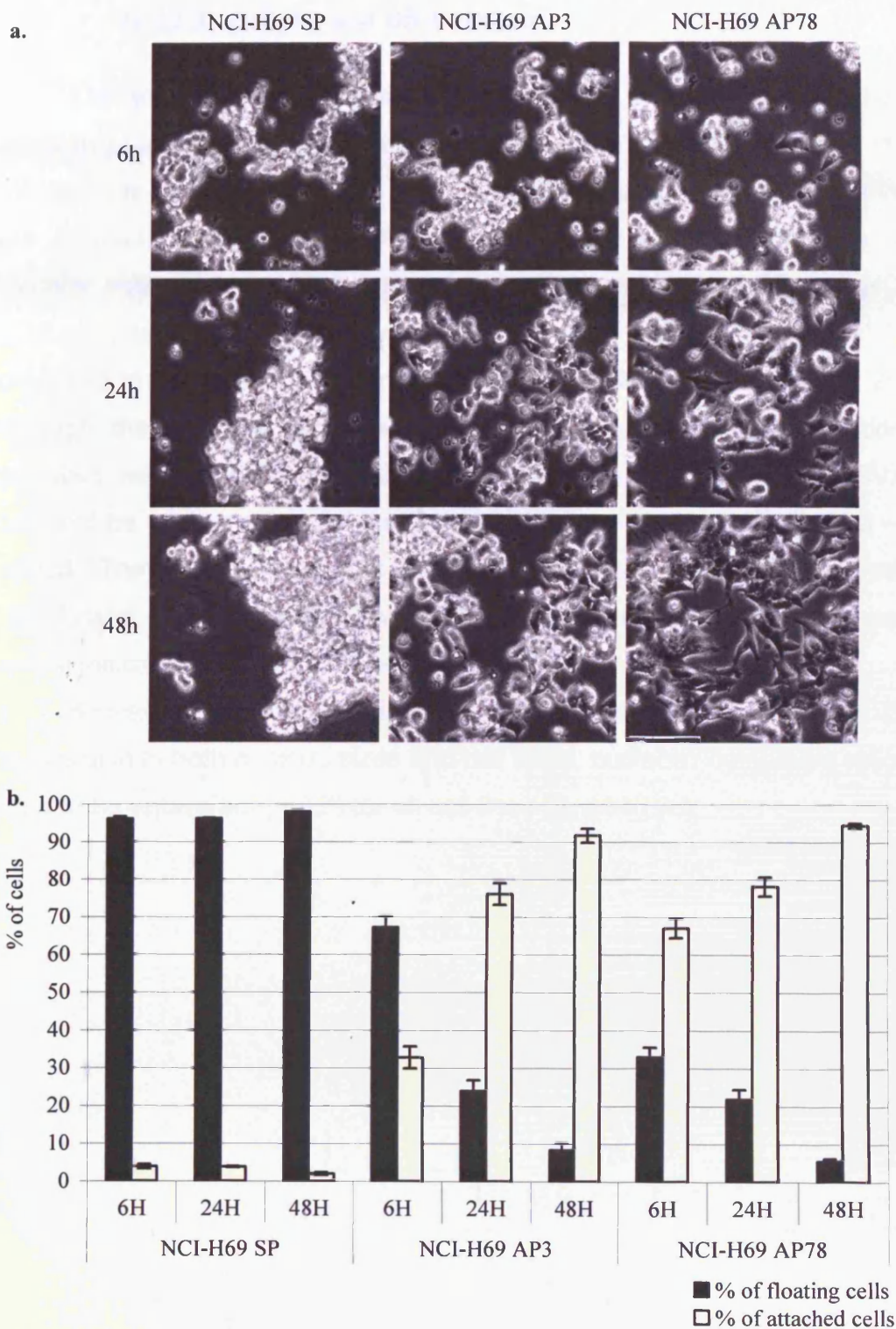


**Figure III.7:** Attachment properties of the different adhesion variants of the NCI-H69 cell line. **a.** The images show the extent of cell spreading for each stage of selection at 6 hours and 24 hours after detachment. Calibration bar represents 50  $\mu\text{m}$ . **b.** Adherence profile at 6, 24 and 48 hours after detachment. Graph depicting the mean  $\pm$  SD of 3 wells of one representative experiment out of 3.

### III.3.2.3. Cell size and DNA content

The evolution of the size of the cells and their nuclei throughout the selection process was evaluated. Individual cells in suspension were imaged; cell diameter was measured on the bright field image, while nuclear diameter was measured using the DRAQ5 fluorescent image. An increase in cell diameter was observed (figure III.8a) in both the NCI-H69 AP3 and NCI-H69 AP78 cell lines (median diameter of 13.55  $\mu\text{m}$  and 15.99  $\mu\text{m}$  respectively) when compared to the parental cell line NCI-H69 SP (mean diameter of 12.28  $\mu\text{m}$ ). Although the data for each cell lines followed a Gaussian distribution, the variances were found to be statistically different, so a one-way-ANOVA test could not be performed and a non-parametric test — Kruskal-Wallis test — was applied. The test showed that the medians varied significantly (p-value < 0.0001) and *post hoc* test showed that the differences between the medians were significant for all pairs (all p-value < 0.001).

Similar finding were obtained for nuclear diameter (figure III.8b). Due to the increase in both nucleus sizes and cell sizes, nucleus / cytoplasm ratio were found to be equivalent (~ 0.7) for all cell lines (figure III.8c).

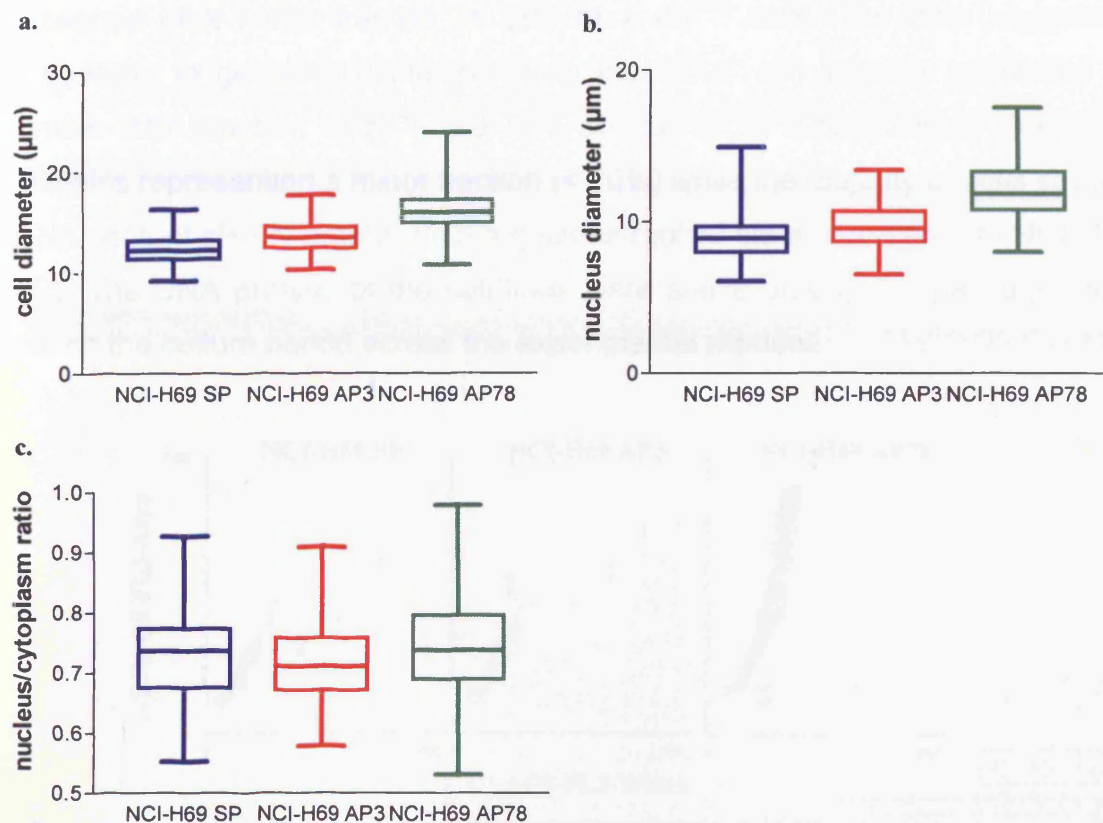


**Figure III.8:** *NCI-H69 variants cell and nuclei diameters.* Cell diameters (a.), nucleus diameters (b.) and nucleus / cytoplasm ratio (c.) are represented using a box-and-whisker diagram depicting medians, minimal and maximal values and 25% and 75% percentile for each data set. Data is representative of two independent experiments.

The results suggest that subtle changes in size have occurred upon NCI-H69 SP to NCI-H69 AP3 enrichment and a significant size increase upon enrichment to NCI-H69 AP78. To investigate this further, DNA content analysis, using flow cytometry and the DNA dye DRAQ5, was undertaken.

The pulse width versus area measurement shown in figure III.9a relates the time-of-flight of the object with the integrated fluorescence signal respectively, providing a means of discriminating doublets. The results permit an interpretation of the ploidy evolution during the enrichment process. The data show that all cell lines demonstrated profiles that suggest active proliferation with S phase fractions of 35 % for NCI-H69 SP, 28 % for NCI-H69 AP3 and 39 % for NCI-H69 AP78. The presence of a minor fraction (< 2%) of  $> 4n^{SP}$  cells could not be accounted for by doublets in the whole SP sample. NCI-H69 AP3 shows a shift to higher DNA content for the whole population and again the



presence of a minor fraction (< 2%) of  $> 4n^{AP3}$  cells. The data suggest a propensity to generate higher ploidy in the SCLC cell lines. A population of similar DNA content to NCI-H69 AP3 appear to be discernible in the AP78 samples representing a minor fraction (< 10%) while the majority of cells show a DNA content clearly greater than a quasi-tetraploid state (compared to NCI-H69 SP). The DNA profiles of the cell lines were stable among the passages and during the culture period across the experimental window.

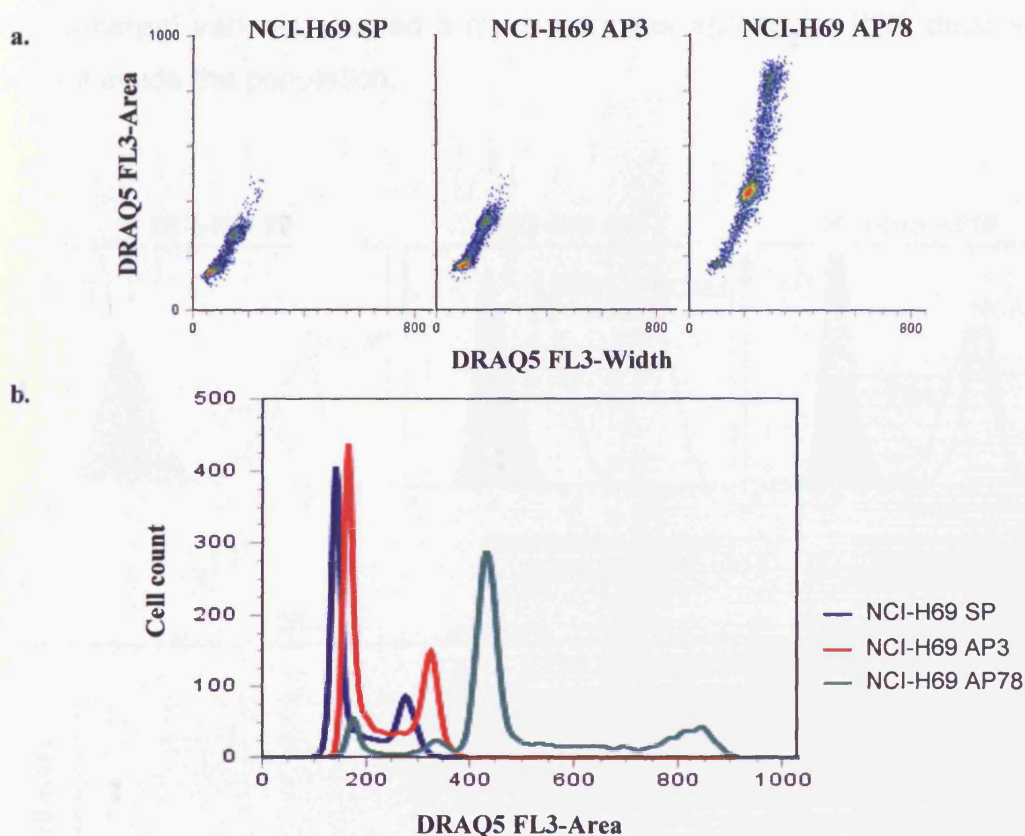


**Figure III.9:** Flow cytometry determination of NCI-H69 variants DNA content. NCI-H69 cell lines stained with DRAQ5 (FL3). **a.** FL3 is plotted (Area vs. Width). **b.** Overlay of DNA histogram to show G1 (peak 1) and G2 (peak 2) fractions. Data is representative of two independent experiments.

#### III.3.2.4. PSA-NCAM

The SCLC marker NCAM and the polysialylated form of NCAM were detected by flow cytometry (figure III.10), immunocytochemistry (figure III.11) and western blotting (figure III.12). Specific antibodies were used to detect PSA-NCAM: the 12F8 antibody recognizes a neuraminidase-sensitive epitope on



NCAM; the 2-2B antibody recognizes PSA chains with more than 10 sialic acid residues (Rougon *et al.*, 1986) and B159 that recognizes NCAM.

Flow cytometry for NCAM revealed that 100% of cells in all variants express NCAM (figure III.10a) and that NCAM expression did not significantly change upon variants enrichment (figure III.10b). NCI-H69 SP showed heterogeneity in the population, going from low decoration of NCAM to high decoration. NCI-H69 AP3 showed low decoration of NCAM. While for NCI-H69 AP78, the signal for NCAM was equivalent to the signal for PSA-NCAM. Both the adherent variants showed a much narrower spread for PSA decoration of NCAM inside the population.

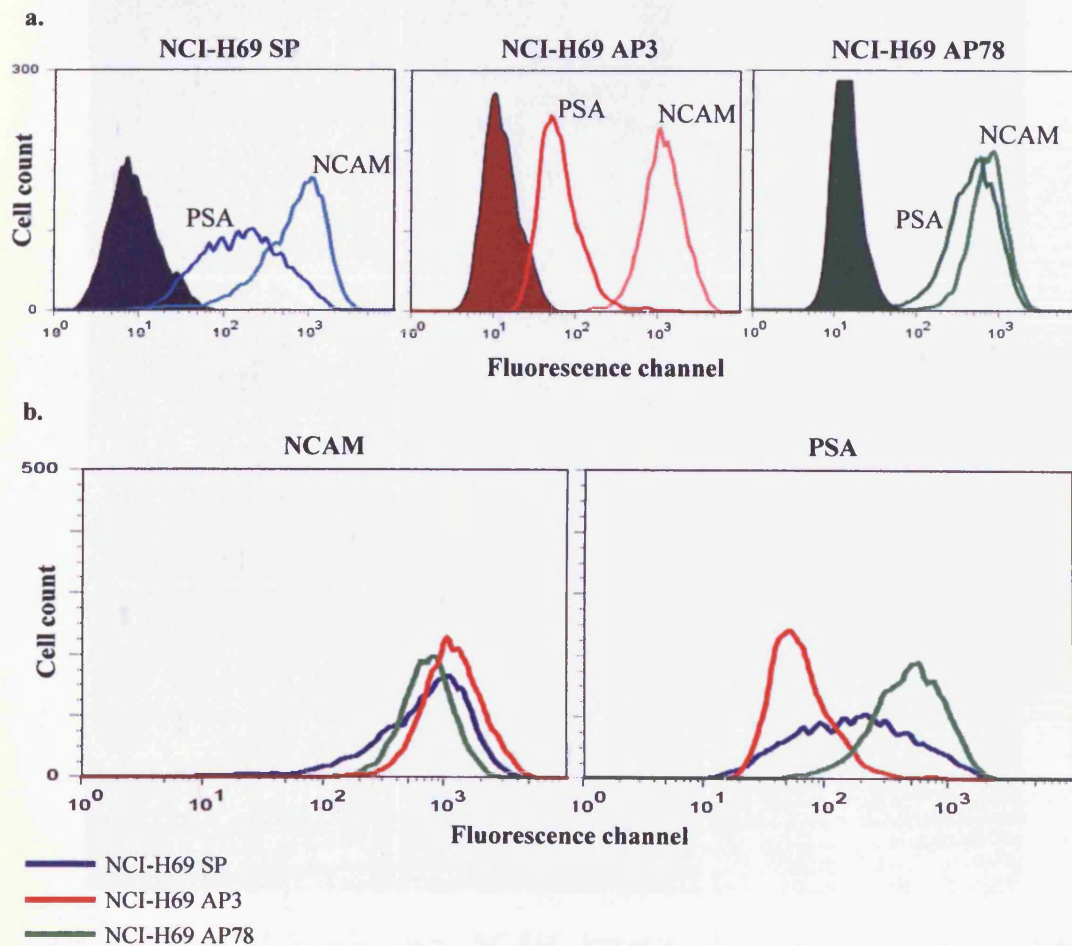


Figure III.10: *PSA and NCAM expression in the NCI-H69 variants.* Expression of NCAM (antibody B159) and PSA-NCAM (antibody 22B) was detected by flow cytometry. **a.** Overlay histogram of NCAM and PSA-NCAM against background fluorescence for all variants. **b.** Overlay histogram of the variants NCAM and PSA-NCAM expression. Results shown are representative of at least two independent experiments.

Dual channel immunofluorescence labeling of NCAM and PSA-NCAM (figure III.11) confirmed the flow cytometry results, that all cells expressed NCAM and further showed that it was a membrane located signal. Immunofluorescence also confirmed the heterogeneity of the staining for PSA-NCAM throughout the NCI-H69 SP population. NCI-H69 AP3 showed many cells with no PSA-NCAM immunoreactivity and very few cells showed a strong signal. While for NCI-H69 AP78 cell line, PSA-NCAM staining was intense and homogeneously distributed.

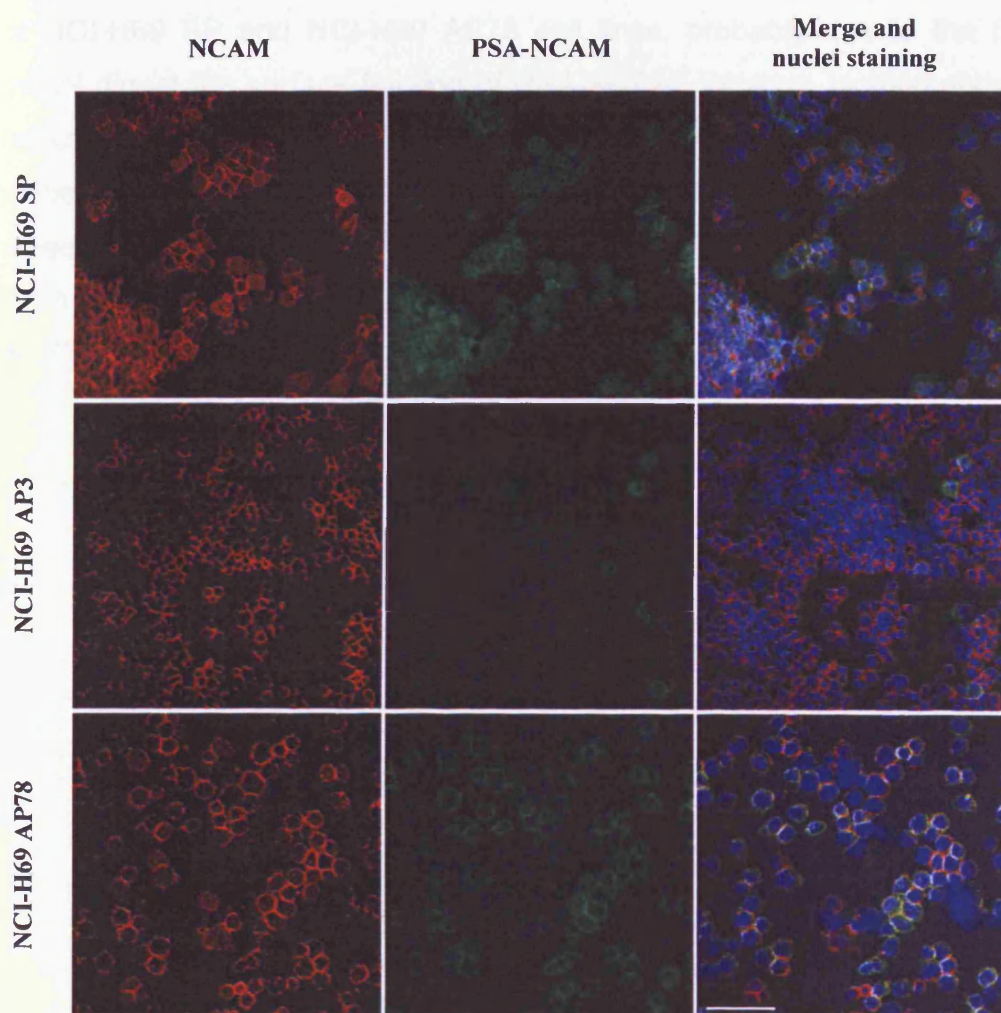
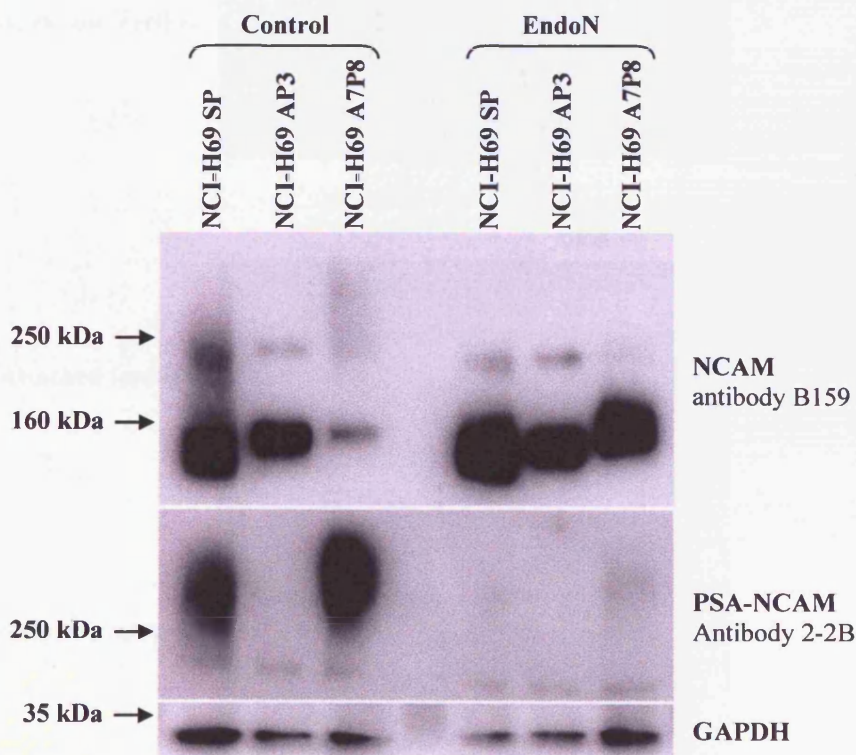


Figure III.11: *PSA-NCAM* and *NCAM* expression in the *NCI-H69* variants. Immunofluorescence detection of *NCAM* (antibody B159) and *PSA-NCAM* (antibody 12F8) on cells prepared as cytopsin. Calibration bar represents 50  $\mu\text{m}$ .



Western blotting experiments showed that for PSA-NCAM and NCAM (figure III.12) all cell lines mainly expressed the 140 kDa isoform with weak expression of the 180kDa isoforms. No expression of the GPI-anchored form was detected, although the ability to detect the 120 kDa form with the B159 antibody was not validated. Moreover, previous studies have shown that the NCI-H69 cell line does not express that form (120 kDa) of NCAM (Moolenaar *et al.*, 1992). Western blotting confirmed that most NCAM is polysialylated in NCI-H69 AP78. Loss of most of the PSA signal after endoN digestion confirmed this specificity of the staining. After endoN digestion a faint signal was still detected for NCI-H69 SP and NCI-H69 AP78 cell lines, probably due to the fact that endoN digest the surface fraction of PSA-NCAM. Western blotting showed low detection of highly polysialylated NCAM in NCI-H69 AP78 with the B159 antibody, maybe due to reduced accessibility of the antigen. Moreover, higher molecular weight PSA-NCAM (slower migration) was detected for NCI-H69 AP78 suggesting longer chain of PSA in the adherent cell line (Seidenfaden *et al.*, 2000).



**Figure III.12:** Immunoblotting detection of NCAM and PSA-NCAM. Cells were treated overnight (15h) with 0.7 U of endoN or heat inactivated endoN (control / 80°C for 15 min) and then processed for western blotting. The blot shown is representative of at least 3 independent experiments.

To test whether PSA-NCAM loss in NCI-H69 AP3 can be designated as an early event or acquired later during the enrichment process. The adherent cells (from several flasks) and the suspension fraction of cells of NCI-H69 SP were isolated, cytospun and stained for PSA and NCAM. Fluorescent signal for NCAM and PSA were found to be similar for both cell populations (figure III.13). No loss of PSA was detected in the adherent fraction, suggesting that the subsequent loss of PSA in the NCI-H69 AP3 variant is not an early event necessary for driving the cell-substrate interactions.

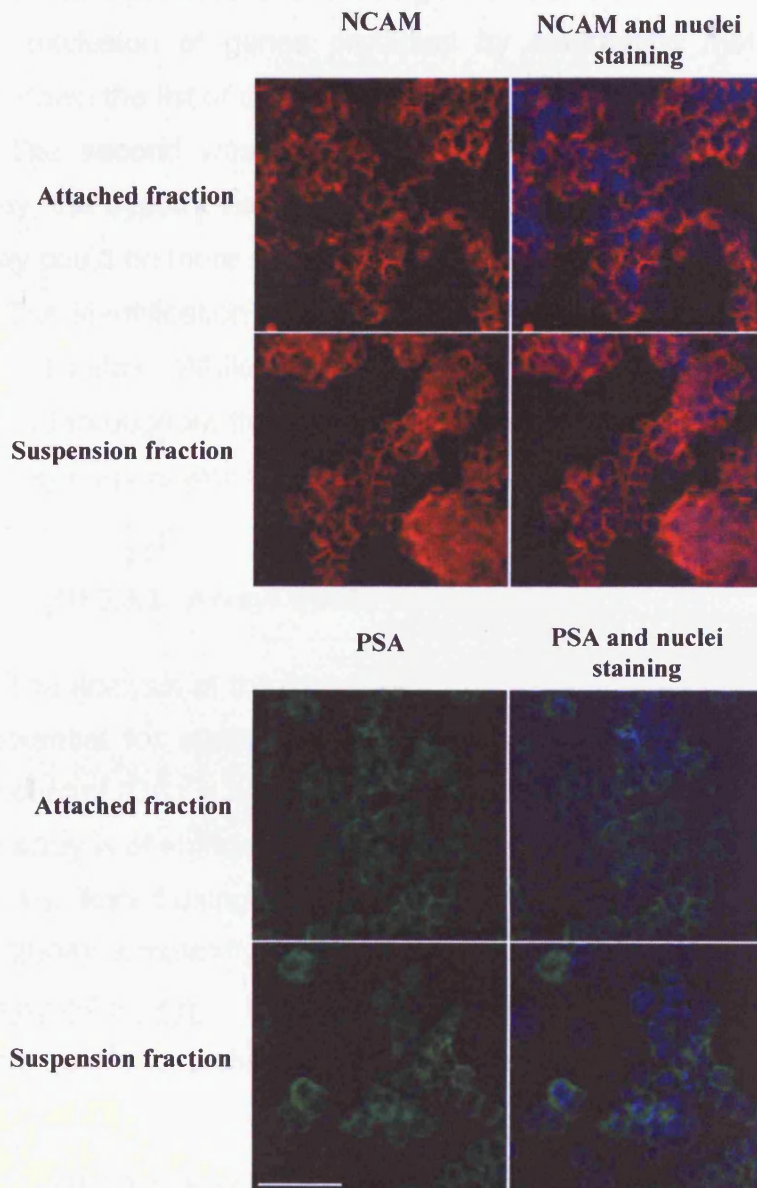


**Figure III.13:** *Fluorescence detection of NCAM and PSA-NCAM in NCI-H69 SP cells.* The attached versus suspension fraction of cells were compared for membrane located signal. All images were taken using conventional wide-field microscopy. Bar represents 50  $\mu\text{m}$ .

### **III.3.3. NCI-H69 model: gene expression changes**

Evaluation of the gene expression across the variants was performed using HG\_U133A\_2.0 arrays and Affymetrix technology, allowing the study of the expression of 14500 well-characterised genes. The 2008 microarray study, comparing the NCI-H69 SP vs. NCI-H69 AP3 vs. NCI-H69 AP78 cell lines, served 2 purposes:

The first was to identify a set of genes with “large” variations between the variants and classification of those genes into relevant ontology and pathways. Mutual exclusion of genes predicted by contrasting methods was used to narrow down the list of candidate genes.

The second was to profile the expression of all genes in a specific pathway, the hypothesis is that small changes of a number of genes in a same pathway could be more relevant than big changes in unrelated pathways.

The identification of candidate genes and further functional analyses are presented below. While the interrogation of specific pathways or ontology is distributed throughout the thesis to retain a biological context and to embed the microarray outputs with further relevant studies.

#### **III.3.3.1. Arrays quality assessment**

The analysis of the expression of a large number of genes gives rise to a high potential for statistical error (exclusion and inclusion), therefore robust quality control (QC) is an essential first step in microarray analysis to determine if each array is of sufficient quality to be included in the study. Chip hybridization quality was tested using 2 packages from the BioConductor project (Gentleman *et al.*, 2004): *simpleaffy* (Wilson and Miller, 2005) and *AffyPLM* (Bolstad, B; <http://bmbolstad.com>). Quality assessment showed that all arrays were of sufficient quality for inclusion in the analysis (Appendix V).

#### **III.3.3.2. Statistical analyses**

Data were first processed and normalised in GeneSpring 7.3.1 using RMA background subtraction and quantile normalisation followed by per gene

normalisation. After filtering for present calls, 7283 probes were removed from further analysis due to lack of expression in all nine arrays. The data for the 14994 remaining probes was then analyzed separately using 3 different statistical methods: Welch T-test, SAM and ANOVA. Results are shown in figure III.14a.

Welch's T-test followed by Benjamini and Hochberg False Discovery Rate was performed on the 14994 probes list using the GeneSpring software, a total of three pair-wise comparisons were performed. A change in gene expression was considered significant if the p-value was less than 0.05 and the fold change at least 2. Under those conditions, 813 probes were identified when comparing NCI-H69 AP3 and NCI-H69 SP, 702 probes when comparing NCI-H69 AP3 and NCI-H69 AP78 and 631 probes when comparing NCI-H69 AP78 and NCI-H69 SP, for a total of 1325 probes up or down-regulated.

SAM was used to perform multi-class comparison on the 14994 probes list. A delta value that captured the largest number of significant genes with the lowest SAM-FDR was chosen. The delta value of 3.48 combined with a SAM-FDR of 0% generated 4134 probes. Pair-wise 2 fold change were then applied using GeneSpring and identified 737 probes when comparing NCI-H69 AP3 and NCI-H69 SP, 668 probes when comparing NCI-H69 AP3 and NCI-H69 AP78 and 605 probes when comparing NCI-H69 AP78 and NCI-H69 SP, yielding a total of 1201 probes.

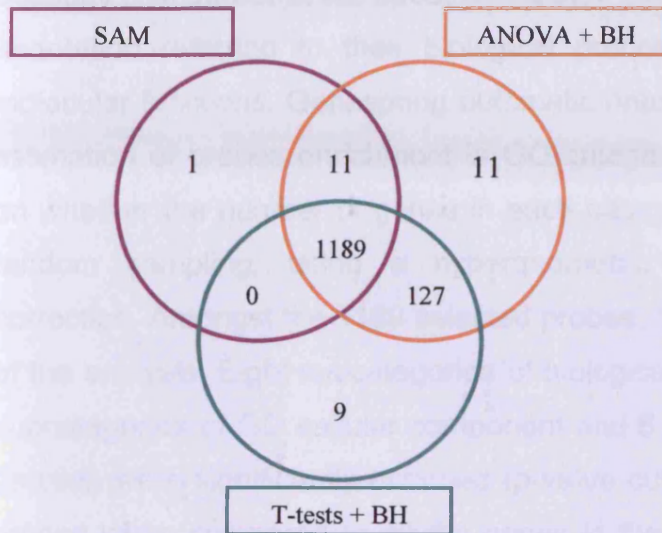
Finally, ANOVA followed by Benjamini and Hochberg False Discovery Rate were performed in GeneSpring, on the 14994 probes list, and a change in gene expression was considered significant if the p-value was less than 0.05. Under those conditions, 7253 probes were identified and 1338 probes after filtering for at least 2 fold change. Pair-wise 2 fold change were then applied using GeneSpring and identified 813 probes when comparing NCI-H69 AP3 and NCI-H69 SP, 730 probes when comparing NCI-H69 AP3 and NCI-H69 AP78 and 655 probes when comparing NCI-H69 AP78 and NCI-H69 SP.

In order to reduce the dimensions of the data and describe the general trend of gene expression changes induced upon the enrichment, only probes identified by the 3 techniques were selected for further analyses. Using this strategy a list of 1189 probes — representing 934 genes — was defined for the rest of the analysis (figure III.14b). The p-values used in the thesis were the

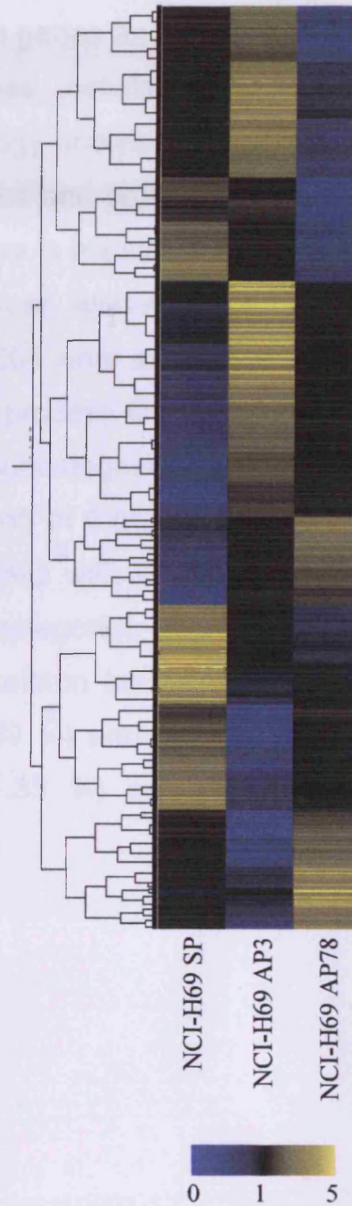
scores taken from the Welch's T-test method. Pair-wise comparisons (figure III.14c) between the variants identified, out of the 1189 selected probes, 737 probes with signal statistically different when comparing NCI-H69 SP and NCI-H69 AP78 (425 upregulation and 312 downregulation in NCI-H69 AP3), 658 probes when comparing NCI-H69 AP3 and NCI-H69 AP78 (225 upregulation and 433 downregulation in NCI-H69 AP78) and 598 probes when comparing NCI-H69 SP and NCI-H69 AP78 (242 upregulation and 356 downregulation in NCI-H69 AP78).



a. Comparison of statistical analysis methods used:



b. 1189 gene list:



c. Pair-wise comparison of the selected remaining probes:

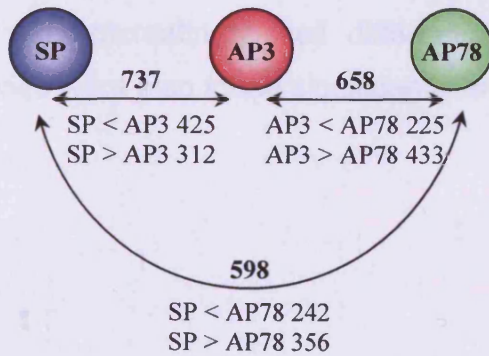


Figure III.14: *Microarray statistical analysis.* a. Venn diagram comparing the results of the 3 statistical methods used: SAM, ANOVA followed by Benjamini and Hochberg False Discovery Rate (BH) and Welch's T-test followed by BH. b. False-colour cluster view of the 1189 gene list representing the expression (average value of the triplicates) of each cell line. c. Variants pair-wise comparison.



### **III.3.3.3. Overview of the ontology analysis**

The biological functions of the differentially expressed genes were explored using the Gene Ontology Browser function in GeneSpring. The gene ontology (Ashburner *et al.*, 2000) associates each genes and their products with annotation referring to their biological processes, cellular components and molecular functions. Genespring automatic ontology analysis tool allows for the estimation of probes enrichment in GO categories and assigns p-value based on whether the number of genes in each category is greater than expected by random sampling, using a hypergeometric test without multiple testing correction. Amongst the 1189 selected probes, 1004 were annotated at the time of the analysis. Eight subcategories of biological process GO SLIM category, 3 subcategories of GO cellular component and 8 subcategories of GO molecular function were significantly enriched (p-value cut-off of 0.05) amongst the 1004 probes when compared to all the genes in the chip with GO annotation (table III.2). As expected for adherence variants, categories found significantly enriched were categories associated with cytoskeleton (as cellular component 11.12 % and molecular function of binding - 6.89 %) and extracellular region (15.27 %). Interestingly, cell differentiation (11.35 %) and death (8.96 %) categories were also found significantly enriched.

**Table III.2: Distribution and enrichment amongst the GO SLIM categories of the 1004 probes.** Significantly (p-value < 0.05) enriched GO SLIM categories are represented in blue and 'offspring' categories are noted below their parent categories within the GO hierarchy.

GO Category	Genes in Category	% of Genes in List in Category	p-Value
<b>GO:8150: biological process</b>			
GO:7275: development	3792	32.37	2.97E-16
GO:9653: morphogenesis	1585	12.85	2.34E-05
GO:9790: embryonic development	361	2.888	0.0419
GO:30154: cell differentiation	1402	11.35	7.58E-05
<b>GO:7582: physiological process</b>			
GO:16265: death	1242	8.964	0.0119
GO:8219: cell death	1232	8.964	0.00974
GO:7610: behavior	816	7.57	1.83E-05
GO:40007: growth	401	3.486	0.0088
<b>GO:5575: cellular component</b>			
GO:5576: extracellular region	1767	15.27	2.09E-07
GO:5578: extracellular matrix (sensu Metazoa)	652	7.381	2.54E-08
<b>GO:5623: cell</b>			
<b>GO:5622: intracellular</b>			
GO:5856: cytoskeleton	1394	11.12	0.000297
<b>GO:3674: molecular function</b>			
GO:4871: signal transducer activity	3746	24.11	0.000928
GO:5198: structural molecule activity	1178	7.656	0.0479
<b>GO:5215: transporter activity</b>			
GO:5489: electron transporter activity	371	2.871	0.0308
<b>GO:5488: binding</b>			
GO:5515: protein binding	9654	56.84	0.000994
GO:5102: receptor binding	1053	9.282	1.09E-06
GO:8092: cytoskeletal protein binding	674	6.89	1.33E-07
GO:3779: actin binding	455	5.263	8.01E-08
GO:30246: carbohydrate binding	377	3.254	0.00486

#### **III.3.4. NCI-H69 model: SCLC phenotype**

Given that several of the NCI-H69 variants mentioned in the literature displayed v-SCLC morphology and biochemical characteristics (Kraus *et al.*, 2002; Seddon *et al.*, 1998), the SCLC phenotype of the variants were investigated using the microarray data. During the analysis, NCI-H69 SP, a classic SCLC cell line, was considered to have maintained its SCLC characteristics under our laboratory culture conditions. To determine whether the enrichment process induced a loss of SCLC biochemical characteristics, the expression of several known-SCLC and NSCLC markers (Kraus *et al.*, 2002) and of microarray-identified SCLC cancer specific markers (Pedersen *et al.*, 2003) was compared across the variants.

In their study, Kraus *et al.* (2002) investigated the expression of 15 SCLC markers, and 5 of them were downregulated in their adherent variant (L-dopa-decarboxylase, chromogranin A, NSE, c-kit and GRP). In this study (figure III.15a / Appendix VII), out of the 15 genes (represented by 33 probes), 3 genes were not detected (Cholecystokinin, progalanin and arginine vasopressin receptor 1 / AVPR1), while 6 genes (8 probes) were found to be significantly modulated between the variants. Four of those genes had their expression downregulated in both NCI-H69 AP3 and NCI-H69 AP78, with expression level higher in the NCI-H69 AP78 cell line when compared to NCI-H69 AP3. The most drastic down-regulation was of gastrin-releasing peptide (84.7 fold SP / AP3 and 21.2 fold AP78 / AP3) and of neurotensin (18.11 fold SP / AP3 and 8.3 fold AP78 / AP3). While enolase 2 (2.2 fold SP / AP3 and 1.4 fold AP78 / AP3) and dopa decarboxylase (2.1 fold SP / AP3 and 1.9 fold AP78 / AP3) were downregulated by around 2 fold. The expression of the oncogene KIT (v-kit Hardy-Zuckerman 4 feline sarcoma viral oncogene homolog) was downregulated in NCI-H69 AP3 when compared to NCI-H69 SP (2.2 fold) and NCI-H69 AP78 (2.5 fold). Neuropilin 1 (nRP) was downregulated in NCI-H69 AP78 when compared to NCI-H69 SP and NCI-H69 AP3 (2 fold and 5.3 fold respectively).

Kraus *et al.* (2002) also investigated the expression of 7 known NSCLC markers, and found that 5 of them were upregulated in their NCI-H69 adherent variant (CD44, Axl, endothelin, thrombospondin and cyclin D1). In the present

study (figure III.15b / Appendix VII), 2 of the SCLC markers were not detected (Axl and endothelin 1) and only CD44 was found upregulated in NCI-H69 AP3 when compared to NCI-H69 SP and NCI-H69 AP78 (3 fold and 5 fold respectively).

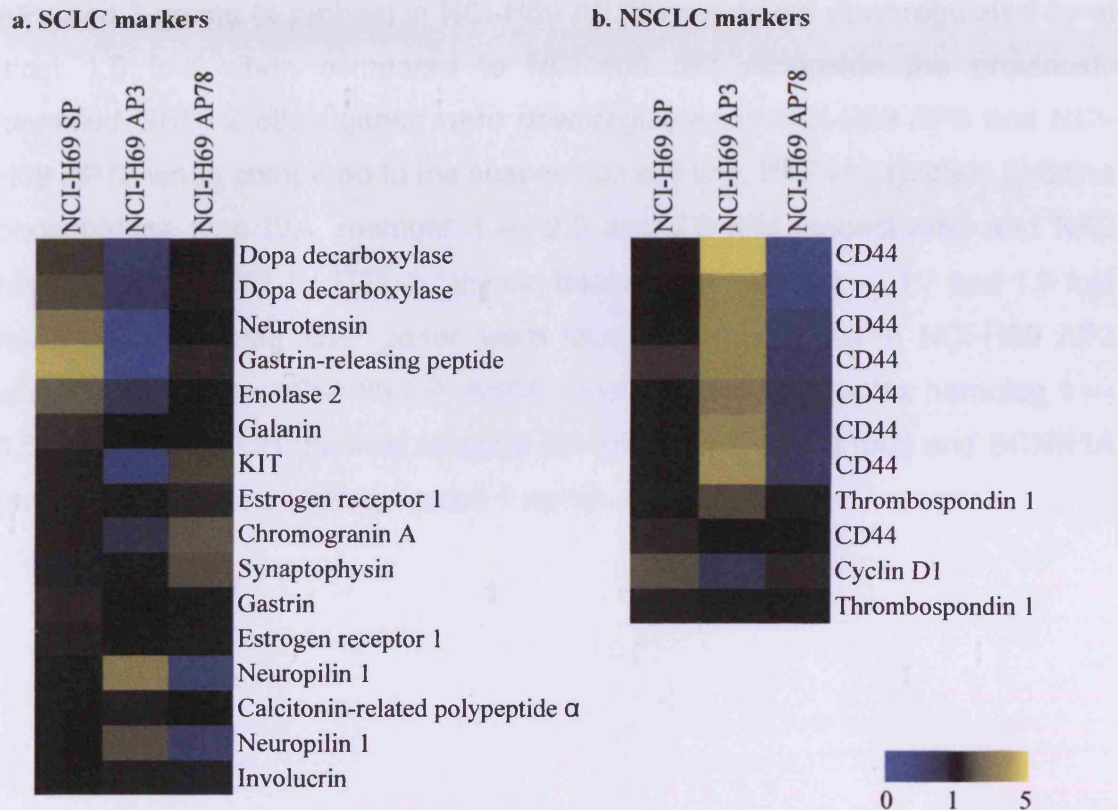


Figure III.15: SCLC and NSCLC markers (Kraus *et al.*, 2002) expression in the NCI-H69 variants. False-colour cluster representing the expression (average value of the triplicates) of each cell line for SCLC marker gene list (a.) and NSCLC marker gene list (b.).

In order to further examine the SCLC characteristics in each of the variants, the expression of previously identified genes was compared across the variants. Pedersen *et al.* (2003), while profiling the transcriptional gene in expression of SCLC, identified 30 genes as SCLC cancer-specific with a median level of expression in SCLC tumour higher than the median of all the samples used in their study. Here, the list of genes (68 Affymetrix probes) was

used to look for downregulation of expression in both adherent variants when compared to NCI-H69 SP (figure III.16 / Appendix VII). One of the marker gene, PNPLA2 (patatin-like phospholipase domain containing 2 / TTS-2.2), was not found expressed by all cell lines, however this result was perhaps not so surprising since, previously, NCI-H69 was found to express only a low amount of it (Pedersen *et al.*, 2003). The expression of 6 genes (10 probes) in NCI-H69 AP3 and 3 genes (4 probes) in NCI-H69 AP78 were found downregulated by at least 1.5 fold when compared to NCI-H69 SP. Alongside the previously identified GRP, 2 other genes were downregulated in NCI-H69 AP3 and NCI-H69 AP78 when compared to the suspension cell line, PTP4A3 (protein tyrosine phosphatase type IVA, member 3 — 2.5 and 1.9 fold respectively) and NK2 homeobox 1 (NKX2-1 / TITF-1 / thyroid transcription factor 1 — 1.7 and 1.9 fold respectively). Three other genes were found downregulated in NCI-H69 AP3 when compared to NCI-H69 SP: ASCL1 (achaete-scute complex homolog 1 — 6.5 to 9 fold), NCOR (nuclear receptor co-repressor 1 — 1.8 fold) and SCNN1A (sodium channel, nonvoltage-gated 1 alpha — 1.6).

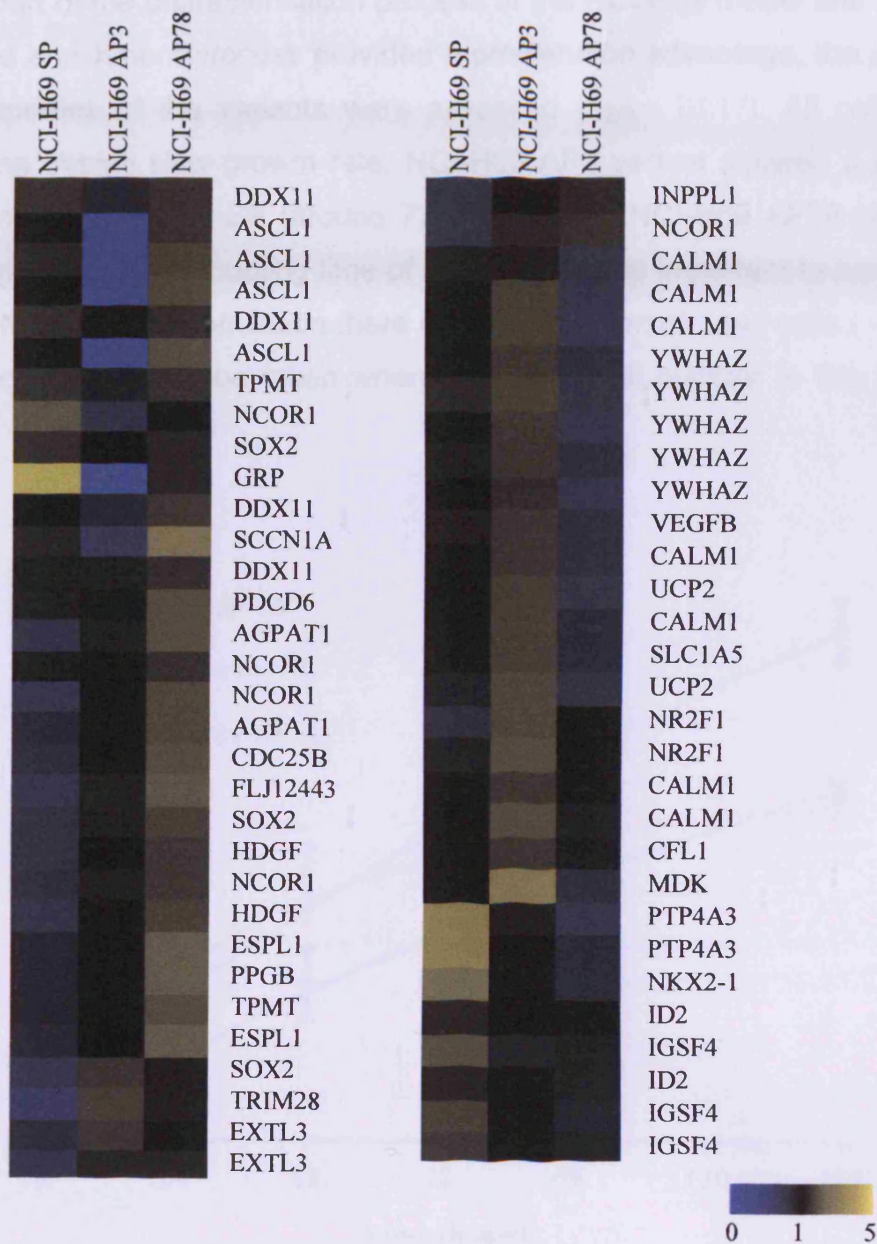
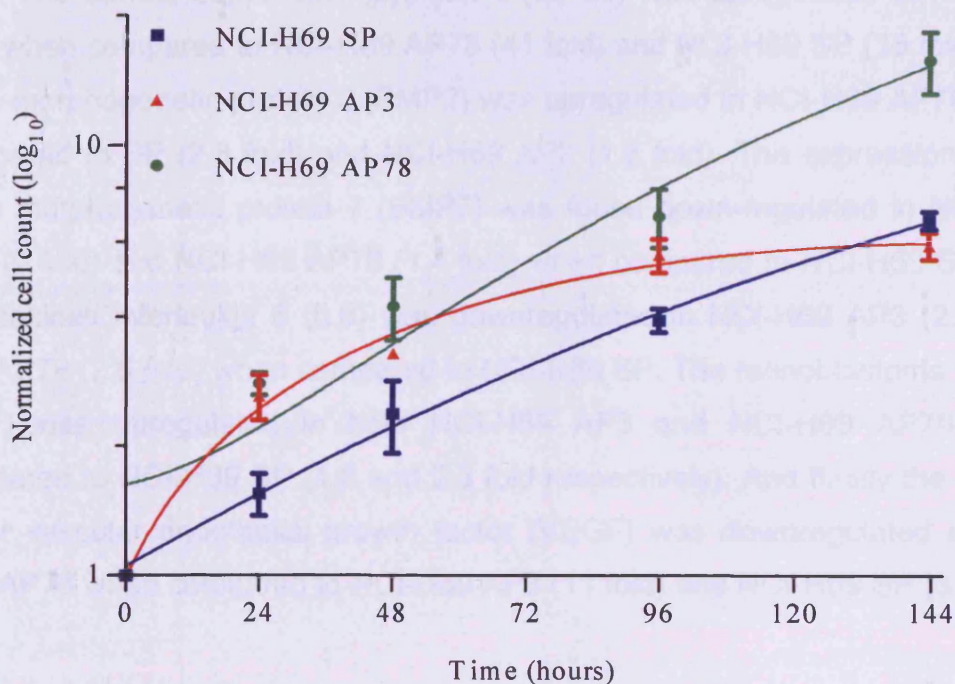


Figure III.16: *SCLC markers* (Pedersen *et al.*, 2003). False-colour cluster representing the expression (average value of the triplicates) of each cell line for SCLC marker gene list.



### III.3.5. NCI-H69 model: growth characteristics

As part of the characterisation process of the NCI-H69 model and to test whether the enrichment process provided a proliferation advantage, the *in vitro* growth properties of the variants were assessed (figure III.17). All cell lines displayed an overall slow growth rate. NCI-H69 AP3 variant showed a similar doubling time to NCI-H69 SP (around 72h). However, NCI-H69 AP78 showed enhanced growth with a doubling time of around 48h. It is important to also note that in the NCI-H69 SP population there is a high fraction of dead cells (~50%). Therefore caution has to be taken when estimating cell number in this model system.



**Figure III.17:** Growth properties of the different variants of the NCI-H69 cell line. Each point, normalised to the starting number of cells, represents the mean  $\pm$  SD of triplicates wells. The experiment is representative of three independent experiments.

Microarray data were interrogated for cell cycle and growth-related gene expression changes in the variants.

Using the cell cycle GO gene list (GO: 7049), 74 probes (55 genes) overlapped with the 1189 gene list (figure III.18 / Appendix VIII). The expression

of 3 cell cycle effectors were found modulated in the variants. The expression of the cyclin A1 (CCNA1) was found downregulated in both NCI-H69 AP3 and NCI-H69 AP78 when compared to NCI-H69 SP (8 fold and 17 fold respectively). The expression of cyclin F (CCNF) was found upregulated in both NCI-H69 AP3 and NCI-H69 AP78 when compared to NCI-H69 SP (1.7 fold and 2.4 respectively). And, the cyclin-dependent kinase inhibitor 1C (CDKN1C / p57 / Kip2) was found upregulated in NCI-H69 AP78 when compared to NCI-H69 SP and NCI-H69 AP3 (1.7 fold and 3 respectively)

Using the cell growth GO gene list (GO: 40007), 35 probes (20 genes) overlapped with the 1189 gene list (figure III.18 / Appendix VIII). The expression of the transforming growth factor, beta 2 (TGFB2) was found up-regulated in NCI-H69 AP3 when compared to NCI-H69 SP (1.9 fold) and NCI-H69 AP78 (3.6 fold). The tumour suppressor glypican 3 (GPC3) was upregulated in NCI-H69 AP3 when compared to NCI-H69 AP78 (41 fold) and NCI-H69 SP (15 fold). The bone morphogenetic protein 2 (BMP2) was upregulated in NCI-H69 AP78 when compared to SP (2.8 fold) and NCI-H69 AP3 (1.8 fold). The expression of the bone morphogenetic protein 7 (BMP7) was found down-regulated in NCI-H69 AP3 (5 fold) and NCI-H69 AP78 (1.4 fold) when compared to NCI-H69 SP. The chemokines interleukin 8 (IL8) was downregulated in NCI-H69 AP3 (2.4 fold) and AP78 (2.6 fold) when compared to NCI-H69 SP. The retinoblastoma 1 gene (RB1) was upregulated in both NCI-H69 AP3 and NCI-H69 AP78 when compared to NCI-H69 SP (1.5 and 2.3 fold respectively). And finally the growth factor vascular endothelial growth factor (VEGF) was downregulated in NCI-H69 AP78 when compared to NCI-H69 AP3 (11 fold) and NCI-H69 SP (6 fold).



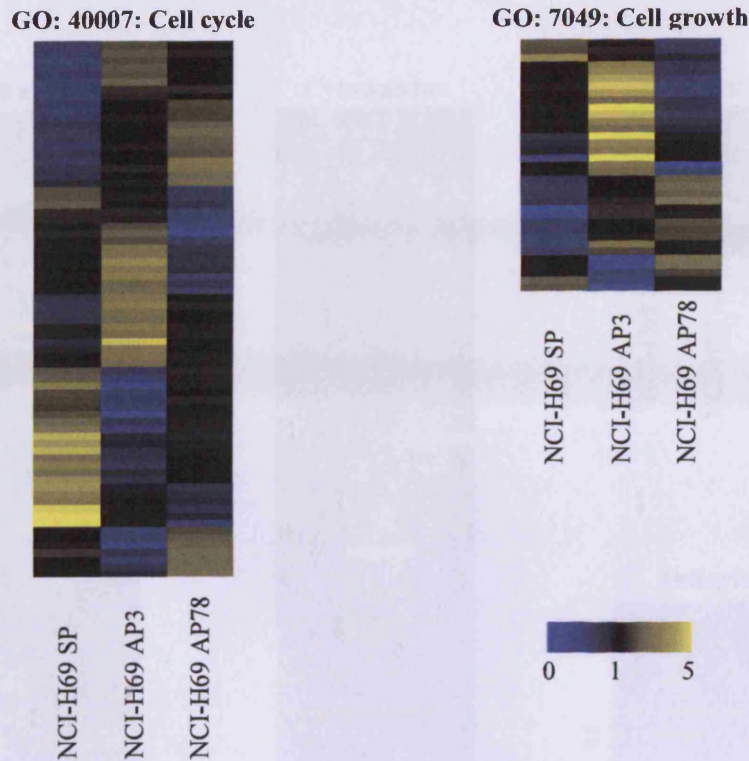
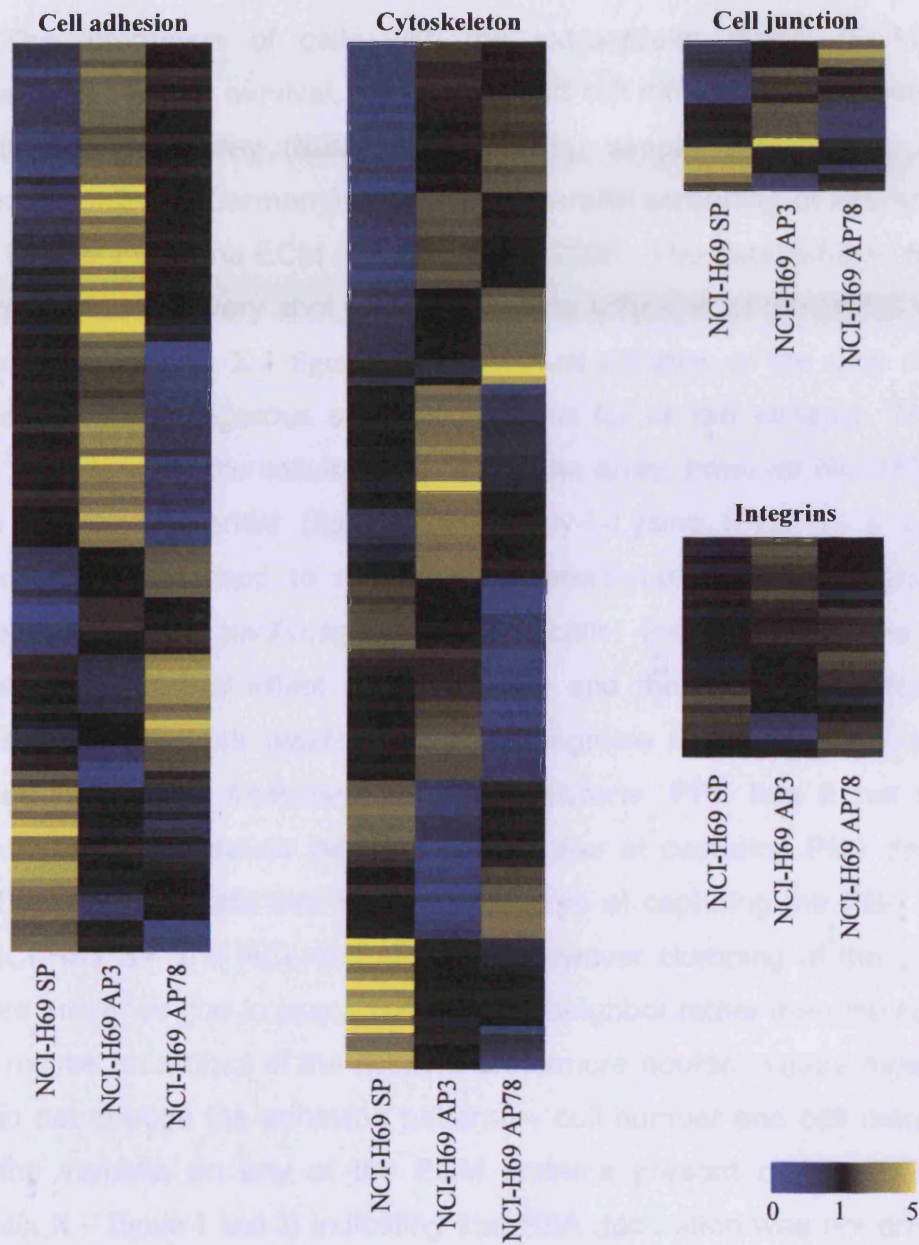


Figure III.18: *Cell cycle and growth-related gene expression.* False-colour cluster representing the expression (average value of the triplicates) of each cell line for the overlap between 1189 gene list and GO: 7049: cell cycle or GO: 40007 cell growth.

### III.3.6. NCI-H69 model: cell adhesion

The microarray data was viewed from two general perspectives. The first addressing cell adhesion properties (figure III.19 / Appendix IX – table 1). The interesting outcome from this global analysis is that out of 110 probes 61 probes showed a higher expression in NCI-H69 AP3 when compared to NCI-H69 AP78 and NCI-H69 SP. The second global analysis addressed cytoskeleton profiling of the variants (figure III.19 / Appendix IX – table 2) in this case all three variants took on different expression profiles suggesting that the enrichment process and selection for adherence resulted in different cytoskeletal composition. Further drill down addressed cell-cell interactions (called cell junction / figure III.19 / Appendix IX – table 3), where each of the variants took on slightly different profiles, although there was no statistically significant differences detected for the cell-substrate interactions (or integrins / figure III.19 / Appendix IX – table 4).



**Figure III.19:** *Cell adhesion and cytoskeleton.* Gene tree clustering representation of the expression (average value of the triplicates) of each cell line for the overlap of 1189 gene list with GO: 7155: cell adhesion, cytoskeleton (GO: 5856: cytoskeleton and GO: 7010: cytoskeleton organisation and biogenesis) or GO: 30054: cell junction and integrins expression.

### III.3.6.1. Cell-ECM adhesion: MSA

The interaction of cells with the extracellular matrix (ECM) plays important roles in cell survival, cell growth and cell differentiation. Therefore, a multiple substrate array (MSA) screen using simple substrate technology (BioCat, Heidelberg, Germany) enabling the parallel screening of interactions of cell to 14 proteins of the ECM (Kuschel *et al.*, 2006). The reassembled full array in image format for every spot shows the acute adhesion of the SCLC variants to the array (Appendix X – figure 3 to 5). Manual agitation of the slide every 10 minutes provides a rigorous selection process for all the variants. Therefore overall there is very little cellular adhesion to the array, however NCI-H69 AP78 display a better potential (figure III.20). Poly-L-Lysine (PLL) is a synthetic molecule generally used to enhance cell attachment to plastic and glass surfaces. For many anchorage-dependent cells, the nature of the culture substrate has a major effect on cell growth and the requirement for serum proteins. Tissue culture plastic has a net negative surface charge which is produced by plasma treatment of the polystyrene. PLL has a net positive charge and could therefore be considered better at capturing PSA decorated cells. The PLL substrate was therefore effective at capturing the PSA positive cells NCI-H69 SP and NCI-H69 A78 cells, however clumping of the cells and therefore presence due to association with its neighbor rather than the substrate per se maybe an artifact of the assay. Furthermore neuraminidase digestion of PSA did not change the adhesion pattern — cell number and cell morphology — of the variants on any of the ECM proteins present on the MSA slide (Appendix X – figure 1 and 2) indicating that PSA decoration was not driving the selection to the substrate.



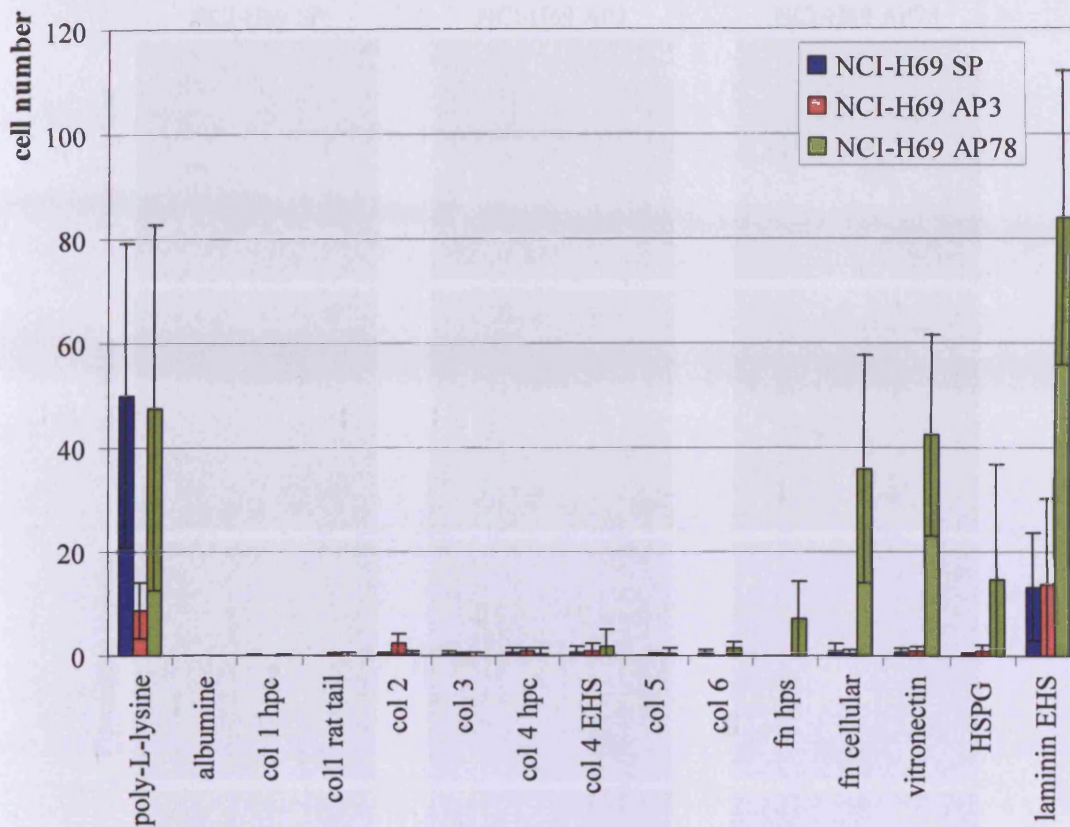


Figure III.20: Adhesion profile of the NCI-H69 variants on ECM proteins. Cells were incubated for 2 h with manual agitation every 10 min. After processing and imaging of the slides, cells on each spot of ECM proteins were counted. The experiment is representative of 3 independent experiments.

Bright field images were acquired to determine general cell morphology and cell-cell interaction characteristics (figure III.21); NCI-H69 SP cells showed significant clumping and a corresponding rounded cell morphology indication of perhaps a somewhat tenuous interaction with the surface; a similar outcome was apparent for NCI-H69 AP78 cells on the HSPG substrate. NCI-H69 AP78 interaction with laminin EHS, vitronectin and cellular fibronectin showed cells with a flattened or lozenge shape indicating a 'real' interaction with the substrate. In all cases these were very due to the presence of a low number of cells (<100).

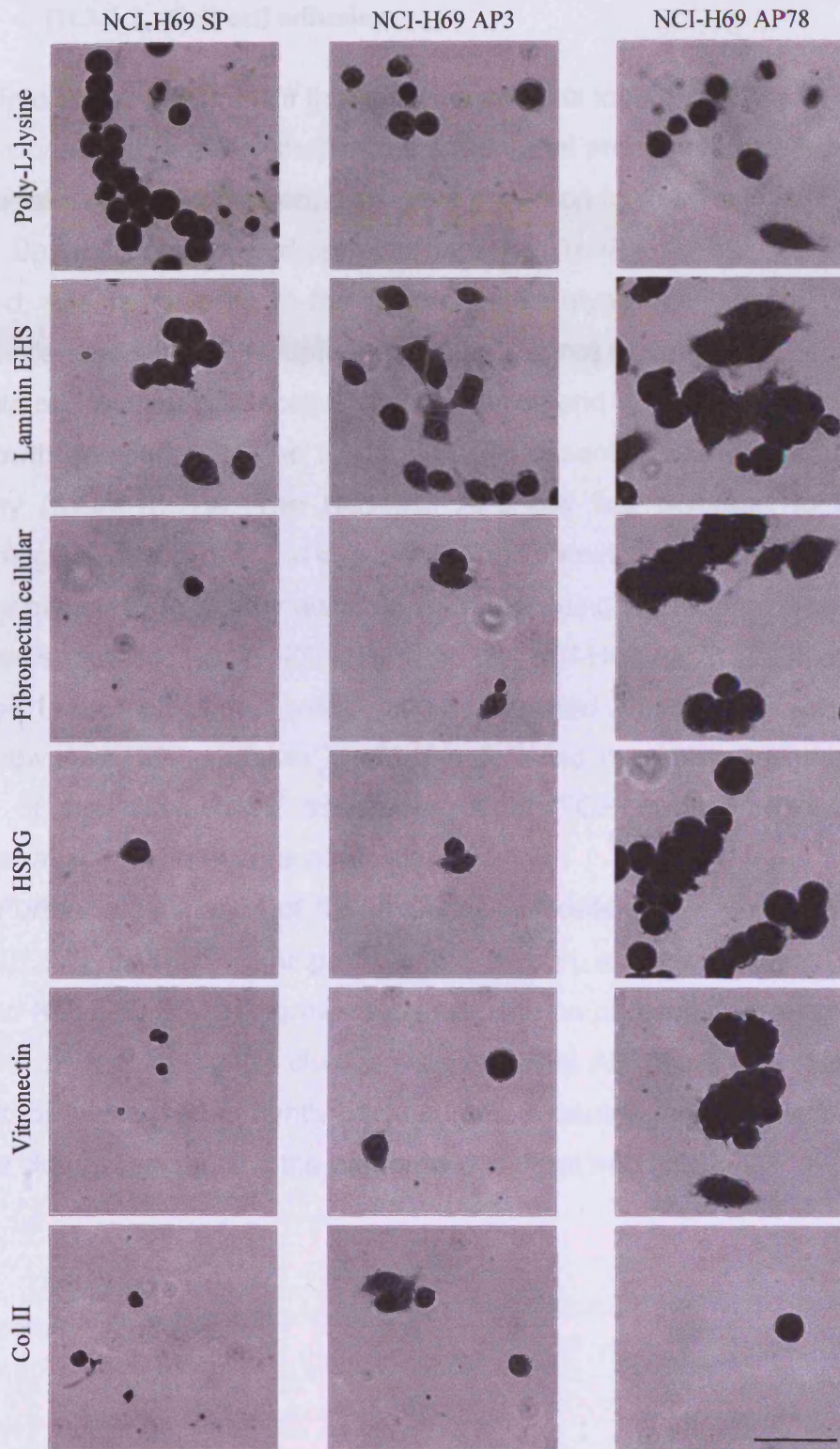


Figure III.21: Cell morphology on MSA ECM proteins spot. Calibration bar represents 50  $\mu\text{m}$ .

### **III.3.6.2. Cell-cell adhesion**

In order to determine if the adherent variants lost their ability to survive in suspension and to assess whether the enrichment process reduced their ability to undertake cell-cell adhesion, cells were grown on hydrophobic surface (figure III.22). Upon culture on hydrophobic surfaces (HOP), no cell adhesion was detected, and reversibility of the adherent phenotype was observed. Indeed, cells challenged with a hydrophobic surface did not undergo cell death, rather they retained normal light scatter characteristics and revert to suspension-form cell growth demonstrating the fundamental or essential property of phenotypic plasticity (figure III.22a). The NCI-H69 AP3 cell line reversed to a type 2 morphology of cells growing in suspension and forming aggregates. Reversal of the phenotype - from loosely attached cells to floating aggregates – can also be observed spontaneously in NCI-H69 AP3. The NCI-H69 AP78 cell line reversed to a type 1 morphology with growth as tightly packed clumps. Both adherent cell lines grown on HOP surfaces for 5 days retained the ability to attach to the plastic of the flask once transferred to a TCP surface (figure III.22b) demonstrating a maintenance of plastic behaviour.

Further examination of the phenotype of cells grown on HOP surfaces (figure III.22c), by H&E staining of paraffin section, showed that both NCI-H69 AP3 and NCI-H69 SP cells grew as clumps with no particular organisation, with NCI-H69 SP forming tighter clumps. The NCI-H69 AP78 cell line clumps were found to be composed of tightly packed cells. A central 'hole' could be seen in all large clumps, suggesting the presence of central necrosis.



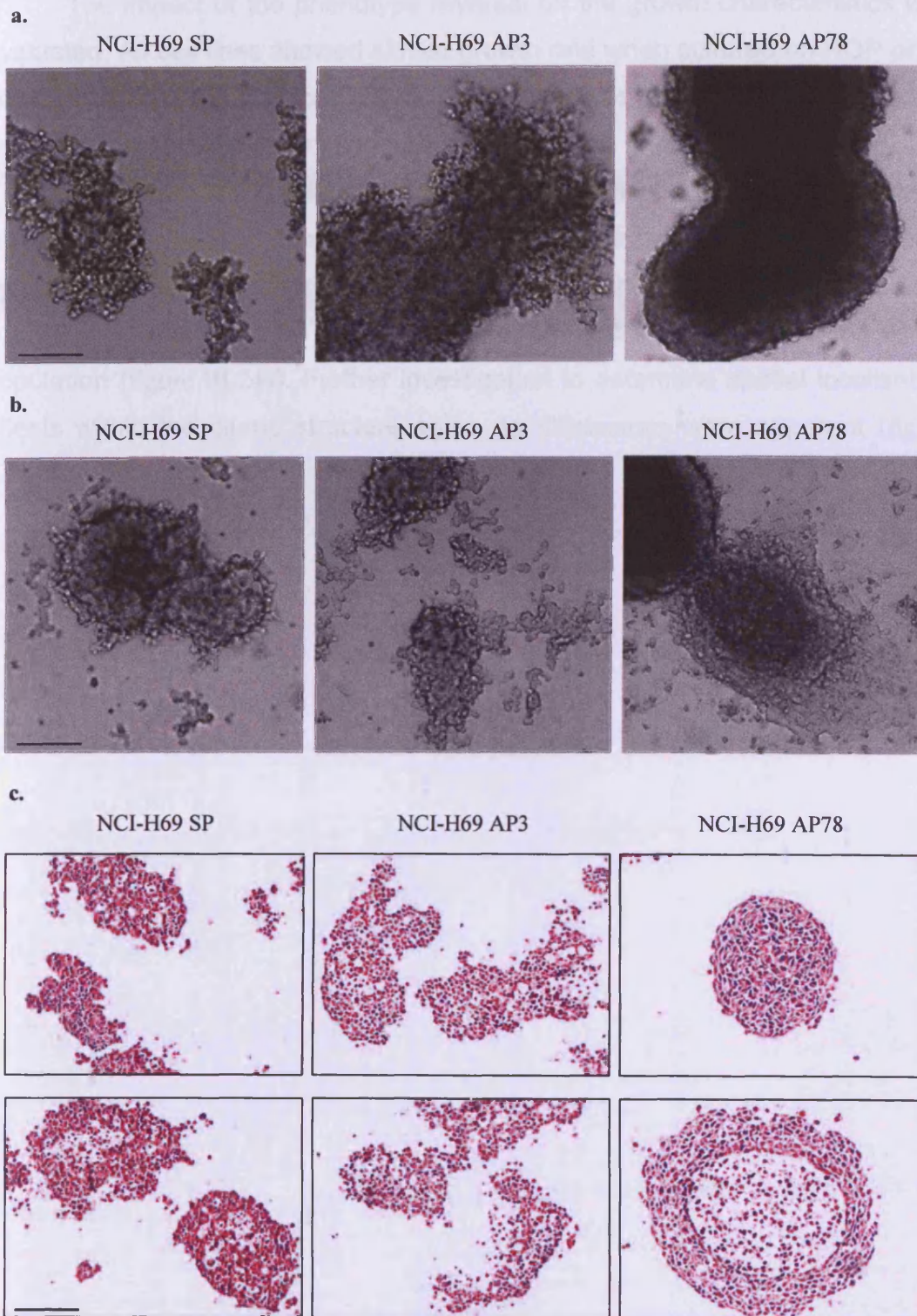


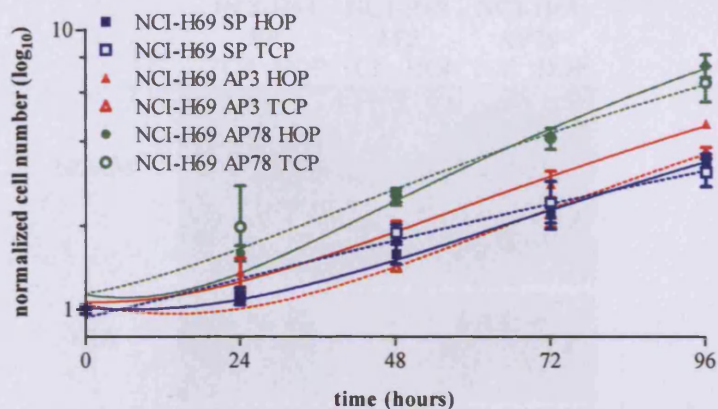
**Figure III.22: Reversibility of the attached phenotype.** The NCI-H69 variants were grown on a hydrophobic substrate. **a.** Pictures depicting cells grown on hydrophobic surface for 9 days. **b.** Pictures depicting cells grown on hydrophobic surface for 5 days, transferred to a tissue culture treated dish and grown for 4 more days. **c.** H&E staining of paraffin section. Calibration bars represent 100 μm.

The impact of the phenotype reversal on the growth characteristics was evaluated. All cell lines showed similar growth rate when cultured on HOP or on corresponding TCP surfaces (figure III.23a). Images acquired every 24 hours over six days showed that clump size increased with time (figure III.23b).

The extent of PSA decoration was also determined (figure III.24) in these same cultures. In each case there was no difference between cells grown on a hydrophobic surface after nine days and its corresponding tissue culture counterpart. This could be said for both NCAM and PSA-NCAM on the whole population (figure III.24a). Further investigation to determine spatial localisation effects within the clump structure again no differences were apparent (figure III.24b).



a.



b.

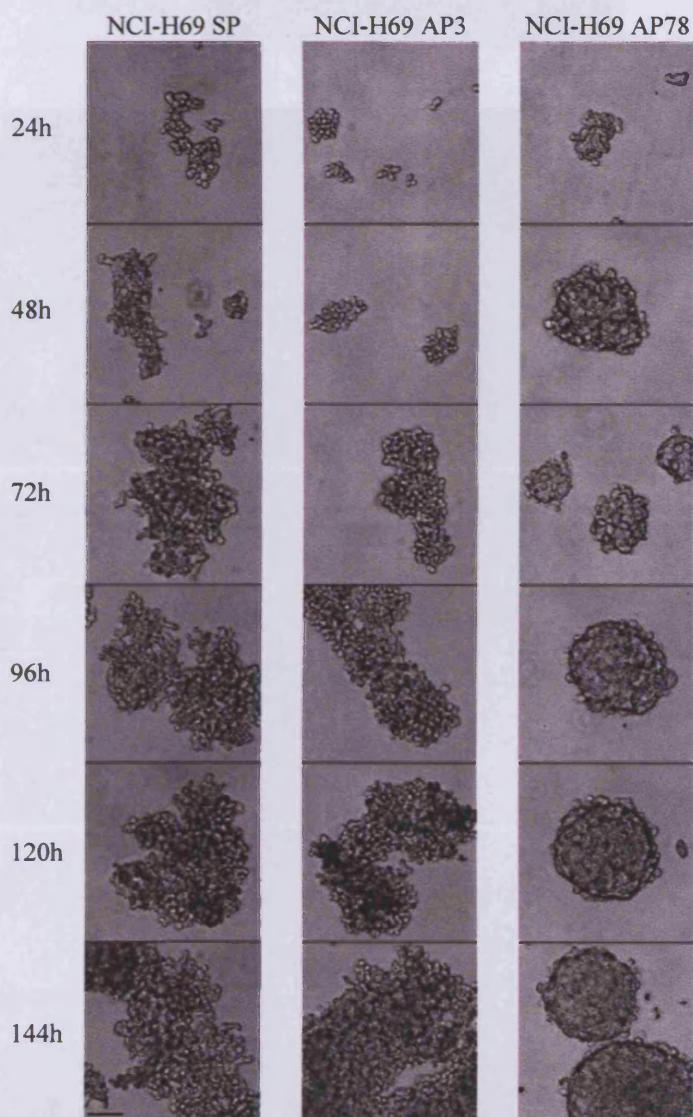


**Figure III.23:** Growth properties of the NCI-H69 model cultured on hydrophobic substrate. **a.** Growth curve of the NCI-H69 model cultured on HOP or TCP dishes. Data represents the mean  $\pm$  SD of triplicates, representative of 2 experiments. Curves were fitted using nonlinear regression. **b.** Pictures of NCI-H69 cell lines grown on hydrophobic substrate taken at random fields every 24h. Calibration bar represents 50  $\mu$ m.

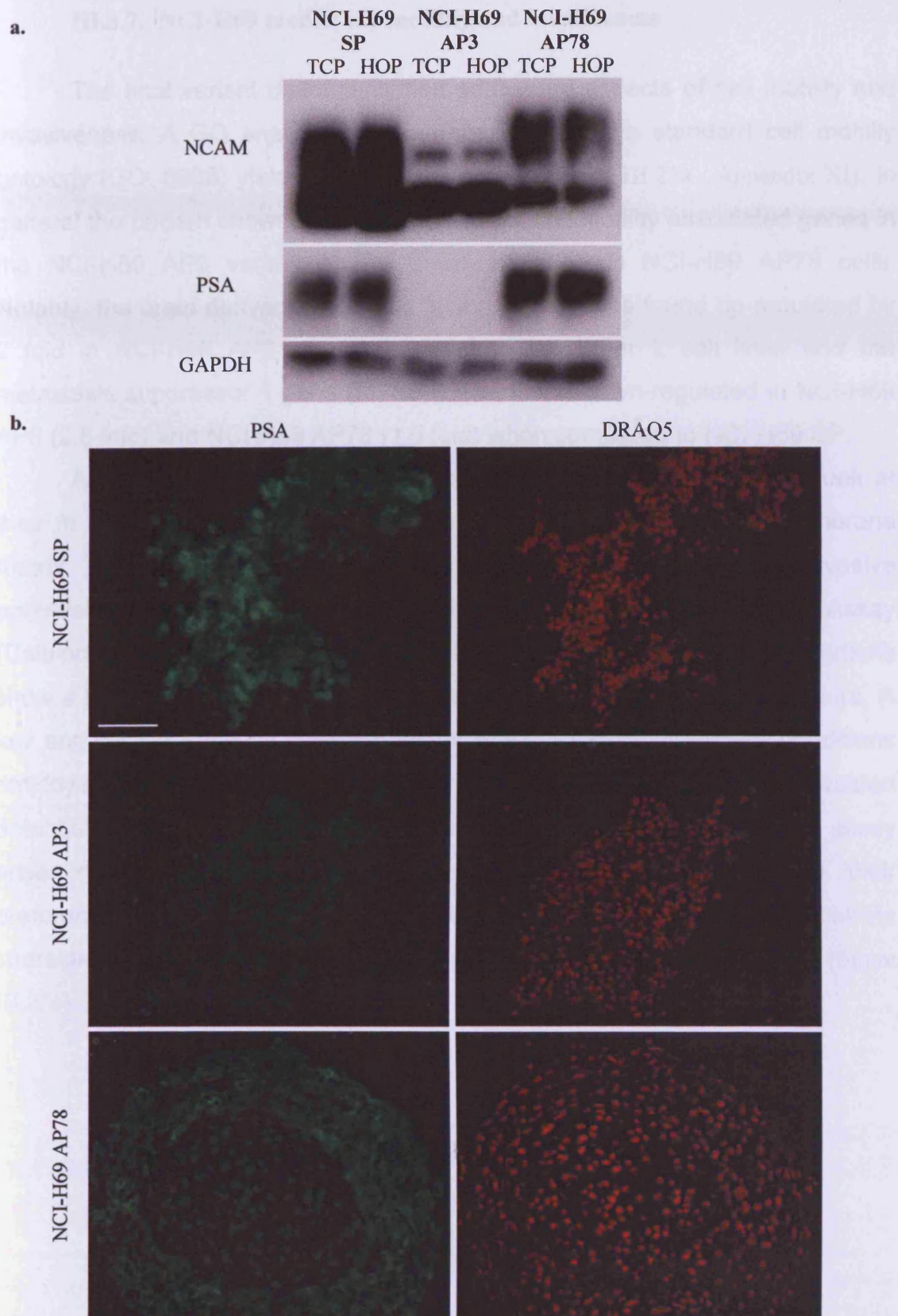


Figure III.24: Expression and localization of NCAM and PSA-NCAM in the NCI-H69 variants grown on hydrophobic surfaces (antibody 22B). **a.** Whole population expression using western blot detection. **b.** Spatial localization within the clump structure using immunofluorescence detection. Calibration bar represents 100  $\mu$ m.

### III.3.7. NCI-H69 model: cell motility and invasiveness

The final variant characterisation addressed aspects of cell motility and invasiveness. A GO analysis was performed using the standard cell motility ontology (GO: 6928) yielding a list of 57 probes (figure III.25a / Appendix XI). In general the pattern showed an up-regulation of cell motility associated genes in the NCI-H69 AP3 variant and a down-regulation in NCI-H69 AP78 cells. Notably, the brain derived neurotrophic factor (BDNF) was found up-regulated by 2 fold in NCI-H69 AP3 when compared to the other 2 cell lines and the metastasis suppressor 1 gene (MTSS1) was found down-regulated in NCI-H69 AP3 (2.5 fold) and NCI-H69 AP78 (1.6 fold) when compared to NCI-H69 SP.

A simple assay to assess the metastatic potential of cells is to look at their *in vitro* 'invasive' capacity through a reconstituted basement membrane matrix. The most common method currently employed to screen the invasive potential of cell lines in the current study the *in vitro* Cell Invasion Assay (Calbiochem, San Diego, CA, USA) was used (see methods). All cell variants show a poor ability to invade the basement membrane matrix after 48 hours. A low and similar invasive potential for all SCLC variants under the conditions employed was apparent (figure III.25b), therefore no modification of the invasion potential of the adherent variant was noted. A major draw back of the assay arises due to the inherent behaviour of the cells in suspension, *i.e.* their preference to clump with each other (cell-cell interactions) over a cell-substrate interaction. Images after a 48 hour incubation indicates this tendency (figure III.25c).



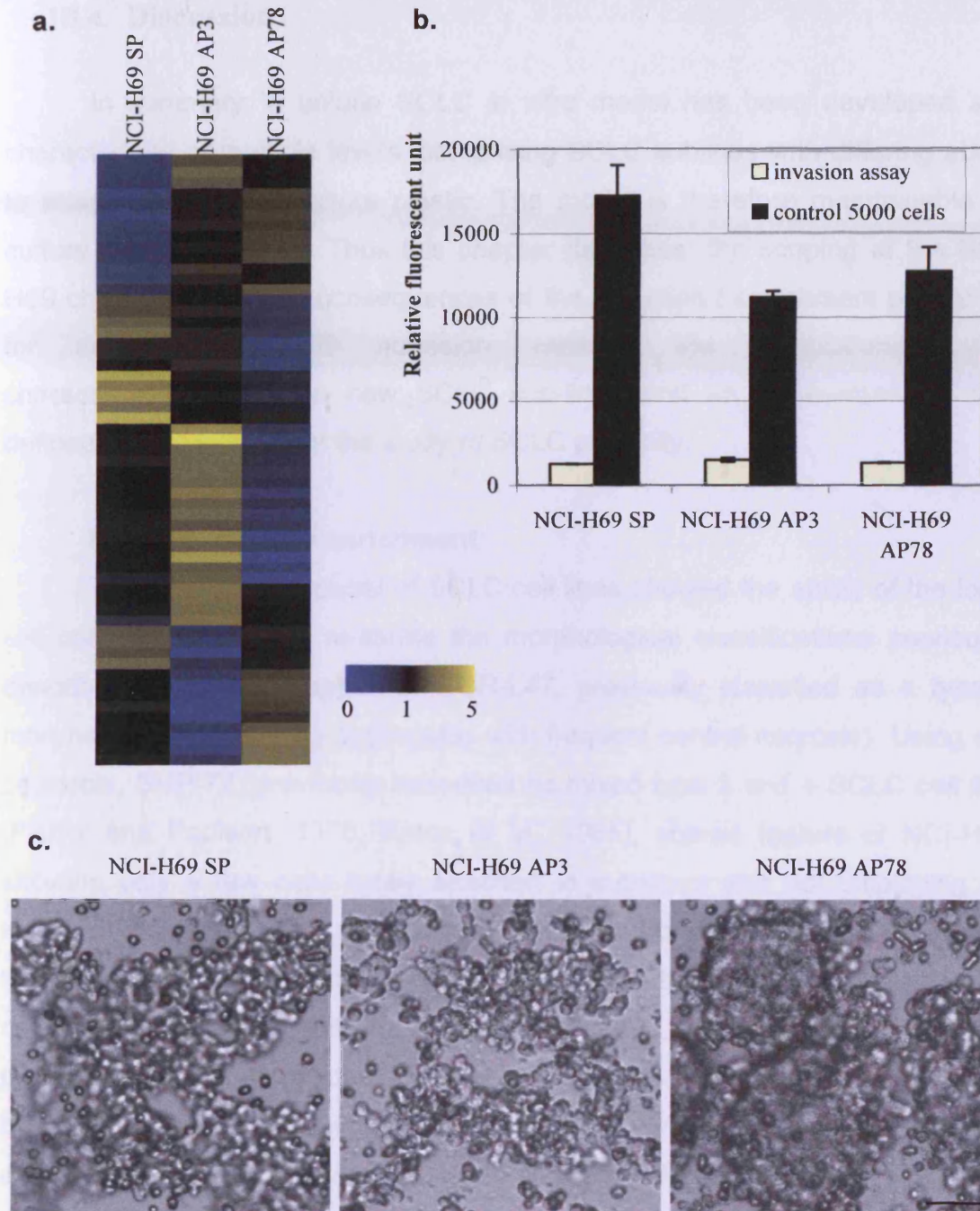


Figure III.25: *Determination of the invasion potential of the NCI-H69 variants.* **a.** False-colour cluster view representing the expression (average value of the triplicates) of each cell line for the overlap between GO: 6928 cell motility and 1189 gene list. **b.** Relative fluorescence unit value of calcein AM stained cells that have passed through the membrane alongside relative fluorescence unit value for 5000 cells. The data represent the mean  $\pm$  SD of 3 wells and is representative of 2 independent experiments. **c.** Images from the top chamber of the invasion assay after 48 h incubation. Calibration bar represents 50  $\mu$ m.

### III.4. Discussion

In summary, a unique SCLC *in vitro* model has been developed and characterised at multiple levels, comprising SCLC sublines with differing ability to attach to standard culture plastic. The model is therefore maintainable by culture technique alone. Thus this chapter describes: the scoping of the NCI-H69 characteristics and consequences of the selection / enrichment procedure for adhesion NCI-H69 adhesion variants; the establishment and characterisation of three new SCLC sub-lines and an assessment of this defined *in vitro* system for the study of SCLC plasticity.

#### **NCI-H69 variants enrichment:**

The study on the panel of SCLC cell lines showed the ability of the local cell culture protocols to re-iterate the morphological classifications previously described with the exception of COR-L47, previously classified as a type 1 morphology (tight floating aggregates with frequent central necrosis). Using our protocols, SHP-77, previously described as mixed type 2 and 4 SCLC cell line (Fisher and Paulson, 1978; Koros *et al.*, 1985), shared feature of NCI-H69 showing only a few cells lightly attached to substrate and not displaying an epithelial phenotype. This morphological distinction of NCI-H69 provided part of the rationale for its selection for further study. Importantly, the majority of SCLC cell lines in the panel, with the exception of COR-L51 and COR-L47, show a propensity for sub-populations of cells to undergo spontaneous non-specific binding to TCP substrate indicating that it is an intrinsic property and that the experiments described have established a rationale for the adoption of NCI-H69 as a representative a classical cell line.

The adhesion variants varied in their ability to attach to the substrate as demonstrated by the adhesion assay developed as a quantitative means of assessing culture status revealing that acute attachment to TCP is a robust method for assessing variant status. This metric is not dependent upon observational assessment of morphology and therefore applicable to multi-laboratory studies scheduled for future collaborations with drug discovery and development groups. Moreover, it will offer the possibility to determine the

variants' attachment properties to various ECM proteins in a time-dependent manner and to determine the heterogeneity among the population.

**NCI-H69 variants characterisation:**

**Gene expression** — The chapter reports a successful establishment of a NCI-H69 state transition model and a methodology for the enrichment of adherence variants for the molecular studies – recognizing that microarray analysis provides ambivalent results when dealing with mixed populations. The results describe an assessment of the stability of the adhesion variant phenotype in the absence of ECM-based cues. To establish a firm basis for our study and to determine the extent of variation between the variants, we have used the expression arrays to investigate the differences between NCI-H69 cells cultured as micro-spheroids and cultures sequentially selected for adherent growth. As expected gene expression modulation was most frequently linked to gene products located in the extracellular region, membrane, associated with cell adhesion and components of the cytoskeleton.

Microarray analysis found downregulation of neuroendocrine characteristics in NCI-H69 AP3 GRP, ASCL1, ENO2 and DDC. All of these SCLC markers are often downregulated in variant SCLC cell lines (Carney *et al.*, 1985; Gazdar *et al.*, 1985; Kraus *et al.*, 2002). Moreover the NSCLC marker, CD44 (Kondo *et al.*, 1998), was upregulated in NCI-H69 AP3. Transition from SCLC to NSCLC observed *in vivo* and *in vitro*, associated with H-ras and c-myc function, has been shown to comprise these phenotypic changes (Barr *et al.*, 1996; Risse-Hackl *et al.*, 1998). Interestingly, those changes were not found in the late adherent variant.

Although the adherent-variants showed increased epithelioid morphology with increasing passage, no modulation of epithelial markers such as cadherin were detected and two claudins (3 and 5) were found down-regulated in both adherent cell lines. As expected frequent modulation of cytoskeleton-related genes was found, including actin beta, actin gamma 2 and actinin  $\alpha$ 1. Interestingly, the tetraspanin CD9 was found downregulated in both adherent cell lines. Absence of CD9 has recently been shown to enhance adhesion-dependent morphologic differentiation of SCLC cells (Saito *et al.*, 2006).

**PSA-NCAM expression** — The NCI-H69 cell line was used in the development of the SCLC variant model because of the hypothesized complex link with PSA decoration (see Introduction). The decrease in PSA decoration of the NCI-H69 AP3 variant was an acquired feature rather than one driving substrate adherence. Furthermore PSA loss is unrelated to a sustained adherence variant since the NCI-H69 AP78 variant shows an increased PSA decoration.

Although PSA expression cannot be related, across the panel, with the adherent phenotype *per se*, a decrease in PSA expression was observed in NCI-H69 AP3 cell line. Thus plasticity for PSA decoration of NCAM is independent of acquisition of the adherence phenotype and therefore provides for plasticity to be expressed at each stage of the transition to variant appearance. Importantly no positive selection for PSA-NCAM is imposed in the enrichment process and we have not adopted a clonal selection method. Thus, the system as described proved a holistic view of the ability of cells to show enrichment preference and what features naturally co-enriched. The interesting characteristic of NCI-H69 adherent cell line of retaining NCAM expression, while down-regulating polysialylation, provides an opportunity to investigate the impact of PSA changes rather than loss of NCAM *per se*.

The panel study established that there was not a simple relationship between *in vitro* TCP adherence properties and the expression of the nominated plasticity marker PSA-NCAM. This neither confirms nor rejects the view the polysialylation of NCAM may provide, through phenotypic plasticity, opportunities for SCLC cells to generate variation which is resolved, through selection, as changes in adherence. This underlies the need to evaluate the stages of transition and the associated plasticity of expression, rather than seeking a correlation of 'end-stages' which may be more representative of clonal variation.

**Cell-ECM adhesion properties** — In order to assess matrix-adhesion properties of the variants, we chose a screening technique (MSA) allowing comparative profiling studies (Kuschel *et al.*, 2006). The limited time frame (2 h) allowed testing of inherent ECM-adhesion capacity rather than adaptation capacity. Agitation every 10 min leads to resuspension and redistribution of

unattached cells (Kuschel *et al.*, 2006) while allowing sufficient time for the molecular response to be initiated (Lotz *et al.*, 1989). However, with the NCI-H69 system, culture agitation provides mean of promoting cell-cell attachment. This is not dissimilar to the formation of microspheroids in standard spinner cultures. Therefore, presence of cells on the array due to cell-cell association rather than cell-substrate *per se* (cell clumping) provided ambivalent results. Despite these technical complications, the MSA experiment showed low affinity of the variants to the used ECM proteins. These results were consistent with previous findings showing that only few NCI-H69 cells adhered to laminin after 1 day, but after 5 days virtually all cells were adherent to laminin showing a flattened morphology (Tsurutani *et al.*, 2005). The MSA experiment also clearly showed the increased affinity of NCI-H69 AP78 to fibronectin, laminin, HSPG and vitronectin. Fibronectin and laminin have been shown to surround SCLC tumour cells (Sethi *et al.*, 1999), suggesting an *in vivo* relevance for the ECM responses of the NCI-H69 variants system.

PSA removal did not affect cell adhesion to ECM proteins. This result is consistent with previous findings, where NCI-H69 variants selected for high or low PSA expression showed no modulation of attachment to the ECM proteins heparan sulfate, laminin, collagen IV and poly-L-lysine (Scheidegger *et al.*, 1994).

*Cell-cell adhesion* — We have established an *in vitro* methodology to test the impact of acute reversal of substrate adhesion opportunities and to test reversal of phenotype and the impact on the capacity of SCLC cells to retain variant growth characteristics. The aim was to assess the impact of variation on cell interactions to interpret *in vitro* growth patterns.

Clearly, long-term enrichment for epithelioid growth did not result in loss of the ability for suspension growth. Even the NCI-H69 AP78 cell line, which offers limited heterogeneity in term of adhesion (under normal conditions only 5% of the NCI-H69 AP78 cells do not adhere to the substrate — these cells do not form clumps and could be dead) was capable of suspension growth with no indication of proliferation disadvantage. Moreover, reversibility of the adherence phenotype in NCI-H69 AP3 resulted in similar growth to the parental cell line, while NCI-H69 AP78 formed tighter clumps.



PSA was also not found to inhibit cell-cell contact. Indeed, NCI-H69 AP78 when forced to grow in suspension formed tightly packed aggregates. The large excluded volume of NCAM-PSA has the potential to control general cell-cell interactions through the hindrance of overall membrane apposition (Rutishauser *et al.*, 1988) or by modified charge and surface dielectric properties. Indeed, sialic acid residues and the proteoglycans (PGs) are considered to be major contributors to the negative charge at the surface of cells as revealed by electrokinetics (Vargas *et al.*, 1990; Vargas *et al.*, 1989). When NCAM with a low PSA content is expressed, adhesion is increased and contact-dependent events are triggered. Recently, Johnson *et al.* (2005) have provided direct evidence that NCAM polysialylation increases intermembrane repulsion and abrogates adhesion. These molecular force measurements show quantitatively that NCAM polysialylation increases the range and magnitude of inter-membrane repulsion. Clearly, PSA-NCAM can regulate both cell-cell and cell-substrate interactions (Acheson *et al.*, 1991).

A previous study showed modulation of cell-cell interactions by PSA. Indeed, NCI-H69 variants (isolated using limiting dilution exploiting NCI-H69 PSA expression heterogeneity) expressing high level of PSA were found to form fewer clumps (Scheidegger *et al.*, 1994). This suggests that if PSA modulates cell-cell adhesion in NCI-H69 SP, others mechanisms must be capable of overriding the exclusion volume effect of PSA-NCAM in permitting NCI-H69 AP78 cell-cell adhesion to be so effective.

*Invasion potential* — Microarray analysis identified two invasion-related genes of interest: BDNF upregulated in NCI-H69 AP3 and MTSS1 down-regulated in both adherent cell lines. The *in vitro* invasion assay showed no difference between phenotypes, however, because invasion *in vivo* is ultimately more complex, involving both trans-endothelial cell invasion and degradation and migration through extracellular matrix (ECM) components and basement membrane, a more realistic model system would include each of these barriers.

In a corresponding recent study (Kraus *et al.*, 2002), spontaneously adherent SCLC sublines were shown by differential gene expression analysis to provide an *in vitro* model of variant differentiation in SCLC, with down-regulation of neuroendocrine markers and up-regulation of epithelial differentiation

markers cyclin D1, endothelin, the cell adhesion molecules CD 44 and integrin subunits  $\alpha 2$ ,  $\beta 3$  and  $\beta 4$ . A phenomenon of enhanced metastasis is also thought to relate to the induction of tumour differentiation, resulting in apoptosis-resistant, morphological variants that lack the neuroendocrine expression of classic (c-) SCLC cells. Sub-cultivation of the adherent sublines on uncoated surfaces reversed their adherent phenotype immediately and under these conditions Akt activity reverts to low levels (Kraus *et al.*, 2002). Understanding the events involved in such a switch in adherent/suspension tumour cell characteristics could suggest the nature and the plasticity of the steps involved in the spreading of this highly metastatic type of lung cancer.

*In vitro growth characteristics* — Growth characteristics of the variants were determined in order to test the operation of proliferation advantage in variant selection and to provide the interpretation parameters for the NCI-H69 model for the assessment of hypothesized modulation of PSA and chemosensitivity characteristics for cell adhesion.

Microarray analysis found that the tumour suppressor RB1 was found to be up-regulated in both adherent cell lines. The P16-cyclin D1-CDK4-RB pathway, central for G1/S cell cycle transition control, is disrupted in most lung cancer. The pathway is disrupted through RB inactivation in SCLC, while cyclin D1, CDK4 and p16 abnormalities are rare in SCLC but common in NSCLC (Wistuba *et al.*, 2001). NCI-H69 has been previously shown to only express traces of non-altered RB1 (Harbour *et al.*, 1988).

Overall, microarray profiling genes has revealed no major changes in cell cycle and cell growth regulators. To explain NCI-H69 AP78 increased proliferation advantage, it is possible that this might arise from the inability to determine the true proliferation kinetics of the NCI-H69 SP due to the lower live fraction.

*Determination of variation in cell size and DNA content* — Further features were also revealed by the continuous enrichment process for SCLC variants. The NCI-H69 AP78 variant showed an increase in DNA content and a corresponding increase in cell size although the nucleus/cell size ratio remained unchanged. It is clearly evident that minimal and sustained culture of cells can

allow for the appearance of clonal variants (e.g. shown here in terms of ploidy levels in NCI-H69). The conclusion is that the NCI-H69 SP to NCI-H69 AP3 transition is an equilibrium shift between two populations with slight differences in ploidy while the NCI-H69 AP3 to NCI-H69 AP78 represents the predomination of a hyper-ploidy clone with some selective advantage. The assumption is that this hyperploidy clone arises from the NCI-H69 AP3 pool as a consequence of a proliferative advantage within a range of adherent cells. This shift in cell and nucleus size is likely to influence on the micropharmacokinetic properties of the variants. To be also noted is the presence of a sub-fraction of NCI-H69 AP78 with similar DNA content to NCI-H69 AP3 cells, underlying the heterogeneity of the population.

**NCI-H69 variants clinical context:**

Recent global gene expression analyses using oligonucleotide microarrays on many SCLC cell lines have showed that all of the xenografts clustered closest to the cell lines from which they originated and had the same expression levels as the cells grown in culture for the majority of genes (Pedersen *et al.*, 2003). This suggests that SCLC *in vitro* biology presents relevant gene expression profiles and target opportunities. Indeed, comparison of array profiles of resected tumours (Bhattacharjee *et al.*, 2001) has revealed that many potential drug targets expressed by SCLC cell lines and xenografts are also expressed in the tumours.

Interestingly we have discovered a large (>15 fold) and apparently specific increase in Glypican-3 (GPC3) mRNA abundance in adherent versus suspension NCI-H69 cells. This result was further confirmed by immunoblotting and FACS analysis (data not shown). GPC-3 is a candidate tumour suppressor gene in SCLC. While increased GPC3 expression has been found in melanoma and hepatocellular carcinoma (Capurro *et al.*, 2005; Nakatsura *et al.*, 2004), GPC3 expression is known to be associated with decreased lung metastasis, less local invasiveness and increased sensitivity to apoptosis (Peters *et al.*, 2003). The encoded glypican has been linked with the control of tumour growth and cell migratory activity through Wnt-signalling (Capurro *et al.*, 2005). Recently, GPC3 has been found to inhibit Hedgehog (Hh) signalling during development (Capurro *et al.*, 2008) and to mediate oncogenecity through insulin

growth factor (IGF)-signalling pathway (Cheng *et al.*, 2008). Thus altered GPC3 expression seems to be highly tissue specific, suggesting that GPC3 could stimulate proliferation in tumours with Wnt signalling influence is dominant and GPC3 inhibit proliferation in tumours with Hh signalling predominant (Filmus and Capurro, 2008). This hypothesis is consistent with the fact that GPC3 is downregulated in breast, ovarian and lung cancer, tumours where Hh pathway is hyperactivated (Filmus and Capurro, 2008).

GPC-3 has been proposed to represent a potential lung tumour suppressor in non-small cell lung carcinoma with reduced expression of GPC-3 reported in a panel of non-small cell lines and a limited number of adenocarcinomas resected from patients with non-small cell lung carcinoma (Kim *et al.*, 2003). Furthermore, these latter studies demonstrated that the expression levels of GPC-3 in normal respiratory bronchiolar epithelial cells (the cell type assumed to give rise to adenocarcinomas) are sensitive to cigarette smoke, with its loss upon exposure proposed as an initiating factor in the aetiology of NSCLC. GPC3 role in lung cancer has yet to be determined. Indeed, a recent study showed that GPC3 was overexpressed in lung squamous cell carcinoma, and again GPC3 expression correlated with cigarette smoking (Aviel-Ronen *et al.*, 2008). To date no information regarding the expression of GPC-3 in clinically defined SCLC tissue samples and how these correlate to the metastatic potential of the primary tumour exists.

## **IV. Chemosensitivity and heterogeneity of the NCI-H69 variants**

### **IV.1. Introduction and aims**

SCLC is a very aggressive disease with 5 years survival of 10% for limited disease and less than 5% for extensive disease. Although surgery and radiotherapy play a great role in managing SCLC, chemotherapy remains the main form of treatment. The combination of cisplatin or carboplatin with etoposide has been used to treat SCLC for over 25 years, and still remains the standard treatment (Murray and Turrisi, 2006). Despite a good initial response to therapy, most SCLC patients suffer from the development of chemotherapeutic resistance and relapse. Therefore, there is a need to apply second-line chemotherapy, which however, frequently results in only a low survival increase. To improve the outcome of SCLC, there is a further need for new therapies, and new drugs such as topotecan, iritonecan, paclitaxel have been studied (Fischer and Arcaro, 2008). Moreover progress in the understanding of SCLC biology has led to the development of new specific targeted therapies. However, to date, no targeted therapy has been approved for use in the treatment of patients with SCLC (Rossi *et al.*, 2008). The topoisomerase I (TOP1) inhibitor topotecan (TPT) is the only single agent approved for the treatment of recurrent SCLC (Garst, 2007), and recent studies suggested that TPT in combination with etoposide or cisplatin could be effective for first line therapy in untreated SCLC (O'Brien *et al.*, 2007). Hence, this indicates the relevance for investigating the action of the agent on later phases of SCLC cancer biology as represented by the SCLC variant models under analysis in the current study. Furthermore, pharmacological aspects of TPT, including the mechanisms of action, metabolism, activity- and toxicity-profiles, are under scrutiny to provide an insights into how to "fine-tune" anticancer treatment and address the mechanisms of resistance (Mathijssen *et al.*, 2002). The availability of a variant SCLC system has the potential to contribute to that knowledge base. Indeed, sublines of the classic small cell lung cancer NCI-H69 line have proven useful in studies on drug resistance and its circumvention with alternative agents such as paclitaxel (Davey *et al.*, 2004) or in assessing the

micropharmacokinetic features of multi-drug resistant cell lines (Coley *et al.*, 1993).

The camptothecin class of agents, such as that represented by TPT (figure IV.1a), induce their pharmacodynamic effects through the targeting of DNA topoisomerase I, an enzyme capable of removing DNA supercoils. The consequences of enzyme inhibition include the engagement of genetic programs leading to cell cycle arrest and apoptosis (Daoud *et al.*, 2003; Pommier, 2004; Pommier *et al.*, 1998). Topotecan stabilizes a covalent topoisomerase-DNA complex, then converted into double-strand DNA breaks by collisions of DNA replication fork, during replication, or progressing RNA polymerase molecules, during transcription (Pommier, 2006). TPT is therefore considered to be S-phase specific, but more recent studies have shown that TPT differentially targets cells in G1, S or G2, with G2 cells presenting the best opportunity for drug resistance (Feeney *et al.*, 2003).

The mechanisms of damage induction, molecular sensing of lesions, the functional and structural impact on cellular processes such as DNA metabolism, together with the transmission of signals to repair, cell cycle or cell death pathways are complex – especially in tumour cell systems in which there is frequently dysfunction in one or more components. Both Top1 and TOP2 DNA topoisomerases solve topological problems during chromosome metabolism, counteracting the accumulation of torsional stress and sister chromatid entanglement at replication forks and preventing the diffusion of topological changes along large chromosomal regions (Bermejo *et al.*, 2007). In the presence of topotecan, TOP1 cleaves the DNA but is unable to religate the single-strand break. This leads to stabilization of TOP1-DNA-bound complexes and the accumulation of DNA strand breaks that may interfere with DNA replication. The origin of strand breakage is thought to reflect the discontinuous nature of DNA replication. A role for the Werner syndrome helicase/3'-exonuclease (WRN), a major component of the DNA repair and replication machinery, has also been recognised. For example, cells not expressing WRN are hypersensitive to topotecan, but not to the TOP2 inhibitor etoposide. The evidence suggests that WRN is involved in the repair of TOP1, but not TOP2-induced DNA damage - most likely via preventing the conversion of DNA single-strand breaks into DSBs during the resolution of stalled replication forks at

TOP1-DNA complexes (Christmann *et al.*, 2008). There has been recent insight into the complexity of the damage induction process and mechanism of action of topotecan, extending the view of the stabilized covalent topoisomerase-DNA complex acting as obstacles to DNA replication forks. Using single-molecule nanomanipulation to monitor the dynamics of human top 1 in the presence of topotecan an accumulation of positive supercoils ahead of the replication machinery causing potentially lethal DNA lesions was demonstrated (Koster *et al.*, 2007)

Cell cycle checkpoints are pivotal mechanisms safeguarding genome stability and their failure impacts on the evolution of variation in tumour populations and drug responsiveness. Two structurally-unrelated protein kinases, CHK1 and CHK2, are implicated in several major checkpoints of the cell cycle, transmitting signals from damage sensing processes to the cell cycle engine. Variations of the ATM/ATR-CHK1/CHK2-CDC25-CDK pathways contribute to the replication checkpoint, to the intra-S phase checkpoint, and to the G2 DNA damage checkpoint (Chen and Poon, 2008). TOP1-mediated DNA lesions elicit checkpoint responses in the DNA damage-activated checkpoint signalling pathways. The tumour suppressor p53 is considered to play a key role in restricting proliferation of abnormal cells. It is activated in response to a variety of cellular stresses, including DNA damage (for review see Levine, 1997). Following TPT treatment, the activation of p53 is most pronounced in S-phase, as observed in A549 cells human lung alveolar cell carcinoma (Zhao *et al.*, 2008). S-phase arrest induced by top 1 inhibition arises from an activation of Chk1 (Zhang *et al.*, 2008) and degradation of Cdc25A phosphatase that occurs independent of p53 status (Levesque *et al.*, 2008). This independence of p53 is pertinent to SCLC since this tumour suppressor gene (TSG) is mutated in more than 90% of SCLCs and more than 50% of NSCLCs (Wistuba *et al.*, 2001). Furthermore, the retinoblastoma TSG is inactivated in over 90% of SCLC but only 15% of NSCLCs, and p16, the other component of the retinoblastoma/p16 pathway, is almost never abnormal in SCLC but is inactivated in more than 50% of NSCLCs (Wistuba *et al.*, 2001). NCI-H69 cells shows evidence of p53 mutant expression, therefore affirming that a strategy using a topoisomerase I inhibitor for arresting in the late-cell cycle. The prognostic significance of p53 mutations in lung cancer is not entirely clear although there is evidence to suggest that



lung cancers with p53 alterations carry a worse prognosis and may be relatively more resistant to chemotherapy and radiation (Campbell *et al.*, 2002; Campling and El-Deiry, 2003).

Several reports have described the hydrolysis reactions of camptothecins in physiological buffers as measured by high performance liquid chromatography (HPLC). Indeed, the maintenance of intracellular active drug for DNA targeting is opposed by the hydrolysis, at the physiological pH, of the active lactone form to the inactive ring-opened form (Chourpa *et al.*, 1998). Therefore any bias in the intracellular equilibrium and the export of drug molecules from the cell impose micropharmacokinetic limitations on TPT availability at the cellular level (Chappell *et al.*, 2008; Cheung *et al.*, 2008; Evans *et al.*, 2004). Moreover, the fluorescent properties of topotecan (figure IV.1b) allows for drug tracking and fluorescence reporting of the drug using the convenient UV absorbance and visible range fluorescence signature of the drug (Burke *et al.*, 1996; Gryczynski *et al.*, 1999).

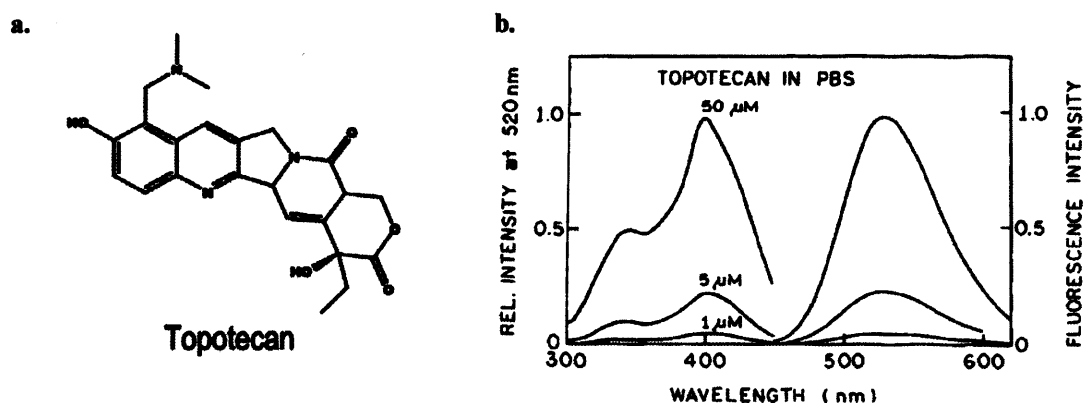


**Figure IV.1:** *Topotecan* — a *camptothecin* derivative. **a.** Structure of the lactone form of topotecan. **b.** Fluorescence spectral properties of topotecan in PBS (from Burke *et al.*, 1996), dose dependent increase of excitation (first peak, maximum at 390 nm) and emission (second peak, maximum at 540 nm).

Topotecan shows effectiveness in a range of cancers, most notably in ovarian cancer and SCLC, but is subject to cellular efflux by membrane-located ABC transporters (Pommier, 2006). The half transporter ABCG2, containing only a single putative transmembrane region and ATP binding motif, has been linked to resistance to TPT. First discovered in multi-drug resistant human

breast (MCF-7) cancer cell line, showing high cross resistance for mitoxantrone, daunorubicin and topotecan (Litman *et al.*, 2000), ABCG2 is found to be expressed in epithelial cells of intestine, colon, liver, and renal tubules, where it acts to reduce the plasma level, and therefore bioavailability of orally administered anti-cancer drugs (Jonker *et al.*, 2000; Maliepaard *et al.*, 2001). The fungal toxin fumitremorgin C (FTC) is a potent inhibitor of the ABCG2 transporter (Rabindran *et al.*, 2000), providing a selective pharmacological tool to evaluate the activity of the transporter in SCLC variants. The roles for ATP-binding cassette (ABC) transporter superfamily members in conferring drug resistance have been extensively described. In a recent study on NSCLC cells it was found that ABCG2 levels accounted for between 80 and 90% of the variation in the resistance to topoisomerase I inhibitors, including topotecan (Nagashima *et al.*, 2006).

ABCG2 has also been identified as a marker for cancer stem cell (CSC) activity, with sub-population expression found in multiple tumour cell types (Wu and Alman, 2008). While the presence of surface markers selectively expressed on CSCs are used to isolate these cells, in many cases exploitation of stem cell characteristics can be used to identify CSCs. One such characteristic is the capacity to extrude dyes, such as Hoechst 33342, via the ABCG2 transporter. Cells that exclude this dye are referred to as side population cells (Challen and Little, 2006). Isolation or identification of stem cells based on the efflux of fluorescent dyes has also been an efficient method to study stem cells, for instance it has been demonstrated that Rhodamine 123 (Rho123) retention is low in the most primitive hematopoietic cells. Indeed, cells with low Hoechst 33342 and Rho123 are highly enriched for stem cell activity (Leemhuis *et al.*, 1996; Wolf *et al.*, 1993). The biological basis for the differential efflux of these dyes in the stem cell compartment is due to the activity of ATP-binding cassette transporters.

The AT-specific DNA minor groove ligand (MGL) 2',5'-bi-1H-benzimidazole, 2',(4-ethoxyphenyl)-5-(4-methyl-1-piperaziny), trichloride (Hoechst 33342) is used extensively for the labeling of DNA in both live and fixed cells. A significant advantage is the enhanced fluorescence shown by the dye molecule upon binding to DNA in the minor groove and more extant to the groove as more molecules bind. The dye has both cytotoxic and mutagenic

properties (Durand and Olive, 1982). In identifying modified intracellular maintenance of Hoechst 33342 dye in side population cells, use is made of the spectral shift in the dye's emission spectrum as the ligand effectively titrates sites on DNA with different binding modes (Smith *et al.*, 1985; Watson *et al.*, 1985). At low dye: DNA base ratios, as experienced at early uptake periods or imposed by enhanced dye efflux, there is an initial favouring of high affinity binding within the minor groove, yielding a violet-biased emission spectrum. The spectral shift allows side population discrimination, by comparing emission at the violet and red regions of the spectrum, on the basis of high level dye exclusion, the side population phenotype is associated with low blue and low red fluorescence (Goodell *et al.*, 2005). Therefore, dye exclusion provides a valuable technique as it identifies a unique population of cells with stem-like characteristics (Sung *et al.*, 2008).

The overall aim of the study was to determine the impact of variant status on the chemosensitivity of SCLC cells with specific reference to the highly relevant agent TPT. The concept was to assess sensitivity (pharmacodynamic response) as an innate property of the variants without the imposition of ECM-driven factors as discussed in the main Introduction chapter. Further, the study sought to search for evidence of the modulation of known mechanisms of resistance for TPT, particularly those related to drug exclusion. The SCLC variants provide a characterised cell system in which to assess changes in the ability to deliver TPT (pharmacokinetic activity) to an intracellular target especially regarding the potential heterogeneity within cell populations. A linked concept was possibility that the variant enrichment process had selected cells with CSC-like properties, in the absence of drug selection that might favour CSC survival, through robustness for establishing proliferative capacity under changed conditions for cell-cell/cell-substrate interactions. Accordingly, an assessment was also undertaken to search for 'CSC-like' sub-compartments in the variants that might impose chemoresistance phenotype given that this feature might not be apparent in short-term bulk population studies but would be highly relevant to Darwinian fitness under selection *in vivo*.

The experimental aims were:

➤ To survey for variation in the expression of ABC transporters and to functionally determine if the NCI-H69 variants display altered pharmacokinetic properties, *i.e.* whether the delivery of drug to the target was affected. Fluorescence tracking and the use of inhibitors allowed for detection of altered sensitivity versus topotecan uptake and efflux properties. To address the problem of tracking and parameterising rapid cellular drug dynamics time series flow cytometry was used to monitor uptake, delivery and stability of the TPT signal in cells.

➤ To determine if there was evidence of changes in subfractions of cells with CSC-like properties. The human lung alveolar cell carcinoma, A549 (Lieber *et al.*, 1976), was used as a control for ABCG2 expression and to provide a technical validation of the side population phenotype measurement by flow cytometry, given that the A549 cell line displays a strong side population phenotype due to functional ABCG2 expression (Scharenberg *et al.*, 2002). Recent studies have identified and isolated a stem cell-like sub-population (24%) from the A549 cell line using the FACS / Hoechst 33342 approach with FTC (Sung *et al.*, 2008) and have revealed differential sensitivity to DNA damage agents.

➤ To determine the long term consequences of a 1 hour bolus exposure to topotecan on cell viability. Due to inherent heterogeneity of the SCLC variants (*i.e.* size, shape and substrate adhesion), determining growth curves using a cell count approach proved to be unreliable and an insensitive approach. A simple colourimetric test, called alamarBlue, was adapted to provide a screening method suitable for both suspension and adherent cells alike, to provide a non-invasive high-throughput format and therefore potentially providing a continuous readout over time.

## **IV.2. Specific Material and Methods**

### **IV.2.1. Drugs and inhibitor**

Hoechst dye No. 33342 (Sigma-Aldrich Ltd, Dorset, UK) was prepared as an aqueous stock solution and added directly with mixing to culture media containing cells. Topotecan (Hycamtin®; GlaxoSmithKline, Brentford, UK) was prepared in sterile water and the stock was stored at -80°C until required. Fumitremorgin C (FTC / Rabindran *et al.*, 1998) was purchased from Sigma (St Louis, MO, USA) resuspended in DMSO (to a stock concentration of 10 mM) and used as previously described (Robey *et al.*, 2001).

### **IV.2.2. Cell lines**

NCI-H69 variants cell lines (NCI-H69 SP, NCI-H69 AP3 and NCI-H69 AP78 — described in chapter III) and the human lung alveolar cell carcinoma, A549 (Lieber *et al.*, 1976), were routinely cultured as previously described (see Materials and methods).

### **IV.2.3. ABCG2 immunodetection**

Immunofluorescence was conducted as previously described (see Materials and methods). Cells were cytopun, fixed with 100% methanol and stained with ABCG2 antibody (Chemicon international, Millipore, Temecula, CA, USA).

### **IV.2.4. Hoechst side population assay**

Single cell suspensions, with or without FTC pretreatment (10 µM / 1h), of A549 cells and of each NCI-H69 variants in complete medium supplemented with 20 mM HEPES were incubated with Hoechst 33342 (5 µM). Hoechst fluorescence was assessed on the FACS Vantage system at various time points on the same sample. Samples were kept at 37°C in a dry-block heater (Techne, Barloworld Scientific Ltd, Stone, UK) between time points. Signals were

acquired with CELLQuest software (Beckton-Dickinson Immunocytometry Systems). Forward scatter (FSC) and side scatter (SSC) were acquired in linear mode. Hoechst 33342 signals derived from UV excitation were detected in linear mode at FL4 via a 620 LP filter (Hoe red) and via a FL5 424 / 44 filter (Hoe blue). All signals were collected for 10000 cells using the forward light scatter as the master signal. Data were analysed using FlowJo (Tree Star, San Carlos, CA, USA).

#### **IV.2.5. TPT uptakes**

Time series: the assay was conducted by incubating single cell suspension of each NCI-H69 variants and SU-DHL-4 cells (used as biological control) — at a concentration of  $4.3 \times 10^5$  cells / mL in fresh medium supplemented with 20 mM HEPES — with 10  $\mu$ M TPT. TPT fluorescence was measured on the FACS Vantage system at various time points on the same sample (t = 0; 5; 10; 20; 30; 40; 50 and 60 min). Samples were kept at 37°C in a dry-block heater (Techne, Barloworld Scientific Ltd, Stone, UK) between time points. Signals were acquired with CELLQuest software (Beckton-Dickinson Immunocytometry Systems). Forward scatter (FSC) and side scatter (SSC) were acquired in linear mode. TPT signals derived from 488 nm excitation were detected in logarithmic mode at FL1 via a 530/30 filter and TPT signals derived from UV excitation were collected in logarithmic mode at FL4 via a 530/30 filter. All signals were collected for 10000 cells using the forward light scatter as the master signal. TPT uptakes at each time point were corrected to control autofluorescence and normalised to the SU-DHL-4 cells TPT uptake at 10 min. Data are expressed as means of normalised median fluorescence intensity for 5 data sets. All data were analyzed with FlowJo (Tree Star, San Carlos, CA, USA) and GraphPad Prism (GraphPad Software, San Diego, CA, USA).

Continuous time series: Cells were incubated with 10 $\mu$ M TPT for 10 min with or without FTC. Fluorescence was acquired on the same sample continuously for 15 min using the FACS Vantage and the settings described above.



**Single time-point analysis:** Cells were preincubated with or without 10  $\mu\text{M}$  FTC followed by 10 min incubation with TPT (10  $\mu\text{M}$ ). Fluorescence was then acquired on 10000 cells using the settings described above.

#### **IV.2.6. alamarBlue assay**

##### **IV.2.6.1. Method design: continuous exposure vs. end-point assay**

**Continuous exposure:** alamarBlue (Ahmed *et al.*) was purchased from AbD Serotec (Kidlington, UK) and used according to the manufacturer's instructions. Confluent cells (~ 70 %) were detached with CDS (adherent cells) or harvested (suspension) from T75 flasks, spun down and resuspended in 2 mL of full medium. Cells were counted and volumes were adjusted to obtain concentrations of  $1 \times 10^4$ ;  $5 \times 10^4$  or  $10 \times 10^4$  cells / mL. Cell solutions (180  $\mu\text{L}$ ) were added to 96-well plates and cells were allowed to settle down for 24 h, before adding 20  $\mu\text{L}$  of AB (to a final concentration of 10 %). Controls with medium only or medium and AB were included. Plates were incubated at 37°C under 5%  $\text{CO}_2$  in a humidified incubator. Cellular proliferation was assessed at 24 h intervals during 72 h under aseptic conditions, by measuring absorbance using POLARStar OPTIMA plate reader (BMG Labtech, Offenburg, Germany). The plate reader was first blanked with the medium only well and absorbance at 540 nm (reduced form) and 600 nm (oxidized form) were measured.

**End-point assay:** the optimum AB incubation time was determined by plating various concentrations of cells ( $1 \times 10^4$ ;  $5 \times 10^4$  or  $10 \times 10^4$  cells / mL) 96-well plates and incubation as described previously. After 48 h, AB was added to the wells with cells as well as the control wells. Absorbance was measured at 540 nm and 600 nm as described previously at various time after AB addition. The optimum starting cell number was determined by plating various concentrations of cells (1000; 2500; 5000; 10000; 30000; 50000 or 70000 cells / well) in 96-well plates as described previously and overnight incubation prior AB addition. Absorbance at 540 nm and 600 nm was measured 15 h after AB addition.

#### IV.2.6.2. Chemosensitivity testing

Cells were prepared as previously described and plated at a concentration of 5000 cell / well. Cells were allowed to settle down for 24 h before adding various concentrations of TPT to the cells. TPT was also added to control wells without cells. After 4 days of incubation under standard culture conditions, AB was added to the test and control wells. Absorbance was measured 15 h after the addition of AB as previously described.

#### IV.2.6.3. % reduction calculation

Due to an overlap between the absorption spectra of the oxidized and the reduced form, results are expressed as percentage of reduced AB and the calculation is — when samples are read at:  $\lambda_1 = 540$  nm and  $\lambda_2 = 600$  nm — as follows:

$$\% \text{ reduced} = \frac{(\epsilon_{\text{ox}} \lambda_2) \times (A \lambda_1) - (\epsilon_{\text{ox}} \lambda_1) \times (A \lambda_2)}{(\epsilon_{\text{red}} \lambda_1) \times (A' \lambda_2) - (\epsilon_{\text{red}} \lambda_2) \times (A' \lambda_1)} \times 100$$

Where:

$\epsilon_{\text{red}} \lambda_1$  = molar extinction coefficient of reduced AB at 540 nm = 104,395

$\epsilon_{\text{red}} \lambda_2$  = molar extinction coefficient of reduced AB at 600 nm = 14,652

$\epsilon_{\text{ox}} \lambda_1$  = molar extinction coefficient of oxidized AB at 540 nm = 47,619

$\epsilon_{\text{ox}} \lambda_2$  = molar extinction coefficient of oxidized AB at 600 nm = 117,216

$A \lambda_1$  = absorbance of test well at 540 nm

$A \lambda_2$  = absorbance of test well at 600 nm

$A' \lambda_1$  = absorbance of negative control (medium and AB) well at 540 nm

$A' \lambda_2$  = absorbance of negative control (medium and AB) well at 600 nm

### IV.3. Results

#### IV.3.1. ABC transporters expression

Microarray analysis showed that, among the ABC transporters known to be involved in drug efflux, only ABCC1 and ABCC5 were expressed above the detection threshold in all variants. ABCG2 signal was found equivalent and flagged as absent for all variants (see figure IV.2).

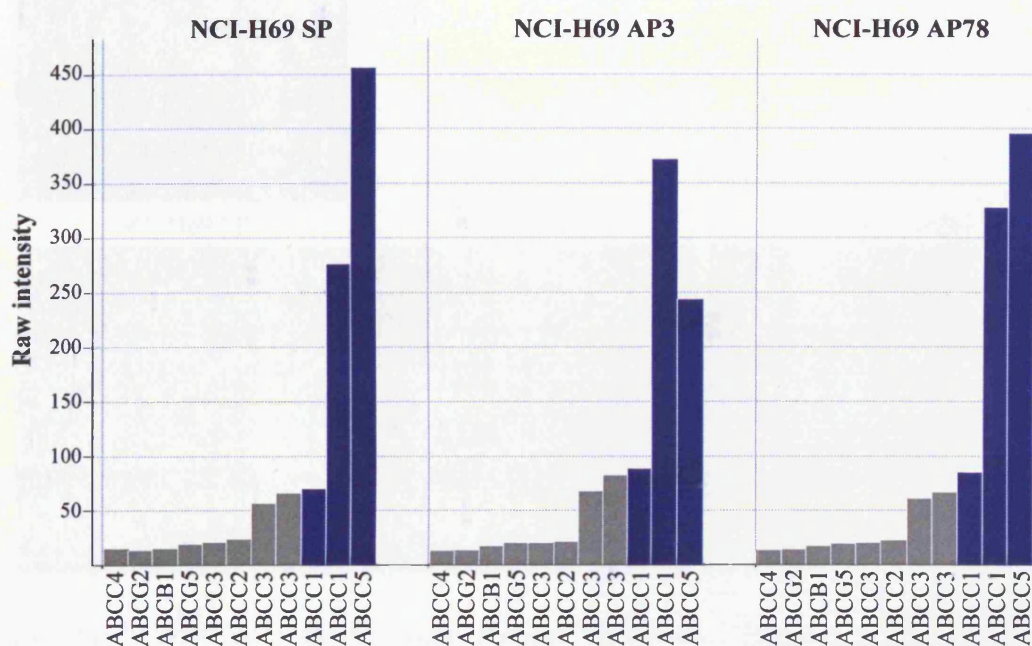


**Figure IV.2:** ABC transporters expression in NCI-H69 variants. Graph representing the raw intensity (without per gene normalisation) of the average value of the triplicates for ABC transporters known to be involved in drug resistance. Grey bars represent genes whose expression was flagged as absent.

ABCG2 expression and localisation was further examined using immunofluorescence (figure IV.3). The human lung alveolar cell carcinoma A549 cell line, previously shown to express ABCG2 (Scharenberg *et al.*, 2002) was used as the positive control for ABCG2 detection. All A549 cell appeared to express ABCG2, however the population showed heterogeneity, with some cells expressing elevated amounts of the transporter protein, possibly representing the side population phenotype cells. All of the variants showed positive staining for ABCG2. The signal seemed to be higher for both adherent

variants compared to the suspension cell line. Again, all variants showed heterogeneity in ABCG2 expression in their cell populations. However, western blotting, using the same antibody, failed to detect ABCG2 in all the NCI-H69 variants and the A549 cell lines, reinforcing the need for a functional analysis of ABCG2.

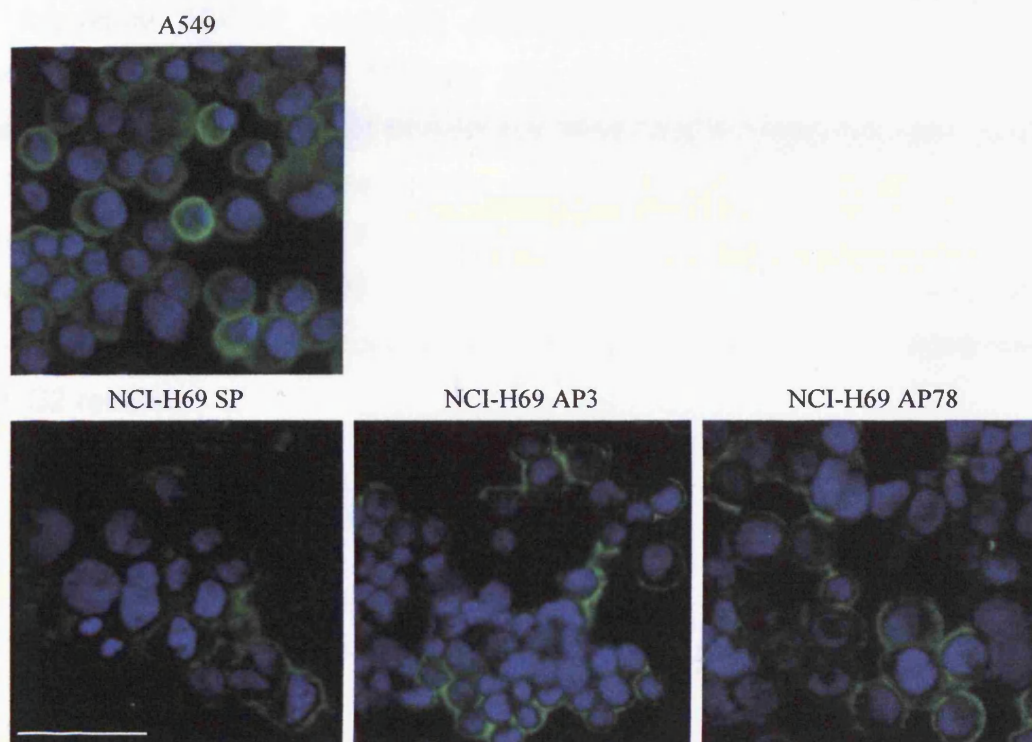


**Figure IV.3:** *ABCG2 immunofluorescence detection.* Images representing the immunodetection of cytospined, methanol fixed cells stained for ABCG2 (x 40 oil magnification). Calibration bar represents 50  $\mu\text{m}$ .

### **IV.3.2. ABCG2 profiling and function**

Functional profiling of ABCG2 activity was performed using flow cytometry detection of the uptake/exclusion of the reporter dye Hoechst 33342 with or without the presence of the ABCG2 inhibitor — Fumitremorgin (FTC). This was initially performed and validated in ABCG2-expressing A549 cell line. Uptake of Hoechst 33342 was significantly higher in cells treated with FTC compared to the non-treated cells (median fluorescence of 195 vs. 232) consistent with functional ABCG2 expression. A clear cell cycle distribution could only be seen on the A549 samples treated with FTC (figure IV.4),

suggesting that stoichiometry was only reached when the efflux pumps were blocked. In addition, 37.5% of non-FTC treated cells had a lower signal than that of the cells in G1 in the treated samples, indicating a sub-fraction of low loading cells.

The Hoechst 33342 profiles for all NCI-H69 cell lines were equivalent for the untreated sample and its corresponding treated counterpart, indicating that no functional ABCG2 could be detected within the limits of the assay. Consistent with previous findings (see chapter III), median fluorescence increased with the degree of enrichment (NCI-H69 SP/132, NCI-H69 AP3/202 and NCI-H69 AP78/320) essentially reflecting the increase in cellular DNA content. The NCI-H69 SP DNA profile was consistent with previous finding (see chapter III), while, NCI-H69 AP3 and NCI-H69 AP78 profiles were slightly skewed. However, this was not sensitive to FTC addition and therefore was not ABCG2 related.



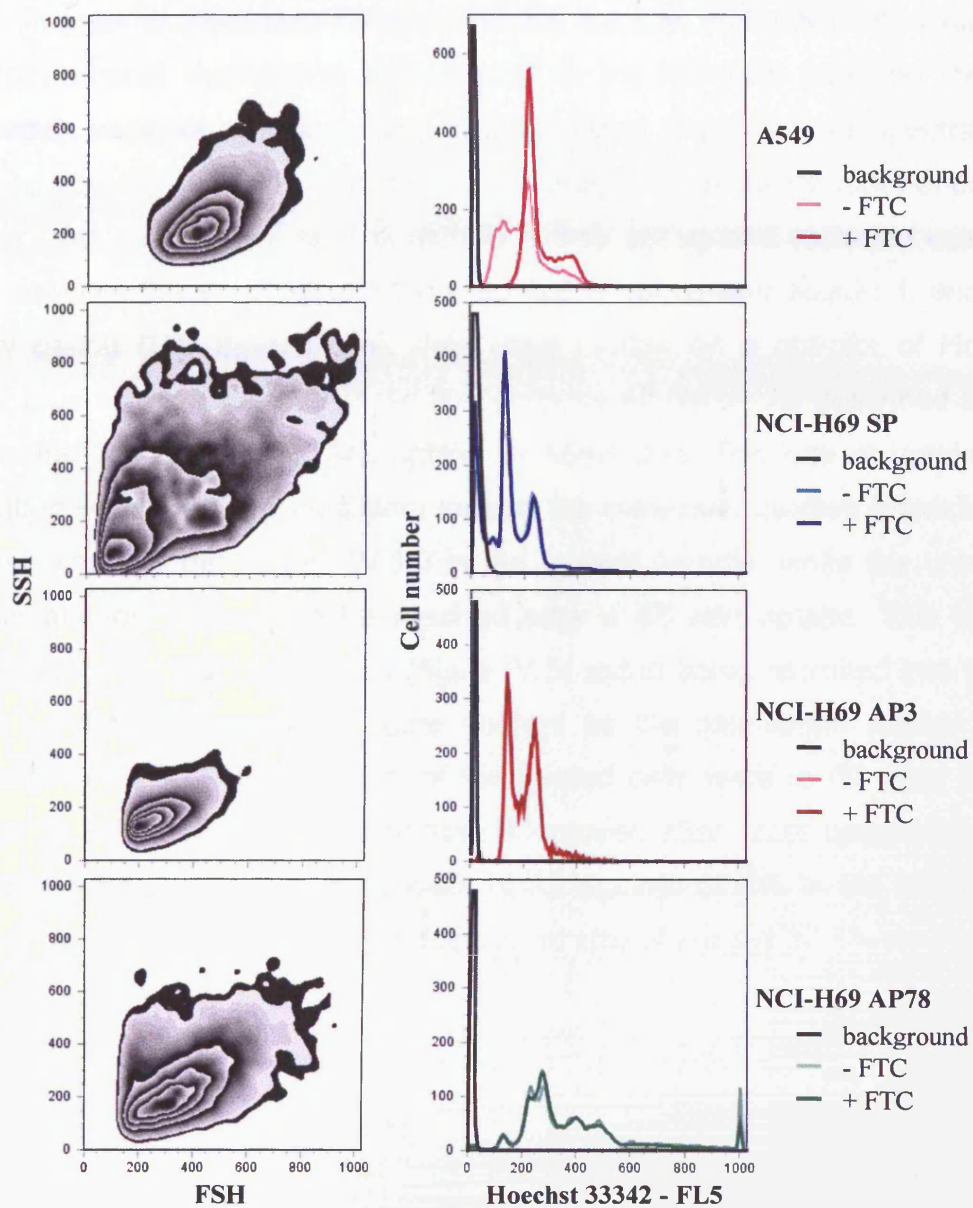


**Figure IV.4:** Hoechst 33342 uptake profiles in the A549 and each of the NCI-H69 variants. The cells were preincubated for 1h with 10  $\mu$ M FTC or DMSO, before incubation with 5  $\mu$ M Hoechst 33342 (60 min). Data shown are representative of n=2.



### **IV.3.3. Identification and analysis of the side population phenotype**

In order to determine if a rare CSC-like fraction, so far not detectable with the conventional techniques, was present in the NCI-H69 variants, the side population analysis approach was applied, since the extent of spectral shift used to identify the side population phenotype is relatively independent of cellular DNA content *per se*. The technique was set up and validated using the A549 cell line. Dual-wavelength Hoechst fluorescence was acquired, and after quality gating (R1/ figure IV.5a), data were plotted on a dot-plot of Hoechst 33342 blue vs. Hoechst 33342 red fluorescence emission. As described above, FTC enhanced Hoechst 33342 uptake in A549 cells. The rate of uptake was also affected by ABCG2 inhibition, indeed the maximum median intensity was reached after 20 min (figure IV.5b) in the treated sample, while the untreated sample plateau seemed to be reached after a 60 min uptake. This can be explained by the number of cells (figure IV.5c and d) being recruited into the R2 sector — the side population gate defined as the diminished region in the presence of FTC — indeed 93% of the treated cells were in R2 after 20 min against 34.8% in the untreated sample. Moreover, after 1h of uptake 99.5% of cells of the FTC treated sample were in R2 against 62.8% in the non-treated sample, making an estimated side population size of around 37.5% for the A549 cells.

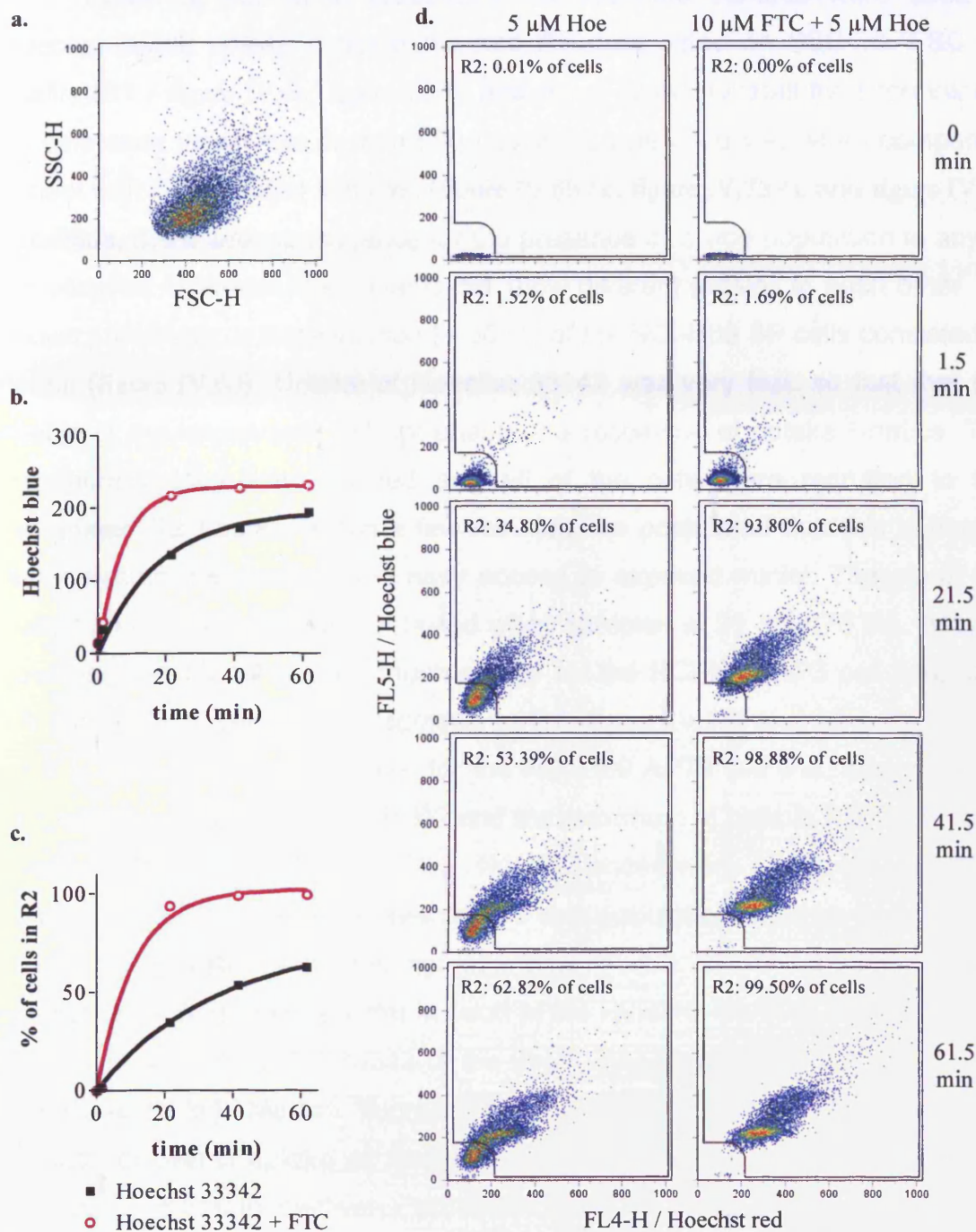


**Figure IV.5:** A549 Hoechst 33342 uptake profiles. **a.** Scatter plot of side vs. forward scatter after quality gating (R1). **b.** Median fluorescence intensity of the FL5-H / Hoechst 33342 blue channel (high affinity binding sites) taken from the whole population (R1 gate) over time. **c.** Recruitment of cells to the R2 segmentation gate (% of whole R1 population) over time. **d.** Time series scatter plot showing the uptake and distribution of the Hoechst 33342 (blue channel) fluorescence vs. Hoechst 33342 (red channel) fluorescence. R2 indicates the segmentation gate for positive labelled cells. Numbers indicate the fraction of cells in the R2 gate. Left column represents control conditions, right column indicates FTC treated cells. All curves were fitted using a non-linear regression.

Following the same procedure, the NCI-H69 variants were used in Hoechst 33342 uptake experiments and the data gated on SSC vs. FSC for quality (R1 / figure IV.6a, figure IV.7a and figure IV.8a). Overall for each variant no difference in accrual or mean fluorescence was observed when comparing control with FTC-treated samples (figure IV.6b / c, figure IV.7b / c and figure IV.8b / c). Thus, there was no evidence for the presence of a side population in any of the variants. However, the variants did show different profiles to each other. As shown previously, a large fraction (~ 30 %) of the NCI-H69 SP cells consisted of debris (figure IV.6d). Uptake of Hoechst 33342 was very fast, so fast that the design of the experiment did not enable the resolution of uptake kinetics. The maximum uptake was reached and all of the cells were recruited to the designated R2 fraction within a few minutes, we postulated that this is due to leaky plasma membranes and easy access to exposed nuclei. Therefore, the maximum of cells in R2 was obtained when sampled at 21 min (75 %). Uptake, however, can be considered much slower for the NCI-H69 AP3 cell line, after 1.5 min, 8 % of cells were displaced to R2 (figure IV.7d) and all cells (98 %) were in R2 after 21 min. Finally, for the NCI-H69 AP78 cell line, after 1.5 min, 13% of the cells were located in R2 and the maximum of cells in R2 (98 %) was obtained after 21 min (figure IV.8d). No differences were observed upon FTC treatment for all NCI-H69 cell lines and no side population could be detected.

Having established the non-operation of the ABCG2 transporter with respect to the surrogate reporter in each of the variants, we then considered the overall uptake of Hoechst 33342 of the three variants (figure IV.6b, figure IV.7b and figure IV.8b). Median fluorescence for the R2 gated cells showed an increase of overall uptake as the cells were enriched for substrate adherence (120, 200 and 350 respectively), probably due to the increase of volume of each of the cell populations (see chapter III). Indeed, volume increments (NCI-H69 AP78 = NCI-H69 AP3 x 1.7 = NCI-H69 SP x 1.4) correlate with Hoechst 33342 median fluorescence increments (NCI-H69 AP78 = NCI-H69 AP3 x 1.75 = NCI-H69 SP x 1.6). This indicates that the concentration of dye per cell is probably equivalent. Therefore, there is no indication that the uptake of the minor groove ligand Hoechst 33342 differs across the variants. This provided the foundation work for the topoisomerase I inhibitor topotecan. In the case of TPT there is no evidence of fluorescence enhancement upon DNA binding (Gryczynski *et al.*,

1999) although the affinity will be significantly lower than for the Hoechst 33342-DNA complex. Parallel studies in the laboratory had indicated the rapid loss (> 50% loss of intracellular fluorescence 5 min after drug removal) of TPT from the cell suggesting that TPT may provide a more sensitive responding molecule for subtle changes in drug efflux capacity. The hypothesis is that the pharmacokinetics of TPT is the same across all the variants and any differences are not ascribable to ABCG2 function.

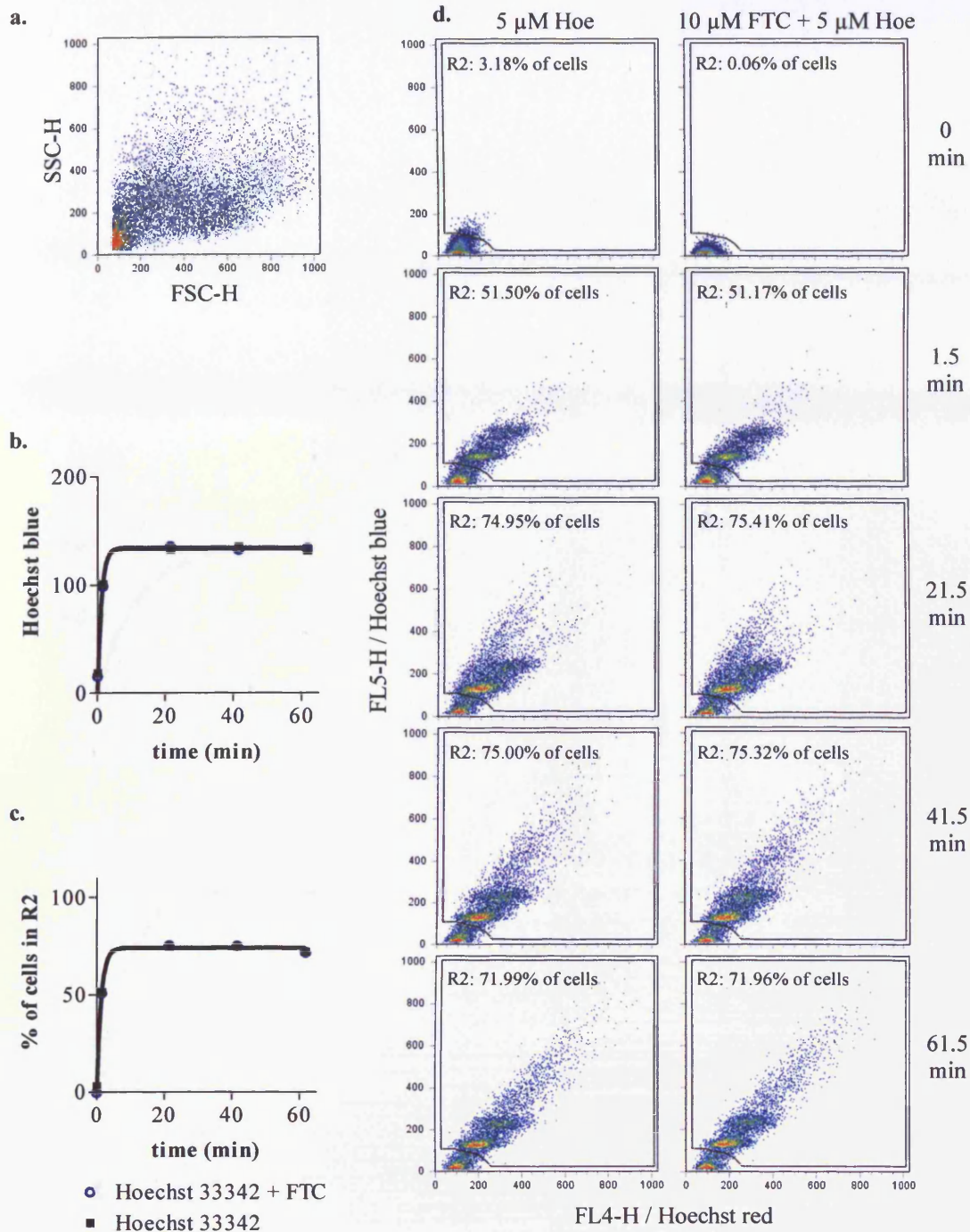


**Figure IV.6:** NCI-H69 SP Hoechst 33342 uptake profiles. **a.** Scatter plot of side vs. forward scatter after quality gating (R1). **b.** Median fluorescence intensity of the FL5-H / Hoechst 33342 blue channel (high affinity binding sites) taken from the whole population (R1 gate) over time. **c.** Recruitment of cells to the R2 segmentation gate (% of whole R1 population) over time. **d.** Time series scatter plot showing the uptake and distribution of the Hoechst 33342 (blue channel) fluorescence vs. Hoechst 33342 (red channel) fluorescence. R2 indicates the segmentation gate for positive labelled cells. Numbers indicate the fraction of cells in the R2 gate. Left column represents control conditions, right column indicates FTC treated cells. All curves were fitted using a non-linear regression.



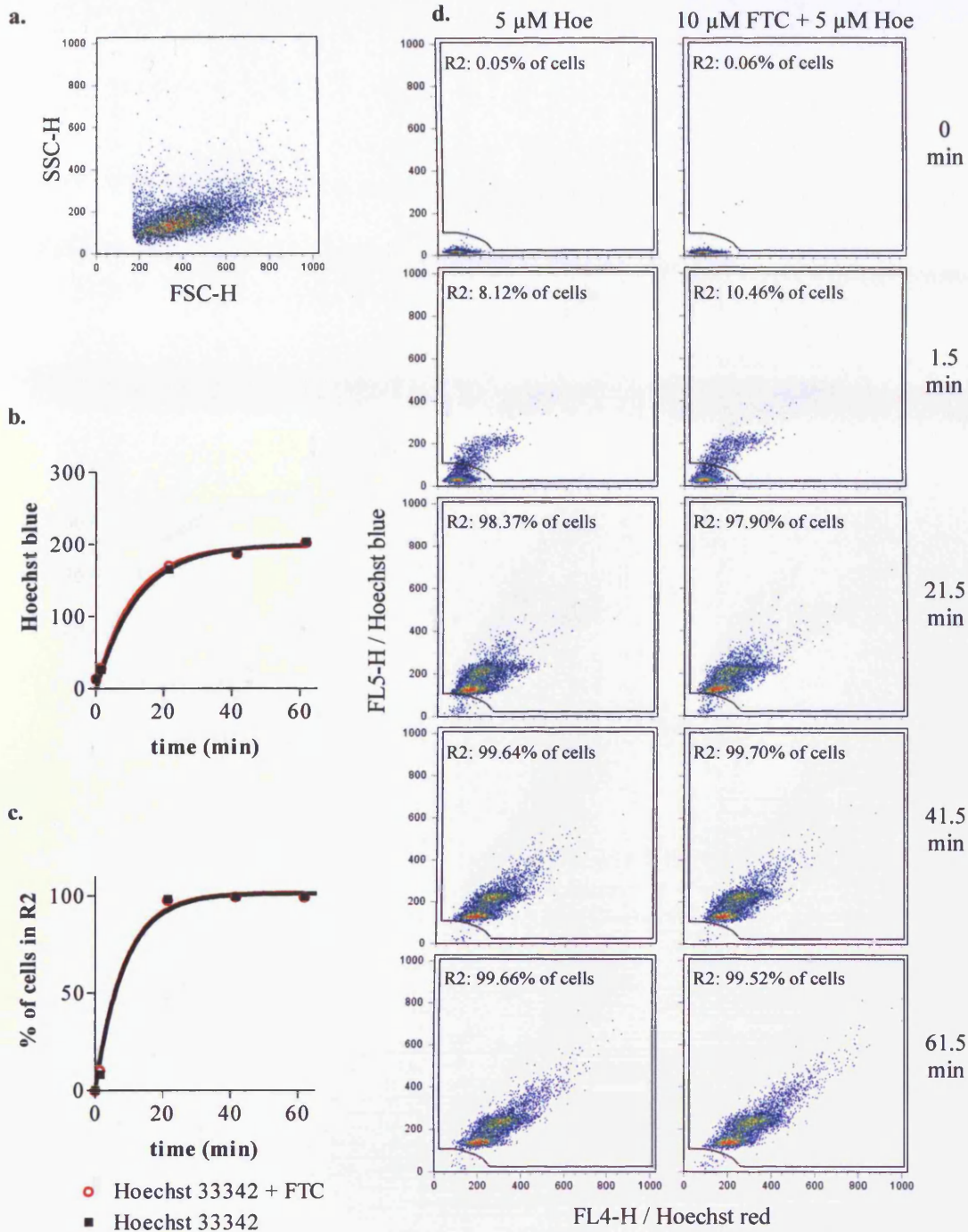


**Figure IV.7:** NCI-H69 AP3 Hoechst uptake profiles. **a.** Scatter plot of side vs. forward scatter after quality gating (R1). **b.** Median fluorescence intensity of the FL5-H / Hoechst 33342 blue channel (high affinity binding sites) taken from the whole population (R1 gate) over time. **c.** Recruitment of cells to the R2 segmentation gate (% of whole R1 population) over time. **d.** Time series scatter plot showing the uptake and distribution of the Hoechst 33342 (blue channel) fluorescence vs. Hoechst 33342 (red channel) fluorescence. R2 indicates the segmentation gate for positive labelled cells. Numbers indicate the fraction of cells in the R2 gate. Left column represents control conditions, right column indicates FTC treated cells. All curves were fitted using a non-linear regression.



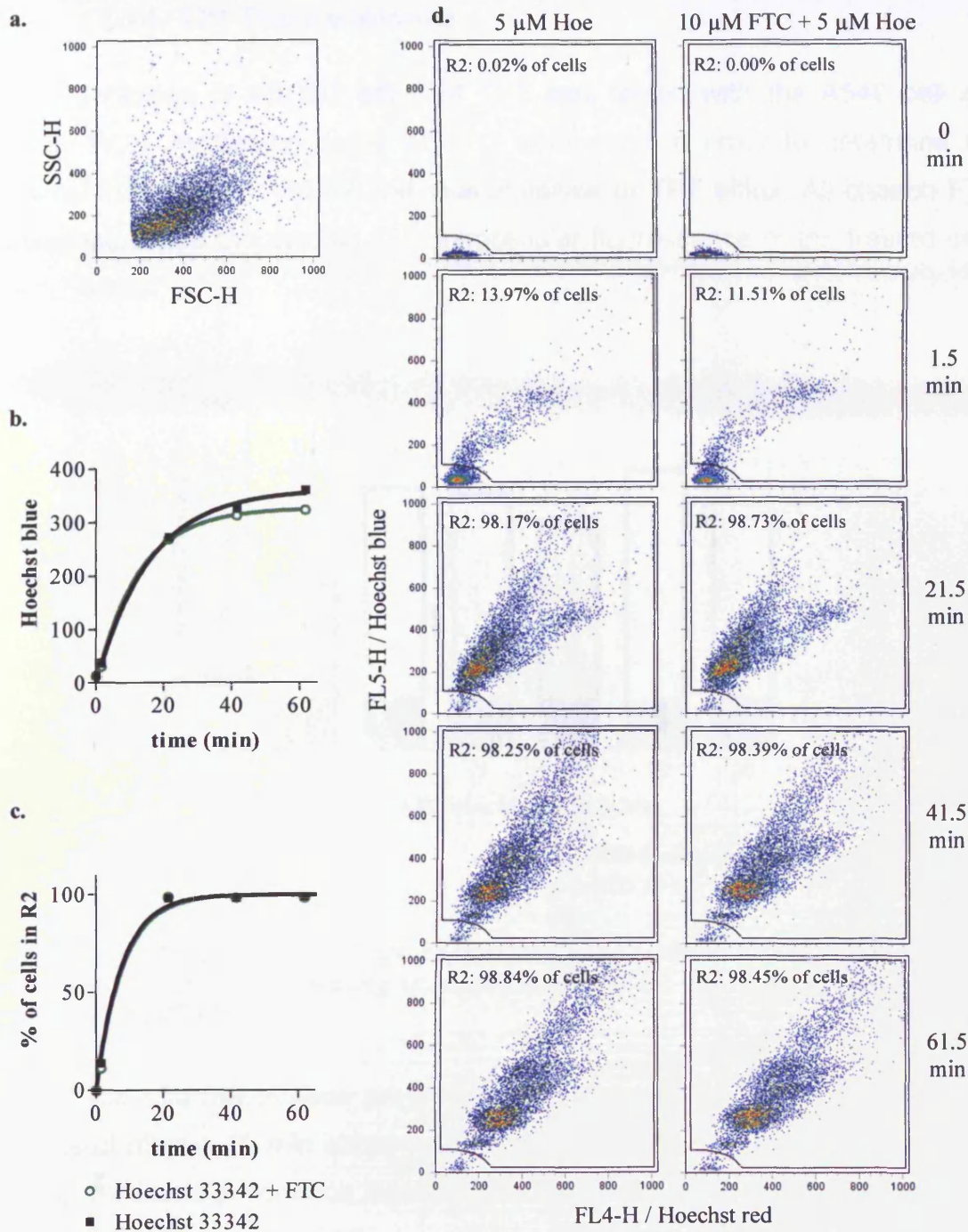


**Figure IV.8:** NCI-H69 AP78 Hoechst uptake profiles. **a.** Scatter plot of side vs. forward scatter after quality gating (R1). **b.** Median fluorescence intensity of the FL5-H / Hoechst 33342 blue channel (high affinity binding sites) taken from the whole population (R1 gate) over time. **c.** Recruitment of cells to the R2 segmentation gate (% of whole R1 population) over time. **d.** Time series scatter plot showing the uptake and distribution of the Hoechst 33342 (blue channel) fluorescence vs. Hoechst 33342 (red channel) fluorescence. R2 indicates the segmentation gate for positive labelled cells. Numbers indicate the fraction of cells in the R2 gate. Left column represents control conditions, right column indicates FTC treated cells. All curves were fitted using a non-linear regression.

#### IV.3.4. TPT Pharmacokinetics

Inhibition of ABCG2 efflux of TPT was tested with the A549 cell line (figure IV.9), increasing doses of FTC were used in order to determine the optimal inhibition of ABCG2 and thus inhibition of TPT efflux. All chosen FTC doses increased the median TPT intracellular fluorescence of the treated cells by 1.7 times.

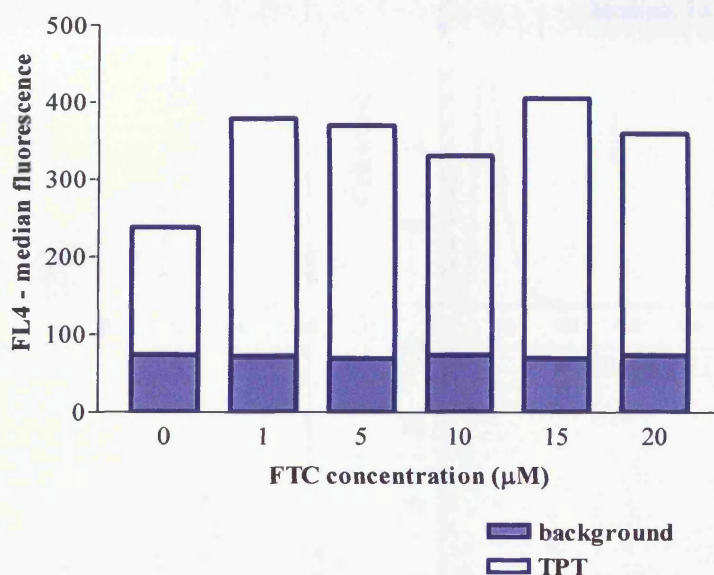


**Figure IV.9:** Modulation of TPT uptake with the ABCG2 inhibitor FTC. A549 cells were pretreated for 1h with increasing concentrations of FTC and followed by a 10 min treatment of TPT (10 µM).

The pharmacokinetic properties of TPT in the NCI-H69 variants were assessed after a 10 min exposure to 10 µM of TPT by flow cytometry (figure IV.10). Median fluorescence signals were similar for the NCI-H69 SP and NCI-H69 AP3 (161.3 and 157.3 respectively). As expected due to higher DNA content and cell volume, overall uptake in the NCI-H69 AP78 population was greater (median fluorescence of 217.7). Interestingly, the spread of fluorescence across the entire population was narrow for the NCI-H69 AP3, while NCI-H69 SP and NCI-H69 AP78 population displayed a broader distribution, probably a reflection in heterogeneity in cell volume, while the NCI-H69 AP3 variant represent an acutely selected population (as indicated by the forward scatter signal).



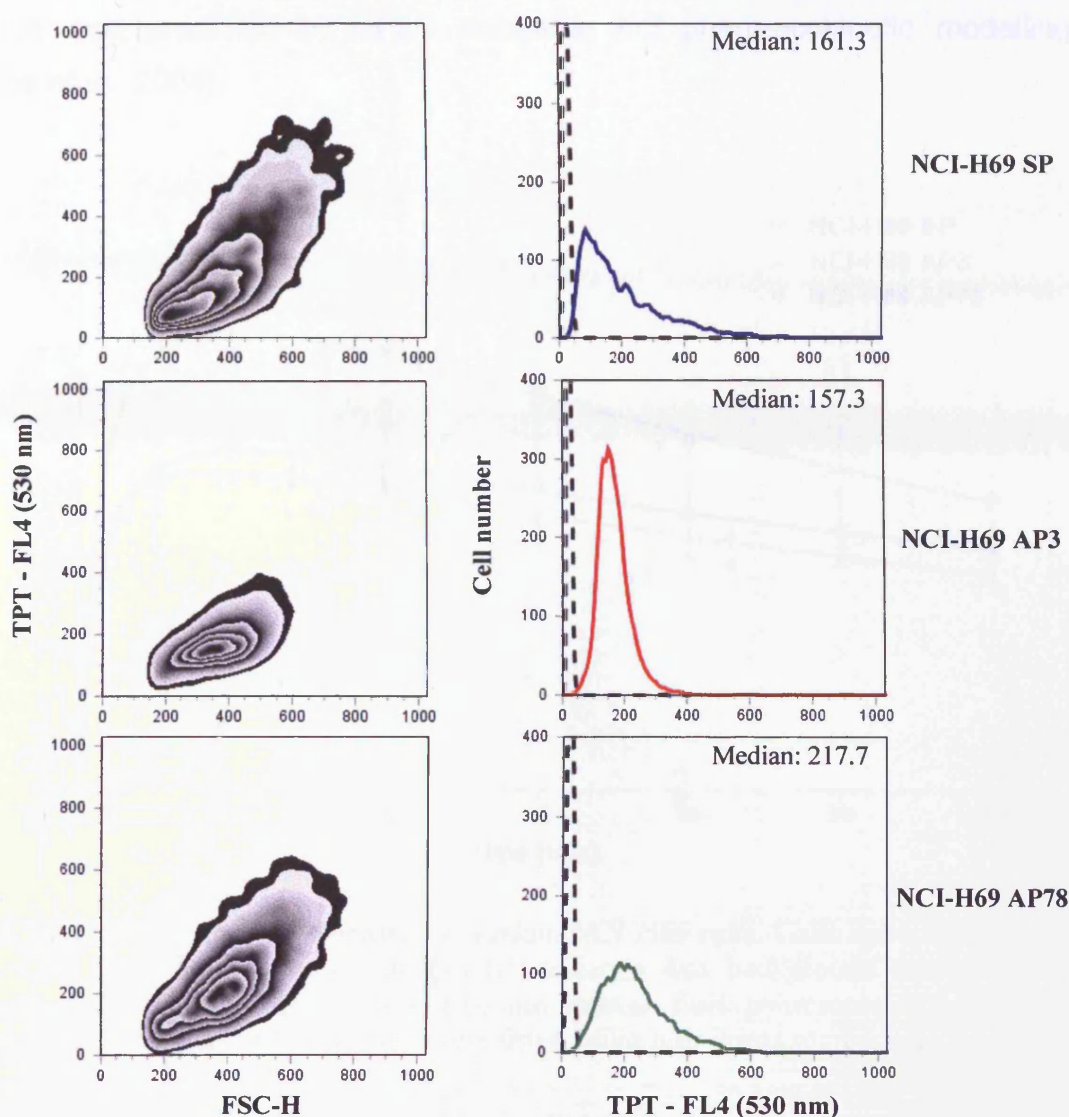
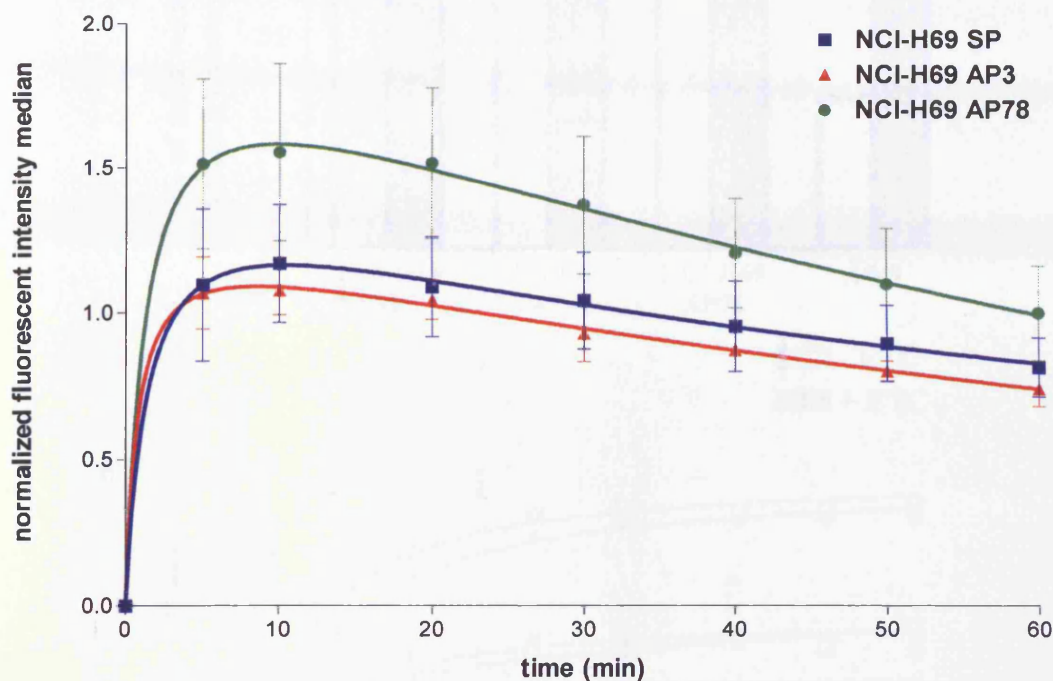


Figure IV.10: Differences of TPT uptake for the NCI-H69 variants. Cells were treated with 10  $\mu$ M of TPT for 10 min. The left column represents the forward scatter vs. TPT fluorescence detected at 530 nm for each NCI-H69 variant. The right column represents the fluorescent intensity distribution profile (the dotted line represent the background fluorescence). The figure represents a typical experiment (n=5).

Topotecan uptake was observed over time by extracting the fluorescence signal at designated time intervals from the same sample (figure IV.11). As observed above, similar levels of fluorescence were detected for the NCI-H69 SP and NCI-H69 AP3 and a higher median signal for the NCI-H69 AP78 cell line throughout the entire 60 min uptake experiment. TPT fluorescence peaked after 10 minutes followed by a slow decline in TPT fluorescence in all cell lines,

this is due to the removal of the lactone form of TPT (active pool of TPT) in the medium and predicted by HPLC analyses and pharmacokinetic modelling (Evans *et al.*, 2004).



**Figure IV.11:** Profiles of TPT uptake for variant NCI-H69 cells. Cells were treated with 10  $\mu$ M of TPT. Each value of median fluorescence was background corrected and normalised to the value of the control at 10 min uptakes. Each point represents the mean  $\pm$  SD of 5 experiments and the curves were fitted using non-linear regression.

As expected, inhibition of ABCG2 had no effect on TPT uptake for all the variants, while TPT uptake was significantly increased in the control A549 cell line upon FTC pre-treatment (figure IV.12a). FTC also had no effect on the overall rate of the uptake (figure IV.12b). For all variants, a plateau was reached after 8 min, with or without FTC. It is important to note that in this experiment the assay was conducted at room temperature, the overall effect was that TPT fluorescence was maintained over the entire 15 minutes, as opposed to the findings in figure IV.11.

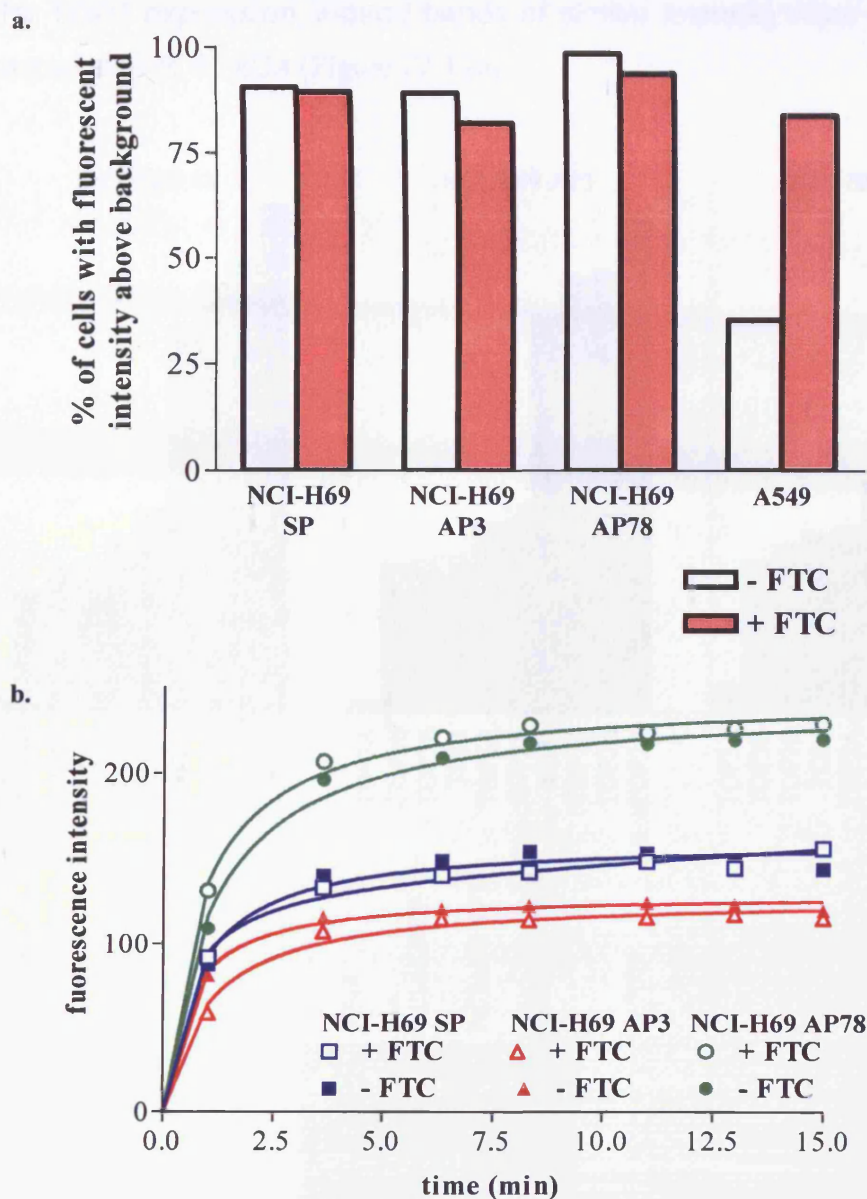


Figure IV.12: FL4 signal of TPT uptakes with or without FTC. **a.** Cells were preincubated 1h with 10  $\mu$ M FTC or DMSO followed by incubation with 10 $\mu$ M TPT for 10 min. **b.** Continuous TPT uptake over 15 min with or without 10  $\mu$ M FTC. Curves were fitted using non-linear regression.

### IV.3.5. TPT pharmacodynamics – the overall response to topotecan

#### IV.3.5.1. Topoisomerase expression

Microarray analysis showed that all subclasses of topoisomerase were present in all the variants and that their expression levels were equivalent in all NCI-H69 cell variants (Figure IV.13a). Western blotting confirmed the microarray



results for TOP1 expression, indeed bands of similar intensity were detected at the expected size of 91 kDa (Figure IV.13b).

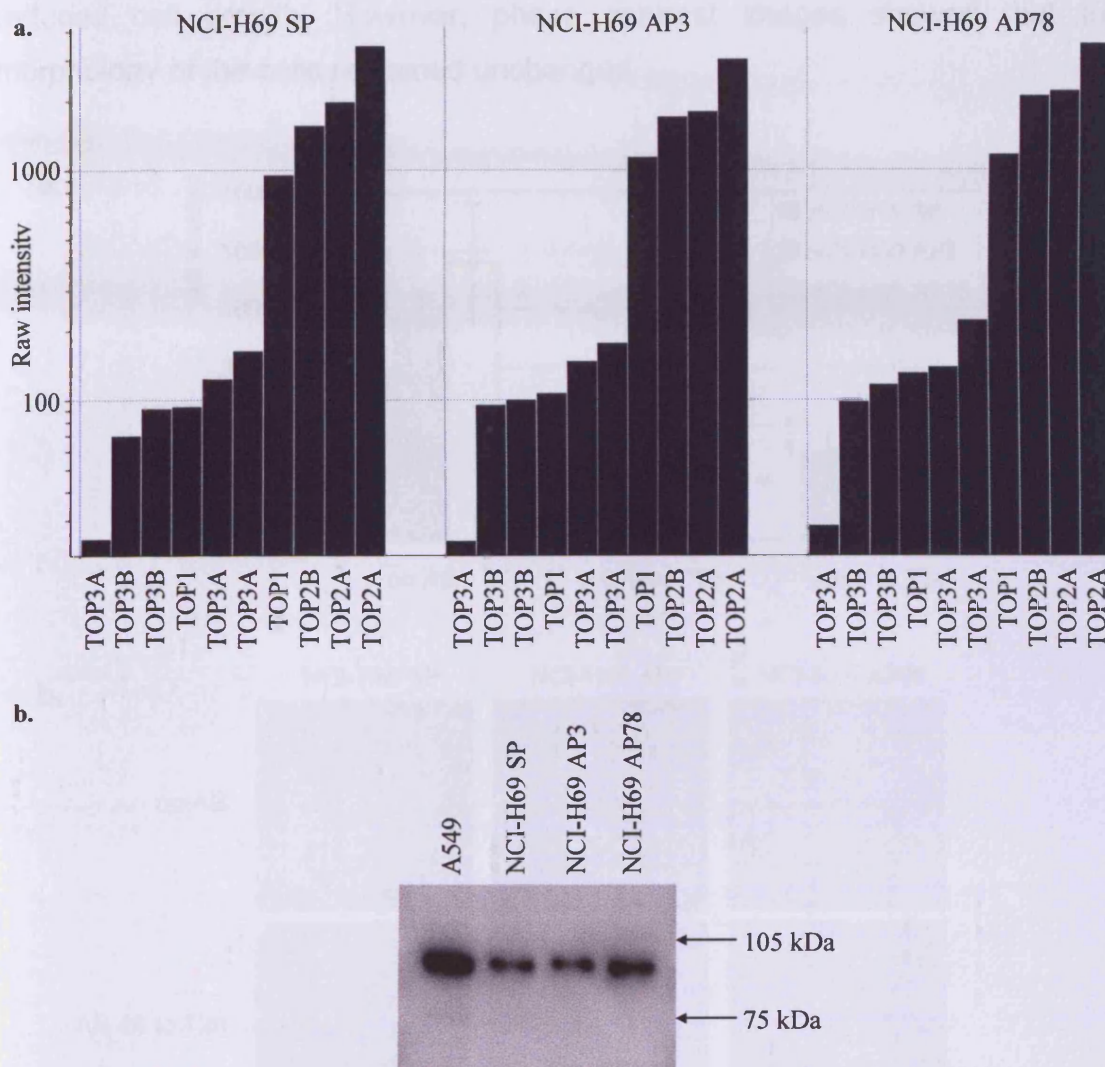


**Figure IV.13:** *Topoisomerase expression across all NCI-H69 variants.* **a.** Microarray analysis of topoisomerases expression. Graph depicting the raw intensity value of the value of the triplicates (without per gene normalisation). **b.** Western blotting detection of topoisomerase I. Western blot shown is representative of 2.

#### IV.3.5.2. alamarBlue method implementation and optimisation

The alamarBlue (AB) assay is a cell proliferation assessment method based on the reduction of the tetrazolium salt, alamarBlue, in cells. The molecule is soluble, stable in culture medium and putatively non-toxic allowing continuous monitoring (Ahmed *et al.*, 1994). However, alamarBlue was revealed to be toxic for NCI-H69 variants. Indeed, cells exposed over 72h to alamarBlue



showed a significant decrease in growth (figure IV.14a). Snap-shots taken after 72h showed that cells died upon exposure to alamarBlue (figure IV.14b). Furthermore, addition of AB for the last 24 h of a 72 h experiment also caused a reduced cell growth. However, phase contrast images showed that the morphology of the cells remained unchanged.

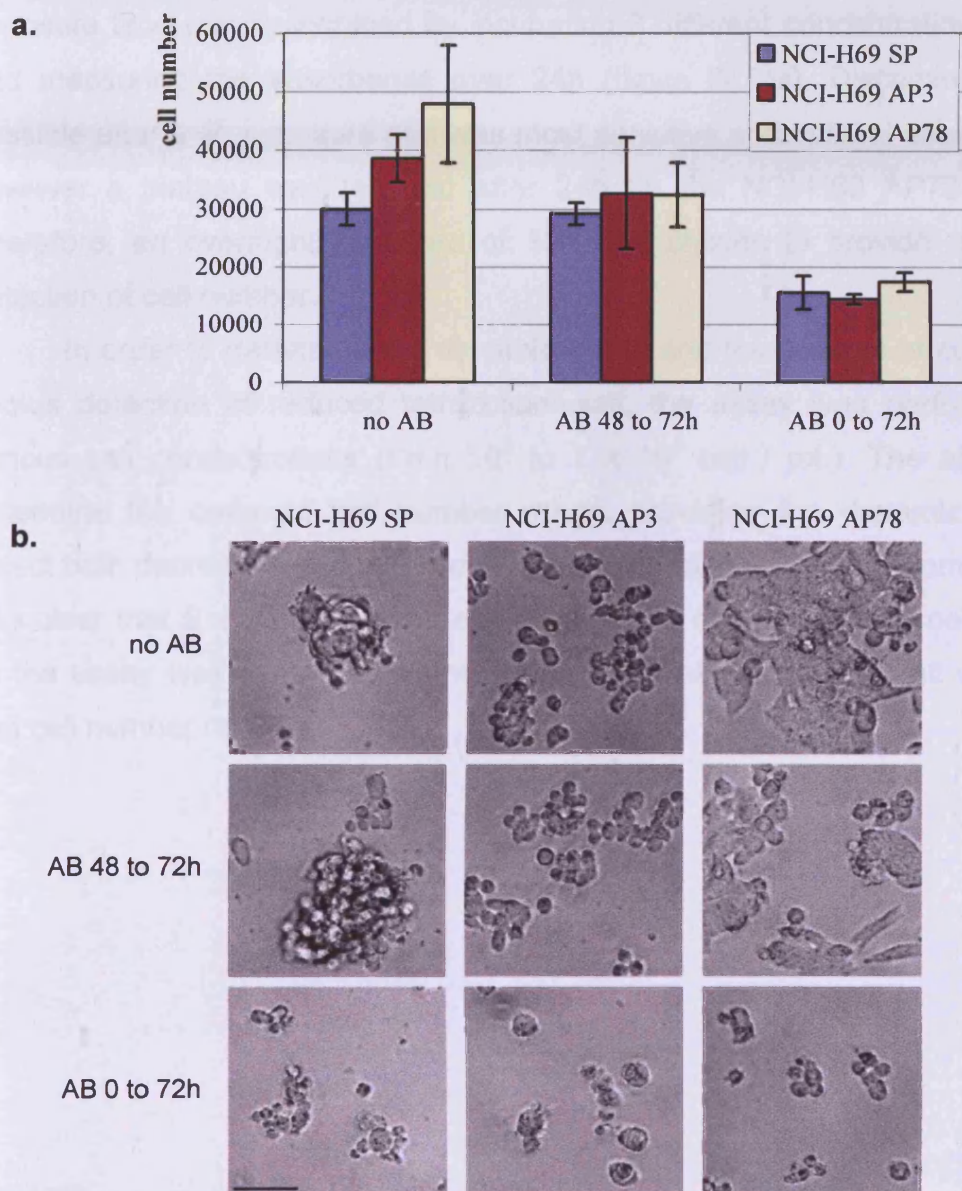


**Figure IV.14:** *Continuous alamarBlue exposure is toxic for all NCI-H69 variants.* Cells were incubated in a 96-well dish for 72h without alamarBlue (AB), with AB added at  $t = 48h$  or  $t = 0h$ . Data is representative of two independent experiment. **a.** After 72h cells were harvested and counted. **b.** Phase contrast images of the variant cells captured at  $t = 72h$  to show the overall morphology. Calibration bar represents  $50 \mu m$ .

Continuous incubation with AB was too invasive and therefore not a viable option, because of its cytotoxic effects. Therefore an end-point assay was developed, ensuring the optimization of the start cell number and minimising overall exposure to AB. In addition the assay had to be able to discriminate different cell numbers (assay sensitivity), by avoiding a shortage of substrate and further reagent reduction to a colourless substrate (figure IV.15). The exposure time was determined by incubating 3 different concentrations of cells and measuring the absorbance over 24h (figure IV.15a). Discrimination was possible after a 4h exposure and was most sensitive and optimal after 12h-24h, however a plateau was reached after 24h for the NCI-H69 AP78 cell line. Therefore, an overnight exposure of 15h was chosen to provide an optimal detection of cell number.

In order to determine the dynamic range and relationship of cell number versus detection of reduced tetrazolium salt, the assay was performed with various cell concentrations (from  $10^3$  to  $7 \times 10^4$  cell / mL). The aim was to determine the optimum cell number range, providing the dynamic range to detect both decreased and enhanced cell growth (figure IV.15b). From the plot it was clear that  $5 \times 10^4$  cells / mL represented the optimal starting cell number, as the assay was sensitive to small changes in cell number for all variants in that cell number range.

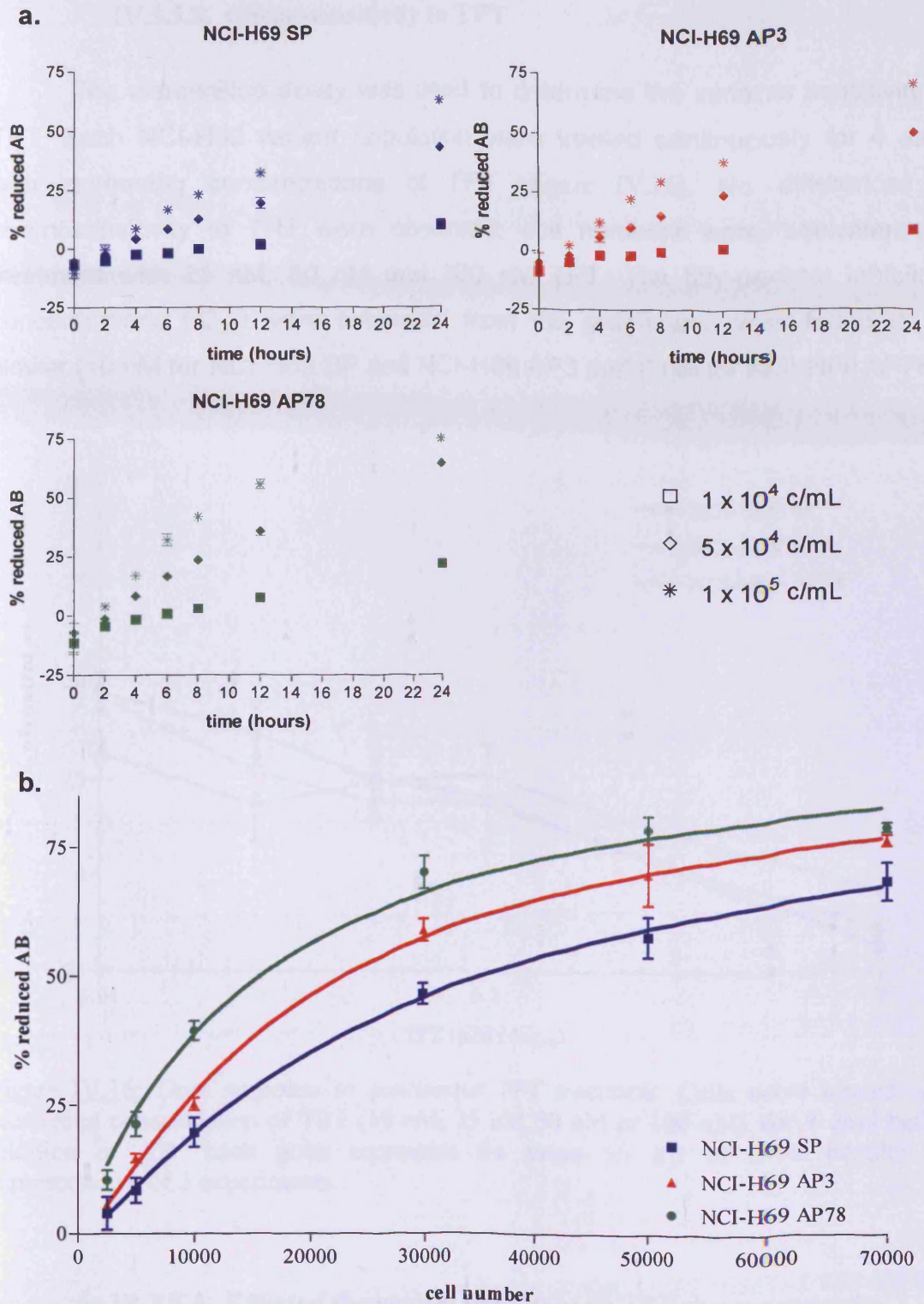


**Figure IV.15: AlamarBlue method optimization.** **a.** 1800, 9000 and 18000 cells / well were exposed to alamarBlue and absorbance was measured at various times over 24h. Results are representative of 2 experiments. Each point represents the mean +/- SD of n=4. **b.** Increasing cell numbers were exposed to alamarBlue for 15h. Results are representative of 2 experiments. Each point represents the mean +/- SD of n=4. Curves were fitted using non-linear regression.



### IV.3.5.3. Chemosensitivity to TPT

The alamarBlue assay was used to determine the variants sensitivity to TPT. Each NCI-H69 variant population were treated continuously for 4 days with increasing concentrations of TPT (figure IV.16). No differences in chemosensitivity to TPT were observed; cell numbers were equivalent for treatment with 25 nM, 50 nM and 100 nM TPT. The fifty-percent inhibitory concentrations ( $IC_{50}$ ) were estimated from the graph and were found to be similar (10 nM for NCI-H69 SP and NCI-H69 AP3 and 6 nM for NCI-H69 AP78).

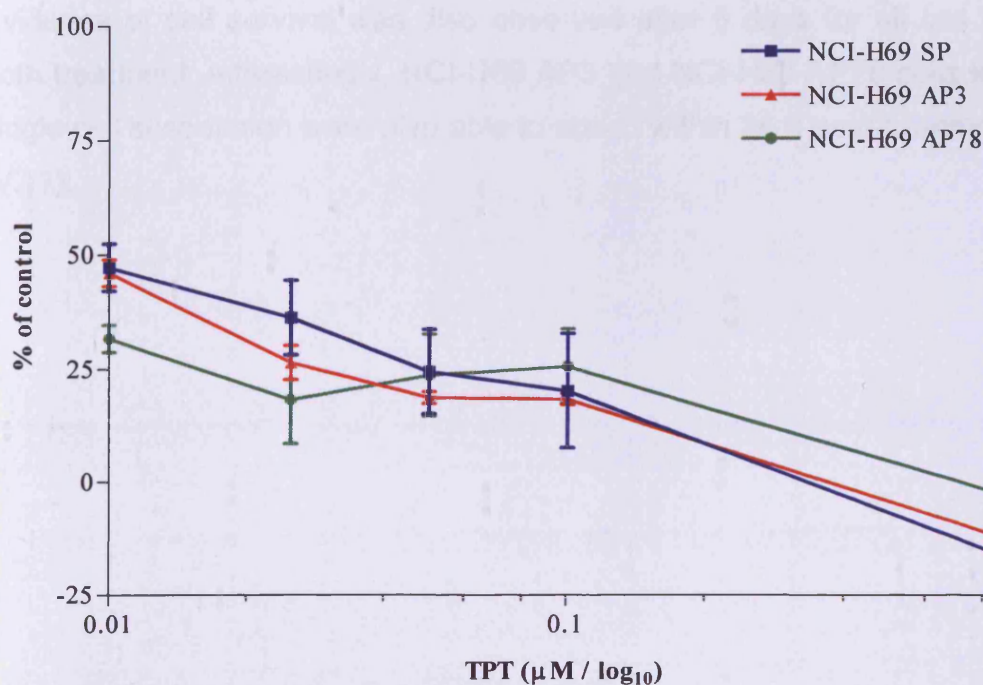


**Figure IV.16:** Dose response to continuous TPT treatment. Cells were treated with increasing concentration of TPT (10 nM, 25 nM 50 nM or 100 nM) for 4 days before addition of AB. Each point represents the mean  $\pm$  SD of  $n=4$ . Results are representative of 3 experiments.

### IV.3.5.4. Effect of the variant phenotype on TPT chemosensitivity

Alongside the alamarBlue studies, another approach was undertaken to determine the consequences of TPT treatment on the NCI-H69 variants, simply by observing cell morphology, cell-substrate interactions and the extent of cell-cell adhesion using phase contrast microscopy. There were two designs of the

treatment experiments performed to decipher the effect of substrate-adhesion on the chemosensitivity of the variants to TPT. The first scenario entailed the removal of the cells from the plastic substrate (*i.e.* NCI-H69 AP3 and NCI-H69 AP78 cells were detached) and treatment as a single cell suspension (figure IV.17) for 1h with 10  $\mu$ M TPT and then re-seeded into a plastic well. Here the aim was to remove conformation-based limitations on drug access. For the second scenario, cells were seeded for a full 24 hours (enabling them to assume their normal cell-cell or cell-substrate phenotypic behaviour) prior to a 1 hour treatment with 10  $\mu$ M TPT (figure IV.18). In all cases cell death was apparent from 48h onwards for all cell lines treated before or after reseeding. Evidence of cell survival was also observed after 5 days for all cell lines and both treatment. Interestingly, NCI-H69 AP3 and NCI-H69 AP78 cells treated as single cell suspension were also able to attach within 24 h post-treatment (figure IV.17).

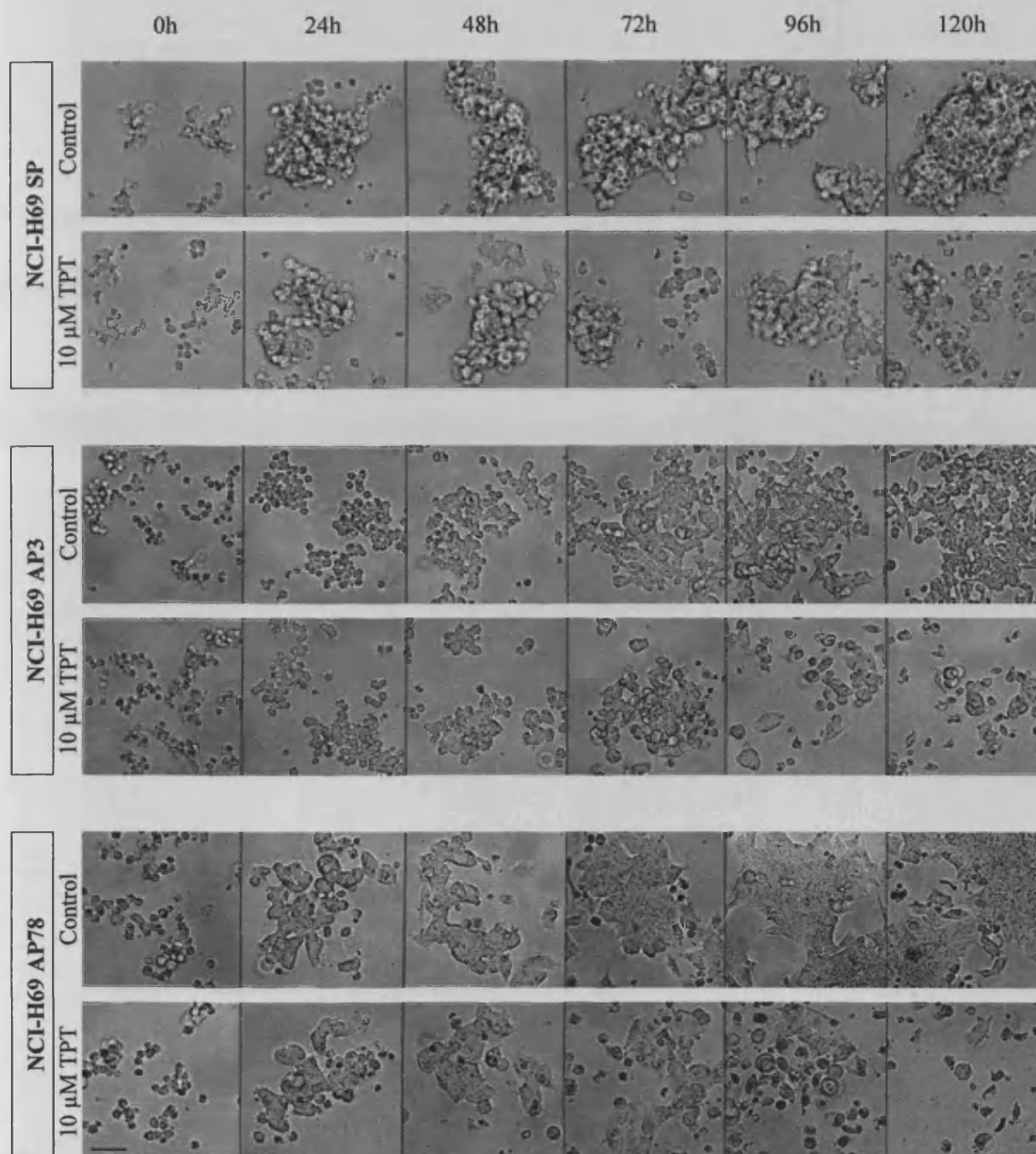


Figure IV.17: TPT treatment of all NCI-H69 variants as single cell suspension. Single cell suspensions were treated for 1h with 10  $\mu$ M TPT and then seeded into individual wells. Images were taken at random separate fields for each time point. Calibration bar represents 50  $\mu$ m.



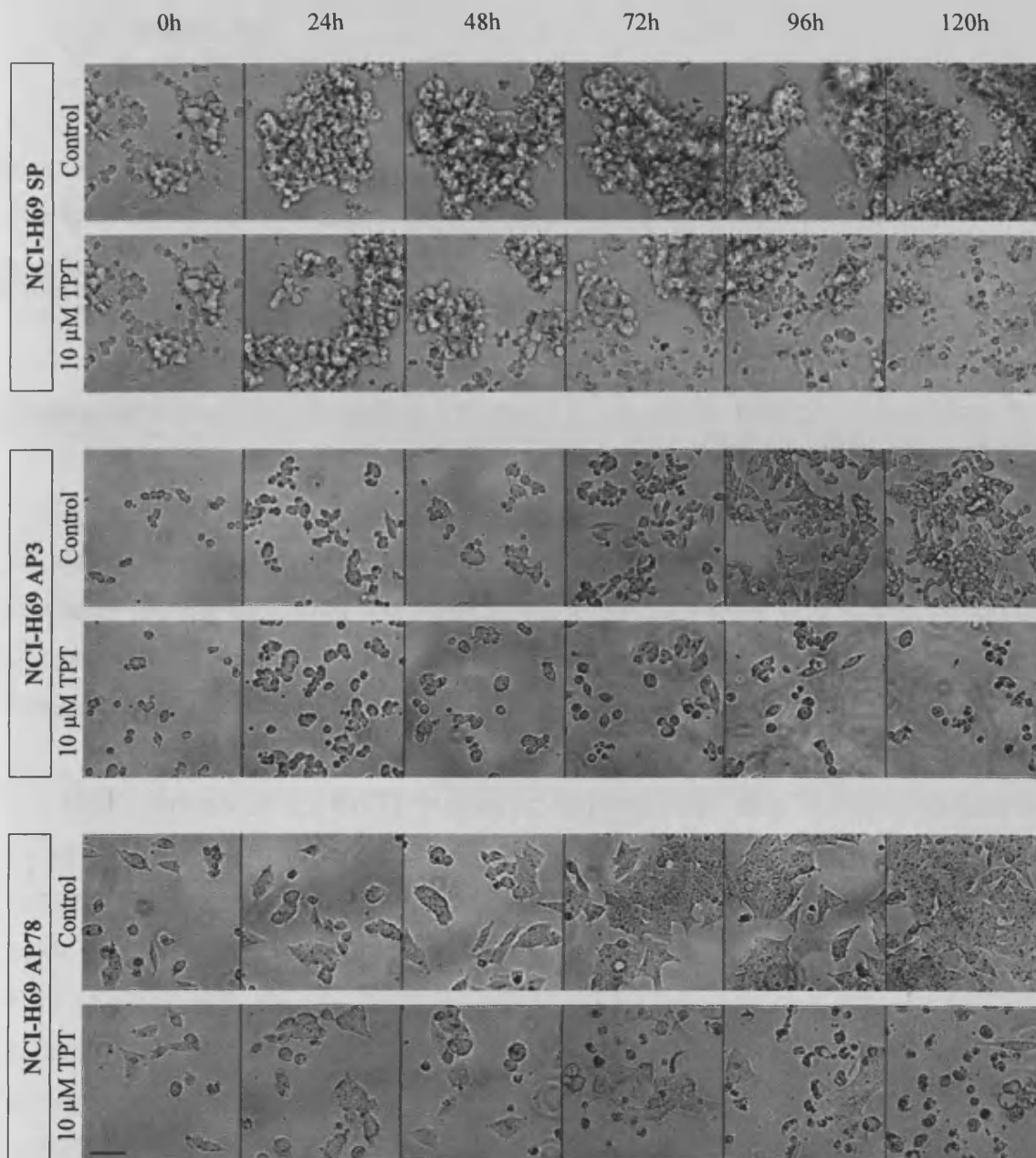


Figure IV.18: TPT treatment of all NCI-H69 variants pre-seeded into wells. Cells were seeded 24 h prior 1h treatment with 10  $\mu$ M TPT. Images were taken at random separate fields for each time point. Calibration bar represents 50  $\mu$ m.

#### **IV.4. Discussion**

SCLC is an aggressive disease with a high initial response rate but typically relapses (Okuno and Jett, 2002). Here the study focused on TPT, as the lead agent for evaluation of chemosensitivity in the SCLC system. TPT is the first TOP1 inhibitor to be approved for second-line treatment of SCLC and is the only single-agent approved for the treatment of recurrent SCLC (Garst, 2007; Ommrod and Spencer, 1999). Furthermore, recent studies have been conducted in the first-line setting and oral TPT shows to be a good candidate for combination therapy with intravenous agents such as small tyrosine kinase inhibitors (O'Brien *et al.*, 2007). Chemoresistance/sensitivity has been studied by development of *in vitro* system based on drug-resistant variant selection. Recently more importance has been given to the possibility of a small fraction of cancer cell populations with stem-like properties, which may define drug resistance properties.

NCI-H69 is not a recognised multi-drug resistant cell line (Campling *et al.*, 1997; Jensen *et al.*, 1997). However, several multi-drug resistant variant of NCI-H69 have been developed. NCI-H69 selected for resistance to etoposide (H69/VP) has been reported previously to sequentially overexpress both the MRP and MDR1 multi-drug conferring genes (Brock *et al.*, 1995). While NCI-H69 selected with daunorubicin (H69/DAU) was found to overexpress ABCB1 (Jensen *et al.*, 1989) and NCI-H69 selected for resistance to adriamycin/doxorubicin (H69AR) was found to overexpress ABCC1 (Cole *et al.*, 1992; Mirski *et al.*, 1987).

*ABC transporters expression* — Members of the ABC transporter superfamily known to be involved in multi-drug resistance, ABCC1 and ABCC5 are the ones most expressed in the NCI-H69 variants. ABCC1 is frequently expressed in SCLC cell lines and tumours, while ABCB1 can be detected in tumours but rarely in cell line (Campling *et al.*, 1997).

FTC efflux-inhibition assays showed that ABCG2 is not functional in any of the NCI-69 cell lines. This is consistent with a negative literature search on ABCG2 expression and SCLC cell lines. To our knowledge no multi-drug

resistant NCI-H69 subline overexpressing ABCG2 has been selected so far. However, the expression of functional drug resistance-related members of the superfamily of ABC transporters, such as ABCB1, ABCC1, or ABCG2 may be affected by drug exposure, although it is likely that cellular pharmacokinetic protection is effected through a single dominant extrusion pump (Nieth and Lage, 2005).

*Pharmacokinetics properties of TPT* — With no detectable ABCG2 activity in any of the NCI-H69 variants it was hypothesized that equivalent amounts of drug are been delivered to intracellular targets in the NCI-H69 cell lines. Hoechst 33342 fluorescence, as a surrogate reporter of DNA targeting rates, shows variation between the sub-lines in a manner that corresponds to the increment in cell volume of the variants. TPT uptakes, however, did not reflect the volume increment in NCI-H69 AP3 compared to NCI-H69 SP, probably due to the low affinity of TPT for DNA and the potential modulation by lactone ring opening changing the ability to export the drug.

A common feature associated with camptothecin resistance is the reduction of the target enzyme activity by downregulation, mutation or a combination of both (Losasso *et al.*, 2008; Sorensen *et al.*, 1995). No variation of TOP1 expression was observed in the NCI-H69 system. Functional assays could find no evidence of changes in drug efflux in the NCI-H69 variants, although positive controls using the ABCG2 expressing lung adenocarcinoma cell line A549 demonstrated the sensibility of the assay. The conclusion is therefore, that the pharmacokinetic of TPT is the same across all the variants and any differences are not ascribable to ABCG2 function. Further, the adherent phenotype state *per se* does not confer drug resistance.

*Cell adhesion-mediated drug resistance* — Although the CAM-DR (Rintoul and Sethi, 2002; Sethi *et al.*, 1999) potential in the NCI-H69 variants has not been tested in the thesis, a poly-L-lysine adherent variant previously developed was found to be resistant to several drugs, through survival signalling, indicating the possibility to enrich drug resistant variants through non-specific substrate adherence (Kraus *et al.*, 2002). Again the conclusion is that variant enrichment does not confer drug resistance.

**Side population phenotype** — ABCG2 shows an intriguing linkage with the CSC phenotype, given that enhanced ABCG2 transporter expression contributes the defining ability of pluripotential side population of cells to exclude the DNA minor groove-binding dye Hoechst 33342 (Hirschmann-Jax *et al.*, 2004). Hoechst 33342 has been proven to be a useful approach to for identification and purification of stem-like cells, side population phenotype (Kruger *et al.*, 2006; Yano *et al.*, 2005).

A549 side population fraction was detected by variation in immunofluorescence staining and Hoechst dye exclusion. According to the findings here, the side population fraction represented up to 37.5% of the cells, consistent with previous finding showing that A549 displays a strong side population (Scharenberg *et al.*, 2002; Sung *et al.*, 2008). Recently, gene expression profiles of A549 side population cells showed up-regulation of ABCG2 (~2.5-fold) compared to non-side population cells, together with other genes (AKR1C1/C2, TM4SF1 and NR0B1) potentially indicative of a poor prognosis in anti-cancer therapy (Seo *et al.*, 2007).

According to the CSC theory, significant ABCG2 function may be restricted to cell sub-populations that may vary considerably in frequency in human tumours and may have uncertain representation in established cell lines from solid tumours. A recent study showed the presence of the side population phenotype in six human lung cancer cell lines (NSCLC adenocarcinoma, squamous cell carcinoma and lung alveolar cell carcinoma) ranging from 1.5 to 6.1% of the total population. This side population showed increased resistance to multiple chemotherapeutic drugs, notably cisplatin, gemcitabine, and vinorelbine, although TPT was not assessed (Ho *et al.*, 2007). No ABCG2-dependent Hoechst 33342 side population was observed in any of the variants and it is reasonable to conclude that CSCs, as defined by side population fractions, are essentially absent from the NCI-H69 system.

**Cancer stem cells characteristics** — CSCs may contribute to tumourigenic and chemoresistant subfractions in a variety of malignancies, including brain tumours, leukemias, and breast carcinomas. Cancer stem cells might be of clinical relevance, indeed it could explain why when 99% of cells are killed by therapy, the tumour is able to grow again (Vezzoni and Parmiani,

2008). Therefore, there is a continuing drive to identify functional markers of neoplastic cells with stem-like properties (Visvader and Lindeman, 2008). Thus there is the possibility that stem-like cells may exist in the NCI-H69 system but are defined by markers and function different from ABCG2. A search for stem-like cell markers, not necessarily defining a stem-like population, that might change upon enrichment was undertaken (figure IV.19). The results revealed modulation ALDH1 (aldehyde dehydrogenase 1 family, member A1) with reduced expression in NCI-H69 AP3. The family of aldehyde dehydrogenases (ALDH) catalyzes the oxidation of aldehydes to carboxylic acids, considered a general detoxification process. ALDH1 has a role in the conversion of retinol to retinoic acid, which is important for proliferation, differentiation and survival (Vasiliou *et al.*, 2000). The heavily glycosylated adhesion molecule CD24, is as yet the only known ligand for P-selectin. Although CD24 is not a specific marker of cancer stem cells, low levels can characterise breast tumour-initiating cells (Visvader and Lindeman, 2008). CD24 expression shows a similar modulation to that of ALDH1 with reduced expression in NCI-H69 AP3. CD44 is an adhesion molecule with multiple isoforms with roles in signalling, migration and homing. The CD44V form is known to confer metastatic properties and was found to show elevated expression in NCI-H69 AP3 (Visvader and Lindeman, 2008). PROM1 (prominin 1 / CD133) is a transmembrane glycoprotein with a potential role in the organization of plasma membrane topology (Bidlingmaier *et al.*, 2008) and show a consistent increase in expression from NCI-H69 SP to NCI-H69 AP78.

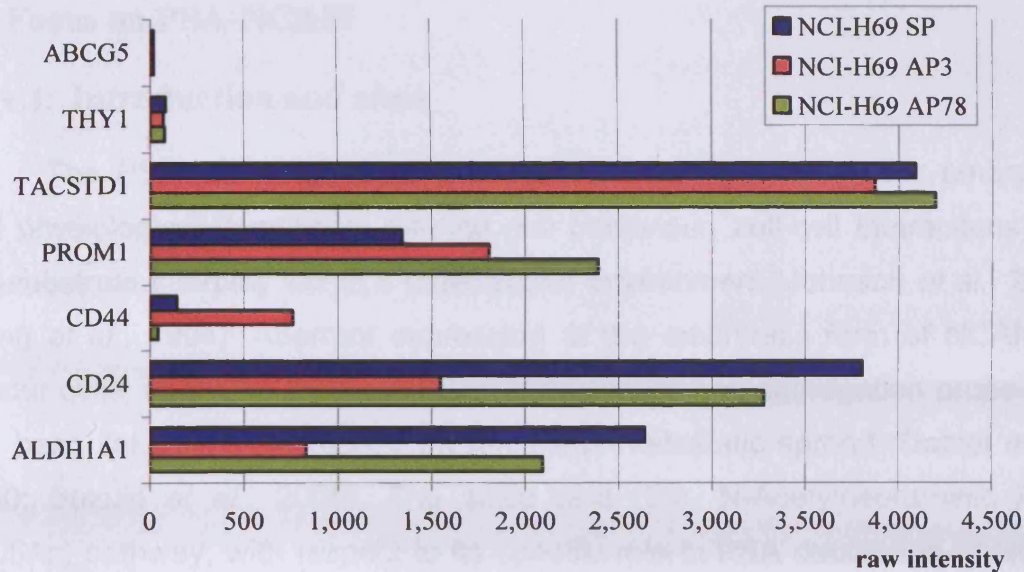


**Figure IV.19:** Solid tumours cancer stem cell markers (from Visvader and Lindeman, 2008) expression in the NCI-H69 model. Graph representing the raw intensity (without per gene normalisation) expression of the average value of the triplicates from the microarray analysis of selected markers of cancer stem cells in solid tumours. ABCG5 / ATP-binding cassette, sub-family G, member 5, THY1 / Thy-1 cell surface antigen, TACSTD1 / tumour-associated calcium signal transducer 1, PROM1 / prominin 1, ALDH1A1 / aldehyde dehydrogenase 1 family, member A1.

So far, to our knowledge, no SCLC cell line has demonstrated a Hoechst 33342 side population phenotype. However, a recent study suggested that a SCLC cancer stem cell type could be defined as a PLAUR (uPAR / urokinase plasminogen activator receptor) positive. The PLAUR<sup>+</sup> cells were also found to express CD44 and ABCB1. Those cells were found to demonstrate significant resistance to 5-fluorouracil, cisplatin and etoposide (Gutova *et al.*, 2007).



## V. Focus on PSA-NCAM

### V.1. Introduction and aims

The PSA-NCAM glycoalyx is subject to modulation under embryonic and physiological conditions, altering cell behaviour, cell-cell interactions and cell-substrate interplay within a multicellular environment (Johnson *et al.*, 2005; Wang *et al.*, 1994). Aberrant expression of the embryonic form of NCAM by tumour cells, changing their adhesion, detachment and aggregation properties, has been linked with increased invasion and metastatic spread (Daniel *et al.*, 2000; Suzuki *et al.*, 2005). The sialic acid (Sia, N-Acetylneuraminic Acid, Neu5Ac) pathway, with respect to its specific role in PSA decoration of NCAM (Bork *et al.*, 2005), is therefore a potential target for the development of new tools and anti-cancer treatments. A focus on the importance of PSA decoration of NCAM in SCLC cells could offer drug design opportunities for post-translational modification, given its restricted expression in normal adult tissues (Walmod *et al.*, 2004). The inhibition of the polysialic acid synthesis pathway, to reduce the metastatic potential of tumour cells, is an exciting new area with very little research published to date.

The pathway for sialic acid biosynthesis comprises a succession of steps. *N*-acetylmannosamine (ManNAc) is the first precursor biosynthesized from UDP-*N*-acetylglucosamine (UDP-GlcNAc) obtained from the extracellular environment. UDP-GlcNAc is then committed to a series of transformation resulting in CMP-sialic acid (CMP-Neu5Ac) production in the nucleus. After transport to the Golgi compartment, CMP-Neu5Ac serves as a donor for glycosylation by one family of sialyltransferases (Wang *et al.*, 2006).

The sialic acid pathway shows tolerance for unnatural ManNAc, indeed several enzymes, including the 2 polysialyltransferases, in this pathway can accept unnatural substrates. This enzymatic permissiveness can be exploited in order to deliver unnatural analogues of sialic acid to the cell surfaces (Charter *et al.*, 2000; Jacobs *et al.*, 2001). Recently, Bertozzi and co-workers have demonstrated that incorporation of unnatural substrates, for example, *N*-butanoylmannosamine (ManBut), can lead to reversible inhibition of polysialic acid expression via this metabolic mechanism. ManBut is subsequently

converted (via the biosynthetic pathway described above) to an unnatural sialic acid derivative that effectively leads to chain termination (Mahal *et al.*, 2001).

The experimental therapeutics theme addressed in this current chapter, is the identification and validation of the 2  $\alpha$ -2,8-polysialyltransferases as drug targets for the development of inhibitors of tumour cell surface polysialic acid decoration. In collaboration with medicinal chemists, we have sought to explore the catalytic domain of the sialyltransferases in order to develop tools to assist in validation of assays for inhibitors of NCAM polysialylation. Our collaborators, Prof Patterson and Dr Falconer (Institute of Cancer Therapeutics, Bradford), have undertaken the design and synthesis of the carbohydrate-based probes informed by computational chemistry. Using molecular modelling of the 'sialyl motif' active site they sought to explore the catalytic domain of the two  $\alpha$ -2,8-polysialyltransferases (ST8SIA) in order to develop probes with the potential for inhibition of NCAM polysialylation. Since no structural information is available on either ST8SIA4 (PST) or ST8SIA2 (STX), they identified the  $\alpha$ -2,3/ $\alpha$ 2,8-sialyltransferase of *Campylobacter jejuni* (CstII) as an appropriate alternative model for informing the synthesis of agents to probe the enzyme active site 101. Significantly, all sialyltransferases accept the same glycosyl donor and the "sialyl motif L", a sequence of 48-49 amino acids is conserved amongst the different enzymes and is potentially required for substrate donor binding (Angata and Fukuda, 2003; Datta *et al.*, 1998). In collaboration with Dr Mire Zloh (University of London) the CstII protein structure was extracted from a complex with a substrate analogue (PDB code 1R07) and used it as a target for unbiased docking. Given the close homology of the active binding site of CstII and that of both ST8SIA4 and ST8SIA2, this provided useful information as to potential interactions between agents to be synthesised and the human polysialyltransferases. This process was used dock small molecule substrate mimics into the active site. Two probes, R1108 (and R890), occupied this space preferentially when the computer was asked to dock the molecule through energy minimisation anywhere on the protein. Further agents were synthesised to explore other design concepts.

Potential ST8SIA4 inhibitors — analogues of sialic acid — are being co-developed and modelled (Institute of Cancer Therapeutics, Bradford) for screening and identifying cellular consequences of modulation. The hypothesis

is that modulation of polysialic acid decoration of the neural cell adhesion molecule (NCAM) using inhibitors of ST8SIA4 (PST) and ST8SIA2 (STX)  $\alpha$ -2,8-polysialyltransferases will suppress its capacity to express changes in tumour cell-cell adhesion, that promote the opportunity, *i.e.* for phenotypic alterations associated with metastatic potential. Key to this is an exploration of the NCI-H69 system as a mean of assessing changes associated with a restriction of PSA decoration of NCAM. The goal is to apply specific inhibitors of NCAM polysialylation as molecular “tools” to explore the impact of post-translational changes in PSA decoration of NCAM on cell-cell contacts, cell adhesion and chemosensitivity.

Here the experimental aims were:

- To analyse and assess, using predominantly microarray analysis, changes in glycosylation pathways in the NCI-H69 system, with a focus on the sialic acid pathway – the aim is to assess the extent of changes in the expression of key pathway members to determine underlying influences that contribute to variation in polysialylation.
- To assess the relative expression of ST8SIA4 (PST) and ST8SIA2 (STX) in the NCI-H69 variants – the aim being to provide evidence of availability for inhibition by targeted inhibitor molecules.
- To undertake cellular studies using the NCI-H69 model in order to understand the impact of exposure to candidate PST inhibitors with a focused library of modified sialic acid derivatives rationalised to penetrate cellular systems and completely inhibit PSA production – the aim being to assess the impact on PSA expression.
- To assess any evidence of apparent off-target activity – here studies involved the microarray analysis to identify candidate off-target activity and the selection of a second cellular system to provide supporting evidence.

## V.2. Specific materials and methods

### V.2.1. Inhibitors and treatment

ST8SIA4 potential inhibitors were developed and provided by Dr Robert Falconer (Institute of Cancer Therapeutics, Bradford). Each compound was shipped lyophilised and kept at -20°C upon resuspension. R1108 was resuspended in 35% methanol to a stock concentration of 20 mM. The other compounds (ICT 2551 / ICT 2553 / ICT 2554 / ICT 2555) were resuspended in 50% methanol to a concentration of 10 mM. Benzyl alcohol and benzyl acetate were purchased from Sigma Aldrich (St Louis, MO, USA) and kept at room temperature.

For treatment with R1108 and the other compounds, cells were seeded in standard culture dish and allowed to attach for 24 h prior addition of drugs. Every treatment experiment included a control treated with methanol.

### V.2.2. Cell lines

NCI-H69 variants cell lines (NCI-H69 SP, NCI-H69 AP3 and NCI-H69 AP78 — described in chapter III) were used to test the inhibitors. Another variant — NCI-H69 AP55 — was also used to perform the microarray analysis (see Appendix e).

The mouse CHO-K1 (Kao and Puck, 1968) and the mouse metallothionein-1 (mMT-1)-overexpressing CHO K1 (mMT-CHO-K1) — described in Appendix b — were provided by Dr John H Beattie at the Rowett Research Institute (Beattie *et al.*, 2005). Following removal of first passage cells from liquid nitrogen, single layer cultures of mMT-CHO-K1 and CHO-K1 cells were maintained, routinely detached, split and resuspended as described previously (see II.2.2.).

### V.2.3. RT-PCR

Primers were purchased from Eurofins MWG (Ebersberg, Germany) shipped lyophilised, resuspended with H<sub>2</sub>O at a concentration of 100 μM and

stored at  $-20^{\circ}\text{C}$ . Table V.1 describes the primers used to amplify ST8SIA2 and ST8SIA4.

Table V.1: RT-PCR primers (from Seidenfaden et al., 2000).

Name	Primers	Product size
ST8SIA2	U: 5' – TACATCTTCGATCGAGACAGCA – 3'	421 bp
	L: 5' – TGCTTCAGGATAAGCTCGTTGA – 3'	
ST8SIA4	U: 5' – TCCGTCATTGAGACTTATTCAT – 3'	262 bp
	L: 5' – CACATTTAATGTTTTGAATTCT – 3'	

Total RNA were extracted (see II.3.2) with TRIZOL (Invitrogen, Carlsbad, CA, USA). Reverse transcription was performed using Reverse-IT™ 1st Strand Synthesis Kit (ABgene, Cambridge, UK), according to the manufacturer instruction. Briefly, 1.5  $\mu\text{g}$  total RNA was added to 500 ng of oligodT in a final volume of 13  $\mu\text{L}$  and incubated at  $70^{\circ}\text{C}$  for 5 min. Then, 5 mM of each dNTP (Bioline, London, UK), 4  $\mu\text{L}$  of 5x reaction buffer and 50 units of Reverse-IT™ reverse transcriptase were added to the mix. Reaction was carried out at  $47^{\circ}\text{C}$  for 30 min followed by reverse transcriptase inactivation at  $75^{\circ}\text{C}$  for 15 min. The reverse transcription reaction was then diluted by 10 and stored at  $-20^{\circ}\text{C}$ .

PCR reaction was performed by mixing in a final volume of 20  $\mu\text{L}$ : 1  $\mu\text{L}$  of reverse transcription dilution with 2 mM of dNTP mix (Bioline, London, UK), 2  $\mu\text{L}$  of 10x reaction buffer (New England Biolabs, Ipswich, MA, USA), 5  $\mu\text{M}$  of each primer and 1 unit of Taq DNA polymerase (New England Biolabs, Ipswich, MA, USA). The reaction was carried out in a thermocycler (MJ Research DNA Engine PTC-200, Bio-Rad, Hemel Hempstead, UK) and the cycling parameters were: Initial denaturation  $95^{\circ}\text{C}$  / 5 min followed by 40 cycles of denaturation  $95^{\circ}\text{C}$  / 15 sec, annealing  $55^{\circ}\text{C}$  / 30 sec and extension  $72^{\circ}\text{C}$  / 30 sec and a final cycle of extension  $72^{\circ}\text{C}$  / 5 min.

Amplifications were visualised by running 10  $\mu\text{L}$  of the PCR reaction along with 2  $\mu\text{L}$  of non-denaturing loading buffer (see Appendix III) on a non-denaturing gel. Samples were loaded on an agarose gel which was prepared

with 1% (w/v) agarose (VWR International Ltd, Lutterworth, UK) in 1x TAE buffer (see Appendix III). Gels were electrophoresed at 70-90 V for 30-60 min and subsequently visualised under a UV transilluminator (UVP, Upland, CA, USA).

#### **V.2.4. Time lapse imaging**

Images were collected over 72 h, every 15 min, for 3 fields per conditions (0.5% methanol / 0.03 mM / 0.1 mM or 0.3 mM R1108). Time-lapse images were analyzed manually using Metamorph software (Molecular Devices). Each cell in the field was tracked individually (figure V.1) and the time to mitosis, duration of mitosis and other key cellular events detected by morphology were recorded. The classification of the event was determined according to key outcomes: a successful mitosis to two daughter cells, a tripolar or quadripolar division, mitosis followed by unsuccessful cytokinesis (polyploidy) event, cell death or unknown (for example, cell leaving the field). The duration of the mitotic event was also extracted (Marquez *et al.*, 2003).



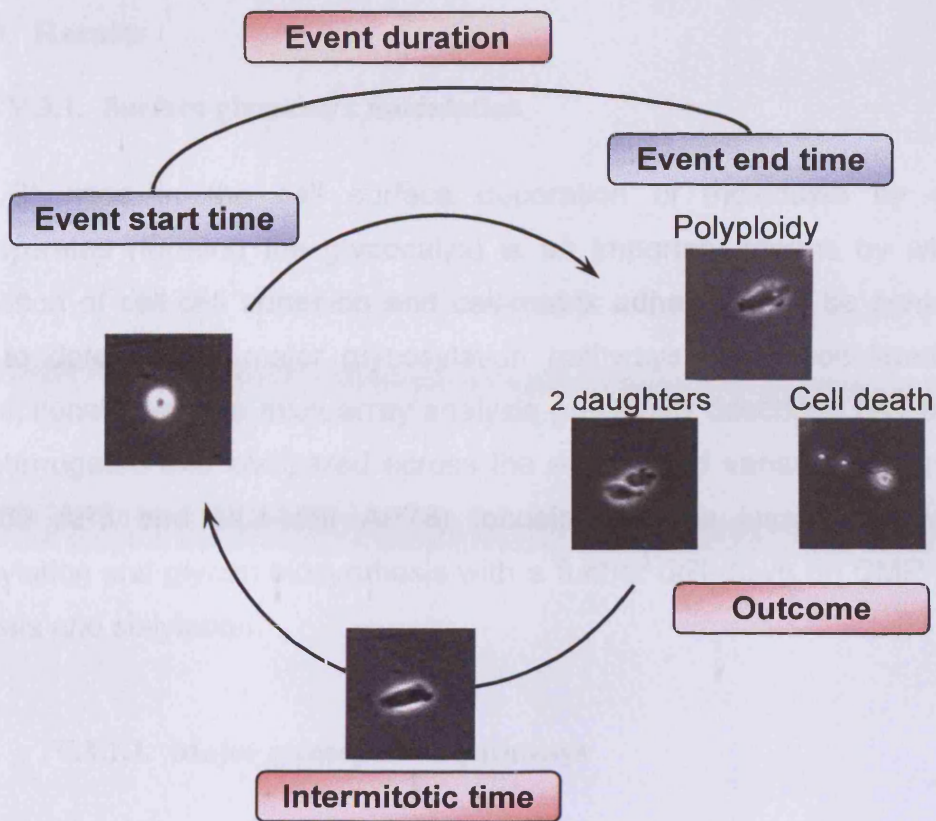


Figure V.1: *Time-lapse imaging analysis*. Schematic representation of the pragmatic approach used to analyze time-lapse images, enabling morphometric extraction of cell behaviour and delivery to mitosis.

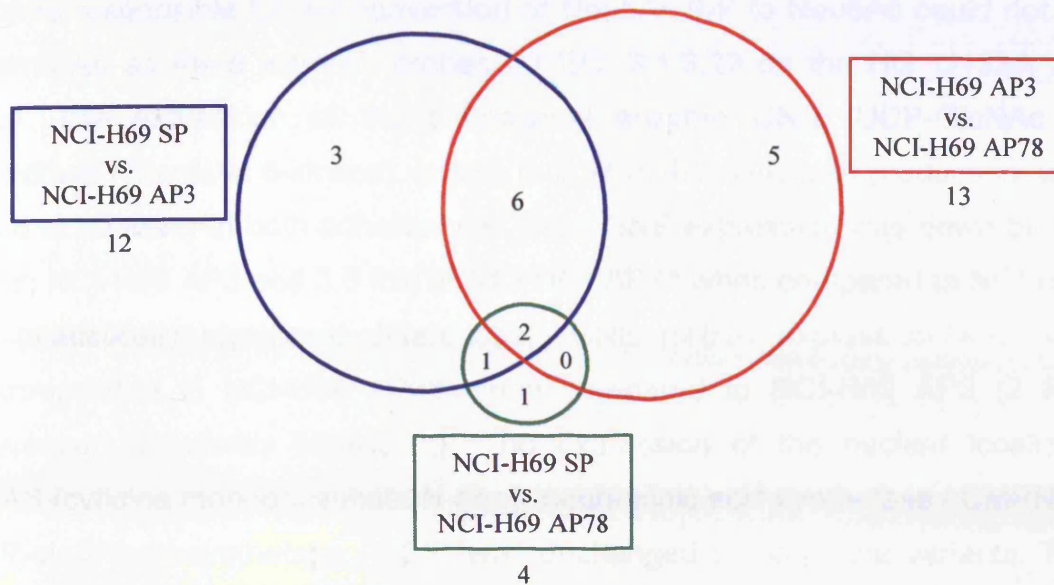
### **V.3. Results**

#### **V.3.1. Surface glycocalyx modulation**

Changes in the cell surface decoration of molecules by complex carbohydrates (forming the glycocalyx) is an important means by which the modulation of cell-cell adhesion and cell-matrix adhesion can be achieved. In order to determine if major glycosylation pathways were modulated at the transcriptional level, the microarray analysis previously described (2008 arrays) was interrogated and compared across the established variants (NCI-H69 SP, NCI-H69 AP3 and NCI-H69 AP78) focusing on the known pathways for glycosylation and glycan biosynthesis with a further drill-down on CMP-Neu5Ac synthesis and sialylation.

##### **V.3.1.1. Major glycosylation pathways**

The list of 1189 probes (representing 2 fold statistically different changes in gene expression among the variants) was compared to a well-defined pathway obtained from Kyoto encyclopedia of genes and genomes (Kanehisa *et al.*) for glycans biosynthesis and metabolism. Figure V.2 shows the partitioning of the changes between the variants (for full list of modulations see Appendix XI). In summary, out of the 302 probes defining the KEGG glycan biosynthesis and metabolism pathway, 12 probes differed in their expression profile by at least 2-fold when NCI-H69 SP and NCI-H69 AP3 were compared, 13 when comparing NCI-H69 AP3 to NCI-H69 AP78 and 4 modulations between NCI-H69 SP and NCI-H69 AP78. Of the modulations, 10 represented an increased mRNA expression in NCI-H69 AP3 compared to NCI-H69 SP and NCI-H69 AP78 (6 and 8 statistically different upregulation by at least 2-fold, respectively). Moreover, 7 showed decreased mRNA expression in NCI-H69 AP73 compared to NCI-H69 SP and NCI-H69 AP78 (6 and 5 statistically different upregulation by at least 2-fold, respectively).

*Glycans biosynthesis and metabolism (KEGG 1.7: 302 probes)*

**Figure V.2:** Venn-diagram representation of glycosylation-related genes expression modulation in the NCI-H69 variants. The list of 2-fold statistically different changes in expression in the 3 variants (1189 gene list) was compared to the pathway for glycans biosynthesis and metabolism.

### V.3.1.2. Sialic acid pathway in the variants

To determine if major changes in the sialic acid pathway were responsible for the decreased PSA decoration of NCAM in the NCI-H69 AP3 variant (see chapter III), and to determine if any of those changes occurred in the NCI-H69 AP78 with a regain of PSA expression. Microarray analysis was undertaken to profile the sialic acid pathway, therefore providing the means to map the relative expression. The analysis was performed by determining the comparative mRNA expression of enzymes catalysing the steps of the sialic acid pathway as well as transporters involved in the transport of the metabolites from the different cell compartments (Wang *et al.*, 2006).

Figure V.3 represents the sialic pathway. The expression of only 1 of the 3 enzymes catalysing the first 4 steps of the biosynthesis was statistically changed by over 2-fold. Indeed, the signal for the N-acetylneuraminic acid synthase (NANS / sialic acid synthase / SAS), converting ManNAc-6-P to Neu5Ac-9-P, was slightly higher for NCI-H69 AP3 when compared to NCI-H69 SP (1.3 fold increase) and NCI-H69 AP78 (1.5 fold increase) and the

differences were statistically different (p-value <0.05). The expression of the enzyme responsible for the conversion of Neu5Ac-9-P to Neu5Ac could not be determined as there were no probes for EC: 3.1.3.29 on the HG\_U133A\_2.0 array. The expression of the bifunctional enzyme GNE (UDP-GlcNAc 2-epimerase / ManNAc 6-kinase), known to control the sialic acid production, was found to be lower in both adherent cell lines. GNE expression was down by 1.7 fold in NCI-H69 AP3 and 3.5 fold in NCI-H69 AP78 when compared to NCI-H69 SP (statistically significant differences). GNE mRNA expression was also downregulated in NCI-H69 AP78 when compared to NCI-H69 AP3 (2 fold difference, statistically significant). The expression of the nuclear localized CMAS (cytidine monophosphate N-acetylneuraminic acid synthetase / CMPNS / CMP-sialic acid synthetase / CSS) was unchanged amongst the variants. The expression of the transporter involved in CMP-Neu5Ac transport from the nucleus to the Golgi — SLC35A1 (solute carrier family 35 member A1 / CMP-sialic acid transporter / CMPST / CST) — was statistically significantly downregulated in NCI-H69 AP3 when compared to NCI-H69 AP78 and NCI-H69 SP (1.5 fold decrease in both cases).

Finally, of the 14 sialyltransferases with probes present on the array, 3 had unreliable signals (flagged as Absent), 8 showed an unchanged expression and 3 had their expression statistically altered. Those 3 enzymes were upregulated in NCI-H69 AP3 when compared to NCI-H69 AP78 and NCI-H69 SP. Moreover, the expression of ST8SIA1 (ST8 alpha-N-acetyl-neuraminide alpha-2,8-sialyltransferase 1 / GD3 synthase) was downregulated in NCI-H69 AP78 when compared to NCI-H69 SP. None of the two sialyltransferases involved in NCAM polysialylation were found to have statistically significant different expression amongst the variants. ST8SIA2 (STX) had unreliable signals (flagged as Absent) on each array. The signal for ST8SIA4 (PST) was lower in the NCI-H69 AP3 compared to NCI-H69 AP78 (1.7 fold decrease) and NCI-H69 SP (1.5 fold decrease). However, the differences were not statistically different.

One other enzyme has been indirectly linked to the polysialylation of NCAM, FUT8 ( $\alpha$  1-6 fucosyltransferase) is responsible for the transfer of a core fucose on N-glycans (Kojima *et al.*, 1996). This enzyme had its expression significantly downregulated in both NCI-H69 AP3 (10 fold decrease) and NCI-



H69 AP78 (8 fold decrease) cell lines when compared to NCI-H69 SP (both adherent cell lines had every FUT8 measurement flagged as absent).

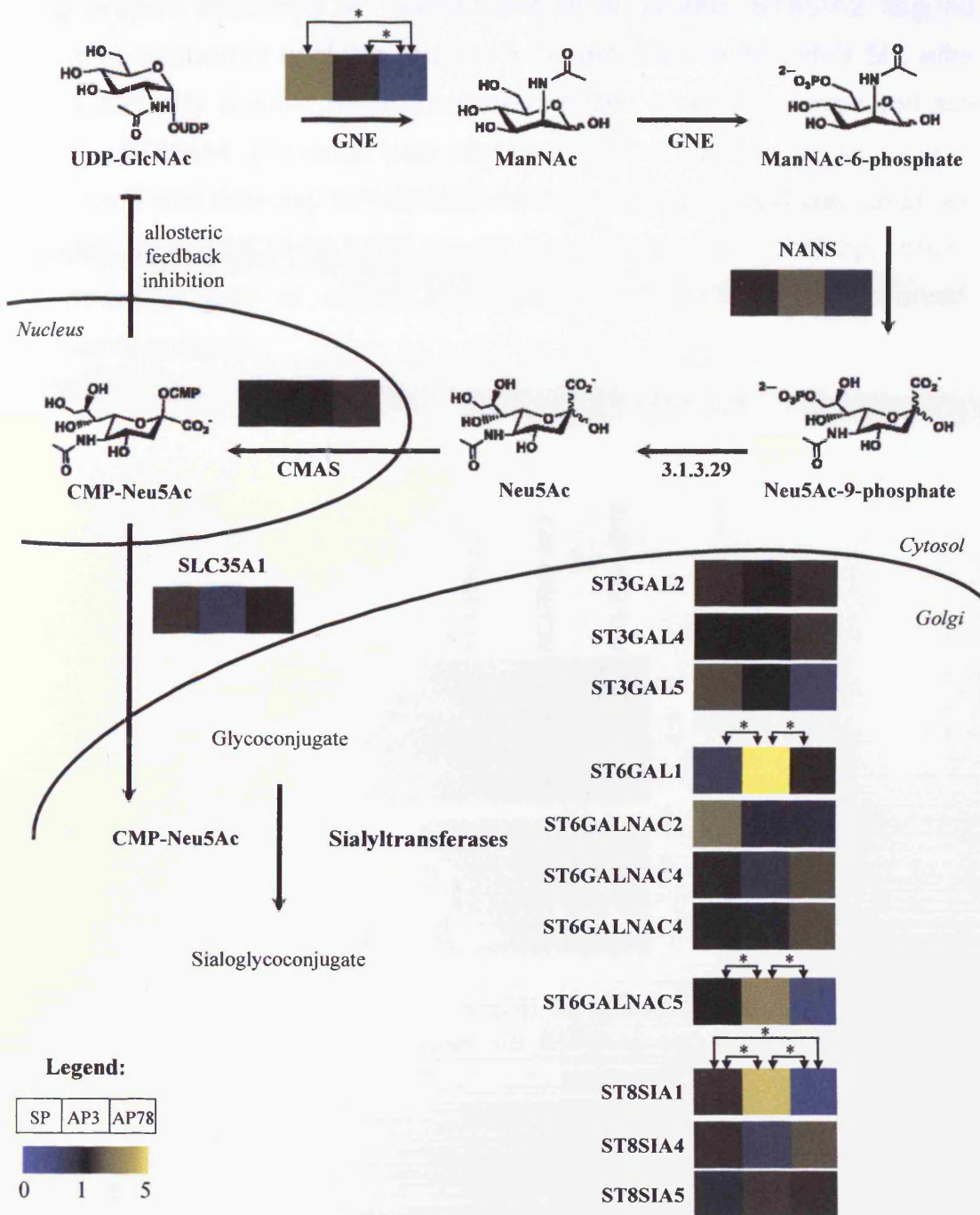
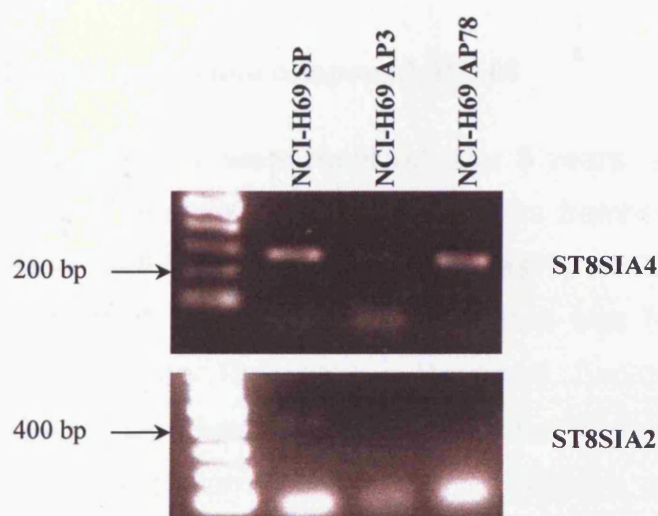


Figure V.3: Sialic acid biosynthesis pathway and sialylation of glycoconjugates (adapted from Wang et al., 2006). Figure depicting the comparative microarray analysis of the sialic pathway in each of the variants (false-colour view representing the average expression of the triplicates). Only sialyltransferases with expression flagged as present in at least one sample are represented here. The gene called 3.1.3.2.9 does not have an associated probe in the HG\_U133A\_2.0. \* indicates statistically different expression by over 2-fold ( $p < 0.05$ ).

As no antibodies were available for the detection of ST8SIA2 and ST8SIA4 proteins, mRNA expression was confirmed by RT-PCR (figure V.4) using primers described by Seidenfaden *et al.* (2000). ST8SIA2 flagged as absent in microarray analysis could only be amplified in NCI-H69 SP, after 40 cycles and only a weak band could be detected around the expected size of 421 bp. ST8SIA4 sequence was amplified after 40 cycles for all variants. A weak band was detected for NCI-H69 AP3 and stronger band was amplified for NCI-H69 SP and NCI-H69 AP78 around the expected size of 262 bp, confirming the downregulation of mRNA expression by NCI-H69 AP3 observed by microarray analysis.



**Figure V.4:** *ST8SIA4* and *ST8SIA2* expression. Ethidium bromide stained gel depicting RT-PCR products, after 40 PCR cycles, for *ST8SIA2* and *ST8SIA4* for each of the NCI-H69 variants.

### V.3.2. Chemical-biology approach to intervention on PSA synthesis

Putative PST inhibitors are being developed at the Institute of Cancer Therapeutics at Bradford University. Those compounds are designed to target the CMP-Neu5Ac binding site on the polysialyltransferases. A compound (R1108) was first developed, and despite poor *in vivo* stability (R1108 had a plasma half-life of less than 2 min), was used to inform the development of



other compounds. Four other compounds were tested (ICT 2551 / ICT 2553 / ICT 2554 / ICT 2555) in a preliminary screen for their effect on the NCI-H69 variants system. Because the last compounds (ICT) were only available in a limited quantity only an essential preliminary screen was performed according to the findings from the R1108 data.

Each compound was sent to Cardiff after quality controls were performed at the Institute of Cancer Therapeutics of Bradford. All compounds are either purified by flash chromatography or HPLC or both. All compounds are then subject to NMR analysis, which gives identity as well as indication of purity. Compounds identity is then checked by mass spectrometry. Therefore all batches were used with the confidence that they had the required quality for biological screening.

#### **V.3.2.1. First generation compound: R1108**

Four batches of R1108 were received over 3 years. Table V.2 presents the nomenclature used here to describe the various batches along with their date of resuspension, method of purification and stability at -20°C.

Long-term effect of storage on R1108 batches was tested by Dr Andy Humphrey (Institute of Cancer Therapeutics, Bradford). Two of the resuspended batches (2 and 3) were sent back to Bradford in order to determine compound stability and evidence of contamination and/or breakdown products of R1108 was present. HPLC analysis revealed that R1108 was stable for longer than a year at -20°C. Indeed, in the 2 batches resuspended in March 2006 and September 2007, R1108 was the major component indicating that the molecule has largely remained intact during storage and transit

Table V.2: R1108 batches.

<b>Batch number</b>	<b>name used in the thesis</b>	<b>date of resuspension</b>	<b>purification</b>
1	R1108/2005	March 2005	HPLC
2	R1108/2006	March 2006	HPLC
3	R1108/2007	Sept 2007	HPLC
4a	R1108/2008a	Feb 2008	HPLC
4b	R1108/2008b	Feb 2008	none

### V.3.2.2. Other compounds.

At this point, real concepts of derivative design were being pursued at Bradford. The intellectual property behind these compounds was also confidential hence each compound was given a unique code ensuring appropriate audit trailing and reporting. Cardiff received one batch of each ICT compound in 2007 (table V.3).

Table V.3: ICT compounds.

<b>name</b>	<b>date of resuspension</b>	<b>purification</b>
ICT 2551	March 2007	HPLC
ICT 2553	March 2007	HPLC
ICT 2554	March 2007	HPLC
ICT 2555	March 2007	HPLC

### V.3.3. Effect on NCAM decoration

#### V.3.3.1. R1108

Previous in-lab screening for R1108 effect on NCAM decoration with increasing concentration of R1108 (0.03 mM; 0.1 mM and 0.3 mM) showed decreased PSA levels after 24 h treatment with R1108. Therefore, the consequence of R1108 treatment on PSA decoration was determined by

western blotting (figure V.5) using 0.3 mM of R1108/2006. The western blot assay showed comparable amounts of PSA after 6 h and 10 h continuous treatment. Neither NCI-H69 SP nor NCI-H69 AP78, cell lines with innate constitutive PSA decoration of NCAM, showed a response to ST8SIA4 putative inhibitor. The tight bands observed on figure V.5 as opposed to the smears seen on figure III.5 or V.6, when immunoblotting for PSA-NCAM, can be explained by a shorter migration time.

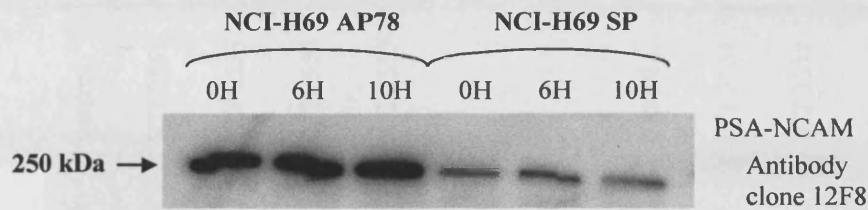


**Figure V.5:** Effect of R1108 treatment on PSA levels. Western blotting showed no effect on PSA decoration of NCAM after 10 hours treatment of NCI-H69 SP and NCI-H69 AP78 with 0.3 mM R1108/2006.

An investigation was undertaken, testing 2 of the batches at 2 doses. No effect on the PSA decoration of NCAM could be observed with different batches of R1108. Table V.4 details concentrations and length of treatment used.

**Table V.4:** Effect of R1108 different batches on PSA decoration of NCAM.

Name	treatment duration	R1108 concentration	cell line used	effect on PSA-NCAM
R1108/2005	/	/	/	/
R1108/2006	0/2/4/6/8/10 h	0.3 mM	NCI-H69 SP and NCI-H69 AP78	none
R1108/2007	48 h	0.3 mM / 1 mM	NCI-H69 AP78	none
R1108/2008a	/	/	/	/
R1108/2008b	/	/	/	/

### V.3.3.2. ICT compounds

The ICT compounds effect on PSA decoration of NCAM was investigated by western blotting. NCI-H69 SP cells were treated for 24h with 0.3 mM or 1

mM of compounds. As shown in figure V.6, in the absence of compounds (control lanes) PSA-NCAM was detected as a smear spreading around 250 kDa. Of the 4 compounds, only ICT 2555 showed a band with reduced intensity after 0.3 mM treatment. Upon 1 mM treatment, while ICT 2551 and 2253 still showed no effect on PSA decoration of NCAM, ICT 2555 and ICT 2554 both showed a reduced PSA-NCAM detection.

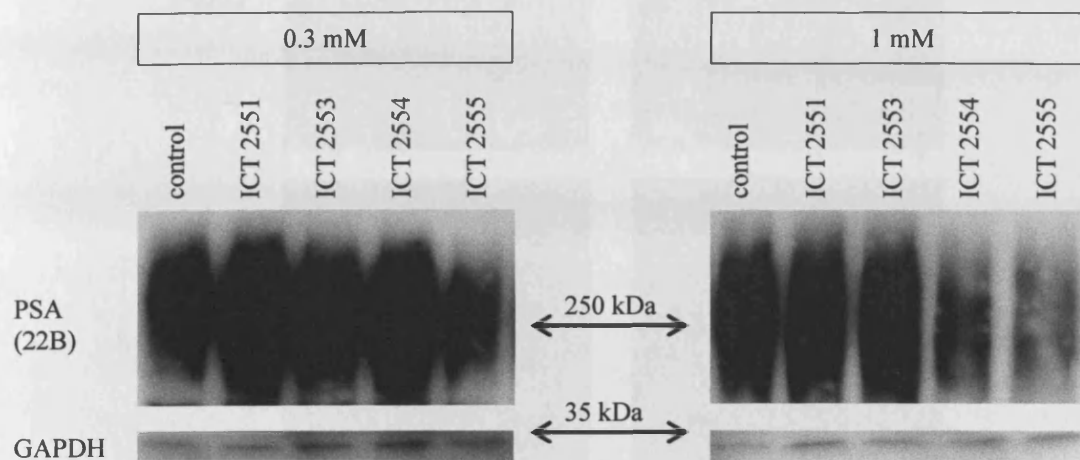


**Figure V.6:** Effect of 24h ICT compounds treatment on NCAM decoration. NCI-H69 SP cells were treated for 24 h continuous treatment with a final concentration of 0.3 mM or 1 mM of compound.

#### V.3.4. Cytotoxicity

As in many biological system, the modulation of a single factor can have unexpected side-effect. In order to determine if the compounds had any related cytotoxicity on the NCI-H69 cell lines, cells were incubated with various amount of compounds and monitored.

##### V.3.4.1. R1108: dose-dependant cytotoxicity

NCI-H69 AP3 and NCI-H69 SP cells were treated continuously over 48 h with 0.3 mM R1108/2006. After 48 h, most cells showed a rounded and shrunken morphology indicating that cells were undergoing cell death (figure V.7). The collected images clearly showed an unexpected response to the

exposure to R1108/2006. The toxic effect also seemed to be independent from ST8SIA4 expression since NCI-H69 AP3 expresses low level of ST8SIA4.

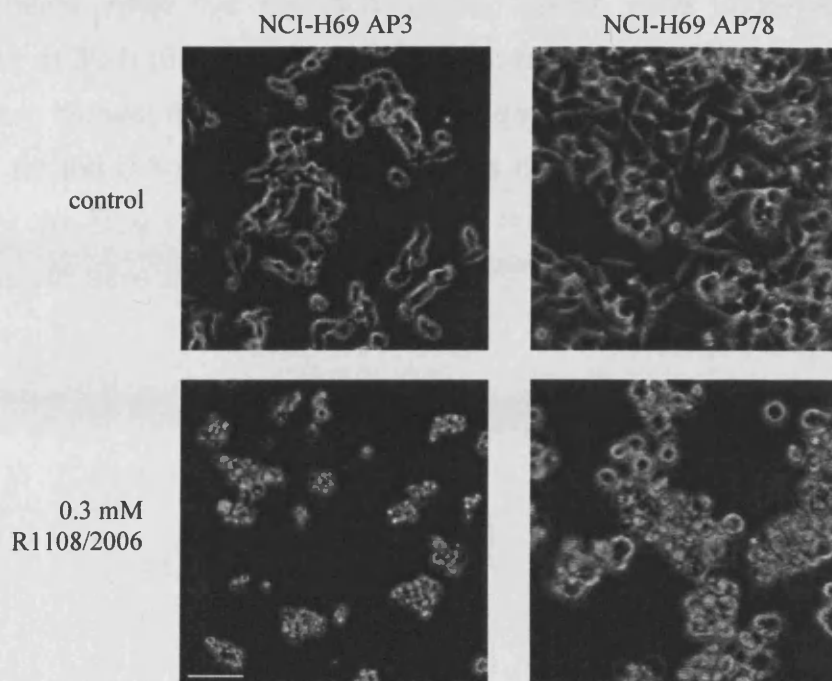


**Figure V.7:** Effect of a 48h R1108 treatment on NCI-H69 variants cell lines. NCI-H69 AP3 and NCI-H69 AP78 cells were treated for 48 h continuous treatment with a final concentration of 0.3 mM R1108/2006. Calibration bar represents 50  $\mu\text{m}$ .

The biological effects of treatment with the unnatural carbohydrate R1108 at different doses were observed using time lapse microscopy. Figure V.8 shows representative phase-contrast images from a time-lapse movie. This investigation was undertaken with NCI-H69 AP3, the adherent variant allowing time lapse analysis and isolation of any possible ST8SIA4 effect due to R1108 treatment. The intention was to record growth (increase in cell number) and to record morphology / combined refractile properties. The control fields showed normal mitotic progression throughout the experiment with cells reaching confluence at 70 h. Cells from the control field had the appearance of bright cells with distinct dark edges. Upon treatment with 0.3 mM R1108/2006 there was no increase in cell number over 70 h. Further, cells showed a change of contrast to a dull / black appearance, probably indicating a highly stressed dying

cell as early as 10 h with clear signs of cell death occurring from 20 h. When lowering the dose, no cell growth was recorded upon treatment with 0.1 mM, while at 0.03 mM some cell growth occurred (10-20 h) however slower than the control fields. After this period of mitotic arrest, cells underwent cell death, observed at 30 h (0.1 mM) and 50 h (0.03 mM). No cell survival was observed for the two highest doses with every cell dead and detaching from the substrate at 40 h for the 0.3 mM dose and all cells dead at 70 h for the 0.1 mM dose. While for the cells incubated with the low dose (0.03 mM), a sub-population of cells was still alive after 70 h of treatment.



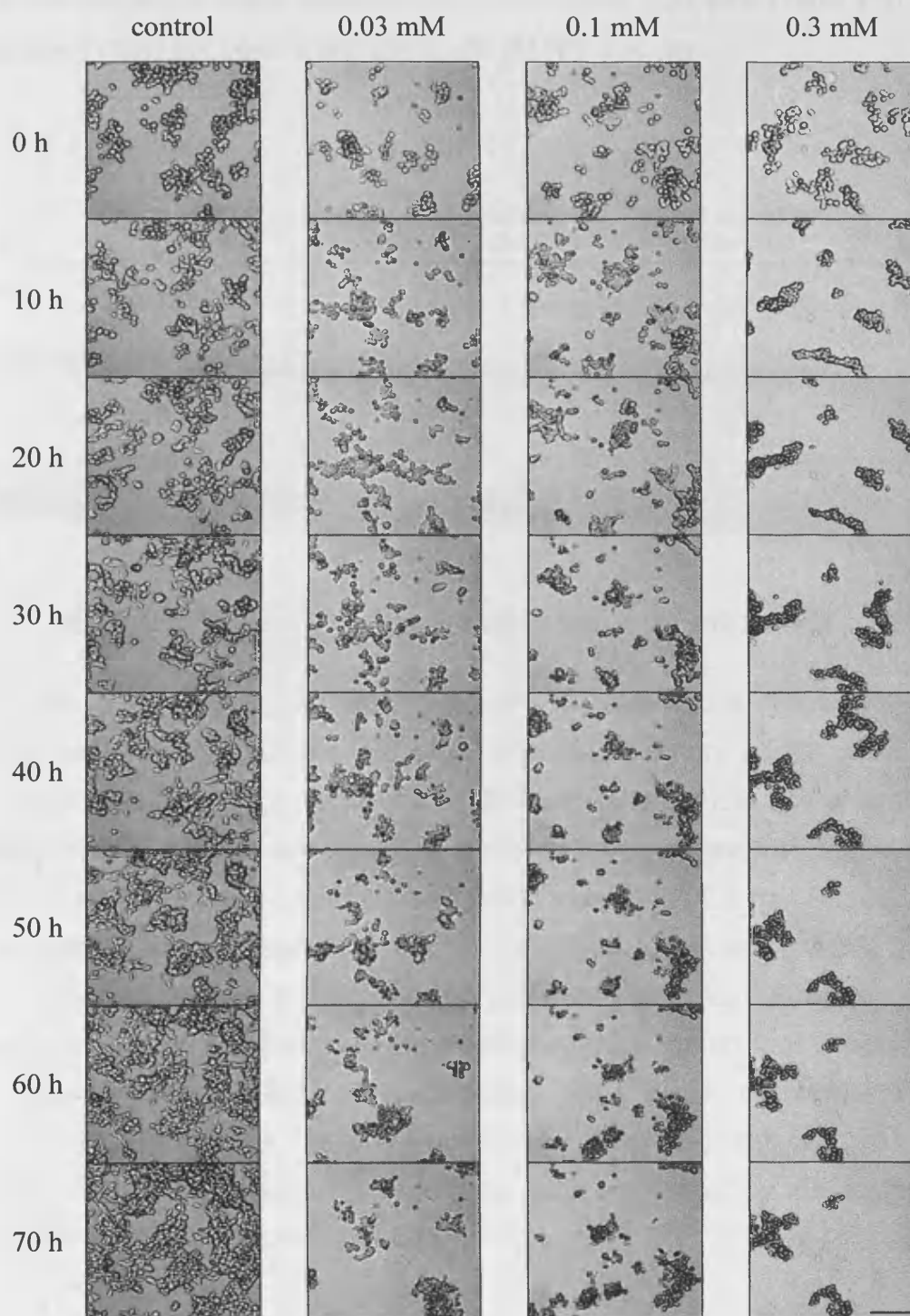


**Figure V.8:** *R1108* toxicity. NCI-H69 AP3 cells were treated continuously over 70 h with 0.03; 0.1 or 0.3 mM *R1108*. Calibration bar represents 100  $\mu\text{m}$ .

These results indicate that *R1108* has a cytotoxic, dose-dependent effect that seems to be independent of the PSA content of the cells, as the response was similar for all variants. However, the cytotoxicity impact has varied across

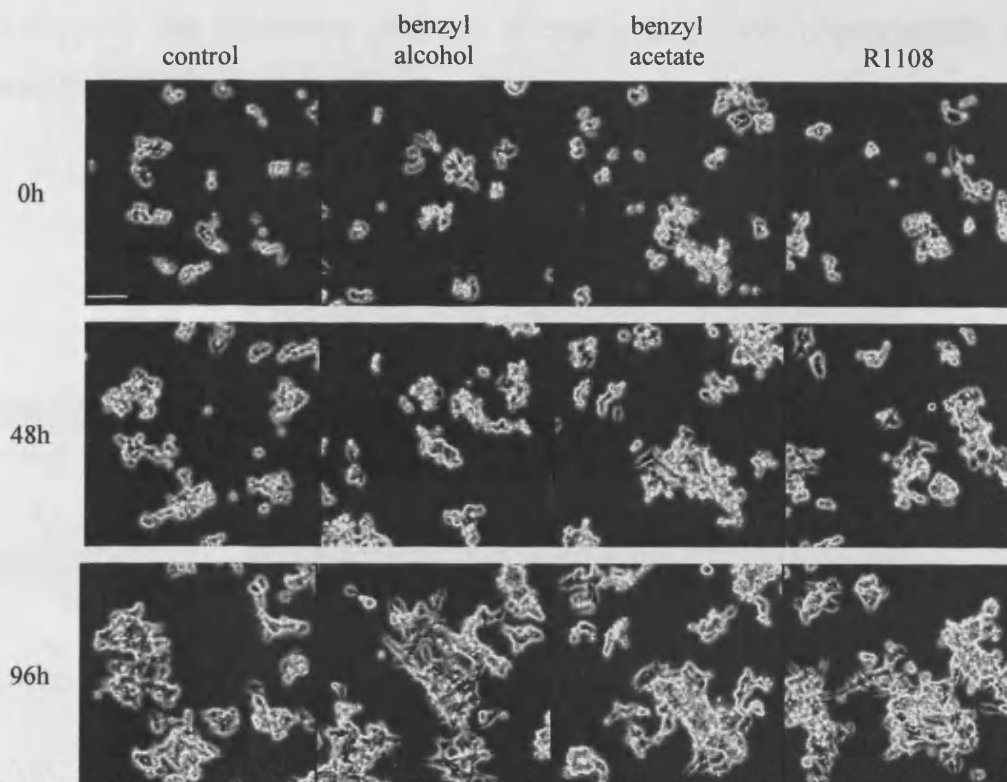
all the batches and to some extent in one of the batch over time (Table V.5). The inconsistency has not been associated with R1108 stability.

Table V.5: R1108 batches — toxicity profile.

<b>Name</b>	<b>Toxicity upon resuspension</b>	<b>Toxicity in Oct 2007</b>	<b>R1108 concentration Nov 2007</b>
R1108/2005	yes	no	/
R1108/2006	yes	yes	> 95%
R1108/2007	no	no	> 95%
R1108/2008a	no	/	/
R1108/2008b	no	/	/

#### **V.3.4.2. A role for R1108 metabolic products in cytotoxicity?**

Due to its chemical structure, R1108 is expected to be labile when exposed to esterases within cells. An esterase reaction would metabolise R1108 and release benzyl alcohol. To determine the potential anti-proliferative effects of R1108 breakdown products, the time lapse assay was repeated as before. NCI-H69 AP3 cells were treated continuously with 0.3 mM R1108/2007, 0.3 mM benzyl alcohol (Sigma-Aldrich, St Louis, MO, USA) and 0.3 mM benzyl acetate (Sigma-Aldrich, St Louis, MO, USA) for 96h. Figure V.9 indicates snapshot at 0 h, 48 h and 96 h of the treatment. Over the 96 h of treatment all cells showed normal growth characteristics, as a result of normal mitotic progression. Furthermore, cellular morphology including cell-cell and cell-substrate interactions showed that the cells were unaffected by the addition of R1108/2007 and any potential breakdown products.



**Figure V.9:** *Benzyl alcohol effect on cells.* NCI-H69 AP3 cells were treated with methanol, 0.3 mM benzyl alcohol, 0.3 mM benzyl acetate or 0.3 mM R1108. Calibration bar represents 50  $\mu\text{m}$ .

#### V.3.4.3. A role for purification regimen of R1108 compound?

As a result of feedback from the medicinal chemists and discussion on the potential source for R1108 cytotoxicity, further analysis was undertaken to address if the cytotoxicity was due to an incomplete purification process. Therefore, un-purified R1108 was tested on the NCI-H69 cell system alongside its fully HPLC-purified counterpart (figure V.10). Time-lapse microscopy analysis showed that long-term incubation with either compound had no cytotoxic effects. NCI-H69 SP cells maintained a highly clustered and refractile morphology, with normal growth characteristics, while NCI-H69 AP78 showed the characteristic flattened adherent phenotype producing monolayer of cells after 120 h (figure V.10a). A higher dose was also tested in order to determine if the lack of cytotoxicity could be concentration-related. NCI-H69 AP3 and NCI-H69 AP78 were treated continuously with 1 mM of R1108/2008a and R1108/2008b over 48 h (figure V.10b). Both cell lines showed normal

morphological cell attributes and an unchanged growth characteristic upon treatment with both compounds.

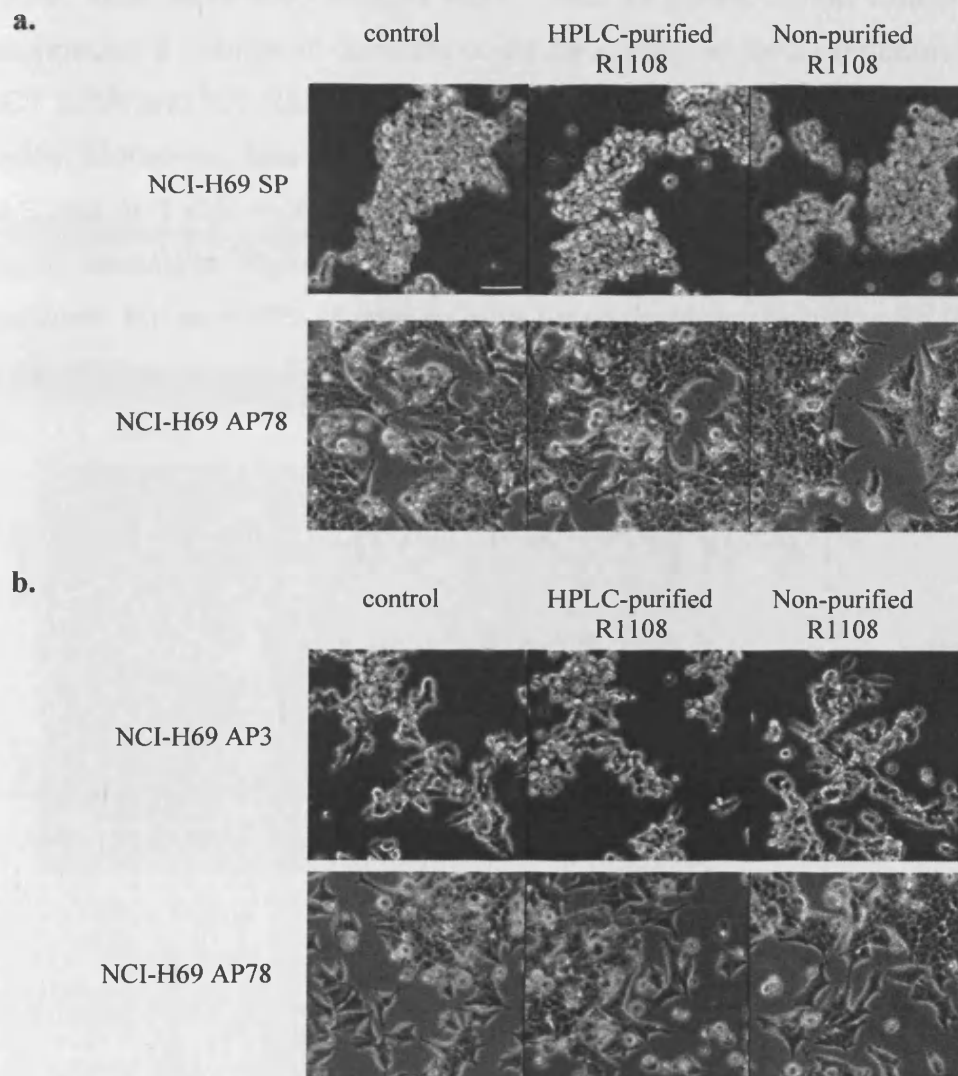


**Figure V.10:** *R1108 purification batches.* **a.** NCI-H69 SP and NCI-H69 AP78 were treated continuously with 0.3 mM R1108/2008a or R1108/2008b for 120 h. **b.** NCI-H69 AP3 and NCI-H69 AP78 were treated continuously with 1 mM R1108/2008a or R1108/2008b for 48 h. Calibration bar represents 50 $\mu$ m.

#### V.3.4.4. ICT compounds

As R1108 had an unexpected toxic effect on cells, the other unnatural sialic acid analogues were tested for toxicity. Cells were initially treated with the same high concentration used for R1108 treatment. Images (figure V.11a) at 24 h after a 0.3 mM treatment showed that NCI-H69 SP cells were unaffected by



treatment with any of the compounds. Indeed, comparable cell growth and cell refractility between the controls and treated wells were observed.

To investigate whether those compounds could induce death at a higher dose, cells were also treated with 1 mM of agent. When treated with 1 mM compound a change in contrast could be observed for 3 compounds, ICT 2553, ICT 2554 and ICT 2555. However, cell numbers remained similar to the control wells. Moreover, flow cytometry cell viability analysis of cells treated with either 0.3 mM or 1 mM indicated that there was no detectable increase in cell death upon treatment (figure V.11b). Indeed, around 50% of the control cells and between 40- and 55% of treated cells were positively stained with PI.

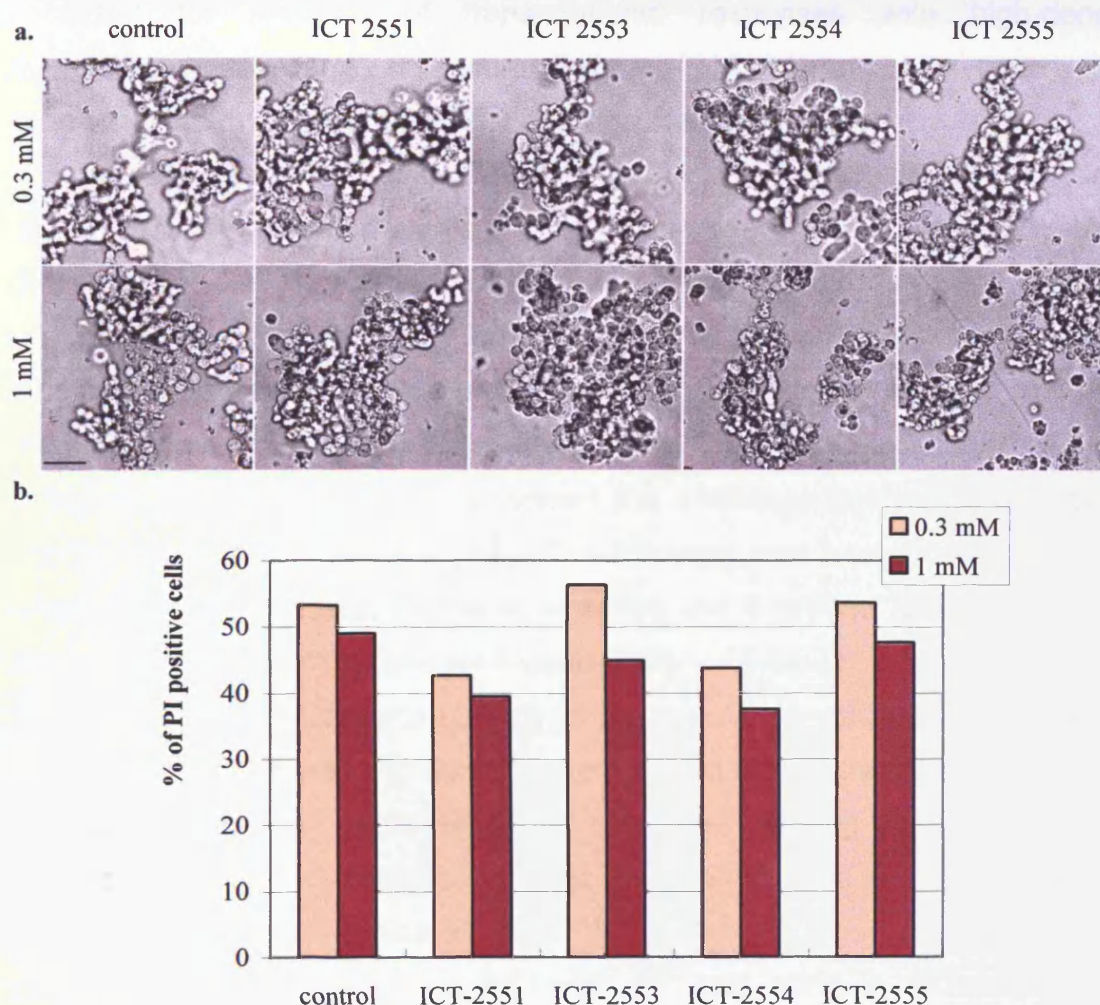


Figure V.11: *Induction of cell death by candidate PST inhibitors.* NCI-H69 SP cells were treated for 24 h with 0.3 mM or 1 mM of each compound (n=1). **a.** Snapshots at 24 h showing cell morphology and cell growth. Calibration bar represents 50  $\mu\text{m}$ . **b.** Flow analysis of PI treated cells.

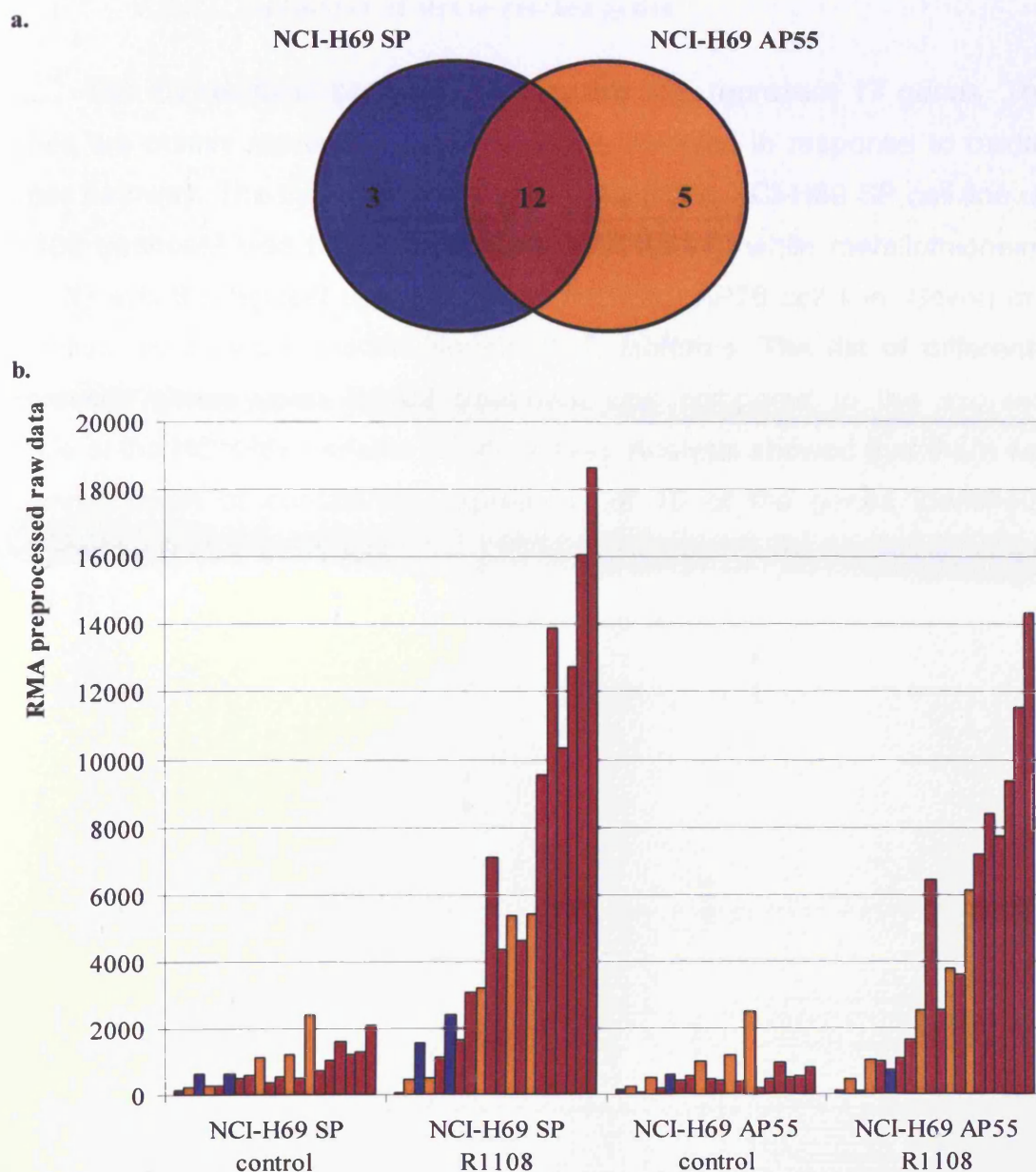
### V.3.5. R1108 toxicity: microarray study

Microarray analysis was performed to determine if the compound-induced cell death was due to specific and/or non-targeted effects and to identify possible mechanisms of cell death. In order to separate the toxicity effect from other possible effects, the drug concentration (0.3 mM R1108/2005) resulting in rapid and total growth inhibition and cell death was chosen. Cells were given sufficient time for a transcriptional response but short enough to avoid the occurrence of cell death. Therefore, NCI-H69 SP and NCI-H69 AP55 were treated continuously for 6 h with 0.3 mM R1108/2005. After 6 h, cells did not show any cell death event, therefore treated and untreated cells were processed for analysis of transcriptional responses with high-density oligonucleotide microarray on Human Genome U133A arrays. Arrays were then probed and scanned as previously described (see chapter II).

Quality control of hybridizations performed as previously described (chapter II and III) identified a chip with high background and noise (see appendix XII — figure 1 and 2). Therefore, two analyses were performed: one with and one without the lesser quality chip. Microarray analysis was performed as described in chapter II. The analysis including the outsider showed only little difference when compared to the analysis excluding it (see appendix XII — figure 3). Indeed, only 4 more probes passed the statistical analysis in the study including the high background array. The following was based on the analysis performed with all arrays, therefore including the 4 probes identified as less reliable properly indicated (see also appendix XII — Table 1).

Application of statistics (T-test) to the microarray data revealed that the signal of 485 probes was significantly altered upon R1108 treatment in NCI-H69 AP55 and 1081 probes in NCI-H69 SP. After filtering for probes for a requirement of a 2-fold change or greater in signal, 15 in NCI-H69 SP and 17 in NCI-H69 AP55 probes remained (figure V.12). Among those alterations, there was only 1 downregulation in NCI-H69 SP and none in NCI-H69 AP55. Moreover, 12 of these alterations were common upregulation in both cell lines. Therefore microarray analysis revealed similar responses to R1108 by both cell lines having different ST8SIA4 expression.





### **V.3.5.1. Induction of stress-related genes**

The 20 identified probes, listed in table V.6, represent 17 genes. These genes are mainly represented by molecules involved in response to oxidative stress pathway. The most highly induced gene in the NCI-H69 SP cell line upon R1108 treatment was heme oxygenase 1 (HMOX1), while metallothionein 1X (MT1X) was the highest upregulation in NCI-H69 AP78 cell line. Seven of the identified genes were metallothionein (MT) isoforms. The list of differentially expressed genes upon R1108 treatment was compared to the expression profile of the NCI-H69 variants (2008 arrays). Analysis showed that there was a downregulation of constitutive expression of 10 of the genes identified as induced by R1108 treatment.

**Table V.6: Transcriptional responses to R1108.** List of the genes with their expression statistically altered. Shaded cells show statistically significant > 2-fold changes. (a) fold change R1108 vs. control for NCI-H69 SP. (b) fold change R1108 vs. control for NCI-H69 AP55. (c) fold change NCI-H69 SP control vs. NCI-H69 AP55 control. Genes that passed only one of the analyses are indicated in italics. The false-colour cluster view represents the expression (average value of the triplicates) for each cell line on the 2008 arrays.

Affymetrix name	gene symbol	description	fold change			2008 array		
			NCI-H69 SP (a)	NCI-H69 AP55 (b)	controls (c)	SP	AP3	AP78
203665_at	<i>HMOX1</i>	<i>heme oxygenase (decycling) 1</i>	16.95	14.2	0.995			
204326_x_at	MT1X	metallothionein 1X	13.71	43.13	0.239			
204745_x_at	MT1G	metallothionein 1G	13.38	19.5	0.415			
208581_x_at	MT1X	metallothionein 1X	12.62	22.37	0.406			
206461_x_at	MT1H	metallothionein 1H	10.62	19.08	0.409			
217165_x_at	MT1F	metallothionein 1F	9.161	9.966	0.784			
212185_x_at	MT2A	metallothionein 2A	8.901	17.77	0.388			
213629_x_at	MT1F	metallothionein 1F	8.293	6.456	0.59			
211456_x_at	RPL35	ribosomal protein L35	6.567	8.533	0.746			
210524_x_at	AF078844	similar to metallothionein 1F	5.43	3.154	0.535			
212907_at	SLC30A1	solute carrier family 30 (zinc transporter), member	3.988	5.258	0.867			
212859_x_at	<i>MT1E</i>	<i>metallothionein 1E</i>	3.563	1.253	0.31			
216336_x_at	MT1M	metallothionein 1M	3.493	2.516	0.639			
221577_x_at	<i>GDF15</i>	<i>growth differentiation factor 15</i>	2.524	1.677	0.0993			
221258_s_at	<i>KIF18A</i>	<i>kinesin family member 18A</i>	0.447	0.794	1.637			
200800_s_at	HSPA1A	heat shock 70kDa protein 1A	4.009	3.142	0.756			
202581_at	HSPA1B	heat shock 70kDa protein 1B	2.687	2.494	0.829			
200799_at	HSPA1A	heat shock 70kDa protein 1A	2.15	2.464	1.172			
203925_at	GCLM	glutamate-cysteine ligase, modifier subunit	1.553	2.135	2.321			
222016_s_at	ZNF323	zinc finger protein 323; ZNF310P, ZNF20-Lp	2.036	2.104	0.959			



### V.3.5.2. MT induction validation

#### V.3.5.2.1. MT induction upon R1108/2006 treatment

Induction of metallothionein at the protein level was confirmed by western blot analysis on the whole cell lysate of NCI-H69 SP and NCI-H69 AP78 cells treated with 0.3 mM R1108/2006 for 0, 6 or 10 h, using the E9 antibody that recognizes MT isoforms 1 and 2 (figure V.13a). Downregulation of MT basal level in NCI-H69 AP78, suggested by the microarray analysis, was not confirmed by western blotting. Whereas, induction in both cell lines was confirmed. Indeed, a similar increase in MT protein expression was observed from 6h after treatment for NCI-H69 SP and NCI-H69 AP78. Moreover, treatment of NCI-H69 AP3 cell line with a non-toxic batch of the compound (R1108/2007) did not induce MT (figure V.13b), confirming that toxicity and MT pathway induction were linked.

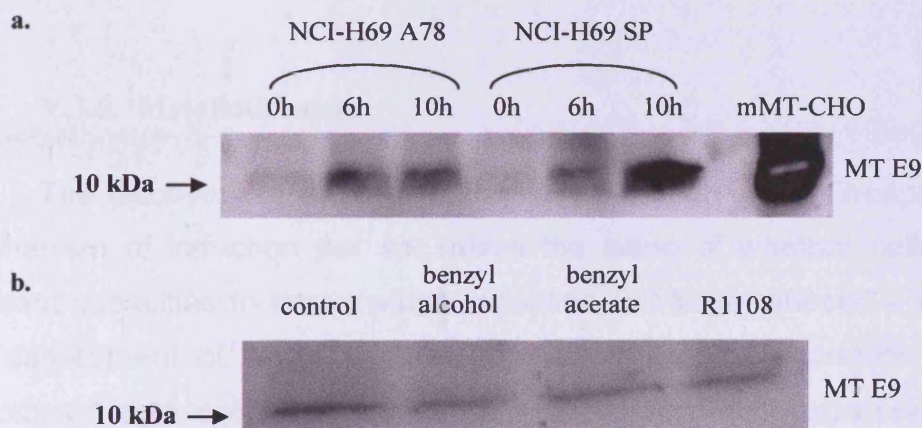


**Figure V.13: Immunoblotting detection of metallothionein induction.** **a.** NCI-H69 AP8 and NCI-H69 SP treated with 0.3mM of R1108/2006 for 0, 6 or 10 h. Data is representative of 2 independent experiments. **b.** NCI-H69 AP3 treated for 24 h with 0.3 mM of R1108/2007, benzyl alcohol or benzyl acetate (n=1).

#### V.3.5.2.2. ICT compounds

In order to assess whether induction of the metallothionein pathway is related to the type of compound, western blotting detection of metallothionein after 6 h treatment with the ICT compounds (data not shown) was performed and showed no induction. However, ICT compounds were found not as toxic as

R1108, therefore a higher concentration of compounds was used along with higher incubation time. After 24 h treatment with 1 mM of the compounds, 2 of the compounds (ICT 2553 and ICT 2554) — who induced changes in contrast of treated cells after 24 h treatment — also induced MT when treated with 1 mM ICT 2553 and ICT 2554 (figure V.14), therefore showing similarity with R1108.

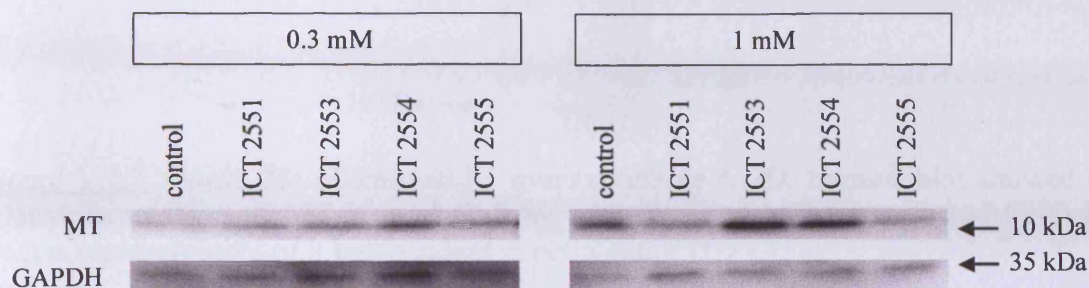


**Figure V.14:** *Immunoblotting detection of metallothionein induction after 24 h treatment.* NCI-H69 SP cells were treated with 0.3 or 1 mM of each PST compounds for 24 h (n=1).

### V.3.6. Metallothionein

The discovery of the metallothionein induction effect, irrespective of the mechanism of induction *per se*, raises the issue of whether cells may have different capacities to demonstrate induction (off-target effects) – complicating the assessment of future second generation agents. Therefore, to test the hypothesis that enhanced constitutive metallothionein expression leads to reduced toxicity of R1108, we used the mouse metallothionein-overexpressing CHO, mMT-CHO-K1 (Smith *et al.*, 2008). The mMT-CHO-K1 cell line overexpresses MT1 (figure V.15). R1108 effects on the transfected and parental CHO-K1 were studied using time-lapse microscopy.



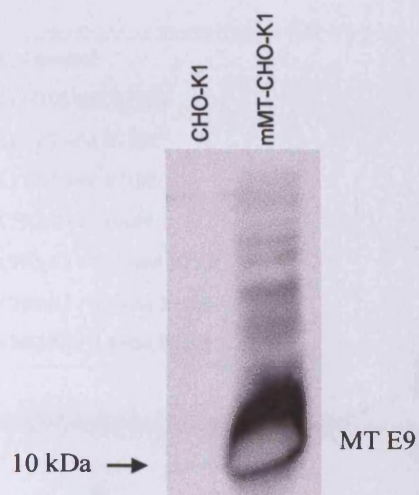


**Figure V.15:** *mouse Metallothionein-1 overexpressing CHO*. Immunoblot showed the relative expression of MT-1 and MT-2 by wild-type and MT-1 transfected CHO-K1. Data is representative of 3 independent experiment.

#### V.3.6.1. Inhibition of CHO growth by R1108

We compared the growth of cells treated with various concentrations of R1108/2006. Figure V.16 shows the growth profile derived from time-lapse analysis. Increasing concentrations of R1108 caused a dose-dependent decrease in growth of parental and transfected cell lines treated *in vitro* for 3 days. No effect on population growth was observed for the low dose of R1108. Growth rate was slower for the transfected cell line at 0.1 mM R1108, as seen by the 70% inhibition of growth rate for the WT and 85% inhibition of growth rate for the transfectant cell line after 60 h. Complete inhibition of the population growth for both cell types was observed at 0.3 mM R1108.



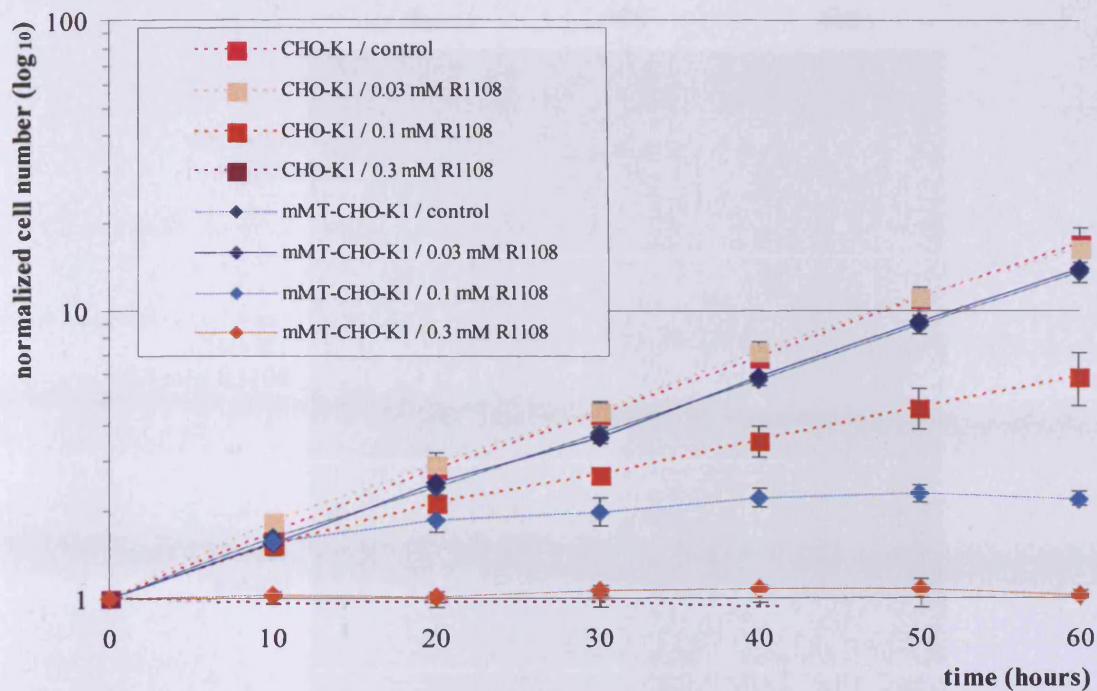


**Figure V.16:** Effect of a range of R1108/2006 concentrations on the growth of the population of CHO-K1 and mMT-CHO-K1. Cells in each field were counted every ten hours (equivalent to 40 frames). Cell numbers for each field were normalised to the number of cells at the beginning of the experiment for that field. Each point represents the mean  $\pm$  SD of  $n = 3$  fields.

However, both CHO-K1 cell lines appeared to be more resistant to R1108 than the NCI-H69 variants. Indeed, even with 0.3 mM R1108 treatment, cell survival could be observed for the transfected as well as for the parental cell type (figure V.17). The control fields of each cell types showed normal mitotic progression with confluence reached at 60 h. Observation of the mitotic process showed that cells treated with 0.3 mM of R1108 underwent mitosis resulting in polyploidy.

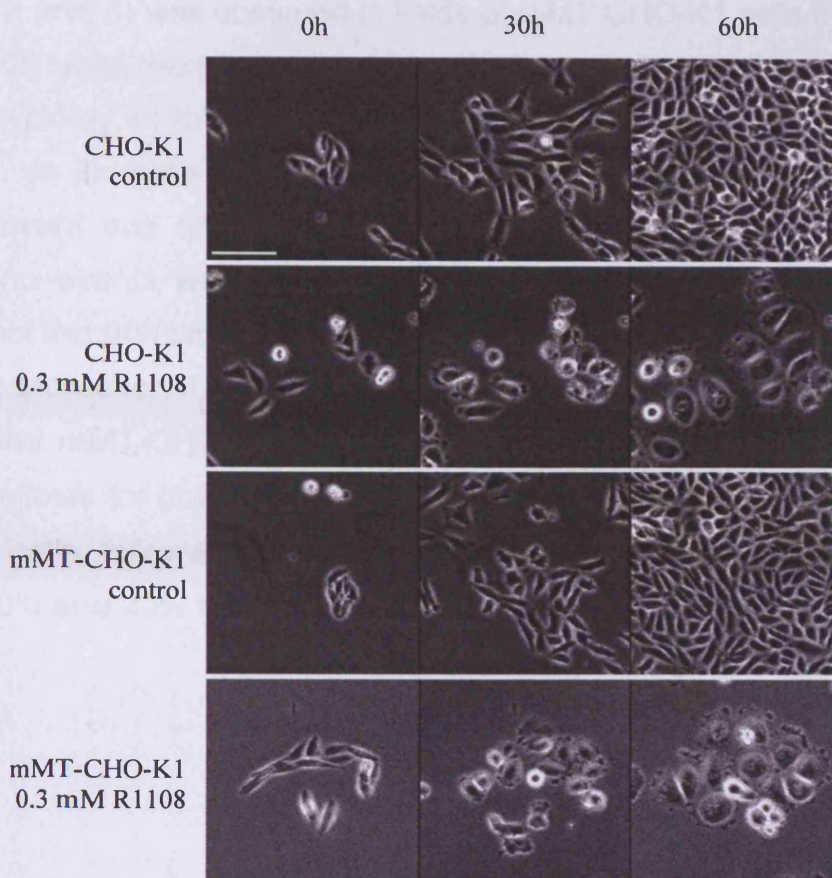


**Figure V.17:** *Effect of various concentrations of R1108 on cell growth.* Still images from the time-lapse sequence taken at 0 h, 30 h and 60 h. Cells were treated with 0.3 mM R1108/2006. Calibration bar represents 50  $\mu$ m.

### V.3.6.2. Effect on mitosis

In-depth analysis of time-lapse by tracking single cells through 3 successive events revealed that R1108 treatment induced a higher incidence of polyploidy events (Figure V.18). Cells in control fields and cells in fields treated with 0.03 mM R1108 (data not shown) progressed normally through the cell cycle (more than 95% of events resulted in successful mitosis). When treated with 0.1 mM R1108, 85% of the first generation of CHO-K1 cells went through a normal mitosis, while 8% of cells underwent polyploidy. The second generation of cells continued mostly through normal mitosis (47%). There was, however a higher polyploid induction (39%). Around half the cells of the third generation still went through normal mitosis. The analysis also showed an increase of cell death throughout the events (3% at first event, 11% at third event). A decreased rate of successful mitosis (73% mitosis at the first event decreased to 30-20%

at event 2 and 3) was observed in fields of mMT-CHO-K1 cells treated with 0.1 mM R1108 while there was an increase in the occurrence of the polyploid event (60% polyploidy for the second generation and 40% for the third). Similar to the CHO-K1, an increase of cell death was observed (0% at first event, 7% at the second event and 8% at third event). When treated with the high dose of R1108, no events were recorded for ~32% of the initially seeded CHO-K1 throughout the 90h time-lapse, while the proportion is ~1.5% for the mMT-CHO-K1 cells. Moreover, 17% of the first generation of CHO-K1 cells died and only 1% for the mMT-CHO-K1. Around 2% of first generation cells went through normal mitosis for both cell types. Finally, 94% of the first generation of mMT-CHO-K1 cells, followed by 82% of the second generation, engaged in polyploid event (40% and 20% for CHO-K1 cells).



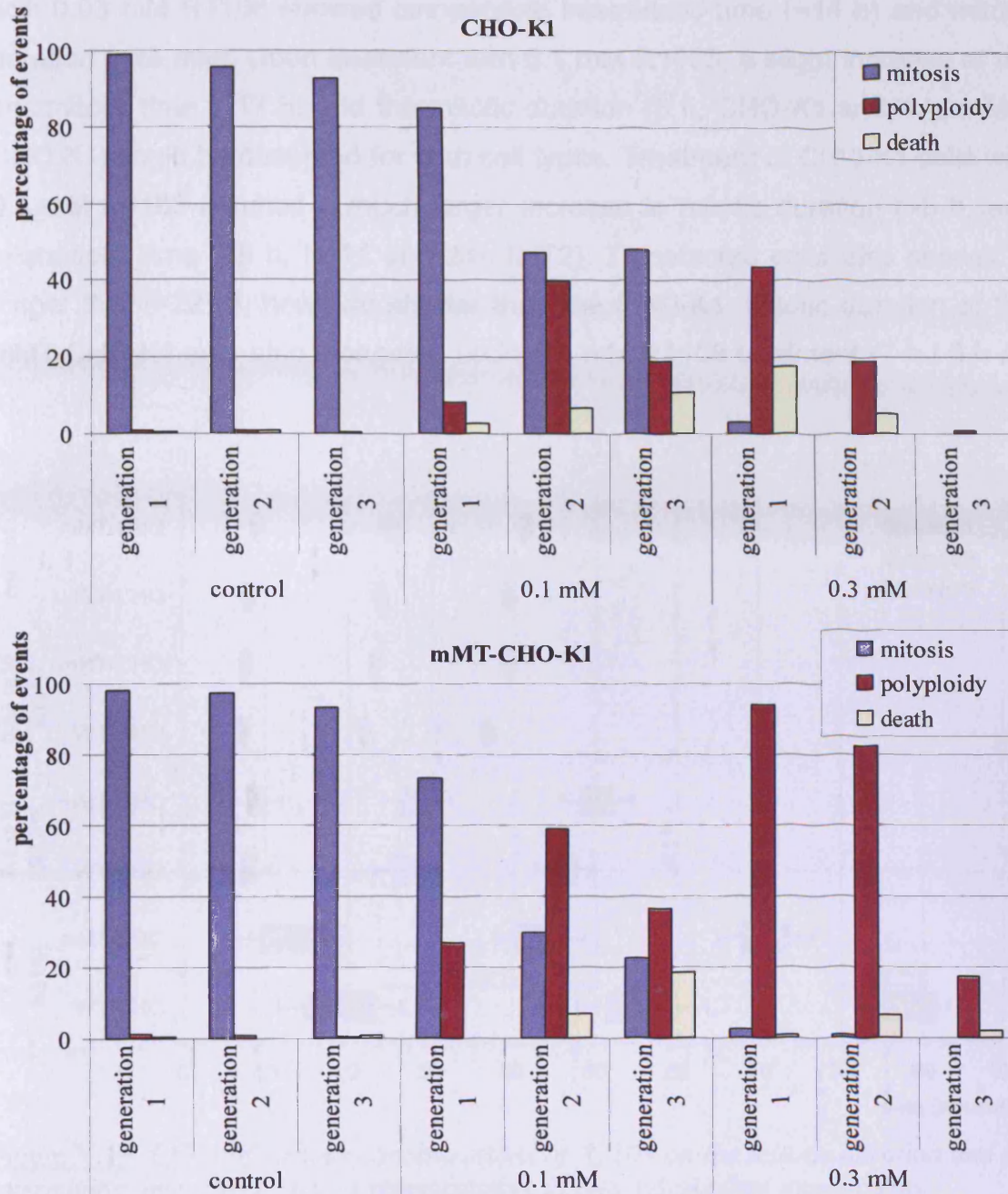
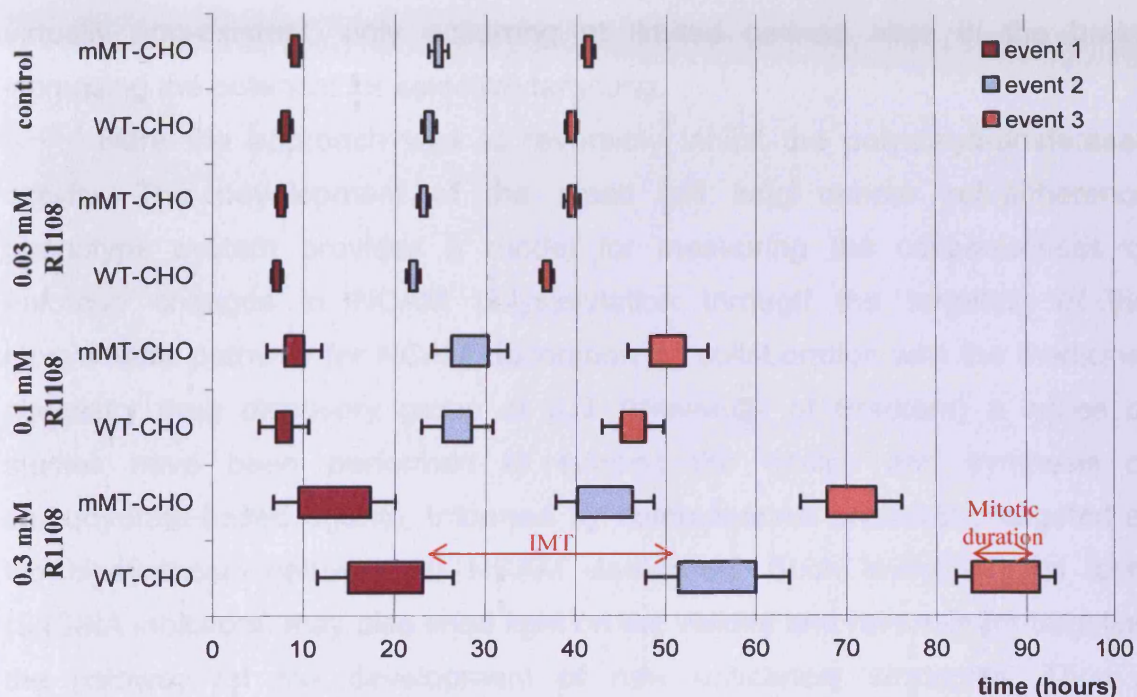


Figure V.18: Effect of increasing concentrations of R1108 on the mitotic outcome of the CHO cell lines over three generation. Data is representative of two independent experiments.

Time-lapse analysis also showed an increase of intermitotic time (IMT / mitosis to mitosis) and mitotic duration. Figure V.19 graphically shows the duration of mitosis and the mean intermitotic time for progenitor cells and subsequent progeny. The data show no significant impact of MT-1 expression on intermitotic time or mitotic duration (controls). Control cells and cells treated

with 0.03 mM R1108 showed comparable intermitotic time (~14 h) and mitotic duration (~48 min). Upon treatment with 0.1 mM R1108, a slight increase of the intermitotic time (~17 h) and the mitotic duration (3 h, CHO-K1 and 4 h, mMT-CHO-K1) could be observed for both cell types. Treatment of CHO-K1 cells with 0.3 mM R1108 induced a much larger increase in mitotic duration (~8 h) and intermitotic time (28 h, IMT1 and 24h IMT2). Transfected cells also showed a longer IMT (~22 h), however shorter than the CHO-K1. Mitotic duration of the mMT-CHO-K1 was also elongated upon 0.3 mM R1108 treatment (7 h / 6 h / 5 h).



**Figure V.19:** Effect of various concentrations of R1108 on the mitotic duration and the intermitotic time (IMT). Data is representative of two independent experiments.

#### V.4. Discussion

PSA decoration of NCAM, by directing tumour growth, invasion and metastasis (Daniel *et al.*, 2001; Seidenfaden *et al.*, 2003; Suzuki *et al.*, 2005) and given its restricted expression in normal adult tissues (Walmod *et al.*, 2004), offers drug design opportunities for post-translational modification. Developmentally, PSA is assembled on the surface of NCAM in the developing brain and facilitates neural tissue development by modulating the inhibition of cell-cell contact – a function potentially re-iterated in micro- and macro-SCLC cell masses. Importantly, in normal cells by adulthood PSA-decorated NCAM is virtually non-existent, only occurring at limited defined sites in the brain, increasing the potential for selective targeting.

Here the approach was to reversibly inhibit the polysialyltransferases activity. The development of the small cell lung cancer cell-adherence phenotype system provides a model for measuring the consequences of enforced changes in NCAM polysialylation through the targeting of the biosynthesis pathway for NCAM decoration. In collaboration with the medicinal chemistry drug discovery group at ICT (University of Bradford) a series of studies have been performed to support the design and synthesis of carbohydrate-based agents, informed by computational chemistry, targeted at the biosynthesis pathway for NCAM decoration. Such investigational tools (ST8SIA inhibitors) may also shed light on the validity and rationale for targeting the pathway for the development of new anticancer strategies. Thus a secondary purpose of the studies reported here was to explore the NCI-H69 model further for possible deployment in candidate drug evaluation programmes given the potential to translate the model into xenograft systems.

*NCI-H69 variants and glycosylation* — Microarray analysis identified mostly variation in expression of glycosylation-related genes in the NCI-H69 AP3 variant. Interestingly, heparanase (HPSE) was found upregulated in NCI-H69 AP78 when compare to NCI-H69 SP and NCI-H69 AP3 (1.8 and 3.7 fold respectively). HPSE has been shown to degrade heparan sulfate (HS) on the cell surface and extracellular matrix, with physiological functions in wound



healing, development and HS turnover (Nasser, 2008). Moreover, HSPE has been found to mediate cell adhesion to ECM, integrin-dependent cell spreading and reorganisation of the actin cytoskeleton. HSPE was also found to function as an adhesion molecule independently of its enzymatic function (Goldshmidt *et al.*, 2003). HPSE overexpression is found in a variety of cancers, where it is implicated in tumour growth, angiogenesis, metastasis and inflammation (Nasser, 2008). Another intriguing identification was the downregulation of the glucuronic acid epimerase (GLCE) in NCI-H69 AP3 when compared to NCI-H69 SP and NCI-H69 AP78 (1.4 and 2.3 fold respectively). GLCE has been previously found to be downregulated in breast cancer (Grigorieva *et al.*, 2008).

*NCI-H69 variants and the sialic acid pathway* — GNE (UDP-GlcNAc 2-epimerase / ManNAc 6-kinase), a key determinant of the sialic pathway was found downregulated in both adherent cell lines. GNE is known to control sialic acid pathway. Indeed, GNE regulates the sialic acid synthesis with an inhibitory feedback from CMP-Neu5Ac. Therefore controlling the cellular sialic acid concentration, limiting both polysialyltransferases and regulating the polysialylation of NCAM (Bork *et al.*, 2005; Keppler *et al.*, 1999). However GNE downregulation in NCI-H69 P78 (the variant cell line with high PSA) showed not effect on PSA expression.

FUT8 (fucosyltransferase 8 (alpha (1,6) fucosyltransferase) was found downregulated in both adherent cell lines. FUT8 adds a fucose in  $\alpha$ 1,6 linkage to the Asn-linked GlcNAc in the *N*-glycan core. FUT8 is the only mammalian protein responsible for core fucose on glycans (Wang *et al.*, 2005b). While early studies suggested that the presence of an  $\alpha$  1,6 core fucose was required for PSA decoration of NCAM by the two transferases (Kojima *et al.*, 1996), in mice *in vivo* various combinations of glycans were found to be polysialylated (including unfucosylated *N*-glycans) (Galuska *et al.*, 2008).

Several factors have been suggested to influence the polysialyltransferases expression level, such as retinoic acid (Angata and Fukuda, 2003). A study also uncovered a role for the developmental transcription factor PAX3 (3 paired box 3) in NCAM polysialylation. Indeed, PAX3 overexpression was linked with increased NCAM polysialylation through

regulation of ST8SIA2 expression (Mayanil *et al.*, 2000). PAX3 expression levels across all the NCI-H69 variants were similar.

*NCI-H69 variants and polysialyltransferases* — Consistent with previous finding (Scheidegger *et al.*, 1995), NCI-H69 SP was found to express both ST8SIA2 and ST8SIA4. ST8SIA2 mRNA could not be detected in both adherent cell lines while low levels were detected in NCI-H69 SP. ST8SIA4 was found to be downregulated in NCI-H69 AP3 but still detectable by RT-PCR. ST8SIA4 mRNA level were found to be equivalent in NCI-H69 SP and NCI-H69 AP78, suggesting ST8SIA4 alone is not responsible for higher PSA content in NCI-H69 AP78. The implications of NCI-H69 SP, expressing both polysialyltransferases while NCI-H69 AP3 and NCI-H69 AP78 express only ST8SIA4 remain to be elucidated.

These results confirm the presence of the enzyme target in all 3 cell types, with different expression level and population heterogeneity, suggesting the usefulness of the NCI-H69 model for inhibition and target validation studies. Moreover, unlike an engineered system with a high expression level of sialyltransferase, the NCI-H69 variant model provides a range of endogenous levels of sialyltransferases expression leading to the dynamic range of PSA decoration found in tumours. This offers the possibility to study the implication of variation in the sialic acid pathway, as well as polysialyltransferases expression, on PSA decoration. NCI-H69 AP3 could also provide a test of potential off-target activity of inhibitors.

*NCI-H69 variants and polysialyltransferases inhibition* — New therapeutic strategies are urgently needed that contain the metastatic disease state without further compromising tumour chemosensitivity. The linked therapeutic concept that underpins the experimental therapeutics context of the thesis is that metastatic potential may be managed for critical periods in therapeutic regimens by limiting the natural exploration of phenotypic plasticity even in tumour cells that have accrued critical genetic lesions. The specific proposal is to engineer features of the tumour cell glycocalyx (in this case PSA decoration of NCAM) to reduce the potential for the expression of critical drivers

for metastatic spread and to extend therapeutic windows for other agents without the accrual of drug resistance. The control of glycocalyx 'plasticity', operating through changes in NCAM decoration, is an attractive proposition both in terms of tools to explore the consequences of plasticity and as a rationale for drug discovery through *in vitro* target validation and mechanisms of action studies. An early model (Acheson *et al.*, 1991) of glycocalyx dynamics makes the striking prediction that PSA could affect not only NCAM function, but also other ligands not directly involved in NCAM-mediated adhesion – widening the possible functional impact of PSA targeted agents.

The chapter primarily focuses on an exemplar first generation compound, while techniques for agent purification and synthesis were also undergoing optimisation. A practical objective of the work was to assess the potential for inhibition of polysialylation and thereby inform the design and synthesis of second generation related compounds. This first compound — R1108 — showed, in an initial screen, knockdown of cell surface detectable PSA-NCAM, with no apparent effects on NCAM expression, but induction of a toxic response. Due to low *in vivo* stability R1108 could not be considered as a possible *in vivo* agent and the synthesis route was not pursued. Nevertheless, in order to inform the synthesis of other compounds, investigations on the cellular consequences and PSA-NCAM of R1108 expression in the SCLC variants were completed.

Studies using R1108 were limited essentially by the quantity of compound available and the inconsistency between the batches, combined with the fact that early analysis were performed while establishing in parallel the NCI-H69 variant system. However, despite the limitations of such a study, undertaking this chemistry-biology collaboration provided the necessary foundation for establishing (i) compound handling, (ii) adequate quantities for analysis and (iii) audit trailing. Four other compounds were also received and, due to restricted quantities, allowed for a single screen for PSA down-regulation and cellular toxicity. It was not possible to ascertain the reason for the inter-batch variability – chemical integrity was assured by NMR, MS and elemental analysis although the possible presence of a minor (less than 1%) impurity contributing to some observed effects cannot be ruled out.

***NCI-H69 variants and polysialyltransferases inhibitors development*** —

Overall, with the exception of ICT 2555, there was no indication of PSA decoration of NCAM knock-down upon treatment with any of the Bradford compounds.

***NCI-H69 variants and R1108 toxicity*** — Despite inter-batch variability, two of the batches showed an intriguing dose-dependent toxicity. R1108 toxicity could not be linked to breakdown products. Therefore, using microarray analysis, we investigated the perturbation of the system with an agent targeting a specific step in the polysialic acid pathway. Interestingly, after 6 hours of treatment, no death-related transcriptional activity was detected and there was no-sialic acid pathway-related genes expression modulation.

The microarray signature of R1108 treatment can be linked to stress-pathways. Indeed, heat shock proteins A1 (HSPA1 / HSP70), heme oxygenase 1 (HMOX1 and metallothioneins (MT) are well know actors involved in stress responses, such as oxidative stress (Ferrandiz and Devesa, 2008; Palmiter, 1998; Schmitt *et al.*, 2007). Also, common induction of some of these proteins could be found — such as HMOX1 and MT2A induction caused by the antineoplastic, gallium nitrate (Yang and Chitambar, 2008) or induction of HMOX1, MT and HSP70 after cadmium exposure — only one study showed a similar signature to R1108. Interestingly, this study showed the induction of HSPA1A, GCLM, MT1, MT2, GDF15, SLC30A1 and HMOX1 in biochemically stretched cardiomyocytes (Frank *et al.*, 2008). Interestingly, cell death and metallothionein seemed to be provoked by the other ICT compounds. However, higher concentration and longer compound/cell contact time were necessary, perhaps reflecting differences in cell membrane penetration of the agents investigated.

***Metallothionein*** — Metallothioneins (MTs) play a role in both zinc and copper homeostasis and comprise a class of ubiquitously-occurring low molecular weight cysteine- and metal-rich proteins, containing conserved sulfur-based metal clusters, with diverse functions including potentially protective effects against oxidative stress and highly toxic metals such as cadmium (Miles *et al.*, 2000). The metal ions, for which MT has a high affinity, are zinc, copper,

cadmium and mercury (Maier *et al.*, 1997; Vallee, 1991). Mice deficient in MT were found to be more susceptible to cadmium (Klaassen and Liu, 1998), supporting it having a function in heavy metal detoxification.

The two main isoforms, MT1 and MT2 are expressed in almost all mammalian tissues (Jin *et al.*, 1998). They are generally expressed at basal levels, while being inducible by a number of factors, such as metals, hormones, inflammatory cytokines and xenobiotics (Jasani and Schmid, 1997). Humans have at least 16 MT genes and seven different genes in humans encode MT1 (Garrett *et al.*, 1998; Jasani *et al.*, 1998). Human MT1E and MT1A levels are increased with Cd<sup>2+</sup>, Zn<sup>2+</sup> or Cu<sup>2+</sup> pre-treatment (Garrett *et al.*, 1998). The most widely expressed mammalian MT1 and MT2 isoforms are rapidly induced in the liver by a wide range of metals, drugs and inflammatory mediators (Coyle *et al.*, 2002).

Although detoxification of heavy metals seems to be a property of MTs, it may not be their primary function. Cells with lower levels of MT are more sensitive to DNA damage while overexpression of MT appears to reduce spontaneous mutagenesis. Using a derivative of the CHO-K1 cell line (Kao and Puck, 1968) overexpression was achieved using an autonomously replicating expression vector. CHO-K1 cells were chosen because of their low endogenous expression of MT even after treatment with metals. The pBPV vector, with a non-inducible promoter, was used here to generate transfectants that overexpressed MT to obtain an induction-independent evaluation of MT protection against R1108 effects. Resistance to exogenously supplied Cd<sup>2+</sup> was established for the present study (Smith *et al.*, 2008) to confirm that the MT-1 overexpressed was functional. Furthermore, a previous study had shown that the endogenous antioxidant status of transfectant and parental cells was similar (Wallace *et al.*, 1996), showing similar levels of glutathione peroxidase, catalase, superoxide dismutase and reduced glutathione. Although, R1108 induced cellular toxicity in the CHO cell line, toxicity levels were lower than for the NCI-H69 cell lines. Indeed, cell death was not observed at the lower dose. Moreover, no significant differences were found between the MT-expressing CHO and the parental cell line, suggesting that R1108 cytotoxicity is not provoked by heavy metal contaminants.



Therefore, R1108 toxicity remains to be explained. Intriguingly a recent study links a possible R1108-gene expression signature to a similar profile induced by biomechanical stretching leading to hypertrophy (Frank *et al.*, 2008). Therefore it would seem appropriate during the next agent synthesis phase of R1108 and the new ICT derivatives to undertake a screen alongside other known agents that cause cell hypertrophy and cell cycle arrest such as sialylated gangliosides (Masson *et al.*, 2005). This would provide further insights on the toxic affect of R1108 and related agents.

The study led to the discovery of potential biomarkers for R1108 agent-related death; provided biological information on the requirements and hence the synthesis of new agents. Therefore in this context the SCLC variant system provides an ideal drug screening model system.

## VI. Discussion

New SCLC therapeutic strategies are urgently needed that contain spreading disease without further compromising tumour chemosensitivity. Variation in the ability of a tumour cell to interact with the extracellular matrix and adjacent cells reflects complex changes at the cell surface and is an evolving theme in attempts to link metastasis and chemoresistance (Sethi *et al.*, 1999). Therapies aimed at the containment of variation in adhesion properties could provide opportunities for the managed suppression of metastatic behaviour, the collateral recruitment of previously unavailable therapeutic targets and the extension of windows of chemosensitivity for novel combination treatments. Cancers result from the accumulation of inherited and somatic mutations in oncogenes and tumour suppressor genes and consideration of how these might evolve in a population has been addressed in modelling studies as potential origins for drug resistance (Iwasa *et al.*, 2006; Michor *et al.*, 2006). At least two models, potentially co-existent, have been put forward to account for heterogeneity and inherent differences in tumour-regenerating capacity: the cancer stem cell (CSC) and clonal evolution models (overview in Vezzi and Parmiani, 2008; Visvader and Lindeman, 2008). Within the SCLC study, evidence of clonal evolution/selection was uncovered together with findings pertinent to the origins of drug resistance as driven in CSCs through efflux-based drug resistance.

The aims of this thesis were restricted to the development and characterisation of a model SCLC system to address the nature and impact of variant generation within classical SCLC cell populations on the possible origins of drug resistance arising from phenotypic plasticity and to develop a therapeutic model for limiting the cellular consequences of plasticity. The approach was technically different from that explored by Sethi and co-workers (Sethi *et al.*, 1999) and that of Kraus *et al.* (Kraus *et al.*, 2002) and Salge *et al.* (Salge *et al.*, 2001) who focused on the impact of ECM interactions, Akt-signalling and changes in matrix metalloproteinases respectively. The overview of the findings is mapped to the adherence plasticity concept in a summary schematic (figure VI.1).

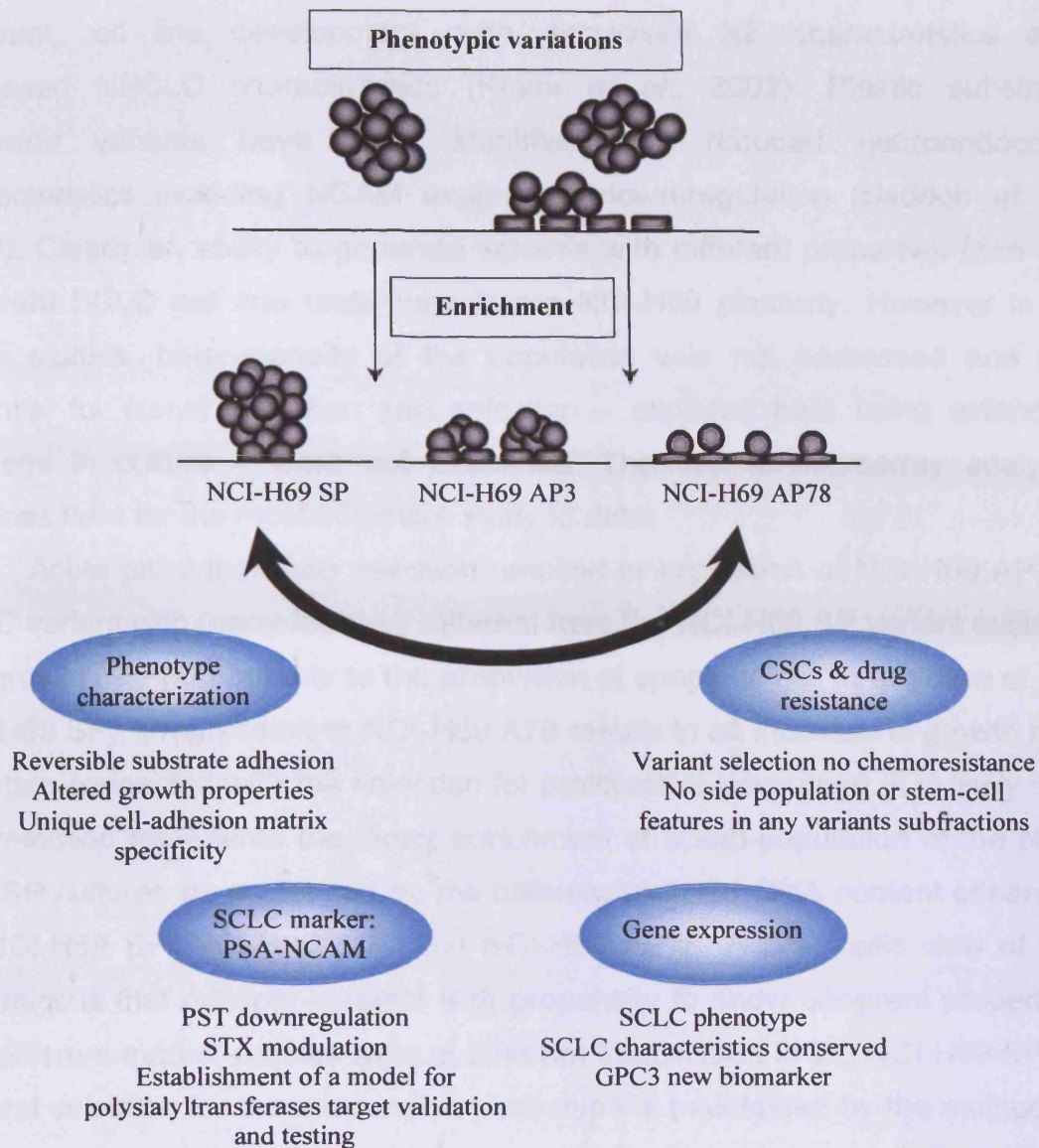


Figure VI.1: Overview of the thesis highlights addressing the stated aims of the study.

### Development and characterisation of a novel SCLC cellular system: Cellular dynamics

*Phenotypic plasticity and SCLC variants* — Several NCI-H69 variants systems have been previously developed and characterised to initiate and address phenotypic variants, in relation to plasticity, signalling status and chemoresistance. BrdU induced NCI-H69 differentiation resulted in the development of substrate adherence, increases in cell-cell adherence junctions and up-regulation of epithelial markers (Gilchrist *et al.*, 2002; Prindull and Zipori, 2004). Poly-L-lysine adherent variants selection has resulted in an apoptosis-

resistant cell line development, with decreased NE characteristics and increased NSCLC characteristics (Kraus *et al.*, 2002). Plastic substrate adhesion variants have been identified with reduced neuroendocrine characteristics including NCAM expression down-regulation (Seddon *et al.*, 1998). Clearly an ability to generate variants with different properties from the NCI-H69 SCLC cell line underlines innate NCI-H69 plasticity. However in all those studies, heterogeneity of the population was not addressed and the potential for clonal evolution and selection – explored here using extended passage in culture – were not examined. The use of microarray analysis provides here for the most complete study to date.

Acute pro-adherence selection resulted in expansion of NCI-H69 AP3 a SCLC variant with many features different from the NCI-H69 SP variant such as low growth rate (attributable to the proportion of apoptotic cell in the case of the NCI-H69 SP). Progression to NCI-H69 A78 results in an increase in growth rate – a state connected with the selection for proliferative advantage. It is likely that the selection represents the direct enrichment of a sub-population of the NCI-H69 SP cultures as evidenced by the differences in G1 DNA content observed for NCI-H69 SP, NCI-H69 AP3 and NCI-H69 AP78. A pragmatic view of the dynamics is that multiple variants with propensity to show adherent properties and different marker profiles exist at different frequencies in the NCI-H69 SP. A general selection for the suspension phenotype is maintained by the method of culture and the microniches formed by cell-cell association. This general selection does not confer any proliferative advantage for cells capable of plasticity and early expression of adherence upon presentation of a suitable substrate. If PSA expression were to impose a negative advantage to proliferation or survival in suspension then expression would be lost. This is clearly not the case. Upon variant selection at NCI-H69 AP3, cultures are now subject to new selection pressures relating to maintenance of the adherence phenotype (demonstrably plastic given its reversibility) and some proliferative advantage. These selection principles upon extended passage result in the overgrowth of the NCI-H69 AP78 sub-population. The microarray analyses therefore define SCLC gene expression profiles (NCI-H69 SP versus NCI-H69 AP78) that conserve SCLC markers irrespective of adherent growth. Furthermore, NCI-H69 AP3-restricted gene expression may therefore represent



pathways for initial microniche exploitation before proliferative advantage becomes a principle of selection.

Thus it is suggested that a lower growth rate in NCI-H69 AP3 (versus NCI-H69 AP78) may be attributable to an active repression, operating even in variants harboured within the NCI-H69 SP population. Candidates for this would be the tumour suppressor GPC-3 and lower neuroendocrine expression (such as GRP) easily identifiable by loss of the marker PSA. Long term enrichment of NCI-H69 AP3 provided an opportunity for proliferative/survival advantage to assert an influence and to allow for a clonal evolution/ expansion. The process produced the hyperploid, fast growing NCI-H69 AP78 variant that sustains the neuroendocrine and SCLC features presented by the NCI-H69 SP culture. The proposed NCI-H69 variant model for heterogeneity and plasticity is represented in figure VI.2.

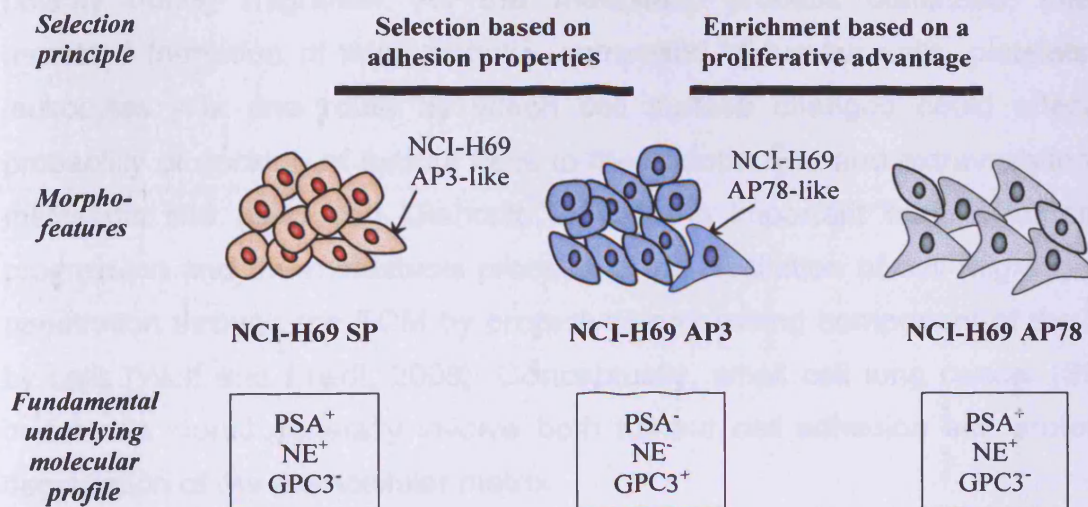


Figure VI.2: *NCI-H69 variant model.*

The model provide a framework for considering the impact of limiting the expression of PSA (originally with the aim of reducing the range of survival/growth support for within a NCI-H69 SP population) and whether this would be synonymous with the phenotype shown by NCI-H69 AP3. If PSA modulation drives cells to a NCI-H69 AP3 state the model predicts enhanced adhesion without generating resistance or proliferative advantage.

*NCI-H69 variants — Implications on metastasis* — The underlying processes governing the various patterns of metastasis observed in different tumour types remains unclear. It appears likely that there are some common features for both phenotypic behavioural changes and the impact of genetic alterations. Studies on disseminated tumour cells found in the bone marrow of patients with various types of solid tumours, including lung tumours, suggest that the cells seem to first disseminate from the early primary lesions and then acquire additional genetic defects (Pantel and Brakenhoff, 2004). The amalgamation of intravital imaging and gene expression profiling methods has started to place into context behavioural processes occurring at early invasion stages (Wang *et al.*, 2005a). Such approaches have highlighted the role of enhanced motility for successful tumour cell invasion of the microenvironment. Changes in specific integrin signals appear to enable cancer cells to detach from neighbouring cells, facilitate matrix remodelling and re-orientate their polarity during migration. As the metastatic process continues, integrin-mediated formation of microemboli - composed of tumour cells, platelets and leukocytes - is one route by which cell surface changes could affect the probability of docking of tumour cells to the endothelium and extravasation at a metastatic site (Guo and Giancotti, 2004). An important feature for cancer progression and the metastasis process is the facilitation of cell migration and penetration through the ECM by proteolytic processing component of the ECM by cells (Wolf and Friedl, 2008). Conceptually, small cell lung cancer (SCLC) metastasis would generally involve both tumour cell adhesion and proteolytic degradation of the extracellular matrix.

The present study shows no evidence that the variants have altered *in vitro* invasion potential although the limitations of the invasion assay used are clear and does not necessary determine *in vivo* behaviour. In a collaborative study with ICT Bradford the suspension and early adherent variant showed similar *in vivo* growth (and retention of the *in vitro* PSA expression profiles) as subcutaneous xenografts. However, it is likely that subcutaneous sites are inappropriate for SCLC invasion modelling but critically demonstrate that *in vivo* culture *per se* does not impose phenotypic reversion. Importantly, *in vivo* there is no 'loss' of cells from the system by serial passage, as imposed *in vitro*, but there remain selective pressures for proliferative advantage. It is possible that



the NCI-H69 AP3 state only comes into play at tumour regions experiencing microniche exploration and penetration through tissue barriers. This view is supported by the findings of an earlier study that attempted to reconcile the observation that the classic SCLC cell line NCI-H69, when grown in suspension expresses only negligible proteolytic activity. Salge *et al.* found that selection for adherent growth generated adherent cells with enhanced matrix metalloproteinases 2 and 9 expression (Salge *et al.*, 2001).

*NCI-H69 variants — implications on chemoresistance* — The variant selection did not result in expansion of a drug resistant clone, although a wider drug screen would be appropriate. However, in attempting to translate the clear demonstration of variation and plasticity in SCLC cell populations into an *in vivo* context the situation becomes more complex. Early tumours may harbour cells with innate non-phenotypic plasticity related drug resistance and the therapeutic intervention itself may act to modulate the dynamics of the metastatic process. The concept of phenotypic plasticity-targeting therapies may be of particular value in limiting responses of target populations to factors generated by a given intervention such as surgery. Retsky *et al.* (1997) have used a mathematical model of breast cancer metastasis to investigate the observed double-peaked frequency of relapse distribution at 18 and 60 months. They attributed relapse to the stimulation of the metastatic growth due to surgery with a proposed mechanism of stimulation via angiogenesis of distant dormant micrometastases (Retsky *et al.*, 2004). Here the hypothesis is that a burst of angiogenesis of distant dormant micrometastases after surgery provides for increased aggressiveness of the tumour and paradoxically a recruitment into a more chemosensitive state (Retsky *et al.*, 2004).

The clonal expansion of the NCI-H69 AP78 variant with proliferative advantage could provide for sub-populations that could both acquire drug resistance according to the Goldie-Coldman model and rapidly repopulate tumours. The choice of TPT for the study was also based on its known cell cycle specificity that would target rapidly growing tumour populations. The current results show that there is no firm connection between variant selection and a natural acquisition of drug resistance.

The Goldie-Coldman model (Goldie and Coldman, 1979) predicts the presence drug-resistant mutants even within the  $10^9$  neoplastic cells nominally present at diagnosis for treatment-naïve primary tumour sites. This has informed a chemotherapeutic approach of rapidly alternating the administration of equally effective drugs to prevent clonal resistance (Panetta, 1998). This 'clonal resistance' problem can occur within a background of phenotypic plasticity enhancing the probability of development of the metastatic phenotype. One of the early models that attempted to describe effective adjuvant chemotherapy is that of Norton and Simon (Norton and Simon, 1986). They assumed that all tumour growth, tumour regression, and tumour regrowth is Gompertzian. The Norton–Simon hypothesis, at variance with the log-cell kill hypothesis (Skipper, 1964), suggested that tumours given less time to regrow between treatments are more likely to be destroyed if therapeutic intent is to effect cell kill or de-population. According to Gompertzian kinetics, as the tumour becomes smaller its growth fraction increases and it regrows at a faster rate. Thus a cure will never be effected if regrowth rate is not matched or exceeded by the rate of cell kill. The implication for treatment is that the only way to overcome this 'kinetic resistance' barrier is the absolute eradication of every viable micrometastatic cell and that intervals between chemotherapy treatment are critical (Clare *et al.*, 2000) – a process that would be enhanced by reducing any ongoing supply of micrometastatic cells. Again, limiting the potential for variant generation, for example through limiting phenotypic plasticity and hence a driver for kinetic resistance. This view suggests that limitation, even without the accrual of drug resistance, of growth potential is as critical as size of the target population. This view suggests that limitation, even without the accrual of drug resistance, of growth potential is as critical as size of the target population.

*Phenotypic plasticity and origins of drug resistance* — Most small cell lung cancer (SCLC) patients relapse within 12 months of starting combination chemotherapy plus radio-therapy, due to the development of acquired chemo- and radio-resistance. This phenomenon has been related to the induction of tumour differentiation, resulting in apoptosis-resistant, morphologically variant

(v-SCLC) cells which lack the neuroendocrine expression of classic (c-) SCLC cells (Kraus *et al.*, 2002).

A study of the isolation of spontaneously adherent SCLC sublines, as part of an attempt to generate an *in vitro* model of variant differentiation in SCLC, found down-regulation of neuroendocrine markers and up-regulation of epithelial differentiation markers cyclin D1, endothelin, the cell adhesion molecules CD 44 and integrin subunits  $\alpha 2$ ,  $\beta 3$  and  $\beta 4$  (Kraus *et al.*, 2002). Interestingly these workers also found that the sensitivity of the adherent SCLC sublines to etoposide, cyclophosphamide and gamma radiation was significantly diminished. This multi-agent resistance was attributed to the differentiation to v-SCLC and cell adhesion triggering an Akt-dependent inhibition of apoptosis with an un-tested prediction that v-SCLC could generate topotecan resistance (Kraus *et al.*, 2002).

Here it is suggested that resistance is likely to be multifactorial. Indeed, in the Kraus *et al.* study no connection was made between the discovered cyclophosphamide resistance and the possible contribution of the aldehyde dehydrogenase 1 (ALDH1A1) expression found to be present in the NCI-H69. The aldehyde dehydrogenase (ALDH) superfamily comprises genes encoding NAD(P)(+)-dependent enzymes that oxidize a wide range of reactive and toxic aldehydes to their corresponding carboxylic acids (Vasiliou *et al.*, 2000). ALDH1A1 has previously been identified in a limited analysis of genes overexpressed in a classical multidrug resistance MDR P-glycoprotein expressing gastric carcinoma cell line (Ludwig *et al.*, 2002). The anticancer agent, cyclophosphamide, is metabolized by cytochrome P450 (CYP), glutathione S-transferase (GST) and aldehyde dehydrogenase enzymes. Aldehyde-dehydrogenase levels have also been correlated with resistance to cyclophosphamide, while resistance induced by enforced overexpression of ALDH1A1 can be reversed by disulfiram, an ALDH1A1 inhibitor (Magni *et al.*, 1996). ALDH1A1 overexpression has been previously recognized as part of possible multidrug resistance patterns associated with drug-metabolizing capacity in cells resistant to cyclophosphamide (Bao *et al.*, 2007) providing a rationale for CSC resistance. Moreover, ALDH1A1 is cancer stem cell marker (Visvader and Lindeman, 2008). ALDH1A1 expression decreased in NCI-H69 AP3 compared to the suspension parent and the NCI-H69 AP78 states. This

observation of in variation ALDH1A1 expression in the variants indicates that variation, in the absence of drug selection, may lay the foundation of drug resistance to agents such as cyclophosphamide. However, on the basis of the lack of efflux-dependent changes in TPT and there being no apparent side population phenotype in the NCI-H69 we suggest that the recruitment of a CSC-like population by adherence selection did not occur.

*Tumour cell glycocalyx and the therapeutic challenge addressed in the PST inhibitor study* — Changes in cell surface decoration by complex carbohydrates (collectively forming a 'glycocalyx') are intimately involved in the shifts in cell-cell and cell-matrix adhesion properties that accompany cellular development, differentiation and metastatic transition (Brooks and Leathem, 1991; Kayser *et al.*, 1998; Nakagoe *et al.*, 2000; Nakagoe *et al.*, 1998; Renkonen *et al.*, 1997). Glycocalyx sugars are assembled from simple monosaccharides, notably *N*-acetylneuraminic (sialic) acid, to form complex oligo- and polysaccharides (Yarema and Bertozzi, 2001) and present potential anti-cancer therapeutic targets (Christofori, 2003; Sell, 1990; Yarema and Bertozzi, 2001). An early step in metastasis involves detachment and escape from the primary tumour (Couzin, 2003) with roles in this critical step for sialic acid metabolism (Brooks and Leathem, 1991; Nakagoe *et al.*, 2000; Nakagoe *et al.*, 1998; Renkonen *et al.*, 1997). A refined model of primary tumour and metastatic growth dynamics, developed by (Koscielny *et al.*, 1985) showed that metastatic initiation could occur at a tumour volume of the primary lesion that was only slightly smaller than that at the time of tumour diagnosis unlike the modelling outcome obtained by others that metastatic initiation occurs very early in the development of the primary tumour if an exponential growth model is adopted (Koscielny *et al.*, 1985). One implication is that metastasis potential containment therapies may become increasingly important as screening programmes evolve and attempt to inform early intervention.

*Phenotypic plasticity and tumour population dynamics- therapeutic implications* — Phenotypic plasticity in tumour cell populations has the undesirable potential to maximise Darwinian fitness for the selection of metastatic and drug-resistant variants. The operation of selection pressures

during the expansion of a tumour cell population could operate on plastic characteristics such as the glycocalyx, affecting cell-cell contacts and increasing the probability of intravasation. Here critical factors would include the initiation time, population expansion kinetics and population size at diagnosis. The chemosensitivity of cells demonstrating neoplasia-favourable but reversible phenotypes, such as cell-adhesion mediated drug resistance (Sethi *et al.*, 1999), would also impact on the prognosis. These factors would act as stochastic drivers for the ongoing growth of variant lineages or cellular cohorts further facilitated by a ratchet-like and sequential accrual of non-reversible genetic changes - including those that impact upon genetic instability and apoptotic susceptibility. On the other hand, limiting the potential for variant generation, for example through phenotype reversal or limiting phenotypic plasticity, is intuitively a route for controlling neoplastic progression but would need to be integrated with active surgical or tumour eradication regimens.

#### **Impact and future work:**

*Drug screening:* The availability of cells with variant properties without apparent sub-populations of CSCs or innate differences in resistance to TPT provides a platform for drug screening against a wider panel of agents. The model allows for the impact of cell adhesion to be excluded or to be explored with respect to difference ECM influences. The availability of NCI-H69 AP78 with an adherent phenotype but retention a many critical NCI-H69 SP markers should allow for clonogenic assays and other HTS-based screens (difficult to achieve with suspension cultures).

*Novel methods of cellular analysis and sorting:* The extensive characterisation for PSA expression and enzymatic removal allows basic studies on the impact of surface charge. Preliminary studies in collaboration with Bangor University have established methodologies for exploiting shifts in cell membrane dielectric properties as a probeless method of cell separation. The current study has also laid the foundations for modulating the surface characteristics, through polysialyltransferases inhibition, and the possible use of dielectrophoretic properties for agent screening. A dielectrophoresis quadrapole



system has been used as a proof of principle study and has succeeded in identifying differences in permittivity characteristics for NCI-H69 SP and NCI-H69 AP3 cells. Further, a sorting micro-technology device has been used to sort phenotypic variations providing a novel (non-labelling) cytometric tool for analysis, identification and monitoring of tumour heterogeneity.

*Glycocalyx targeting agents:* Collaboration with Prof Patterson and Dr Falconer (Institute of Cancer Therapeutics, Bradford) will be pursued to develop new polysialyltransferases inhibitors. The primary focus will be the development of an *in vitro* assay for inhibition studies, before testing on a rat glioma overexpressing SIAT8SIA2 and the NCI-H69 model reflecting population heterogeneity. Further characterisation of the NCI-H69 model, in terms of PSA-NCAM and NCAM kinetics upon polysialyltransferases inhibition will also be needed.

*Modulation of SCLC behaviour in 3D ECM systems:* In collaboration with Prof Peter Friedl (Department of Cell Biology, Nijmegen, The Netherlands) the variant SCLC system is under study with a focus on the visualisation of cell-matrix interactions by using 3D extracellular-matrix-based cell-culture models and advanced imaging procedures. The preliminary studies are aimed at observing the adherent form behaviour in the 3D Collagen Matrix Assay assessed by Time-Lapse videomicroscopy (Wolf and Friedl, 2008). The *in situ* drug responses for cells in this system would be of particular interest with respect to polysialyltransferase inhibition.

*In vitro/in vivo 3D microtumour systems:* Our demonstration of the striking retention of cellular interaction and growth patterns of the NCI-H69 AP78 variant when forced into 3-D growth on hydrophobic surfaces suggest that the NCI-H69 system could be translated to a hollow fibre system (Shnyder *et al.*, 2006; Shnyder *et al.*, 2005; Suggitt *et al.*, 2006) to study the impact on drug sensitivity. Preliminary studies have established the cell loading requirements for NCI-H69 variants growth and recovery from fibres.

*Cancer biomarkers from cell biology to clinic:* The cancer biomarker problem in SCLC suggests a need for better cancer characterisation (Sawyers,

2008), particularly in anticipation of new therapies that aim to target SCLC biology. In collaboration with Dr Allen Gibbs (Llandough Hospital, Department of Histopathology, Cardiff and Vale NHS Trust), we have identified histopathological specimens representing SCLC clinical presentation of primary tumour with no detectable metastases – these primary samples showed very high levels of NCAM expression (figure VI.3). Here the future aim would be to survey using immunofluorescence for the ‘markers’ identified in our NCI-H69 system to gauge co-expression and set the variant system into context. Here a priority is the expression of GPC3 protein.

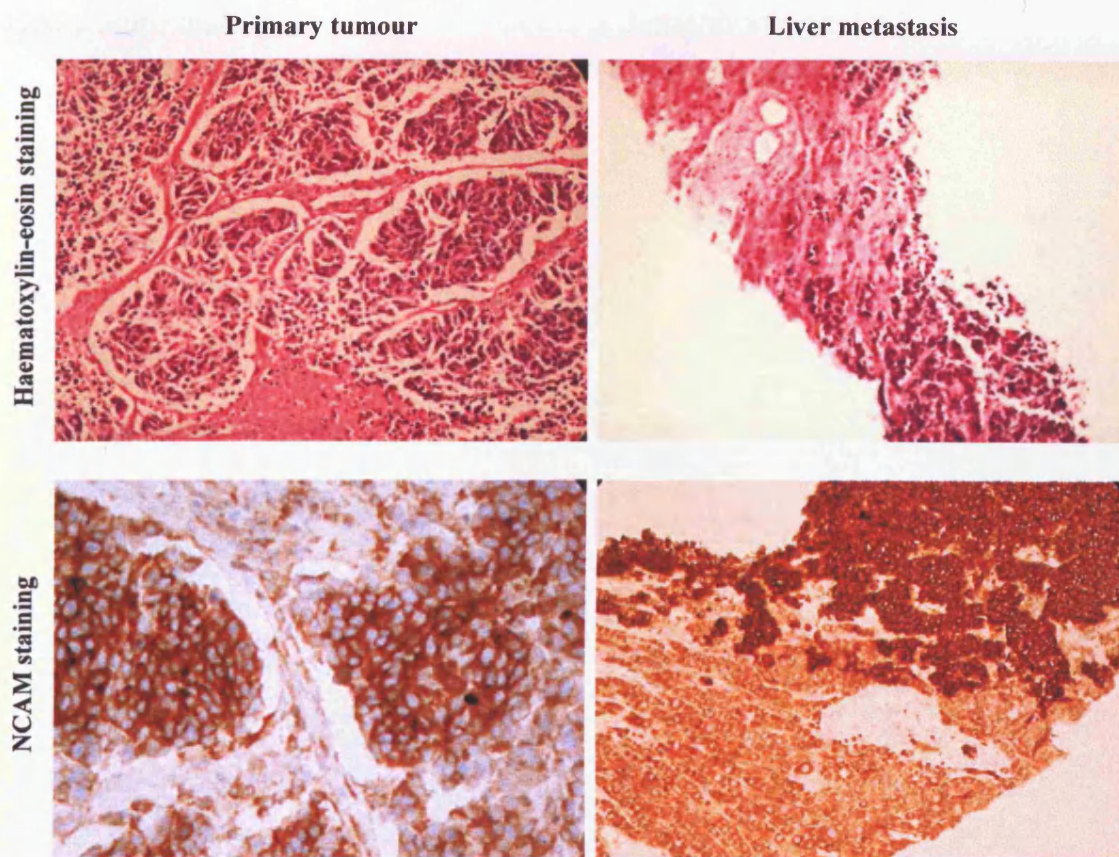


**Figure VI.3:** *SCLC*. Localized small cell carcinoma of the lung vs. liver metastasis stained with haematoxylin-eosin or NCAM.

## **Appendix I: Reagents and suppliers**

Chloroform	Fisher Scientific (Loughborough, UK)
Coverslips	VWR international Ltd (Lutterworth, UK)
Ethanol, analytical grade	Fisher Scientific (Loughborough, UK)
Glass microscope slides	Raymond A. Lamb (Eastbourne, UK).
Isopropanol	Fisher Scientific (Loughborough, UK)
Methanol, analytical grade	Fisher Scientific (Loughborough, UK)
PBS (cell culture)	Gibco (Invitrogen, Carlsbad, CA, USA)
Cell culture dishes	Corning (Loughborough, UK)

## Appendix II: Western blotting solutions

### Solutions for Western Blotting:

#### **Lysis buffer**

Tris	50mM	GE Healthcare (Little Chalfont, UK)
EGTA	5mM	Sigma (St Louis, MO, USA)
NaCl	150mM	Sigma (St Louis, MO, USA)
Triton	1%	GE Healthcare (Little Chalfont, UK)
PMSF	1mM	Sigma (St Louis, MO, USA)
Aprotinin	8µg/mL	Sigma (St Louis, MO, USA)
Leupeptin	10µg/mL	Sigma (St Louis, MO, USA)
H <sub>2</sub> O		

#### **3x sample loading buffer**

TRIS-Cl pH 6.8	240mM	GE Healthcare (Little Chalfont, UK)
SDS	6%	GE Healthcare (Little Chalfont, UK)
Glycerol	30%	GE Healthcare (Little Chalfont, UK)
DTT	0.2M	Sigma (St Louis, MO, USA)
Bromophenol blue	0.05%	Sigma (St Louis, MO, USA)
H <sub>2</sub> O		

#### **Upper gel buffer**

Tris	545mM	GE Healthcare (Little Chalfont, UK)
SDS	0.4%	GE Healthcare (Little Chalfont, UK)
H <sub>2</sub> O		
pH adjusted to 6.8		

#### **Lower gel buffer**

Tris	1.2M	GE Healthcare (Little Chalfont, UK)
SDS	0.4%	GE Healthcare (Little Chalfont, UK)
H <sub>2</sub> O		
pH adjusted to 8.8		

#### **Resolving gel**

	7.5%	10%	12.5%
Lower gel buffer	1.5mL	1.5mL	1.5mL
acrylamide/bisacrylamide* 40%	1.1mL	1.5mL	1.9mL
ammonium persulfate** 10%	60µL	60µL	60µL
TEMED**	6µL	6µL	6µL
H <sub>2</sub> O	3.3mL	2.9mL	2.5mL

\*Sigma (St Louis, MO, USA) \*\*GE Healthcare (Little Chalfont, UK)

<b>Stacking gel</b>	4%	5%
Upper gel buffer	600µL	600µL
acrylamide/bisacrylamide* 40%	250µL	300µL
ammonium persulfate** 10%	25µL	25µL
TEMED**	2.5µL	2.5µL
H <sub>2</sub> O	1.6mL	1.5mL

\*Sigma (St Louis, MO, USA) \*\*GE Healthcare (Little Chalfont, UK)

**Running buffer**

Glycine	192mM	GE Healthcare (Little Chalfont, UK)
Tris	25mM	GE Healthcare (Little Chalfont, UK)
SDS	0.1%	GE Healthcare (Little Chalfont, UK)

**Transfer buffer**

Glycine	192mM	GE Healthcare (Little Chalfont, UK)
Tris	25mM	GE Healthcare (Little Chalfont, UK)

**Blocking solution**

Blocking Reagent	3%	GE Healthcare (Little Chalfont, UK)
Tween-20	0.1%	GE Healthcare (Little Chalfont, UK)
PBS		Sigma (St Louis, MO, USA)

**Wash solution (PBS-T)**

Tween-20	0.1%	GE Healthcare (Little Chalfont, UK)
PBS		Sigma (St Louis, MO, USA)

## **Appendix III: RT-PCR solutions**

### **Solutions for RT-PCR:**

#### ***50x TAE buffer***

Tris base                      2 M                      Fisher Scientific (Loughborough, uk)

Sodium acetate·3H<sub>2</sub>O      1 M                      Fisher Scientific (Loughborough, uk)

EDTA·Na<sub>2</sub>·2H<sub>2</sub>O            50 mM                  Sigma (St Louis, MO, USA)

H<sub>2</sub>O

pH adjusted to 7.2 with glacial acetic acid (Fisher Scientific, Loughborough, uk)

#### ***5x non-denaturing sample loading buffer***

Glycerol                      50%                      GE Healthcare (Little Chalfont, UK)

Bromophenol blue          0.05% (w/v)          Sigma (St Louis, MO, USA)

H<sub>2</sub>O



**Appendix IV: SCLC cell lines panel PSA-NCAM expression.**

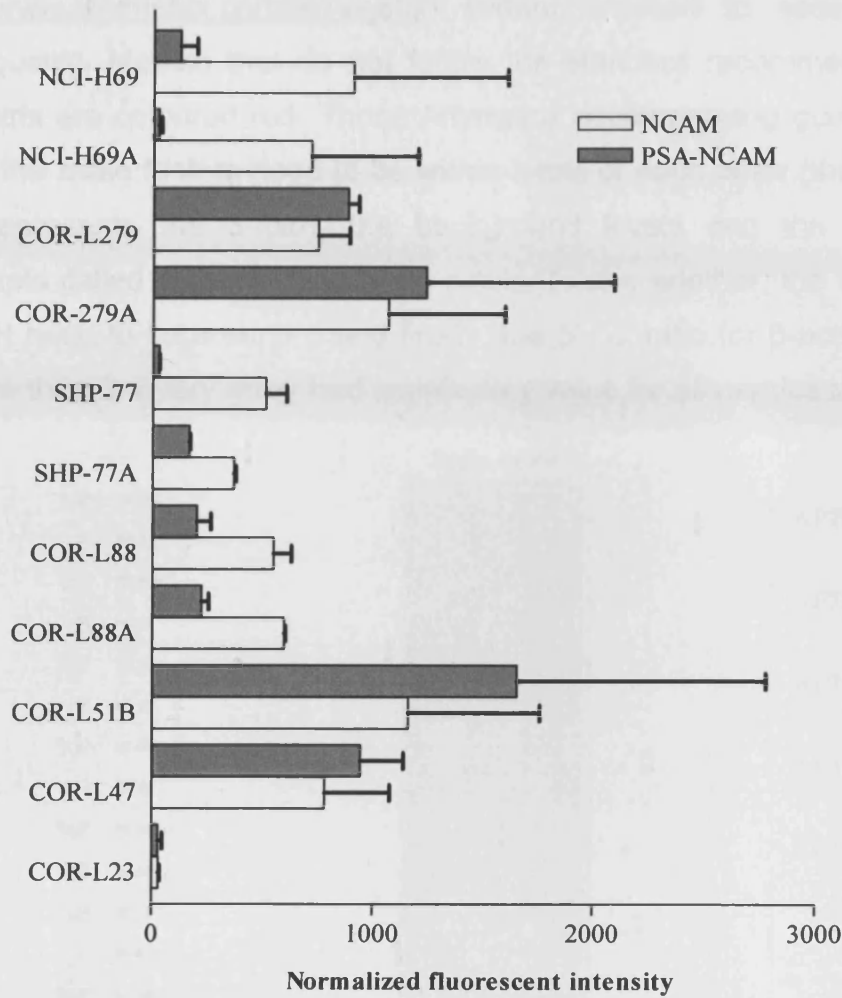


**Figure 1:** *SCLC cell lines panel PSA-NCAM expression.* Flow cytometry analysis of PSA-NCAM and NCAM expression.

## Appendix V: 2008 arrays quality assessment

Figure 1 shows the report from the simpleaffy package on the 5 metrics (<http://www.affymetrix.com/index.affx>) commonly used to assess Affymetrix array quality. Metrics that do not follow the standard recommendations from Affymetrix are coloured red. Those Affymetrix accompanying guidelines are as follow: the scale factors need to be within 3-fold of each other (the blue shaded area represents the 3-fold), the background levels and the proportion of transcripts called present need to be similar to one another, the 5' / 3' ratio for GAPDH need to be around 1 and finally, the 5' / 3' ratio for  $\beta$ -actin need to not be more than 3. Every array had satisfactory value for all metrics tested.

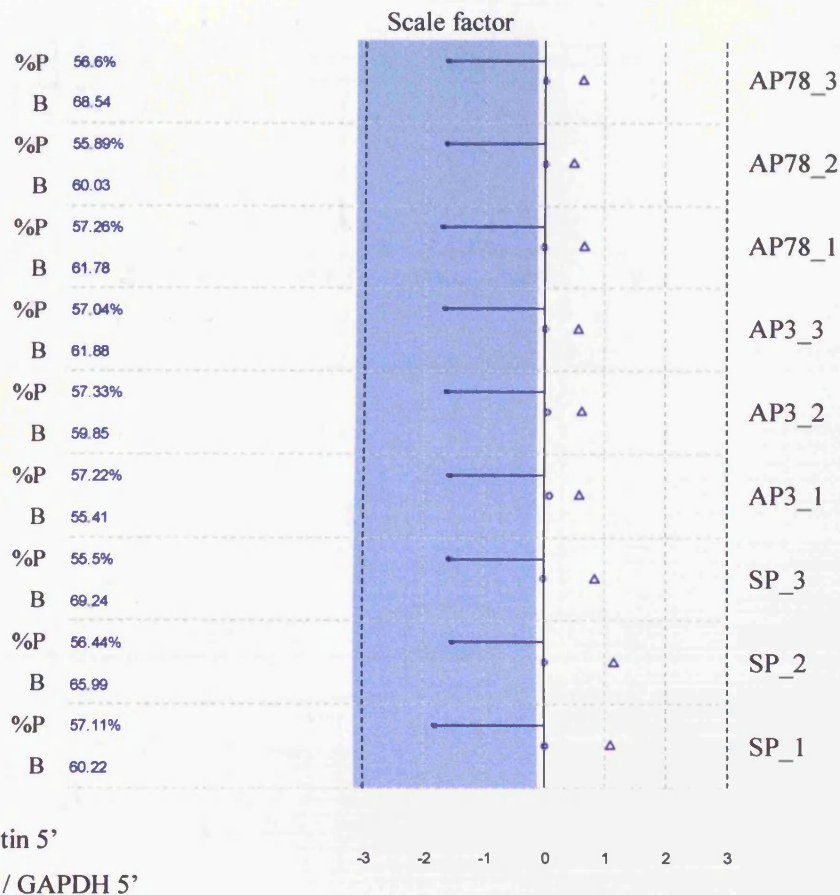


Figure 1: 2008 arrays — MAS5 computed quality control report. Simpleaffy package generated quality control showing 5 metrics (background (B), percent present (%P), scale factor, GAPDH 5'/3' ratio and Actin 5'/3' ration) commonly used to asses arrays quality.

Figure 2 shows the report from the AffyPLM package. Every array showed a NUSE (*normalised unscaled standard error*) value around 1 and a RLE (*relative log expression*) value around 0, thus each array passed the quality test. (RLE) and (NUSE) plots

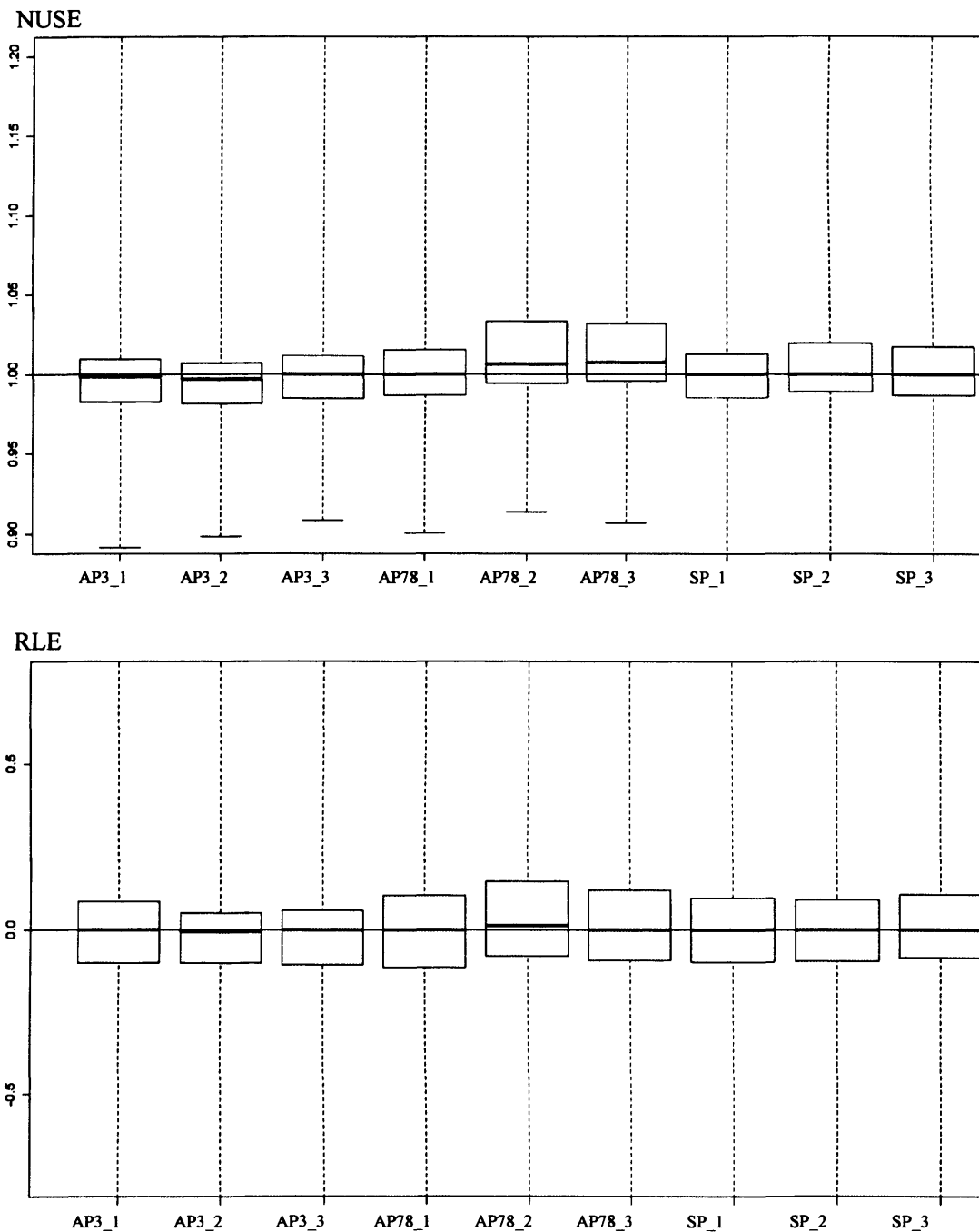
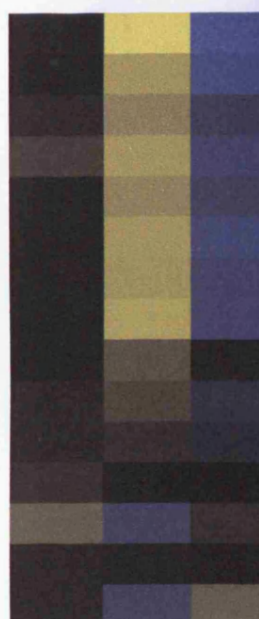
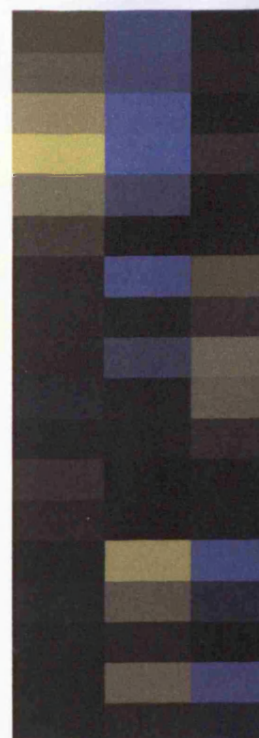


Figure 2: 2008 arrays — AffyPLM package for Bioconductor quality assessment — RLE and NUSE plots.

## Appendix VI: SCLC characteristics

**Table 1: SCLC and NSCLC markers expression in the NCI-H69 variants (Kraus et al., 2002).** False-colour cluster view representing the expression of each cell line (average value of the triplicates).

Affymetrix name	Gene symbol	description	SP	AP3	AP78
<i>SCLC markers</i>					
214347_s_at	DDC	dopa decarboxylase			
205311_at	DDC	dopa decarboxylase			
206291_at	NTS	neurotensin			
206326_at	GRP	gastrin-releasing peptide			
201313_at	ENO2	enolase 2 (gamma, neuronal)			
207466_at	GAL	galanin			
205051_s_at	KIT	Proto-oncogene tyrosine-protein kinase Kit			
215551_at	ESR1	estrogen receptor 1			
204697_s_at	CHGA	chromogranin A (parathyroid secretory protein 1)			
213200_at	SYP	synaptophysin			
211119_at	ESR2	estrogen receptor 2 (ER beta)			
208138_at	GAST	gastrin			
205225_at	ESR1	estrogen receptor 1			
212298_at	NRP1	neuropilin 1			
214632_at	NRP2	neuropilin 2			
217561_at	CALCA	calcitonin/calcitonin-related polypeptide, alpha			
210510_s_at	NRP1	neuropilin 1			
214599_at	IVL	involucrin			
<i>NSCLC markers</i>					
212063_at	CD44	CD44 antigen			
217523_at	CD44	CD44 antigen			
208399_s_at	EDN3	endothelin 3			
212014_x_at	CD44	CD44 antigen			
210916_s_at	CD44	CD44 antigen			
209835_x_at	CD44	CD44 antigen			
204490_s_at	CD44	CD44 antigen			
204489_s_at	CD44	CD44 antigen			
201110_s_at	THBS1	thrombospondin 1			
209561_at	THBS3	thrombospondin 3			
204776_at	THBS4	thrombospondin 4			
216062_at	CD44	CD44 antigen			
208712_at	CCND1	cyclin D1			
215775_at	THBS1	Thrombospondin 1			
206758_at	EDN2	endothelin 2			





**Table 2: SCLC markers expression in the NCI-H69 variants (Pedersen *et al.*, 2003).** False-colour cluster view representing the expression of each cell line (average value of the triplicates).

Affymetrix name	Gene symbol	description	SP	AP3	AP78
213378_s_at	DDX11	DEAD/H (Asp-Glu-Ala-Asp/His) box polypeptide 11			
209988_s_at	ASCL1	achaete-scute complex-like 1 (Drosophila)			
209987_s_at	ASCL1	achaete-scute complex-like 1 (Drosophila)			
213768_s_at	ASCL1	achaete-scute complex-like 1 (Drosophila)			
208149_x_at	DDX11	DEAD/H (Asp-Glu-Ala-Asp/His) box polypeptide 11			
209985_s_at	ASCL1	achaete-scute complex-like 1 (Drosophila)			
203671_at	TPMT	thiopurine S-methyltransferase			
217152_at	NCOR1	Nuclear receptor co-repressor 1			
214178_s_at	SOX2	SRY (sex determining region Y)-box 2			
206326_at	GRP	gastrin-releasing peptide			
210206_s_at	DDX11	DEAD/H (Asp-Glu-Ala-Asp/His) box polypeptide 11			
203453_at	SCNN1A	sodium channel, nonvoltage-gated 1 alpha			
208159_x_at	DDX11	DEAD/H (Asp-Glu-Ala-Asp/His) box polypeptide 11			
203415_at	PDCD6	programmed cell death 6			
213721_at	SOX2	SRY (sex determining region Y)-box 2			
209202_s_at	EXTL3	exostoses (multiple)-like 3			
211051_s_at	EXTL3	exostoses (multiple)-like 3			
201598_s_at	INPPL1	inositol polyphosphate phosphatase-like 1			
200856_x_at	NCOR1	nuclear receptor co-repressor 1			
213722_at	SOX2	SRY (sex determining region Y)-box 2			
216484_x_at	HDGF	Hepatoma-derived growth factor			
200854_at	NCOR1	nuclear receptor co-repressor 1			
200896_x_at	HDGF	hepatoma-derived growth factor			
200855_at	NCOR1	nuclear receptor co-repressor 1			
200857_s_at	NCOR1	nuclear receptor co-repressor 1			
203672_x_at	TPMT	thiopurine S-methyltransferase			
209506_s_at	NR2F1	nuclear receptor subfamily 2, group F, member 1			
209505_at	NR2F1	Nuclear receptor subfamily 2, group F, member 1			
214848_at	YWHAZ	14-3-3 zeta			
200641_s_at	YWHAZ	14-3-3 zeta			
200639_s_at	YWHAZ	14-3-3 zeta			
200638_s_at	YWHAZ	14-3-3 zeta			
200640_at	YWHAZ	14-3-3 zeta			
209030_s_at	IGSF4	immunoglobulin superfamily, member 4			
209031_at	IGSF4	Immunoglobulin superfamily, member 4			
209032_s_at	IGSF4	immunoglobulin superfamily, member 4			

## Appendix VII: Cell cycle and growth

**Table 1:** *Overlap between 1189 gene list and GO: 7049 cell cycle. False-colour cluster view representing the expression of each cell line (average value of the triplicates).*

Affymetrix name	Gene symbol	description	SP	AP3	AP78
200040_at	KHDRBS1	KH domain cont. RNA bind. signal transduction assoc. 1			
40225_at	GAK	cyclin G associated kinase			
218308_at	TACC3	transforming, acidic coiled-coil containing protein 3			
203062_s_at	MDC1	mediator of DNA damage checkpoint 1			
203725_at	GADD45A	growth arrest and DNA-damage-inducible, alpha			
219264_s_at	PPP2R3B	protein phosphatase 2, regulatory subunit B", beta			
202329_at	CSK	c-src tyrosine kinase			
211928_at	DNCH1	dynein, cytoplasmic, heavy polypeptide 1			
209784_s_at	JAG2	jagged 2			
213260_at	FOXC1	Forkhead box C1			
32137_at	JAG2	jagged 2			
202288_at	FRAP1	FK506 binding protein 12-rapamycin associated protein 1			
205289_at	BMP2	bone morphogenetic protein 2			
203132_at	RB1	retinoblastoma 1 (including osteosarcoma)			
204827_s_at	CCNF	cyclin F			
209361_s_at	PCBP4	poly(rC) binding protein 4			
202934_at	HK2	hexokinase 2			
205290_s_at	BMP2	bone morphogenetic protein 2			
216205_s_at	MFN2	mitofusin 2			
209260_at	SFN	stratifin			
202336_s_at	PAM	peptidylglycine alpha-amidating monooxygenase			
202731_at	PDCD4	programmed cell death 4			
212593_s_at	PDCD4	programmed cell death 4			
203786_s_at	TPD52L1	tumor protein D52-like 1			
210372_s_at	TPD52L1	tumor protein D52-like 1			
205848_at	GAS2	growth arrest-specific 2			
210512_s_at	VEGF	vascular endothelial growth factor			
213906_at	MYBL1	v-myb myeloblastosis viral oncogene homolog-like 1			
203588_s_at	TFDP2	transcription factor Dp-2 (E2F dimerization partner 2)			
218723_s_at	RGC32	response gene to complement 32			
208212_s_at	ALK	anaplastic lymphoma kinase (Ki-1)			
209035_at	MDK	midkine (neurite growth-promoting factor 2)			
218718_at	PDGFC	platelet derived growth factor C			
220407_s_at	TGFB2	transforming growth factor, beta 2			
209909_s_at	TGFB2	transforming growth factor, beta 2			



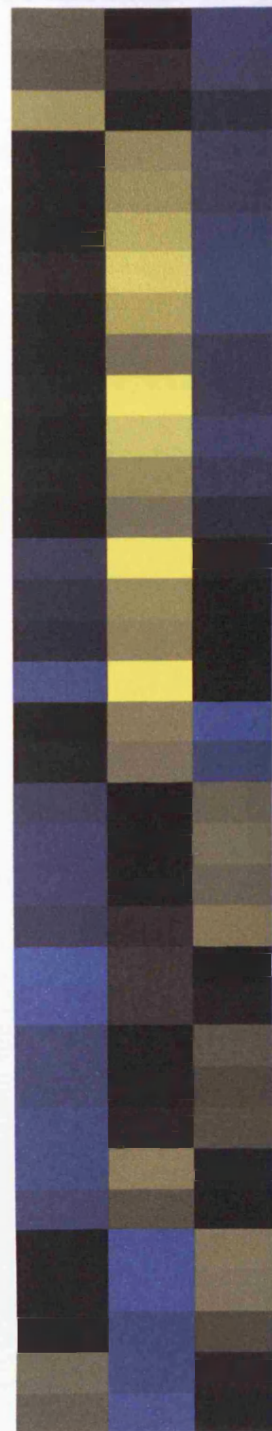


204890_s_at	LCK	lymphocyte-specific protein tyrosine kinase
204891_s_at	LCK	lymphocyte-specific protein tyrosine kinase
212414_s_at	SEPT6	septin 6 ; cytokine-like nuclear factor n-pac
212413_at	SEPT6	septin 6
205698_s_at	MAP2K6	mitogen-activated protein kinase kinase 6
213666_at	SEPT6	septin 6
211538_s_at	HSPA2	heat shock 70kDa protein 2
212415_at	SEPT6	septin 6
206939_at	DCC	deleted in colorectal carcinoma
31874_at	GAS2L1	growth arrest-specific 2 like 1
201012_at	ANXA1	annexin A1
209590_at	BMP7	Bone morphogenetic protein 7 (osteogenic protein 1)
212698_s_a	SEPT10	septin 10
202388_at	RGS2	regulator of G-protein signalling 2, 24kDa
206404_at	FGF9	fibroblast growth factor 9 (glia-activating factor)
220386_s_at	EML4	echinoderm microtubule associated protein like 4
209591_s_at	BMP7	bone morphogenetic protein 7 (osteogenic protein 1)
203037_s_at	MTSS1	metastasis suppressor 1
214720_x_at	SEPT10	septin 10
202409_at	LOC492304	putative insulin-like growth factor II associated protein
207002_s_at	PLAGL1	pleiomorphic adenoma gene-like 1
209318_x_at	PLAGL1	pleiomorphic adenoma gene-like 1
205659_at	HDAC9	histone deacetylase 9
212805_at	KIAA0367	KIAA0367
207943_x_at	PLAGL1	pleiomorphic adenoma gene-like 1
212806_at	KIAA0367	KIAA0367
202859_x_at	IL8	interleukin 8
209466_x_at	PTN	pleiotrophin
211506_s_at	IL8	interleukin 8
211737_x_at	PTN	pleiotrophin (HBGF8, NFGF1)
209465_x_at	PTN	pleiotrophin (HGF8, NFGF1)
205899_at	CCNA1	cyclin A1
201307_at	SEPT11	septin 11
205541_s_at	GSPT2	G1 to S phase transition 2
206506_s_at	SUPT3H	suppressor of Ty 3 homolog (S. cerevisiae)
213183_s_at	CDKN1C	Cyclin-dependent kinase inhibitor 1C (p57, Kip2)
213348_at	CDKN1C	Cyclin-dependent kinase inhibitor 1C (p57, Kip2)
219534_x_at	CDKN1C	cyclin-dependent kinase inhibitor 1C (p57, Kip2)
204021_s_at	PURA	purine-rich element binding protein A



**Table 2: Cell growth.** Overlap between 1189 gene list and GO: 40007 growth. False-colour cluster view representing the expression of each cell line (average value of the triplicates).

Affymetrix name	Gene symbol	description	SP	AP3	AP78
200920_s_at	BTG1	B-cell translocation gene 1, anti-proliferative			
200921_s_at	BTG1	B-cell translocation gene 1, anti-proliferative			
204471_at	GAP43	growth associated protein 43			
201539_s_at	FHL1	four and a half LIM domains 1			
210298_x_at	FHL1	four and a half LIM domains 1			
201540_at	FHL1	four and a half LIM domains 1			
215442_s_at	TSHR	thyroid stimulating hormone receptor			
215443_at	TSHR	thyroid stimulating hormone receptor			
220407_s_at	TGFB2	transforming growth factor, beta 2			
210055_at	TSHR	thyroid stimulating hormone receptor			
210299_s_at	FHL1	four and a half LIM domains 1			
214505_s_at	FHL1	four and a half LIM domains 1			
221675_s_at	CHPT1	choline phosphotransferase 1			
201998_at	ST6GAL1	ST6 beta-galactosamide alpha-2,6-sialyltransferase 1			
214321_at	NOV	nephroblastoma overexpressed gene			
204501_at	NOV	nephroblastoma overexpressed gene			
209220_at	GPC3	glypican 3			
203729_at	EMP3	epithelial membrane protein 3			
209909_s_at	TGFB2	transforming growth factor, beta 2			
202288_at	FRAP1	FK506 binding protein 12-rapamycin associated prot. 1			
205289_at	BMP2	bone morphogenetic protein 2			
203132_at	RB1	retinoblastoma 1 (including osteosarcoma)			
205290_s_at	BMP2	bone morphogenetic protein 2			
205402_x_at	PRSS2	protease, serine, 2 (trypsin 2)			
216470_x_at	PRSS	protease, serine, 1, 2, 3; Trypsinogen C			
208699_x_at	TKT	transketolase (Wernicke-Korsakoff syndrome)			
208700_s_at	TKT	transketolase (Wernicke-Korsakoff syndrome)			
214602_at	COL4A4	collagen, type IV, alpha 4			
204379_s_at	FGFR3	fibroblast growth factor receptor 3			
222006_at	FGFR3	fibroblast growth factor receptor 3			
203372_s_at	SOCS2	suppressor of cytokine signaling 2			
203373_at	SOCS2	suppressor of cytokine signaling 2			
219255_x_at	IL17RB	interleukin 17 receptor B			
209590_at	BMP7	Bone morphogenetic protein 7 (osteogenic protein 1)			
209591_s_at	BMP7	Bone morphogenetic protein 7 (osteogenic protein 1)			

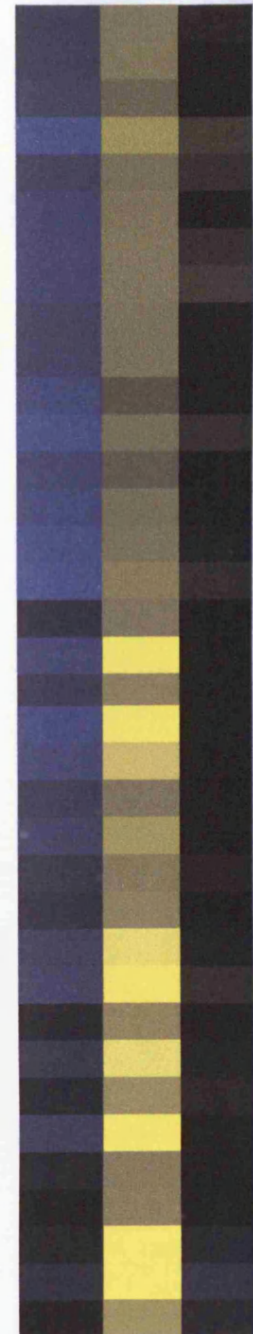




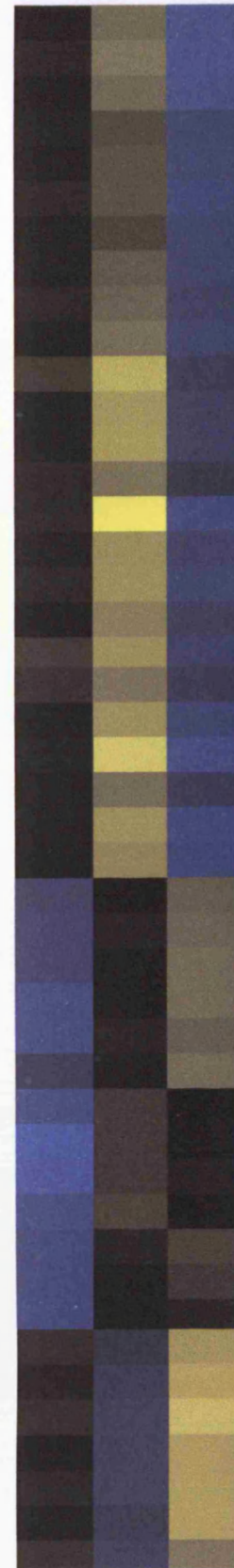
## Appendix VIII: Cell adhesion

**Table 1:** *Overlap between 1189 gene list and GO: 7155: cell adhesion.* False-colour cluster view representing the expression of each cell line (average value of the triplicates).

Affymetri x name	Gene symbol	description	SP	AP3	AP78
1007_s_at	DDR1	discoidin domain receptor family, member 1			
200635_s_at	PTPRF	protein tyrosine phosphatase, receptor type, F			
200636_s_at	PTPRF	protein tyrosine phosphatase, receptor type, F			
200637_s_at	PTPRF	protein tyrosine phosphatase, receptor type, F			
200770_s_at	LAMC1	laminin, gamma 1 (formerly LAMB2)			
200771_at	LAMC1	laminin, gamma 1 (formerly LAMB2)			
201015_s_at	JUP	junction plakoglobin			
201028_s_at	CD99	CD99 antigen			
201029_s_at	CD99	CD99 antigen			
201579_at	FAT	FAT tumor suppressor homolog 1			
201645_at	TNC	tenascin C (hexabrachion)			
201842_s_at	EFEMP1	EGF-containing fibulin-like ECM protein 1			
202007_at	NID1	nidogen 1			
202008_s_at	NID1	nidogen 1			
202267_at	LAMC2	laminin, gamma 2			
203184_at	FBN2	fibrillin 2 (congenital contractural arachnodactyly)			
203394_s_at	HES1	hairy and enhancer of split 1, (Drosophila)			
203413_at	NELL2	NEL-like 2 (chicken) ; NEL-like 2 (chicken)			
203528_at	SEMA4D	semaphorin 4D			
203562_at	FEZ1	fasciculation and elongation protein zeta 1 (zygin I)			
203726_s_at	LAMA3	laminin, alpha 3			
204359_at	FLRT2	fibronectin leucine rich transmembrane protein 2			
204489_s_at	CD44	CD44 antigen			
204490_s_at	CD44	CD44 antigen			
205154_at	LRRN5	leucine rich repeat neuronal 5			
205206_at	KAL1	Kallmann syndrome 1 sequence			
205523_at	HAPLN1	hyaluronan and proteoglycan link protein 1			
205524_s_at	HAPLN1	hyaluronan and proteoglycan link protein 1			
205656_at	PCDH17	protocadherin 17			
206247_at	MICB	MHC class I polypeptide-related sequence B			
206382_s_at	BDNF	brain-derived neurotrophic factor			
206470_at	PLXNC1	plexin C1			
206471_s_at	PLXNC1	plexin C1			
206935_at	PCDH8	protocadherin 8			
207169_x_at	DDR1	discoidin domain receptor family, member 1			
208779_x_at	DDR1	discoidin domain receptor family, member 1			



209436_at	SPON1	spondin 1, extracellular matrix protein
209437_s_at	SPON1	spondin 1, extracellular matrix protein
209835_x_at	CD44	CD44 antigen
209847_at	CDH17	cadherin 17, LI cadherin (liver-intestine)
209897_s_at	SLIT2	slit homolog 2 (Drosophila)
210749_x_at	DDR1	discoidin domain receptor family, member 1
210916_s_at	CD44	CD44
212014_x_at	CD44	CD44 antigen
212063_at	CD44	CD44 antigen
212298_at	NRP1	neuropilin 1
212713_at	MFAP4	microfibrillar-associated protein 4
213241_at	PLXNC1	plexin C1
213438_at	NFASC	neurofascin
213808_at	ADAM23	ADAM metallopeptidase domain 23
213993_at	SPON1	spondin 1, extracellular matrix protein
213994_s_at	SPON1	spondin 1, extracellular matrix protein
215020_at	NRXN3	neurexin 3
216167_at	LRRN5	leucine rich repeat neuronal 5
217523_at	CD44	CD44 antigen
217901_at	DSG2	Desmoglein 2
219414_at	CLSTN2	calsyntenin 2
219737_s_at	PCDH9	protocadherin 9
219738_s_at	PCDH9	protocadherin 9
221933_at	NLGN4X	neuroligin 4, X-linked
36499_at	CELSR2	cadherin, EGF LAG seven-pass G-type receptor 2
200931_s_at	VCL	vinculin
201976_s_at	MYO10	myosin X
205402_x_at	PRSS2	protease, serine, 2 (trypsin 2)
208636_at	ACTN1	Actinin, alpha 1
208637_x_at	ACTN1	actinin, alpha 1
209209_s_at	FERMT2	fermitin family homolog (Drosophila)
209210_s_at	FERMT2	fermitin family homolog (Drosophila)
211340_s_at	MCAM	melanoma cell adhesion molecule
212724_at	RND3	Rho family GTPase 3
214198_s_at	DGCR2	DiGeorge syndrome critical region gene 2
214212_x_at	FERMT2	fermitin family homolog (Drosophila)
216470_x_at	PRSS1,2,3	protease, serine, 1, 2, 3 (trypsin 1, 2, 3)
221408_x_at	PCDHB12	protocadherin beta 12
203780_at	EVA1	epithelial V-like antigen 1
204114_at	NID2	nidogen 2 (osteonidogen)
204619_s_at	CSPG2	chondroitin sulfate proteoglycan 2 (versican)
204620_s_at	CSPG2	chondroitin sulfate proteoglycan 2 (versican)
206394_at	MYBPC2	myosin binding protein C, fast type
207717_s_at	PKP2	plakophilin 2
210945_at	COL4A6	collagen, type IV, alpha 6





211473_s_at	COL4A6	collagen, type IV, alpha 6
211571_s_at	CSPG2	chondroitin sulfate proteoglycan 2 (versican)
212070_at	GPR56	G protein-coupled receptor 56
213992_at	COL4A6	collagen, type IV, alpha 6
215646_s_at	CSPG2	chondroitin sulfate proteoglycan 2 (versican)
215785_s_at	CYFIP2	cytoplasmic FMR1 interacting protein 2
219302_s_at	CNTNAP2	contactin associated protein-like 2
221731_x_at	CSPG2	chondroitin sulfate proteoglycan 2 (versican)
222020_s_at	HNT	neurotrimin
201005_at	CD9	CD9 antigen (p24)
202363_at	SPOCK	testican
202859_x_at	IL8	interleukin 8
203037_s_at	MTSS1	metastasis suppressor 1
203953_s_at	CLDN3	claudin 3
203954_x_at	CLDN3	claudin 3
204482_at	CLDN5	claudin 5
204955_at	SRPX	sushi-repeat-containing protein, X-linked
205042_at	GNE	glucosamine-2-epimerase/N-acetylmannosaminekinase
205185_at	SPINK5	serine peptidase inhibitor, Kazal type 5
205669_at	NCAM2	neural cell adhesion molecule 2
207149_at	CDH12	cadherin 12, type 2 (N-cadherin 2)
209114_at	TSPAN1	tetraspanin 1
211506_s_at	IL8	interleukin 8
213620_s_at	ICAM2	intercellular adhesion molecule 2
215571_at	NCAM2	Neural cell adhesion molecule 2
218087_s_at	SORBS1	sorbin and SH3 domain containing 1
220999_s_at	CYFIP2	cytoplasmic FMR1 interacting protein 2
37965_at	PARVB	parvin, beta
37966_at	PARVB	parvin, beta

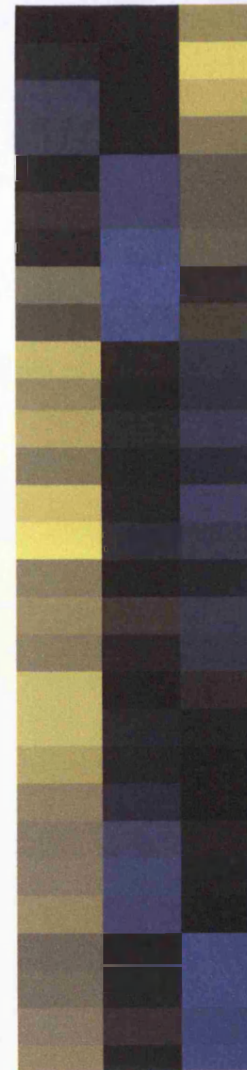
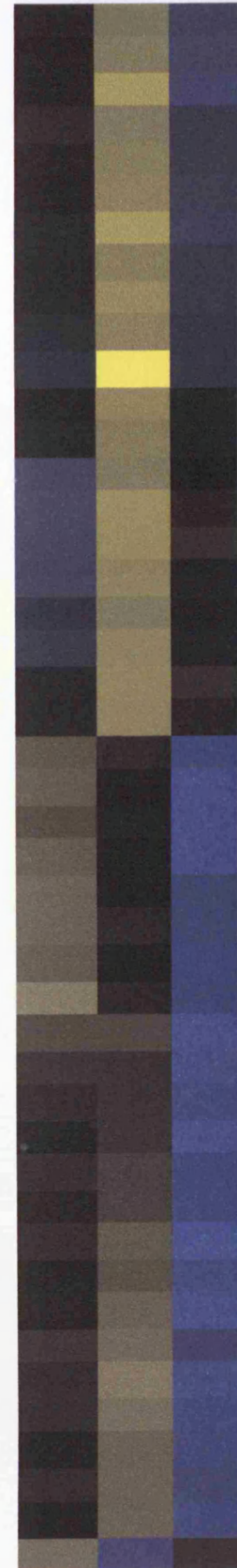




**Table 2:** *Overlap between 1189 gene list and GO: 5856: cytoskeleton and GO: 7010: cytoskeleton organisation and biogenesis. False-colour cluster view representing the expression of each cell line (average value of the triplicates).*

Affymetrix name	Gene symbol	description	SP	AP3	AP78
200609_s_at	WDR1	WD repeat domain 1			
208636_at	ACTN1	Actinin, alpha 1			
200611_s_at	WDR1	WD repeat domain 1			
X00351_5_at	ACTB	actin, beta			
201976_s_at	MYO10	myosin X			
211928_at	DNCH1	dynein, cytoplasmic, heavy polypeptide 1			
200859_x_at	FLNA	filamin A, alpha (actin binding protein 280)			
208637_x_at	ACTN1	actinin, alpha 1			
213746_s_at	FLNA	filamin A, alpha (actin binding protein 280)			
202389_s_at	HD	huntingtin (Huntington disease)			
210935_s_at	WDR1	WD repeat domain 1			
214752_x_at	FLNA	filamin A, alpha (actin binding protein 280)			
201564_s_at	FSCN1	fascin homolog 1, actin-bundling protein			
209209_s_at	FERMT2	fermitin family homolog (Drosophila)			
208621_s_at	VIL2	villin 2 (ezrin)			
209210_s_at	FERMT2	fermitin family homolog (Drosophila)			
212338_at	MYO1D	myosin ID			
201015_s_at	JUP	junction plakoglobin			
209008_x_at	KRT8	keratin 8 ; keratin 8			
221047_s_at	MARK1	MAP/microtubule affinity-regulating kinase 1			
201596_x_at	KRT18	keratin 18			
214721_x_at	CDC42EP4	CDC42 effector protein (Rho GTPase binding) 4			
201648_at	JAK1	Janus kinase 1 (a protein tyrosine kinase)			
212566_at	MAP4	microtubule-associated protein 4			
202274_at	ACTG2	actin, gamma 2, smooth muscle, enteric			
214736_s_at	ADD1	adducin 1 (alpha)			
218966_at	MYO5C	myosin VC			
208030_s_at	ADD1	adducin 1 (alpha)			
200931_s_at	VCL	vinculin			
210933_s_at	FSCN1	fascin homolog 1, actin-bundling protein			
209234_at	KIF1B	kinesin family member 1B			
214212_x_at	FERMT2	fermitin family homolog (Drosophila)			
201349_at	SLC9A3R1	solute carrier family 9, member 3 regulator 1			
216205_s_at	MFN2	mitofusin 2			
212724_at	RND3	Rho family GTPase 3			
214771_x_at	M-RIP	myosin phosphatase-Rho interacting protein			
203780_at	EVA1	epithelial V-like antigen 1			
220773_s_at	GPHN	gephyrin			
207717_s_at	PKP2	plakophilin 2			
200696_s_at	GSN	gelsolin (amyloidosis, Finnish type)			

212551_at	CAP2	CAP, adenylate cyclase-associated protein, 2
212554_at	CAP2	CAP, adenylate cyclase-associated protein, 2
203562_at	FEZ1	fasciculation and elongation protein zeta 1 (zygin I)
203662_s_at	TMOD1	tropomodulin 1
203661_s_at	TMOD1	tropomodulin 1
220119_at	EPB41L4A	erythrocyte membrane protein band 4.1 like 4A
208212_s_at	ALK	anaplastic lymphoma kinase (Ki-1)
209789_at	CORO2B	coronin, actin binding protein, 2B
220120_s_at	EPB41L4A	erythrocyte membrane protein band 4.1 like 4A
59375_at	MYO15B	myosin XVB pseudogene
217901_at	DSG2	Desmoglein 2
219173_at	MYO15B	myosin XVB pseudogene
31874_at	GAS2L1	growth arrest-specific 2 like 1
202039_at	TIAF1	TGFB1-induced anti-apoptotic factor 1
203333_at	KIFAP3	kinesin-associated protein 3
204891_s_at	LCK	lymphocyte-specific protein tyrosine kinase
204890_s_at	LCK	lymphocyte-specific protein tyrosine kinase
202052_s_at	RAI14	retinoic acid induced 14
209191_at	TUBB6	tubulin, beta 6
209850_s_at	CDC42EP2	CDC42 effector protein (Rho GTPase binding) 2
209615_s_at	PAK1	p21/Cdc42/Rac1-activated kinase 1
201034_at	ADD3	adducin 3 (gamma)
212390_at	PDE4DIP	phosphodiesterase 4D interacting protein
213388_at	PDE4DIP	phosphodiesterase 4D interacting protein
214099_s_at	PDE4DIP	phosphodiesterase 4D interacting protein
201752_s_at	ADD3	adducin 3 (gamma)
205882_x_at	ADD3	adducin 3 (gamma)
207705_s_at	KIAA0980	KIAA0980 protein
203881_s_at	DMD	dystrophin
204042_at	WASF3	WAS protein family, member 3
204513_s_at	ELMO1	engulfment and cell motility 1
214130_s_at	PDE4DIP	phosphodiesterase 4D interacting protein
205872_x_at	PDE4DIP	phosphodiesterase 4D interacting protein
212392_s_at	PDE4DIP	phosphodiesterase 4D interacting protein
214129_at	PDE4DIP	Phosphodiesterase 4D interacting protein
210305_at	PDE4DIP	phosphodiesterase 4D interacting protein
204201_s_at	PTPN13	protein tyrosine phosphatase, non-receptor type 13
205848_at	GAS2	growth arrest-specific 2
204797_s_at	EML1	echinoderm microtubule associated protein like 1
205347_s_at	TMSL8	thymosin-like 8
216060_s_at	DAAM1	dishevelled associated activator of morphogenesis 1
206710_s_at	EPB41L3	erythrocyte membrane protein band 4.1-like 3
211776_s_at	EPB41L3	erythrocyte membrane protein band 4.1-like 3
212681_at	EPB41L3	erythrocyte membrane protein band 4.1-like 3
201012_at	ANXA1	annexin A1





202921_s_at	ANK2	ankyrin 2, neuronal
216195_at	ANK2	Ankyrin 2, neuronal
202920_at	ANK2	ankyrin 2, neuronal
203037_s_at	MTSS1	metastasis suppressor 1
203961_at	NEBL	nebulette
204734_at	KRT15	keratin 15
214156_at	MYRIP	myosin VIIA and Rab interacting protein
220386_s_at	EML4	echinoderm microtubule associated protein like 4
214051_at	MGC39900	hypothetical protein MGC39900
201307_at	SEPT11	septin 11
203928_x_at	MAPT	microtubule-associated protein tau
219106_s_at	KBTD10	kelch repeat and BTB (POZ) domain containing 10
206401_s_at	MAPT	microtubule-associated protein tau
216526_x_at	HLA-C	major histocompatibility complex, class I, C
208812_x_at	HLA-C	major histocompatibility complex, class I, C
208885_at	LCPI	lymphocyte cytosolic protein 1 (L-plastin)
214459_x_at	HLA-C	major histocompatibility complex, class I, C
202391_at	BASP1	brain abundant, membrane attached signal protein 1
212365_at	MYO1B	myosin IB
218980_at	FHOD3	formin homology 2 domain containing 3
37965_at	PARVB	parvin, beta
203139_at	DAPK1	death-associated protein kinase 1
203636_at	MID1	midline 1 (Opitz/BBB syndrome)
218211_s_at	MLPH	melanophilin
212364_at	MYO1B	myosin IB
203637_s_at	MID1	midline 1 (Opitz/BBB syndrome)
37966_at	PARVB	parvin, beta
205899_at	CCNA1	cyclin A1
208188_at	KRT9	keratin 9 (epidermolytic palmoplantar keratoderma)
215575_at	PDE4DIP	phosphodiesterase 4D interacting protein
218087_s_at	SORBS1	sorbin and SH3 domain containing 1
208690_s_at	PDLIM1	PDZ and LIM domain 1 (elfin)

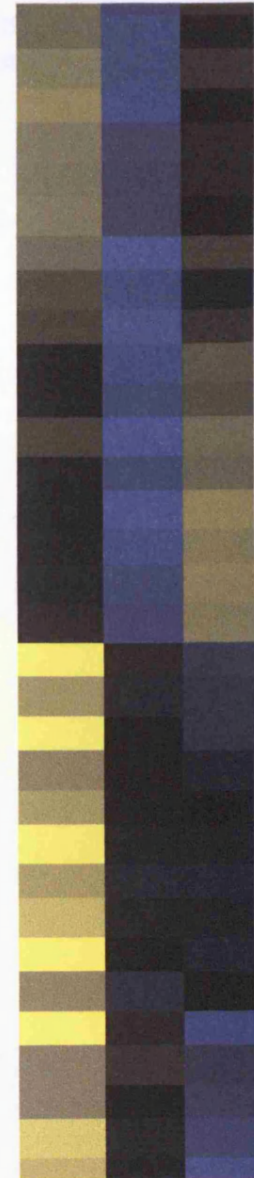


**Table 3:** *Overlap between 1189 gene list and GO: 30054: cell junction.* False-colour cluster view representing the expression of each cell line (average value of the triplicates).

Affymetrix name	Gene symbol	description	SP	AP3	AP78
200931_s_at	VCL	vinculin	Dark Blue	Black	Dark Blue
207717_s_at	PKP2	plakophilin 2	Dark Blue	Black	Yellow
219321_at	MPP5	membrane protein, palmitoylated 5	Dark Blue	Black	Dark Blue
201015_s_at	JUP	junction plakoglobin	Dark Blue	Black	Black
202329_at	CSK	c-src tyrosine kinase	Dark Blue	Black	Black
208636_at	ACTN1	Actinin, alpha 1	Dark Blue	Black	Black
208637_x_at	ACTN1	actinin, alpha 1	Dark Blue	Black	Black
203726_s_at	LAMA3	laminin, alpha 3	Dark Blue	Black	Dark Blue
206710_s_at	EPB41L3	erythrocyte membrane protein band 4.1-like 3	Dark Blue	Black	Dark Blue
211776_s_at	EPB41L3	erythrocyte membrane protein band 4.1-like 3	Dark Blue	Black	Dark Blue
212681_at	EPB41L3	erythrocyte membrane protein band 4.1-like 3	Dark Blue	Black	Dark Blue
217901_at	DSG2	Desmoglein 2	Dark Blue	Yellow	Black
203953_s_at	CLDN3	claudin 3	Dark Blue	Black	Black
203954_x_at	CLDN3	claudin 3	Dark Blue	Black	Black
218087_s_at	SORBS1	sorbin and SH3 domain containing 1	Dark Blue	Black	Dark Blue
204482_at	CLDN5	claudin 5	Dark Blue	Black	Black
205079_s_at	MPDZ	multiple PDZ domain protein	Dark Blue	Black	Black



**Table 4: Integrins expression.** False-colour cluster view representing the expression of each cell line (average value of the triplicates).

Affymetrix name	Gene symbol	description	SP	AP3	AP78
206766_at	ITGA10	integrin, alpha 10			
204627_s_at	ITGB3	integrin, beta 3			
216261_at	ITGB3	integrin, beta 3			
201656_at	ITGA6	integrin, alpha 6			
205816_at	ITGB8	integrin, beta 8			
215240_at	ITGB3	integrin, beta 3			
211488_s_at	ITGB8	integrin, beta 8			
211905_s_at	ITGB4	integrin, beta 4			
215177_s_at	ITGA6	integrin, alpha 6			
213475_s_at	ITGAL	integrin, alpha L			
216190_x_at	ITGB1	integrin, beta 1			
201124_at	ITGB5	integrin, beta 5			
204628_s_at	ITGB3	integrin, beta 3			
202351_at	ITGAV	integrin, alpha V			
211945_s_at	ITGB1	integrin, beta 1			
216178_x_at	ITGB1	integrin, beta 1			
215878_at	ITGB1	integrin, beta 1			
206493_at	ITGA2B	integrin, alpha 2b			
214927_at	ITGBL1	Integrin, beta-like 1			
206009_at	ITGA9	integrin, alpha 9			
205884_at	ITGA4	integrin, alpha 4			
205885_s_at	ITGA4	integrin, alpha 4			
213416_at	ITGA4	integrin, alpha 4			
205055_at	ITGAE	integrin, alpha E			
214020_x_at	ITGB5	Integrin, beta 5			





### Appendix IX: MSA

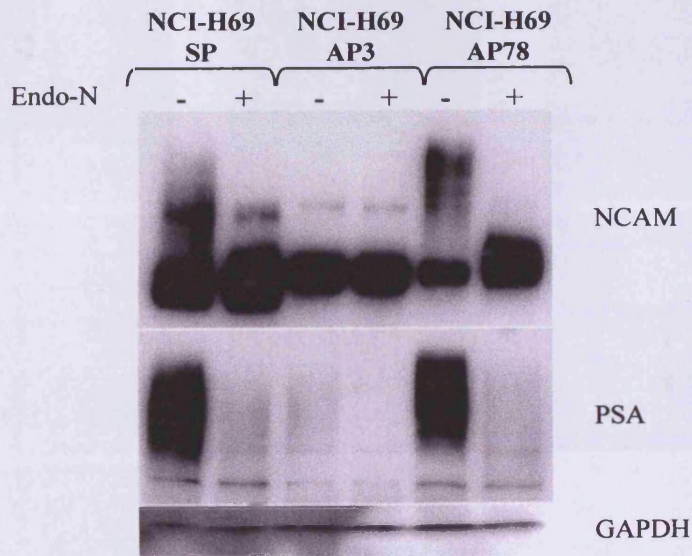
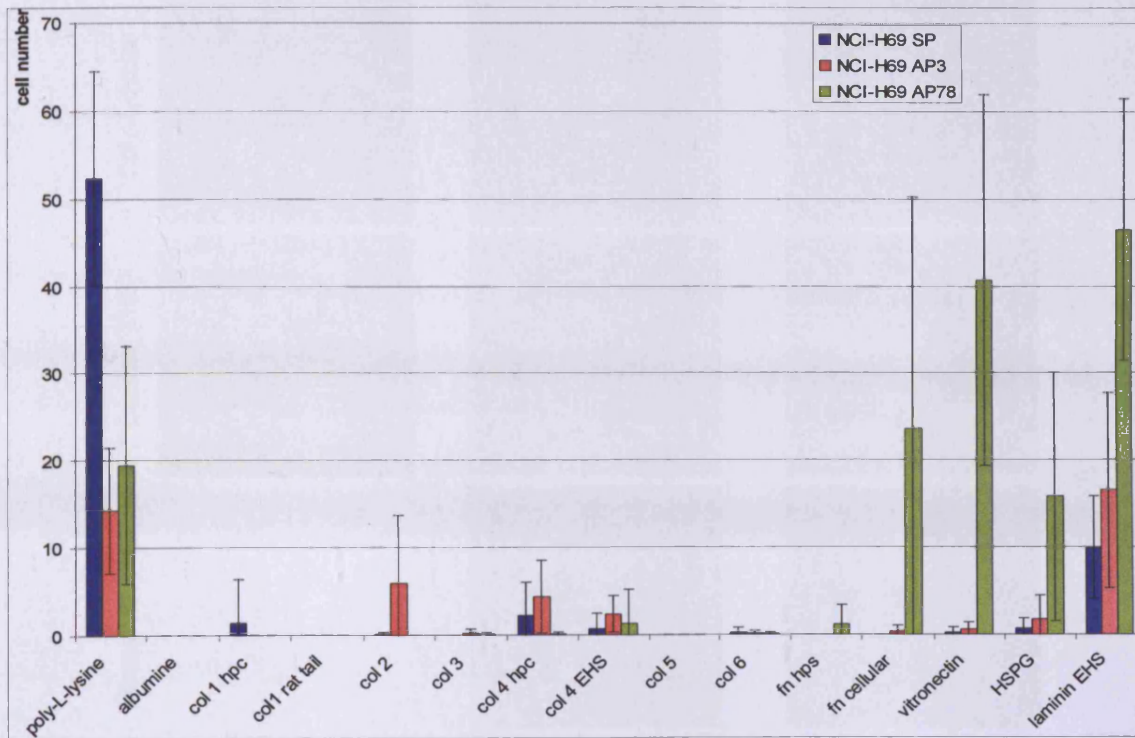


**Figure 1:** MSA adhesion profile after PSA digestion. Cells were treated overnight (15H) with 0.7 U of endoN or heat inactivated endoN (80°C for 15min). **a.** MSA adhesion profile. **b.** Western blotting confirmation of endoN digestion of PSA.

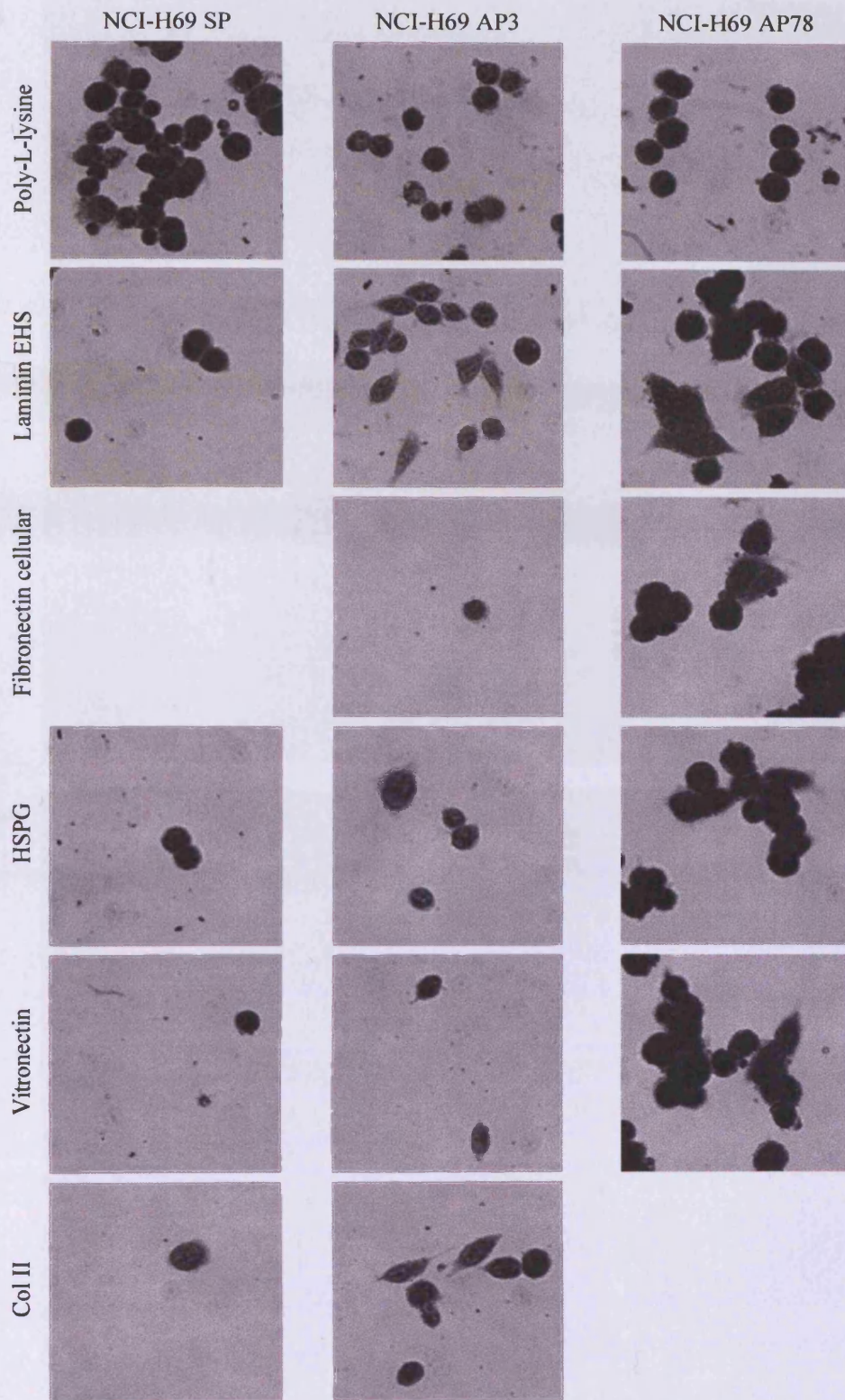
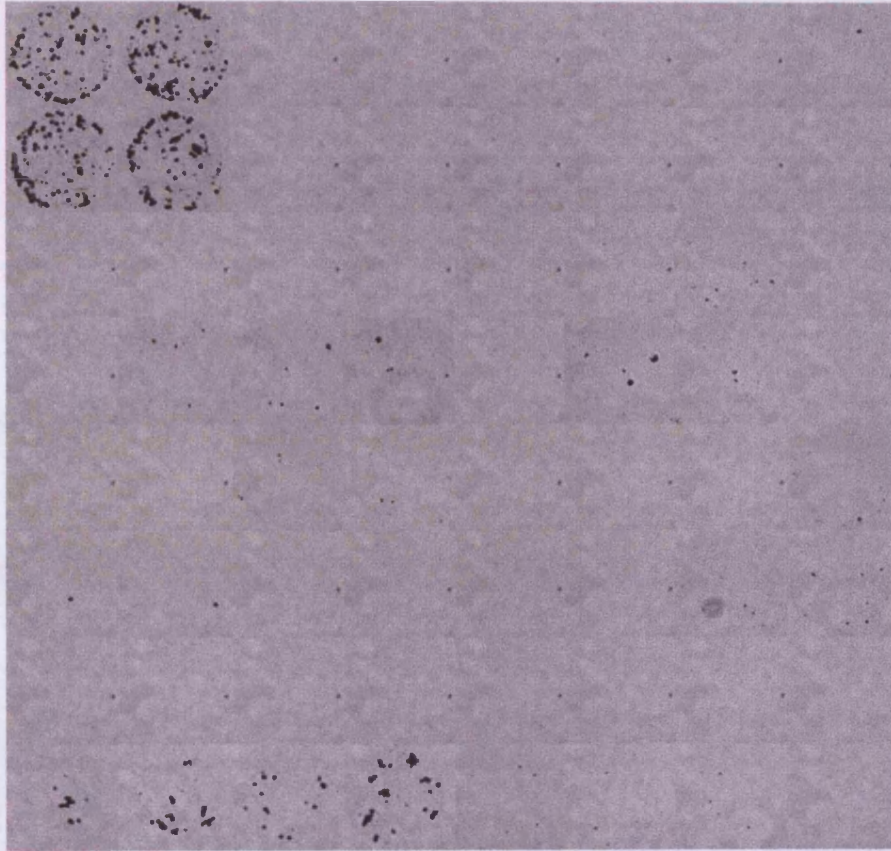


Figure 2: Cell morphology on MSA ECM proteins spot after endoN digestion



control



endoN  
digestion

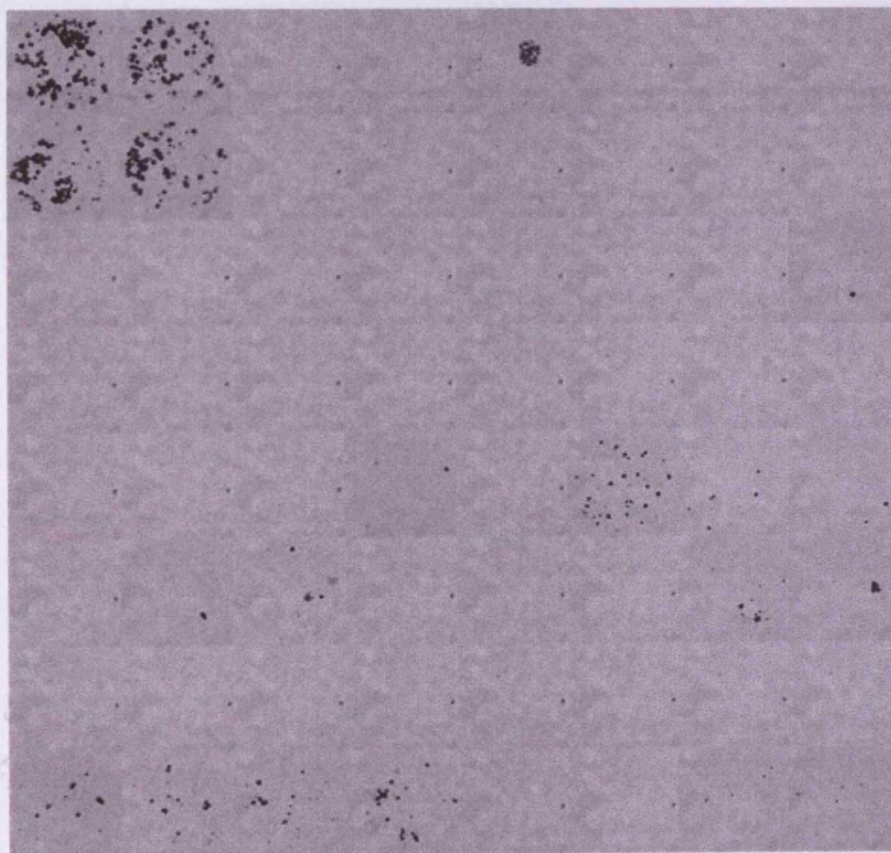
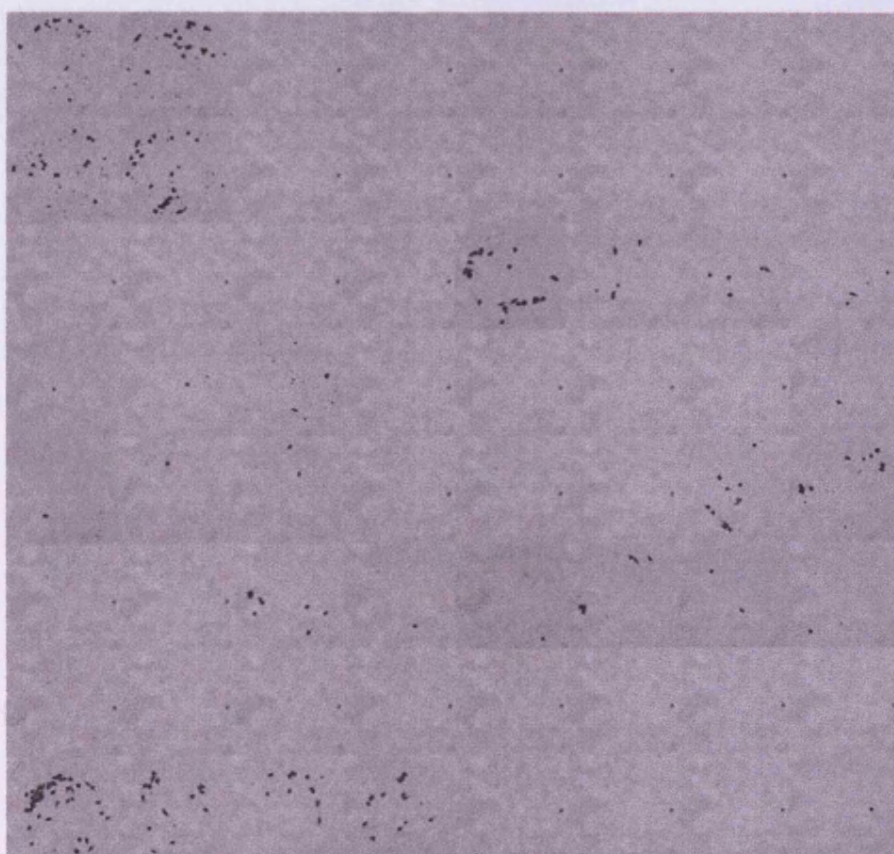


Figure 3: Reassembled full MSA array — NCI-H69 SP.

control



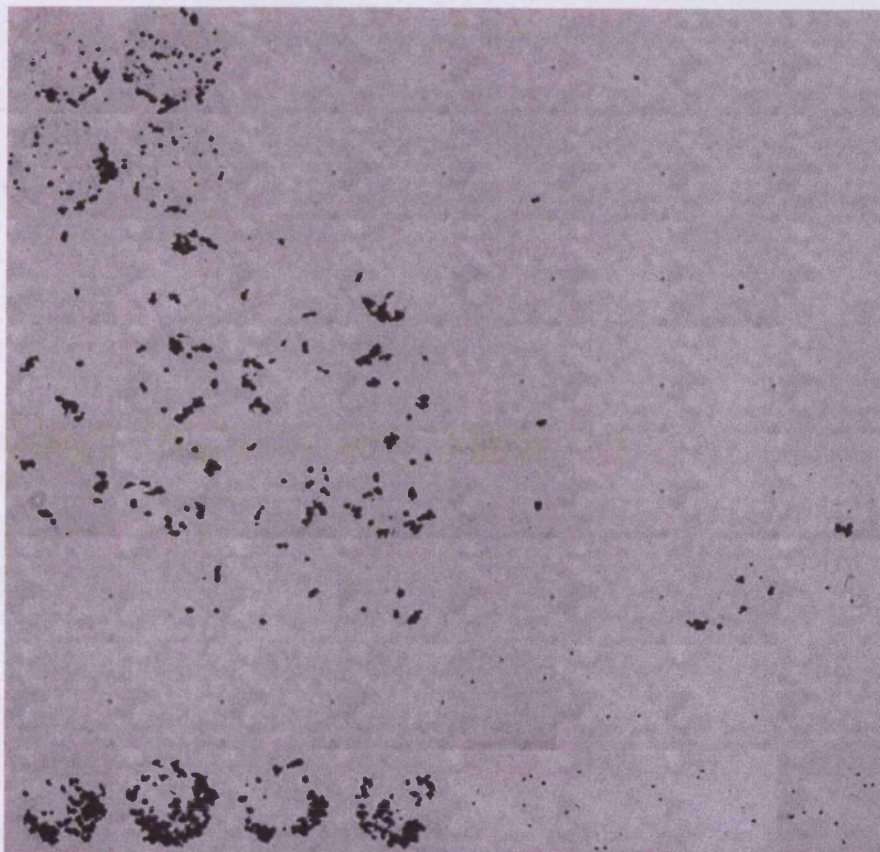
endoN  
digestion



**Figure 4:** Reassembled full MSA array — NCI-H69 AP3.



control



endoN  
digestion

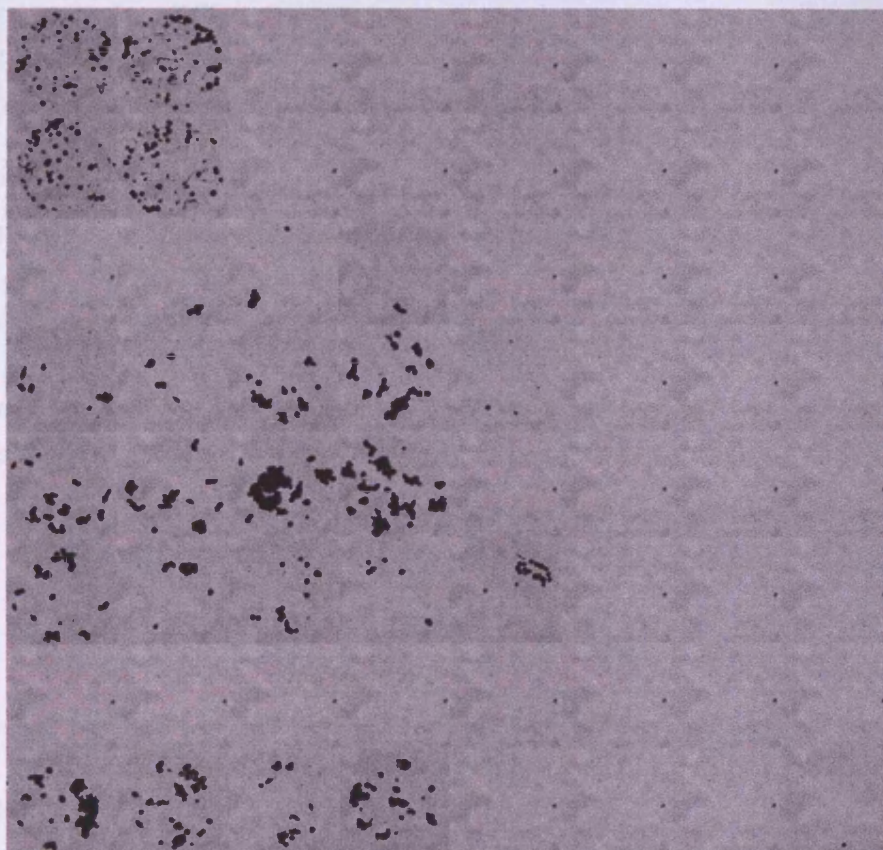


Figure 5: Reassembled full MSA array — NCI-H69 AP78.



## Appendix X: Cell motility

**Table 1: Cell motility.** Overlap between GO 6928 cell motility and 1189 gene list. False-colour cluster view representing the expression of each cell line (average value of the triplicates).

Affymetrix name	Gene symbol	description	SP	AP3	AP78
200770_s_at	LAMC1	laminin, gamma 1	Dark Blue	Dark Blue	Dark Blue
200771_at	LAMC1	laminin, gamma 1	Dark Blue	Dark Blue	Dark Blue
212048_s_at	YARS	tyrosyl-tRNA synthetase	Dark Blue	Dark Blue	Dark Blue
200859_x_at	FLNA	filamin A, alpha	Dark Blue	Dark Blue	Dark Blue
208637_x_at	ACTN1	actinin, alpha 1	Dark Blue	Dark Blue	Dark Blue
213746_s_at	FLNA	filamin A, alpha	Dark Blue	Dark Blue	Dark Blue
214752_x_at	FLNA	filamin A, alpha	Dark Blue	Dark Blue	Dark Blue
213260_at	FOXC1	Forkhead box C1	Dark Blue	Dark Blue	Dark Blue
32137_at	JAG2	jagged 2	Dark Blue	Dark Blue	Dark Blue
209784_s_at	JAG2	jagged 2	Dark Blue	Dark Blue	Dark Blue
208636_at	ACTN1	Actinin, alpha 1	Dark Blue	Dark Blue	Dark Blue
HSAC07/X00351_5_at	ACTB	actin, beta	Dark Blue	Dark Blue	Dark Blue
200931_s_at	VCL	vinculin	Dark Blue	Dark Blue	Dark Blue
200920_s_at	BTG1	B-cell translocation gene 1	Dark Blue	Dark Blue	Dark Blue
200921_s_at	BTG1	B-cell translocation gene 1	Dark Blue	Dark Blue	Dark Blue
204035_at	SCG2	secretogranin II (chromogranin C)	Dark Blue	Dark Blue	Dark Blue
212190_at	SERPINE2	serpin peptidase inhibitor, clade E	Dark Blue	Dark Blue	Dark Blue
204513_s_at	ELMO1	engulfment and cell motility 1	Dark Blue	Dark Blue	Dark Blue
209108_at	TSPAN6	tetraspanin 6	Dark Blue	Dark Blue	Dark Blue
209109_s_at	TSPAN6	tetraspanin 6	Dark Blue	Dark Blue	Dark Blue
201005_at	CD9	CD9 antigen (p24)	Dark Blue	Dark Blue	Dark Blue
211506_s_at	IL8	interleukin 8	Dark Blue	Dark Blue	Dark Blue
202859_x_at	IL8	interleukin 8	Dark Blue	Dark Blue	Dark Blue
209114_at	TSPAN1	tetraspanin 1	Dark Blue	Dark Blue	Dark Blue
202363_at	SPOCK	testican	Dark Blue	Dark Blue	Dark Blue
203562_at	FEZ1	zygin 1	Dark Blue	Dark Blue	Dark Blue
205206_at	KAL1	Kallmann syndrome 1 sequence	Dark Blue	Dark Blue	Dark Blue
206001_at	NPY	neuropeptide Y	Dark Blue	Dark Blue	Dark Blue
206382_s_at	BDNF	brain-derived neurotrophic factor	Dark Blue	Dark Blue	Dark Blue
209541_at	IGF1	insulin-like growth factor 1	Dark Blue	Dark Blue	Dark Blue
220407_s_at	TGFB2	transforming growth factor, beta 2	Dark Blue	Dark Blue	Dark Blue
212298_at	NRP1	neuropilin 1	Dark Blue	Dark Blue	Dark Blue

215020_at	NRXN3	neurexin 3
209909_s_at	TGFB2	transforming growth factor, beta 2
203726_s_at	LAMA3	laminin, alpha 3
210839_s_at	ENPP2	autotaxin
209147_s_at	PPAP2A	phosphatidic acid phosphatase type 2A
209392_at	ENPP2	autotaxin
210946_at	PPAP2A	phosphatidic acid phosphatase type 2A
210512_s_at	VEGF	vascular endothelial growth factor
206939_at	DCC	deleted in colorectal carcinoma
216268_s_at	JAG1	jagged 1 (Alagille syndrome)
209099_x_at	JAG1	jagged 1 (Alagille syndrome)
209897_s_at	SLIT2	slit homolog 2 (Drosophila)
201012_at	ANXA1	annexin A1
209590_at	BMP7	Bone morphogenetic protein 7
209591_s_at	BMP7	bone morphogenetic protein 7
203037_s_at	MTSS1	metastasis suppressor 1
203928_x_at	MAPT	microtubule-associated protein tau
209985_s_at	ASCL1	achaete-scute complex-like 1
213768_s_at	ASCL1	achaete-scute complex-like 1
209987_s_at	ASCL1	achaete-scute complex-like 1
209988_s_at	ASCL1	achaete-scute complex-like 1
206401_s_at	MAPT	microtubule-associated protein tau
216526_x_at	HLA-C	major histocompatibility complex classIC
208812_x_at	HLA-C	major histocompatibility complex classIC
214459_x_at	HLA-C	major histocompatibility complex classIC





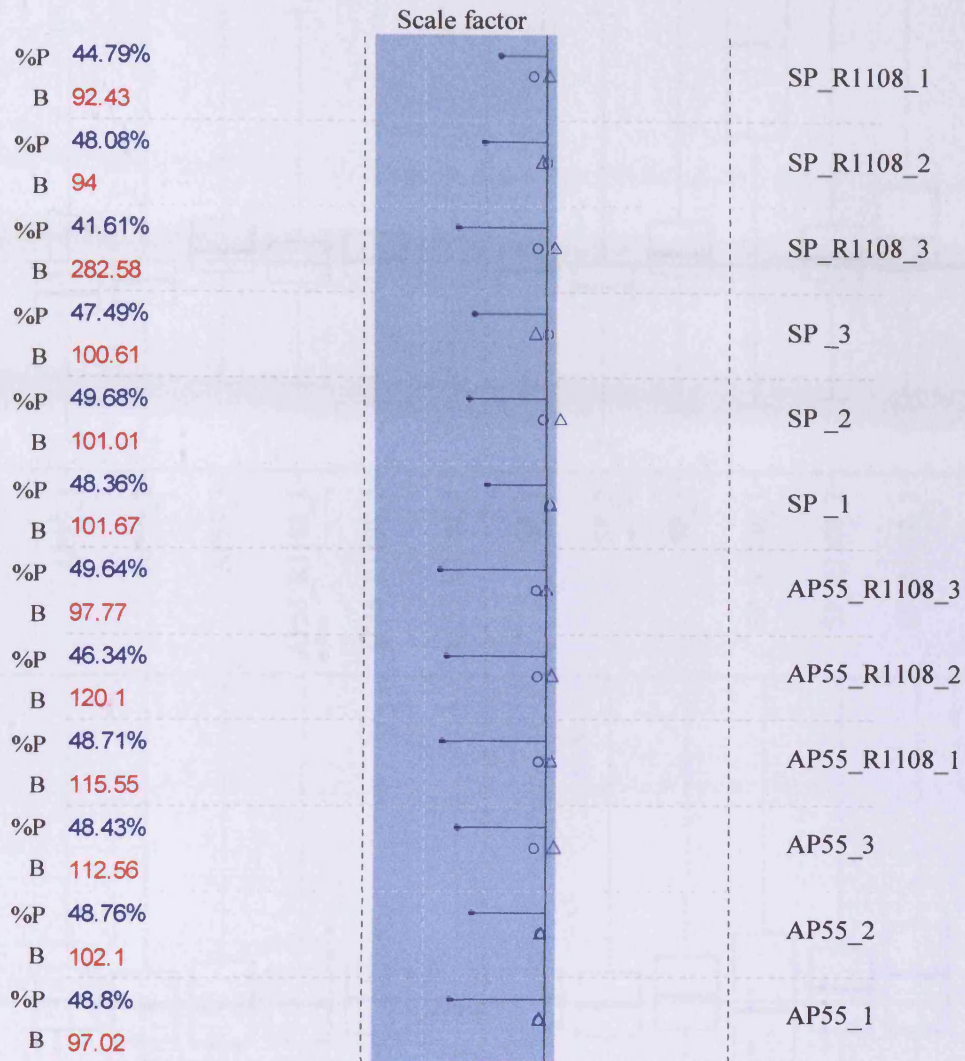
## Appendix XI: Glycosylation

Table 1: *Glycans structure and biosynthesis (KEGG 1.7)*. False-colour cluster view representing the expression of each cell line (average value of the triplicates).

Affymetrix name	gene symbol	description	SP	AP3	AP78
54037_at	HPS4	Hermansky-Pudlak syndrome 4			
218402_s_at	HPS4	Hermansky-Pudlak syndrome 4			
218854_at	SART2	squamous cell carcinoma antigen recognized by T cells 2			
201998_at	ST6GAL1	ST6 beta-galactosamide alpha-2,6-sialyltransferase 1			
220979_s_at	ST6GALNAC5	ST6 (alpha-N-acetyl-neuraminyl-2,3-beta-galactosyl-1,3)-N-acetylgalactosaminide alpha-2,6-sialyltransferase 5			
203066_at	GALNAC4S-6ST	N-acetylgalactosamine 4-sulfate 6-O-sulfotransferase			
209892_at	FUT4	fucosyltransferase 4 (alpha (1,3) fucosyltransferase, myeloid-specific)			
210073_at	ST8SIA1	ST8 alpha-N-acetyl-neuraminide alpha-2,8-sialyltransferase 1			
213552_at	GLCE	glucuronyl C5-epimerase			
203921_at	CHST2	carbohydrate (N-acetylglucosamine-6-O) sulfotransferase 2			
219403_s_at	HPSE	heparanase			
217788_s_at	GALNT2	UDP-N-acetyl-alpha-D-galactosamine:polypeptide N-acetylgalactosaminyltransferase 2			
217452_s_at	B3GALT2	UDP-Gal:betaGlcNAc beta 1,3-galactosyltransferase, polypeptide 2			
210121_at	B3GALT2	UDP-Gal:betaGlcNAc beta 1,3-galactosyltransferase, polypeptide 2			
202673_at	DPM1	dolichyl-phosphate mannosyltransferase polypeptide 1, catalytic subunit			
211812_s_at	B3GALT3	UDP-Gal:betaGlcNAc beta 1,3-galactosyltransferase, polypeptide 3			
205505_at	GCNT1	glucosaminyl (N-acetyl) transferase 1, core 2 (beta-1,6-N-acetylglucosaminyltransferase)			
203988_s_at	FUT8	fucosyltransferase 8 (alpha (1,6) fucosyltransferase)			



## Appendix XII: 2005 arrays quality assessment



Δ actin 3' / actin 5'

○ GAPDH 3' / GAPDH 5'

-3 -2 -1 0 1 2 3

Figure 1: 2005 arrays — MAS5 computed quality control report. Simpleaffy package generated quality control showing 5 metrics (background (B), percent present (%P), scale factor, GAPDH 5'/3' ratio and Actin 5'/3' ration) commonly used to asses arrays quality.

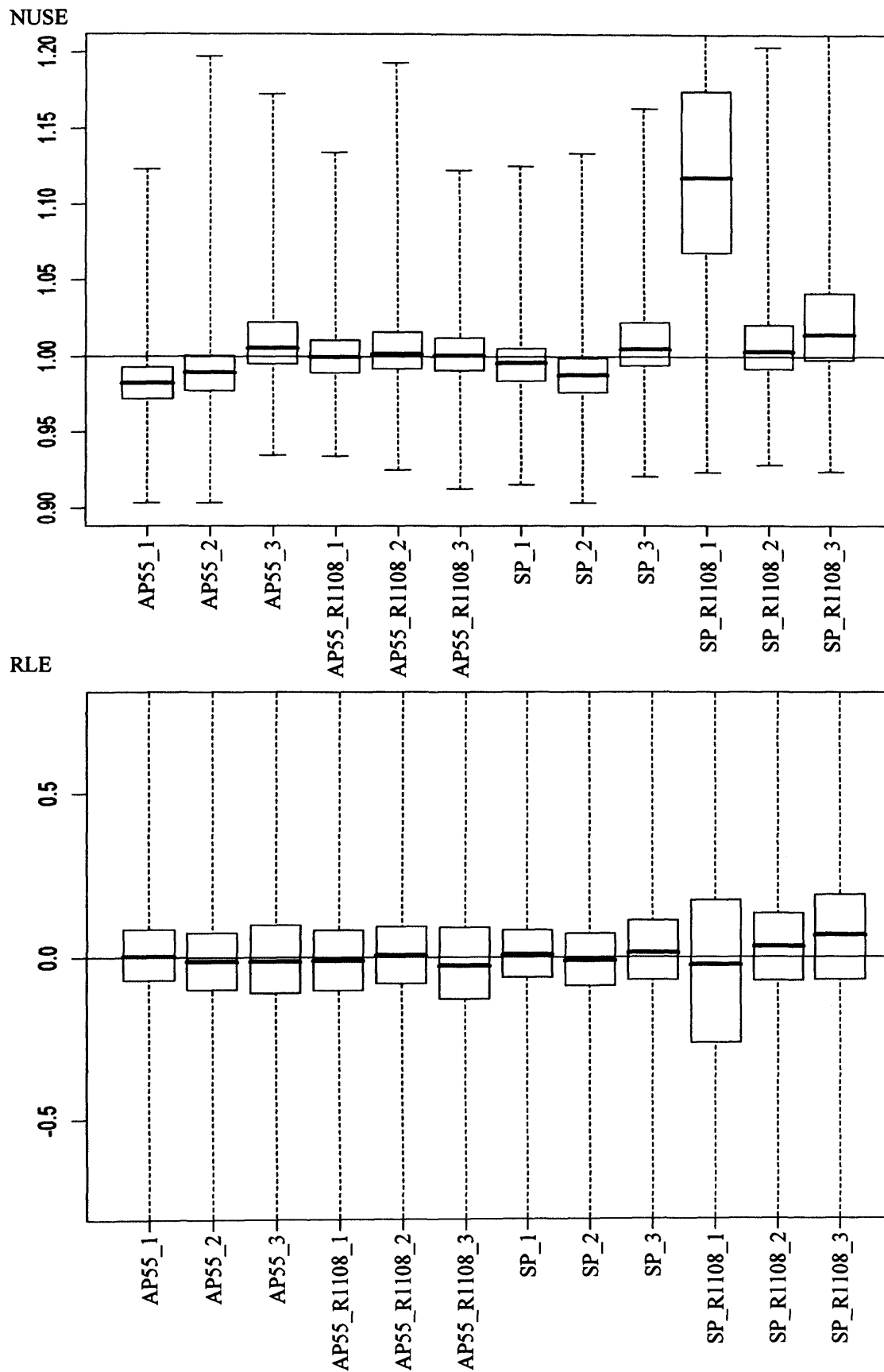


Figure 2: 2008 arrays. AffyPLM package for Bioconductor quality assessment — RLE and NUSE plots.



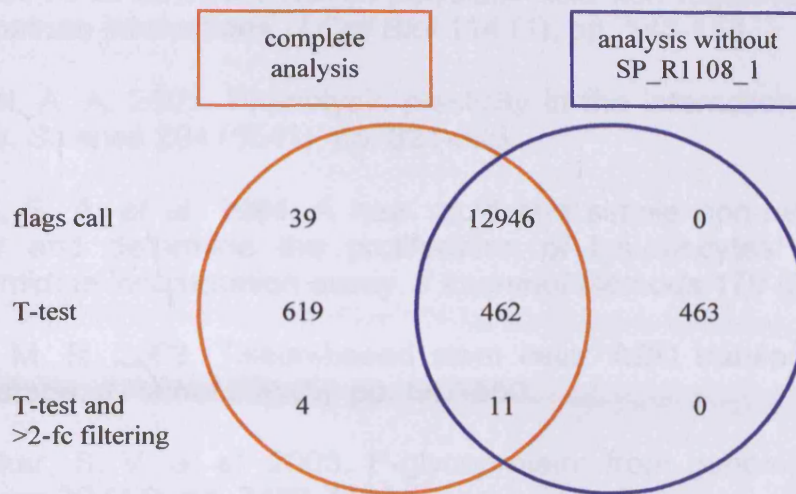


Figure 3: Microarray analysis accounting for failed quality control array.

Table 1: Microarray analysis accounting for failed quality control array. The table lists the results of analyses including (a) or excluding (b) the high background array.

Affymetrix name	gene symbol	description	fold change		T-test p-value	
			(a)	(b)	(a)	(b)
203665_at	HMOX1	heme oxygenase (decycling) 1	16.95	13.43	0.0154	0.146
212859_x_at	MT1E	metallothionein 1E	3.563	3.604	0.0294	0.193
221577_x_at	GDF15	growth differentiation factor 15	2.524	2.506	0.00244	0.0822
221258_s_at	KIF18A	kinesin family member 18A	0.447	0.531	0.0452	0.163

- Acheson, A. *et al.* 1991. NCAM polysialic acid can regulate both cell-cell and cell-substrate interactions. *J Cell Biol* 114 (1), pp. 143-153.
- Agrawal, A. A. 2001. Phenotypic plasticity in the interactions and evolution of species. *Science* 294 (5541), pp. 321-326.
- Ahmed, S. A. *et al.* 1994. A new rapid and simple non-radioactive assay to monitor and determine the proliferation of lymphocytes: an alternative to [3H]thymidine incorporation assay. *J Immunol Methods* 170 (2), pp. 211-224.
- Alison, M. R. 2003. Tissue-based stem cells: ABC transporter proteins take centre stage. *J Pathol* 200 (5), pp. 547-550.
- Ambudkar, S. V. *et al.* 2003. P-glycoprotein: from genomics to mechanism. *Oncogene* 22 (47), pp. 7468-7485.
- Angata, K. and Fukuda, M. 2003. Polysialyltransferases: major players in polysialic acid synthesis on the neural cell adhesion molecule. *Biochimie* 85 (1-2), pp. 195-206.
- Aoudjit, F. and Vuori, K. 2001. Integrin signaling inhibits paclitaxel-induced apoptosis in breast cancer cells. *Oncogene* 20 (36), pp. 4995-5004.
- Ashburner, M. *et al.* 2000. Gene ontology: tool for the unification of biology. The Gene Ontology Consortium. *Nat Genet* 25 (1), pp. 25-29.
- Aviel-Ronen, S. *et al.* 2008. Glypican-3 is overexpressed in lung squamous cell carcinoma, but not in adenocarcinoma. *Mod Pathol* 21 (7), pp. 817-825.
- Baillie-Johnson, H. *et al.* 1985. Establishment and characterisation of cell lines from patients with lung cancer (predominantly small cell carcinoma). *Br J Cancer* 52 (4), pp. 495-504.
- Balsara, B. R. and Testa, J. R. 2002. Chromosomal imbalances in human lung cancer. *Oncogene* 21 (45), pp. 6877-6883.
- Bao, F. *et al.* 2007. Comparative gene expression analysis of a chronic myelogenous leukemia cell line resistant to cyclophosphamide using oligonucleotide arrays and response to tyrosine kinase inhibitors. *Leuk Res* 31 (11), pp. 1511-1520.
- Barr, L. F. *et al.* 1996. Cell-substratum interactions mediate oncogene-induced phenotype of lung cancer cells. *Cell Growth Differ* 7 (9), pp. 1149-1156.
- Beadsmoore, C. J. and Screatton, N. J. 2003. Classification, staging and prognosis of lung cancer. *Eur J Radiol* 45 (1), pp. 8-17.
- Beattie, J. H. *et al.* 2005. Metallothionein overexpression and resistance to toxic stress. *Toxicol Lett* 157 (1), pp. 69-78.

- Beier, D. *et al.* 2008. Temozolomide preferentially depletes cancer stem cells in glioblastoma. *Cancer Res* 68 (14), pp. 5706-5715.
- Benjamini, Y. and Hochberg, Y. 1995. Controlling the False Discovery Rate: A Practical and Powerful Approach to Multiple Testing. *Journal of the Royal Statistical Society. Series B (Methodological)* 57 (1), pp. 289-300.
- Bermejo, R. *et al.* 2007. Top1- and Top2-mediated topological transitions at replication forks ensure fork progression and stability and prevent DNA damage checkpoint activation. *Genes Dev* 21 (15), pp. 1921-1936.
- Bernards, R. and Weinberg, R. A. 2002. A progression puzzle. *Nature* 418 (6900), p. 823.
- Bernstein, B. E. *et al.* 2007. The mammalian epigenome. *Cell* 128 (4), pp. 669-681.
- Berrier, A. L. and Yamada, K. M. 2007. Cell-matrix adhesion. *J Cell Physiol* 213 (3), pp. 565-573.
- Bhattacharjee, A. *et al.* 2001. Classification of human lung carcinomas by mRNA expression profiling reveals distinct adenocarcinoma subclasses. *Proc Natl Acad Sci U S A* 98 (24), pp. 13790-13795.
- Bidlingmaier, S. *et al.* 2008. The utility and limitations of glycosylated human CD133 epitopes in defining cancer stem cells. *J Mol Med* 86 (9), pp. 1025-1032.
- Biedler, J. L. and Riehm, H. 1970. Cellular resistance to actinomycin D in Chinese hamster cells in vitro: cross-resistance, radioautographic, and cytogenetic studies. *Cancer Res* 30 (4), pp. 1174-1184.
- Bissell, M. J. and Radisky, D. 2001. Putting tumours in context. *Nat Rev Cancer* 1 (1), pp. 46-54.
- Blazek, E. R. *et al.* 2007. Daoy medulloblastoma cells that express CD133 are radioresistant relative to CD133- cells, and the CD133+ sector is enlarged by hypoxia. *Int J Radiat Oncol Biol Phys* 67 (1), pp. 1-5.
- Borges, M. *et al.* 1997. An achaete-scute homologue essential for neuroendocrine differentiation in the lung. *Nature* 386 (6627), pp. 852-855.
- Bork, K. *et al.* 2005. The intracellular concentration of sialic acid regulates the polysialylation of the neural cell adhesion molecule. *FEBS Lett* 579 (22), pp. 5079-5083.
- Brabletz, T. *et al.* 2005. Opinion: migrating cancer stem cells - an integrated concept of malignant tumour progression. *Nat Rev Cancer* 5 (9), pp. 744-749.

- Brock, I. *et al.* 1995. Sequential coexpression of the multidrug resistance genes MRP and *mdr1* and their products in VP-16 (etoposide)-selected H69 small cell lung cancer cells. *Cancer Res* 55 (3), pp. 459-462.
- Brooks, S. A. and Leathem, A. J. 1991. Prediction of lymph node involvement in breast cancer by detection of altered glycosylation in the primary tumour. *Lancet* 338 (8759), pp. 71-74.
- Bru, A. *et al.* 2003. The universal dynamics of tumor growth. *Biophys J* 85 (5), pp. 2948-2961.
- Bunting, K. D. 2002. ABC transporters as phenotypic markers and functional regulators of stem cells. *Stem Cells* 20 (1), pp. 11-20.
- Burger, M. *et al.* 2003. Functional expression of CXCR4 (CD184) on small-cell lung cancer cells mediates migration, integrin activation, and adhesion to stromal cells. *Oncogene* 22 (50), pp. 8093-8101.
- Burke, T. G. *et al.* 1996. Fluorescence detection of the anticancer drug topotecan in plasma and whole blood by two-photon excitation. *Anal Biochem* 242 (2), pp. 266-270.
- Buttery, R. C. *et al.* 2004. Small cell lung cancer: the importance of the extracellular matrix. *Int J Biochem Cell Biol* 36 (7), pp. 1154-1160.
- Campbell, A. M. *et al.* 2002. Clinical and molecular features of small cell lung cancer. *Cancer Biol Ther* 1 (2), pp. 105-112.
- Campling, B. G. and El-Deiry, W. S. 2003. Clinical implication of p53 mutation in lung cancer. *Mol Biotechnol* 24 (2), pp. 141-156.
- Campling, B. G. *et al.* 1997. Expression of the MRP and MDR1 multidrug resistance genes in small cell lung cancer. *Clin Cancer Res* 3 (1), pp. 115-122.
- Capurro, M. I. *et al.* 2005. Glypican-3 promotes the growth of hepatocellular carcinoma by stimulating canonical Wnt signaling. *Cancer Res* 65 (14), pp. 6245-6254.
- Capurro, M. I. *et al.* 2008. Glypican-3 inhibits Hedgehog signaling during development by competing with patched for Hedgehog binding. *Dev Cell* 14 (5), pp. 700-711.
- Carney, D. N. *et al.* 1985. Establishment and identification of small cell lung cancer cell lines having classic and variant features. *Cancer Res* 45 (6), pp. 2913-2923.
- Cavallaro, U. and Christofori, G. 2004. Cell adhesion and signalling by cadherins and Ig-CAMs in cancer. *Nat Rev Cancer* 4 (2), pp. 118-132.

- Challen, G. A. and Little, M. H. 2006. A side order of stem cells: the SP phenotype. *Stem Cells* 24 (1), pp. 3-12.
- Chambers, A. F. *et al.* 2002. Dissemination and growth of cancer cells in metastatic sites. *Nat Rev Cancer* 2 (8), pp. 563-572.
- Chappell, M. J. *et al.* 2008. A coupled drug kinetics-cell cycle model to analyse the response of human cells to intervention by topotecan. *Comput Methods Programs Biomed* 89 (2), pp. 169-178.
- Charter, N. W. *et al.* 2000. Biosynthetic incorporation of unnatural sialic acids into polysialic acid on neural cells. *Glycobiology* 10 (10), pp. 1049-1056.
- Chen, Y. and Poon, R. Y. 2008. The multiple checkpoint functions of CHK1 and CHK2 in maintenance of genome stability. *Front Biosci* 13, pp. 5016-5029.
- Chen, Y. N. *et al.* 1990. Characterization of adriamycin-resistant human breast cancer cells which display overexpression of a novel resistance-related membrane protein. *J Biol Chem* 265 (17), pp. 10073-10080.
- Cheng, W. *et al.* 2008. Glypican-3-mediated oncogenesis involves the Insulin-like growth factor-signaling pathway. *Carcinogenesis* 29 (7), pp. 1319-1326.
- Cheung, S. Y. *et al.* 2008. Exploration of the intercellular heterogeneity of topotecan uptake into human breast cancer cells through compartmental modelling. *Math Biosci* 213 (2), pp. 119-134.
- Chomczynski, P. and Sacchi, N. 1987. Single-step method of RNA isolation by acid guanidinium thiocyanate-phenol-chloroform extraction. *Anal Biochem* 162 (1), pp. 156-159.
- Chourpa, I. *et al.* 1998. Kinetics of lactone hydrolysis in antitumor drugs of camptothecin series as studied by fluorescence spectroscopy. *Biochim Biophys Acta* 1379 (3), pp. 353-366.
- Christmann, M. *et al.* 2008. WRN protects against topo I but not topo II inhibitors by preventing DNA break formation. *DNA Repair (Amst)* 7 (12), pp. 1999-2009.
- Christofori, G. 2003. Changing neighbours, changing behaviour: cell adhesion molecule-mediated signalling during tumour progression. *Embo J* 22 (10), pp. 2318-2323.
- Clare, S. E. *et al.* 2000. Molecular biology of breast cancer metastasis. The use of mathematical models to determine relapse and to predict response to chemotherapy in breast cancer. *Breast Cancer Res* 2 (6), pp. 430-435.
- Close, B. E. and Colley, K. J. 1998. In vivo autopolysialylation and localization of the polysialyltransferases PST and STX. *J Biol Chem* 273 (51), pp. 34586-34593.



- Cole, S. P. *et al.* 1992. Overexpression of a transporter gene in a multidrug-resistant human lung cancer cell line. *Science* 258 (5088), pp. 1650-1654.
- Coley, H. M. *et al.* 1993. The efflux of anthracyclines in multidrug-resistant cell lines. *Biochem Pharmacol* 46 (8), pp. 1317-1326.
- Couture, L. *et al.* 2006. The ATP-binding cassette transporters and their implication in drug disposition: a special look at the heart. *Pharmacol Rev* 58 (2), pp. 244-258.
- Couzin, J. 2003. Medicine. Tracing the steps of metastasis, cancer's menacing ballet. *Science* 299 (5609), pp. 1002-1006.
- Coyle, P. *et al.* 2002. Metallothionein: the multipurpose protein. *Cell Mol Life Sci* 59 (4), pp. 627-647.
- Cremer, H. *et al.* 1994. Inactivation of the N-CAM gene in mice results in size reduction of the olfactory bulb and deficits in spatial learning. *Nature* 367 (6462), pp. 455-459.
- Crnic, I. *et al.* 2004. Loss of neural cell adhesion molecule induces tumor metastasis by up-regulating lymphangiogenesis. *Cancer Res* 64 (23), pp. 8630-8638.
- D'Haeseleer, P. 2005. How does gene expression clustering work? *Nat Biotechnol* 23 (12), pp. 1499-1501.
- Daniel, L. *et al.* 2001. A nude mice model of human rhabdomyosarcoma lung metastases for evaluating the role of polysialic acids in the metastatic process. *Oncogene* 20 (8), pp. 997-1004.
- Daniel, L. *et al.* 2000. Polysialylated-neural cell adhesion molecule expression in rat pituitary transplantable tumors (spontaneous mammatropic transplantable tumor in Wistar-Furth rats) is related to growth rate and malignancy. *Cancer Res* 60 (1), pp. 80-85.
- Daoud, S. S. *et al.* 2003. Impact of p53 knockout and topotecan treatment on gene expression profiles in human colon carcinoma cells: a pharmacogenomic study. *Cancer Res* 63 (11), pp. 2782-2793.
- Datta, A. K. *et al.* 1998. Mutation of the sialyltransferase S-sialylmotif alters the kinetics of the donor and acceptor substrates. *J Biol Chem* 273 (16), pp. 9608-9614.
- Davey, R. A. *et al.* 2004. Cellular models of drug- and radiation-resistant small cell lung cancer. *Anticancer Res* 24 (2A), pp. 465-471.
- Dean, M. *et al.* 2001. The human ATP-binding cassette (ABC) transporter superfamily. *Genome Res* 11 (7), pp. 1156-1166.

- Dennis, J. *et al.* 1982. Surface sialic acid reduces attachment of metastatic tumour cells to collagen type IV and fibronectin. *Nature* 300 (5889), pp. 274-276.
- Derynck, R. and Akhurst, R. J. 2007. Differentiation plasticity regulated by TGF-beta family proteins in development and disease. *Nat Cell Biol* 9 (9), pp. 1000-1004.
- DeVita, V. T., Jr. *et al.* 1975. Combination versus single agent chemotherapy: a review of the basis for selection of drug treatment of cancer. *Cancer* 35 (1), pp. 98-110.
- Ditlevsen, D. K. *et al.* 2003. The role of phosphatidylinositol 3-kinase in neural cell adhesion molecule-mediated neuronal differentiation and survival. *J Neurochem* 84 (3), pp. 546-556.
- Ditlevsen, D. K. *et al.* 2008. NCAM-induced intracellular signaling revisited. *J Neurosci Res* 86 (4), pp. 727-743.
- Downward, J. 2004. PI 3-kinase, Akt and cell survival. *Semin Cell Dev Biol* 15 (2), pp. 177-182.
- Doyle, L. A. *et al.* 1990. An adherent subline of a unique small-cell lung cancer cell line downregulates antigens of the neural cell adhesion molecule. *J Clin Invest* 86 (6), pp. 1848-1854.
- Doyle, L. A. and Ross, D. D. 2003. Multidrug resistance mediated by the breast cancer resistance protein BCRP (ABCG2). *Oncogene* 22 (47), pp. 7340-7358.
- Duesberg, P. and Li, R. 2003. Multistep carcinogenesis: a chain reaction of aneuploidizations. *Cell Cycle* 2 (3), pp. 202-210.
- Durand, R. E. and Olive, P. L. 1982. Cytotoxicity, Mutagenicity and DNA damage by Hoechst 33342. *J Histochem Cytochem* 30 (2), pp. 111-116.
- Durand, R. E. and Sutherland, R. M. 1972. Effects of intercellular contact on repair of radiation damage. *Exp Cell Res* 71 (1), pp. 75-80.
- Ee, P. L. *et al.* 2004. Modulation of breast cancer resistance protein (BCRP/ABCG2) gene expression using RNA interference. *Mol Cancer Ther* 3 (12), pp. 1577-1583.
- Epstein, A. L. *et al.* 1976. Biology of the human malignant lymphomas. III. Intracranial heterotransplantation in the nude, athymic mouse. *Cancer* 37 (5), pp. 2158-2176.
- Epstein, R. J. 2005. Maintenance therapy to suppress micrometastasis: the new challenge for adjuvant cancer treatment. *Clin Cancer Res* 11 (15), pp. 5337-5341.

- Errington, R. J. *et al.* 2005. Advanced microscopy solutions for monitoring the kinetics and dynamics of drug-DNA targeting in living cells. *Adv Drug Deliv Rev* 57 (1), pp. 153-167.
- Evans, N. D. *et al.* 2004. A mathematical model for the in vitro kinetics of the anti-cancer agent topotecan. *Math Biosci* 189 (2), pp. 185-217.
- Eyden, B. 2004. Fibroblast phenotype plasticity: relevance for understanding heterogeneity in "fibroblastic" tumors. *Ultrastruct Pathol* 28 (5-6), pp. 307-319.
- Eyre, T. A. *et al.* 2006. The HUGO Gene Nomenclature Database, 2006 updates. *Nucleic Acids Res* 34 (Database issue), pp. D319-321.
- Falco, J. P. *et al.* 1990. v-rasH induces non-small cell phenotype, with associated growth factors and receptors, in a small cell lung cancer cell line. *J Clin Invest* 85 (6), pp. 1740-1745.
- Fan, X. *et al.* 2006. Notch pathway inhibition depletes stem-like cells and blocks engraftment in embryonal brain tumors. *Cancer Res* 66 (15), pp. 7445-7452.
- Feeney, G. P. *et al.* 2003. Tracking the cell cycle origins for escape from topotecan action by breast cancer cells. *Br J Cancer* 88 (8), pp. 1310-1317.
- Feinberg, A. P. 2007. Phenotypic plasticity and the epigenetics of human disease. *Nature* 447 (7143), pp. 433-440.
- Feinberg, A. P. *et al.* 2006. The epigenetic progenitor origin of human cancer. *Nat Rev Genet* 7 (1), pp. 21-33.
- Ferraldeschi, R. *et al.* 2007. Modern management of small-cell lung cancer. *Drugs* 67 (15), pp. 2135-2152.
- Ferrandiz, M. L. and Devesa, I. 2008. Inducers of heme oxygenase-1. *Curr Pharm Des* 14 (5), pp. 473-486.
- Fialkow, P. J. 1979. Clonal origin of human tumors. *Annu Rev Med* 30, pp. 135-143.
- Filmus, J. and Capurro, M. 2008. The role of glypican-3 in the regulation of body size and cancer. *Cell Cycle* 7 (18), pp. 2787-2790.
- Fischer, B. and Arcaro, A. 2008. Current status of clinical trials for small cell lung cancer. *Rev Recent Clin Trials* 3 (1), pp. 40-61.
- Fischer, B. *et al.* 2007. Targeting receptor tyrosine kinase signalling in small cell lung cancer (SCLC): what have we learned so far? *Cancer Treat Rev* 33 (4), pp. 391-406.

Fisher, E. R. and Paulson, J. D. 1978. A new in vitro cell line established from human large cell variant of oat cell lung cancer. *Cancer Res* 38 (11 Pt 1), pp. 3830-3835.

Frank, D. *et al.* 2008. Gene expression pattern in biomechanically stretched cardiomyocytes: evidence for a stretch-specific gene program. *Hypertension* 51 (2), pp. 309-318.

Frank, N. Y. *et al.* 2005. ABCB5-mediated doxorubicin transport and chemoresistance in human malignant melanoma. *Cancer Res* 65 (10), pp. 4320-4333.

Friedl, P. and Wolf, K. 2003. Tumour-cell invasion and migration: diversity and escape mechanisms. *Nat Rev Cancer* 3 (5), pp. 362-374.

Fujimoto, I. *et al.* 2001. Regulation of cell adhesion by polysialic acid. Effects on cadherin, immunoglobulin cell adhesion molecule, and integrin function and independence from neural cell adhesion molecule binding or signaling activity. *J Biol Chem* 276 (34), pp. 31745-31751.

Fukuda, S. *et al.* 2004. Negative regulatory effect of an oligodendrocytic bHLH factor OLIG2 on the astrocytic differentiation pathway. *Cell Death Differ* 11 (2), pp. 196-202.

Galuska, S. P. *et al.* 2008. Enzyme-dependent variations in the polysialylation of the neural cell adhesion molecule (NCAM) in vivo. *J Biol Chem* 283 (1), pp. 17-28.

Garrett, S. H. *et al.* 1998. Differential expression of human metallothionein isoform I mRNA in human proximal tubule cells exposed to metals. *Environ Health Perspect* 106 (12), pp. 825-832.

Garst, J. 2007. Topotecan: An evolving option in the treatment of relapsed small cell lung cancer. *Ther Clin Risk Manag* 3 (6), pp. 1087-1095.

Gazdar, A. F. *et al.* 1985. Characterization of variant subclasses of cell lines derived from small cell lung cancer having distinctive biochemical, morphological, and growth properties. *Cancer Res* 45 (6), pp. 2924-2930.

Gazdar, A. F. *et al.* 1980. Establishment of continuous, clonable cultures of small-cell carcinoma of lung which have amine precursor uptake and decarboxylation cell properties. *Cancer Res* 40 (10), pp. 3502-3507.

Gentleman, R. C. *et al.* 2004. Bioconductor: open software development for computational biology and bioinformatics. *Genome Biol* 5 (10), p. R80.

Georgi, A. B. *et al.* 2002. Timing of events in mitosis. *Curr Biol* 12 (2), pp. 105-114.

- Gilchrist, A. J. *et al.* 2002. Cell adhesion-mediated transformation of a human SCLC cell line is associated with the development of a normal phenotype. *Exp Cell Res* 276 (1), pp. 63-78.
- Goldie, J. H. and Coldman, A. J. 1979. A mathematic model for relating the drug sensitivity of tumors to their spontaneous mutation rate. *Cancer Treat Rep* 63 (11-12), pp. 1727-1733.
- Goldshmidt, O. *et al.* 2003. Heparanase mediates cell adhesion independent of its enzymatic activity. *Faseb J* 17 (9), pp. 1015-1025.
- Goodell, M. A. 2002. Multipotential stem cells and 'side population' cells. *Cytotherapy* 4 (6), pp. 507-508.
- Goodell, M. A. *et al.* 2005. Isolation and characterization of side population cells. *Methods Mol Biol* 290, pp. 343-352.
- Greaves, M. 2007. Darwinian medicine: a case for cancer. *Nat Rev Cancer* 7 (3), pp. 213-221.
- Grigorieva, E. *et al.* 2008. Decreased expression of human D-glucuronyl C5-epimerase in breast cancer. *Int J Cancer* 122 (5), pp. 1172-1176.
- Grossman, D. *et al.* 2001. Transgenic expression of survivin in keratinocytes counteracts UVB-induced apoptosis and cooperates with loss of p53. *J Clin Invest* 108 (7), pp. 991-999.
- Grunert, S. *et al.* 2003. Diverse cellular and molecular mechanisms contribute to epithelial plasticity and metastasis. *Nat Rev Mol Cell Biol* 4 (8), pp. 657-665.
- Gryczynski, I. *et al.* 1999. Fluorescence spectral properties of the anticancer drug topotecan by steady-state and frequency domain fluorometry with one-photon and multi-photon excitation. *Photochem Photobiol* 69 (4), pp. 421-428.
- Gudermann, T. and Roelle, S. 2006. Calcium-dependent growth regulation of small cell lung cancer cells by neuropeptides. *Endocr Relat Cancer* 13 (4), pp. 1069-1084.
- Guo, W. and Giancotti, F. G. 2004. Integrin signalling during tumour progression. *Nat Rev Mol Cell Biol* 5 (10), pp. 816-826.
- Gurrola-Diaz, C. *et al.* 2003. Reduced expression of the neuron restrictive silencer factor permits transcription of glycine receptor alpha1 subunit in small-cell lung cancer cells. *Oncogene* 22 (36), pp. 5636-5645.
- Gutova, M. *et al.* 2007. Identification of uPAR-positive chemoresistant cells in small cell lung cancer. *PLoS ONE* 2 (2), p. e243.
- Hakomori, S. 2002. Glycosylation defining cancer malignancy: new wine in an old bottle. *Proc Natl Acad Sci U S A* 99 (16), pp. 10231-10233.



- Han, H. J. *et al.* 2008. SATB1 reprogrammes gene expression to promote breast tumour growth and metastasis. *Nature* 452 (7184), pp. 187-193.
- Harbour, J. W. *et al.* 1988. Abnormalities in structure and expression of the human retinoblastoma gene in SCLC. *Science* 241 (4863), pp. 353-357.
- Hardwick, L. J. *et al.* 2007. The emerging pharmacotherapeutic significance of the breast cancer resistance protein (ABCG2). *Br J Pharmacol* 151 (2), pp. 163-174.
- Hart, L. S. and El-Deiry, W. S. 2008. Invincible, but not invisible: imaging approaches toward in vivo detection of cancer stem cells. *J Clin Oncol* 26 (17), pp. 2901-2910.
- Hartmann, T. N. *et al.* 2005. CXCR4 chemokine receptor and integrin signaling co-operate in mediating adhesion and chemoresistance in small cell lung cancer (SCLC) cells. *Oncogene* 24 (27), pp. 4462-4471.
- Hartmann, T. N. *et al.* 2004. The role of adhesion molecules and chemokine receptor CXCR4 (CD184) in small cell lung cancer. *J Biol Regul Homeost Agents* 18 (2), pp. 126-130.
- Hazlehurst, L. A. *et al.* 2000. Adhesion to fibronectin via beta1 integrins regulates p27kip1 levels and contributes to cell adhesion mediated drug resistance (CAM-DR). *Oncogene* 19 (38), pp. 4319-4327.
- Heasley, L. E. 2001. Autocrine and paracrine signaling through neuropeptide receptors in human cancer. *Oncogene* 20 (13), pp. 1563-1569.
- Hershey, A. D. *et al.* 2008. Assessing quality and normalization of microarrays: case studies using neurological genomic data. *Acta Neurol Scand.*
- Higgins, C. F. and Linton, K. J. 2004. The ATP switch model for ABC transporters. *Nat Struct Mol Biol* 11 (10), pp. 918-926.
- Hirschmann-Jax, C. *et al.* 2005. A distinct "side population" of cells in human tumor cells: implications for tumor biology and therapy. *Cell Cycle* 4 (2), pp. 203-205.
- Hirschmann-Jax, C. *et al.* 2004. A distinct "side population" of cells with high drug efflux capacity in human tumor cells. *Proc Natl Acad Sci U S A* 101 (39), pp. 14228-14233.
- Ho, M. M. *et al.* 2007. Side population in human lung cancer cell lines and tumors is enriched with stem-like cancer cells. *Cancer Res* 67 (10), pp. 4827-4833.

- Hodkinson, P. S. *et al.* 2006. ECM overrides DNA damage-induced cell cycle arrest and apoptosis in small-cell lung cancer cells through beta1 integrin-dependent activation of PI3-kinase. *Cell Death Differ* 13 (10), pp. 1776-1788.
- Hodkinson, P. S. *et al.* 2007. Extracellular matrix regulation of drug resistance in small-cell lung cancer. *Int J Radiat Biol* 83 (11-12), pp. 733-741.
- Hoffman, P. C. *et al.* 2000. Lung cancer. *Lancet* 355 (9202), pp. 479-485.
- Hoffmann, R. and Valencia, A. 2004. A gene network for navigating the literature. *Nat Genet* 36 (7), p. 664.
- Hollenstein, K. *et al.* 2007. Structure and mechanism of ABC transporter proteins. *Curr Opin Struct Biol* 17 (4), pp. 412-418.
- Huang, Y. *et al.* 2004. Membrane transporters and channels: role of the transportome in cancer chemosensitivity and chemoresistance. *Cancer Res* 64 (12), pp. 4294-4301.
- Huang, Y. and Sadee, W. 2006. Membrane transporters and channels in chemoresistance and -sensitivity of tumor cells. *Cancer Lett* 239 (2), pp. 168-182.
- Hynes, R. O. 1999. Cell adhesion: old and new questions. *Trends Cell Biol* 9 (12), pp. M33-37.
- Igney, F. H. and Krammer, P. H. 2002. Death and anti-death: tumour resistance to apoptosis. *Nat Rev Cancer* 2 (4), pp. 277-288.
- Irizarry, R. A. *et al.* 2003. Summaries of Affymetrix GeneChip probe level data. *Nucleic Acids Res* 31 (4), p. e15.
- Iwasa, Y. *et al.* 2006. Evolution of resistance during clonal expansion. *Genetics* 172 (4), pp. 2557-2566.
- Iyengar, P. and Tsao, M. S. 2002. Clinical relevance of molecular markers in lung cancer. *Surg Oncol* 11 (4), pp. 167-179.
- Jacobs, C. L. *et al.* 2001. Substrate specificity of the sialic acid biosynthetic pathway. *Biochemistry* 40 (43), pp. 12864-12874.
- Jagadeeswaran, R. *et al.* 2007. Activation of HGF/c-Met pathway contributes to the reactive oxygen species generation and motility of small cell lung cancer cells. *Am J Physiol Lung Cell Mol Physiol* 292 (6), pp. L1488-1494.
- Jasani, B. *et al.* 1998. Clonal overexpression of metallothionein is induced by somatic mutation in morphologically normal colonic mucosa. *J Pathol* 184 (2), pp. 144-147.

- Jasani, B. and Schmid, K. W. 1997. Significance of metallothionein overexpression in human tumours. *Histopathology* 31 (3), pp. 211-214.
- Jechlinger, M. *et al.* 2003. Expression profiling of epithelial plasticity in tumor progression. *Oncogene* 22 (46), pp. 7155-7169.
- Jensen, P. B. *et al.* 1997. In vitro cross-resistance and collateral sensitivity in seven resistant small-cell lung cancer cell lines: preclinical identification of suitable drug partners to taxotere, taxol, topotecan and gemcitabine. *Br J Cancer* 75 (6), pp. 869-877.
- Jensen, P. B. *et al.* 1989. In vitro evaluation of the potential of aclarubicin in the treatment of small cell carcinoma of the lung (SCCL). *Br J Cancer* 60 (6), pp. 838-844.
- Jin, T. *et al.* 1998. Toxicokinetics and biochemistry of cadmium with special emphasis on the role of metallothionein. *Neurotoxicology* 19 (4-5), pp. 529-535.
- Johnson, C. P. *et al.* 2005. Direct evidence that neural cell adhesion molecule (NCAM) polysialylation increases intermembrane repulsion and abrogates adhesion. *J Biol Chem* 280 (1), pp. 137-145.
- Jones, P. A. and Baylin, S. B. 2007. The epigenomics of cancer. *Cell* 128 (4), pp. 683-692.
- Jonker, J. W. *et al.* 2000. Role of breast cancer resistance protein in the bioavailability and fetal penetration of topotecan. *J Natl Cancer Inst* 92 (20), pp. 1651-1656.
- Joyce, J. A. 2005. Therapeutic targeting of the tumor microenvironment. *Cancer Cell* 7 (6), pp. 513-520.
- Juliano, R. L. 2002. Signal transduction by cell adhesion receptors and the cytoskeleton: functions of integrins, cadherins, selectins, and immunoglobulin-superfamily members. *Annu Rev Pharmacol Toxicol* 42, pp. 283-323.
- Juliano, R. L. and Ling, V. 1976. A surface glycoprotein modulating drug permeability in Chinese hamster ovary cell mutants. *Biochim Biophys Acta* 455 (1), pp. 152-162.
- Kanehisa, M. *et al.* 2004. The KEGG resource for deciphering the genome. *Nucleic Acids Res* 32 (Database issue), pp. D277-280.
- Kannagi, R. *et al.* 2004. Carbohydrate-mediated cell adhesion in cancer metastasis and angiogenesis. *Cancer Sci* 95 (5), pp. 377-384.
- Kao, F. T. and Puck, T. T. 1968. Genetics of somatic mammalian cells, VII. Induction and isolation of nutritional mutants in Chinese hamster cells. *Proc Natl Acad Sci U S A* 60 (4), pp. 1275-1281.

- Kasper, C. *et al.* 2000. Structural basis of cell-cell adhesion by NCAM. *Nat Struct Biol* 7 (5), pp. 389-393.
- Kastan, M. B. 2007. Wild-type p53: tumors can't stand it. *Cell* 128 (5), pp. 837-840.
- Kayser, K. *et al.* 1998. Pulmonary metastases of breast carcinomas: ligandohistochemical, nuclear, and structural analysis of primary and metastatic tumors with emphasis on period of occurrence of metastases and survival. *J Surg Oncol* 69 (3), pp. 137-146.
- Keppler, O. T. *et al.* 1999. UDP-GlcNAc 2-epimerase: a regulator of cell surface sialylation. *Science* 284 (5418), pp. 1372-1376.
- Kerr, I. D. 2002. Structure and association of ATP-binding cassette transporter nucleotide-binding domains. *Biochim Biophys Acta* 1561 (1), pp. 47-64.
- Khan, M. Z. *et al.* 1993. Induction of phenotypic changes in SCLC cell lines in vitro by hexamethylene bisacetamide, sodium butyrate, and cyclic AMP. *Ann Oncol* 4 (6), pp. 499-507.
- Kim, H. *et al.* 2003. The heparan sulfate proteoglycan GPC3 is a potential lung tumor suppressor. *Am J Respir Cell Mol Biol* 29 (6), pp. 694-701.
- Kim, Y. H. *et al.* 2006. Combined microarray analysis of small cell lung cancer reveals altered apoptotic balance and distinct expression signatures of MYC family gene amplification. *Oncogene* 25 (1), pp. 130-138.
- Kiselyov, V. V. *et al.* 2005. Structural biology of NCAM homophilic binding and activation of FGFR. *J Neurochem* 94 (5), pp. 1169-1179.
- Kiss, J. Z. *et al.* 2001. The role of neural cell adhesion molecules in plasticity and repair. *Brain Res Brain Res Rev* 36 (2-3), pp. 175-184.
- Klaassen, C. D. and Liu, J. 1998. Metallothionein transgenic and knock-out mouse models in the study of cadmium toxicity. *J Toxicol Sci* 23 Suppl 2, pp. 97-102.
- Kleene, R. and Schachner, M. 2004. Glycans and neural cell interactions. *Nat Rev Neurosci* 5 (3), pp. 195-208.
- Kojima, N. *et al.* 1996. Characterization of mouse ST8Sia II (STX) as a neural cell adhesion molecule-specific polysialic acid synthase. Requirement of core alpha1,6-linked fucose and a polypeptide chain for polysialylation. *J Biol Chem* 271 (32), pp. 19457-19463.
- Kondo, K. *et al.* 1998. High frequency expressions of CD44 standard and variant forms in non-small cell lung cancers, but not in small cell lung cancers. *J Surg Oncol* 69 (3), pp. 128-136.

- Kondo, T. *et al.* 2004. Persistence of a small subpopulation of cancer stem-like cells in the C6 glioma cell line. *Proc Natl Acad Sci U S A* 101 (3), pp. 781-786.
- Konemann, S. *et al.* 2000. Cell heterogeneity and subpopulations in solid tumors characterized by simultaneous immunophenotyping and DNA content analysis. *Cytometry* 41 (3), pp. 172-177.
- Koros, A. M. *et al.* 1985. Stability and utility of the unique human small cell carcinoma line SHP-77. *Cancer Res* 45 (6), pp. 2725-2731.
- Koscielny, S. *et al.* 1985. A simulation model of the natural history of human breast cancer. *Br J Cancer* 52 (4), pp. 515-524.
- Koster, D. A. *et al.* 2007. Antitumour drugs impede DNA uncoiling by topoisomerase I. *Nature* 448 (7150), pp. 213-217.
- Kouniavsky, G. *et al.* 2002. Stromal extracellular matrix reduces chemotherapy-induced apoptosis in colon cancer cell lines. *Clin Exp Metastasis* 19 (1), pp. 55-60.
- Kraus, A. C. *et al.* 2002. In vitro chemo- and radio-resistance in small cell lung cancer correlates with cell adhesion and constitutive activation of AKT and MAP kinase pathways. *Oncogene* 21 (57), pp. 8683-8695.
- Krueger, A. *et al.* 2001. FLICE-inhibitory proteins: regulators of death receptor-mediated apoptosis. *Mol Cell Biol* 21 (24), pp. 8247-8254.
- Krug, L. M. *et al.* 2004. Vaccination of small cell lung cancer patients with polysialic acid or N-propionylated polysialic acid conjugated to keyhole limpet hemocyanin. *Clin Cancer Res* 10 (3), pp. 916-923.
- Kruger, J. A. *et al.* 2006. Characterization of stem cell-like cancer cells in immune-competent mice. *Blood* 108 (12), pp. 3906-3912.
- Kruh, G. D. and Belinsky, M. G. 2003. The MRP family of drug efflux pumps. *Oncogene* 22 (47), pp. 7537-7552.
- Krystal, G. W. *et al.* 1996. Autocrine growth of small cell lung cancer mediated by coexpression of c-kit and stem cell factor. *Cancer Res* 56 (2), pp. 370-376.
- Krystal, G. W. *et al.* 2002. Inhibition of phosphatidylinositol 3-kinase-Akt signaling blocks growth, promotes apoptosis, and enhances sensitivity of small cell lung cancer cells to chemotherapy. *Mol Cancer Ther* 1 (11), pp. 913-922.
- Kuschel, C. *et al.* 2006. Cell adhesion profiling using extracellular matrix protein microarrays. *Biotechniques* 40 (4), pp. 523-531.
- Lakshmiathy, U. and Verfaillie, C. 2005. Stem cell plasticity. *Blood Rev* 19 (1), pp. 29-38.



- Lantuejoul, S. *et al.* 1998. Neural cell adhesion molecules (NCAM) and NCAM-PSA expression in neuroendocrine lung tumors. *Am J Surg Pathol* 22 (10), pp. 1267-1276.
- Leemhuis, T. *et al.* 1996. Isolation of primitive human bone marrow hematopoietic progenitor cells using Hoechst 33342 and Rhodamine 123. *Exp Hematol* 24 (10), pp. 1215-1224.
- Letai, A. G. 2008. Diagnosing and exploiting cancer's addiction to blocks in apoptosis. *Nat Rev Cancer* 8 (2), pp. 121-132.
- Levesque, A. A. *et al.* 2008. Defective p53 signaling in p53 wild-type tumors attenuates p21waf1 induction and cyclin B repression rendering them sensitive to Chk1 inhibitors that abrogate DNA damage-induced S and G2 arrest. *Mol Cancer Ther* 7 (2), pp. 252-262.
- Levine, A. J. 1997. p53, the cellular gatekeeper for growth and division. *Cell* 88 (3), pp. 323-331.
- Ley, K. 2003. The role of selectins in inflammation and disease. *Trends Mol Med* 9 (6), pp. 263-268.
- Lieber, M. *et al.* 1976. A continuous tumor-cell line from a human lung carcinoma with properties of type II alveolar epithelial cells. *Int J Cancer* 17 (1), pp. 62-70.
- Ling, V. and Thompson, L. H. 1974. Reduced permeability in CHO cells as a mechanism of resistance to colchicine. *J Cell Physiol* 83 (1), pp. 103-116.
- Litman, T. *et al.* 2000. The multidrug-resistant phenotype associated with overexpression of the new ABC half-transporter, MXR (ABCG2). *J Cell Sci* 113 ( Pt 11), pp. 2011-2021.
- Losasso, C. *et al.* 2008. A single mutation in the 729 residue modulates human DNA topoisomerase IB DNA binding and drug resistance. *Nucleic Acids Res* 36 (17), pp. 5635-5644.
- Lotz, M. M. *et al.* 1989. Cell adhesion to fibronectin and tenascin: quantitative measurements of initial binding and subsequent strengthening response. *J Cell Biol* 109 (4 Pt 1), pp. 1795-1805.
- Lowe, S. W. *et al.* 1994. p53 status and the efficacy of cancer therapy in vivo. *Science* 266 (5186), pp. 807-810.
- Ludwig, A. *et al.* 2002. Identification of differentially expressed genes in classical and atypical multidrug-resistant gastric carcinoma cells. *Anticancer Res* 22 (6A), pp. 3213-3221.
- Magni, M. *et al.* 1996. Induction of cyclophosphamide-resistance by aldehyde-dehydrogenase gene transfer. *Blood* 87 (3), pp. 1097-1103.

- Mahal, L. K. *et al.* 2001. A small-molecule modulator of poly-alpha 2,8-sialic acid expression on cultured neurons and tumor cells. *Science* 294 (5541), pp. 380-381.
- Maier, H. *et al.* 1997. Metallothionein overexpression in human brain tumours. *Acta Neuropathol (Berl)* 94 (6), pp. 599-604.
- Maliepaard, M. *et al.* 2001. Subcellular localization and distribution of the breast cancer resistance protein transporter in normal human tissues. *Cancer Res* 61 (8), pp. 3458-3464.
- Mani, S. A. *et al.* 2008. The epithelial-mesenchymal transition generates cells with properties of stem cells. *Cell* 133 (4), pp. 704-715.
- Mao, Q. and Unadkat, J. D. 2005. Role of the breast cancer resistance protein (ABCG2) in drug transport. *Aaps J* 7 (1), pp. E118-133.
- Marquez, N. *et al.* 2003. Single cell tracking reveals that Msh2 is a key component of an early-acting DNA damage-activated G2 checkpoint. *Oncogene* 22 (48), pp. 7642-7648.
- Masson, E. *et al.* 2005. Glucosamine induces cell-cycle arrest and hypertrophy of mesangial cells: implication of gangliosides. *Biochem J* 388 (Pt 2), pp. 537-544.
- Mathijssen, R. H. *et al.* 2002. Pharmacology of topoisomerase I inhibitors irinotecan (CPT-11) and topotecan. *Curr Cancer Drug Targets* 2 (2), pp. 103-123.
- Maulik, G. *et al.* 2002. Modulation of the c-Met/hepatocyte growth factor pathway in small cell lung cancer. *Clin Cancer Res* 8 (2), pp. 620-627.
- Mayanil, C. S. *et al.* 2000. Overexpression of murine Pax3 increases NCAM polysialylation in a human medulloblastoma cell line. *J Biol Chem* 275 (30), pp. 23259-23266.
- McGee, S. F. *et al.* 2006. Mammary gland biology and breast cancer. Conference on Common Molecular Mechanisms of Mammary Gland Development and Breast Cancer Progression. *EMBO Rep* 7 (11), pp. 1084-1088.
- Merry, A. H. and Merry, C. L. 2005. Glycoscience finally comes of age. *EMBO Rep* 6 (10), pp. 900-903.
- Meuwissen, R. *et al.* 2003. Induction of small cell lung cancer by somatic inactivation of both Trp53 and Rb1 in a conditional mouse model. *Cancer Cell* 4 (3), pp. 181-189.

Michor, F. *et al.* 2006. Evolution of resistance to cancer therapy. *Curr Pharm Des* 12 (3), pp. 261-271.

Miles, A. T. *et al.* 2000. Induction, regulation, degradation, and biological significance of mammalian metallothioneins. *Crit Rev Biochem Mol Biol* 35 (1), pp. 35-70.

Millenaar, F. F. *et al.* 2006. How to decide? Different methods of calculating gene expression from short oligonucleotide array data will give different results. *BMC Bioinformatics* 7, p. 137.

Minn, A. J. *et al.* 1995. Expression of bcl-xL can confer a multidrug resistance phenotype. *Blood* 86 (5), pp. 1903-1910.

Minna, J. D. *et al.* 2002. Focus on lung cancer. *Cancer Cell* 1 (1), pp. 49-52.

Mirski, S. E. *et al.* 1987. Multidrug resistance in a human small cell lung cancer cell line selected in adriamycin. *Cancer Res* 47 (10), pp. 2594-2598.

Moolenaar, C. E. *et al.* 1992. Alternative splicing of neural-cell-adhesion molecule mRNA in human small-cell lung-cancer cell line H69. *Int J Cancer* 51 (2), pp. 238-243.

Moore, S. M. *et al.* 1998. The presence of a constitutively active phosphoinositide 3-kinase in small cell lung cancer cells mediates anchorage-independent proliferation via a protein kinase B and p70s6k-dependent pathway. *Cancer Res* 58 (22), pp. 5239-5247.

Moustakas, A. and Heldin, C. H. 2007. Signaling networks guiding epithelial-mesenchymal transitions during embryogenesis and cancer progression. *Cancer Sci* 98 (10), pp. 1512-1520.

Murphy, N. R. and Hellwig, R. J. 1996. Improved nucleic acid organic extraction through use of a unique gel barrier material. *Biotechniques* 21 (5), pp. 934-936, 938-939.

Murray, N. and Turrisi, A. T., 3rd 2006. A review of first-line treatment for small-cell lung cancer. *J Thorac Oncol* 1 (3), pp. 270-278.

Nagashima, S. *et al.* 2006. BCRP/ABCG2 levels account for the resistance to topoisomerase I inhibitors and reversal effects by gefitinib in non-small cell lung cancer. *Cancer Chemother Pharmacol* 58 (5), pp. 594-600.

Nakagawa, M. *et al.* 1992. Reduced intracellular drug accumulation in the absence of P-glycoprotein (mdr1) overexpression in mitoxantrone-resistant human MCF-7 breast cancer cells. *Cancer Res* 52 (22), pp. 6175-6181.

Nakagoe, T. *et al.* 2000. Expression of Lewis(a), sialyl Lewis(a), Lewis(x) and sialyl Lewis(x) antigens as prognostic factors in patients with colorectal cancer. *Can J Gastroenterol* 14 (9), pp. 753-760.

- Nakagoe, T. *et al.* 1998. Immunohistochemical expression of ABH/Lewis-related antigens in primary breast carcinomas and metastatic lymph node lesions. *Cancer Detect Prev* 22 (6), pp. 499-505.
- Nakanishi, T. *et al.* 2003. Functional characterization of human breast cancer resistance protein (BCRP, ABCG2) expressed in the oocytes of *Xenopus laevis*. *Mol Pharmacol* 64 (6), pp. 1452-1462.
- Nakatsura, T. *et al.* 2004. Identification of glypican-3 as a novel tumor marker for melanoma. *Clin Cancer Res* 10 (19), pp. 6612-6621.
- Nasser, N. J. 2008. Heparanase involvement in physiology and disease. *Cell Mol Life Sci* 65 (11), pp. 1706-1715.
- Nguyen, C. *et al.* 1986. Localization of the human NCAM gene to band q23 of chromosome 11: the third gene coding for a cell interaction molecule mapped to the distal portion of the long arm of chromosome 11. *J Cell Biol* 102 (3), pp. 711-715.
- Nieth, C. and Lage, H. 2005. Induction of the ABC-transporters Mdr1/P-gp (Abcb1), mrpl (Abcc1), and bcrp (Abcg2) during establishment of multidrug resistance following exposure to mitoxantrone. *J Chemother* 17 (2), pp. 215-223.
- Ninomiya, H. *et al.* 2006. Genetic instability in lung cancer: concurrent analysis of chromosomal, mini- and microsatellite instability and loss of heterozygosity. *Br J Cancer* 94 (10), pp. 1485-1491.
- Njoh, K. L. *et al.* 2006. Spectral analysis of the DNA targeting bisalkylaminoanthraquinone DRAQ5 in intact living cells. *Cytometry A* 69 (8), pp. 805-814.
- Norton, L. 1997. Conceptual basis for advances in the systemic drug therapy of breast cancer. *Semin Oncol* 24 (4 Suppl 11), pp. S11-12-S11-12.
- Norton, L. and Simon, R. 1986. The Norton-Simon hypothesis revisited. *Cancer Treat Rep* 70 (1), pp. 163-169.
- Nowell, P. C. 1976. The clonal evolution of tumor cell populations. *Science* 194 (4260), pp. 23-28.
- Nurse, P. 2000. A long twentieth century of the cell cycle and beyond. *Cell* 100 (1), pp. 71-78.
- O'Brien, L. E. *et al.* 2002. Opinion: Building epithelial architecture: insights from three-dimensional culture models. *Nat Rev Mol Cell Biol* 3 (7), pp. 531-537.
- O'Brien, M. *et al.* 2007. Recent advances with topotecan in the treatment of lung cancer. *Oncologist* 12 (10), pp. 1194-1204.

Okuno, S. H. and Jett, J. R. 2002. Small cell lung cancer: current therapy and promising new regimens. *Oncologist* 7 (3), pp. 234-238.

Oltersdorf, T. *et al.* 2005. An inhibitor of Bcl-2 family proteins induces regression of solid tumours. *Nature* 435 (7042), pp. 677-681.

Ormrod, D. and Spencer, C. M. 1999. Topotecan: a review of its efficacy in small cell lung cancer. *Drugs* 58 (3), pp. 533-551.

Oshita, F. *et al.* 2002. Increased expression of integrin beta1 is a poor prognostic factor in small-cell lung cancer. *Anticancer Res* 22 (2B), pp. 1065-1070.

Palmiter, R. D. 1998. The elusive function of metallothioneins. *Proc Natl Acad Sci U S A* 95 (15), pp. 8428-8430.

Panetta, J. C. 1998. A mathematical model of drug resistance: heterogeneous tumors. *Math Biosci* 147 (1), pp. 41-61.

Pantel, K. and Brakenhoff, R. H. 2004. Dissecting the metastatic cascade. *Nat Rev Cancer* 4 (6), pp. 448-456.

Paratcha, G. *et al.* 2003. The neural cell adhesion molecule NCAM is an alternative signaling receptor for GDNF family ligands. *Cell* 113 (7), pp. 867-879.

Pedersen, N. *et al.* 2003. Transcriptional gene expression profiling of small cell lung cancer cells. *Cancer Res* 63 (8), pp. 1943-1953.

Peli, J. *et al.* 1999. Oncogenic Ras inhibits Fas ligand-mediated apoptosis by downregulating the expression of Fas. *Embo J* 18 (7), pp. 1824-1831.

Pepper, S. D. *et al.* 2007. The utility of MAS5 expression summary and detection call algorithms. *BMC Bioinformatics* 8, p. 273.

Perl, A. K. *et al.* 1999. Reduced expression of neural cell adhesion molecule induces metastatic dissemination of pancreatic beta tumor cells. *Nat Med* 5 (3), pp. 286-291.

Peters, M. G. *et al.* 2003. Inhibition of invasion and metastasis by glypican-3 in a syngeneic breast cancer model. *Breast Cancer Res Treat* 80 (2), pp. 221-232.

Polgar, O. *et al.* 2008. ABCG2: structure, function and role in drug response. *Expert Opin Drug Metab Toxicol* 4 (1), pp. 1-15.

Pommier, Y. 2004. Camptothecins and topoisomerase I: a foot in the door. Targeting the genome beyond topoisomerase I with camptothecins and novel anticancer drugs: importance of DNA replication, repair and cell cycle checkpoints. *Curr Med Chem Anticancer Agents* 4 (5), pp. 429-434.



- Pommier, Y. 2006. Topoisomerase I inhibitors: camptothecins and beyond. *Nat Rev Cancer* 6 (10), pp. 789-802.
- Pommier, Y. *et al.* 1998. Mechanism of action of eukaryotic DNA topoisomerase I and drugs targeted to the enzyme. *Biochim Biophys Acta* 1400 (1-3), pp. 83-105.
- Ponte-Sucre, A. 2007. Availability and applications of ATP-binding cassette (ABC) transporter blockers. *Appl Microbiol Biotechnol* 76 (2), pp. 279-286.
- Prindull, G. and Zipori, D. 2004. Environmental guidance of normal and tumor cell plasticity: epithelial mesenchymal transitions as a paradigm. *Blood* 103 (8), pp. 2892-2899.
- Rabindran, S. K. *et al.* 1998. Reversal of a novel multidrug resistance mechanism in human colon carcinoma cells by fumitremorgin C. *Cancer Res* 58 (24), pp. 5850-5858.
- Rabindran, S. K. *et al.* 2000. Fumitremorgin C reverses multidrug resistance in cells transfected with the breast cancer resistance protein. *Cancer Res* 60 (1), pp. 47-50.
- Rajagopalan, H. *et al.* 2003. The significance of unstable chromosomes in colorectal cancer. *Nat Rev Cancer* 3 (9), pp. 695-701.
- Ramaswamy, S. *et al.* 2003. A molecular signature of metastasis in primary solid tumors. *Nat Genet* 33 (1), pp. 49-54.
- Rapp, U. R. *et al.* 2008. Oncogene-induced plasticity and cancer stem cells. *Cell Cycle* 7 (1), pp. 45-51.
- Renkonen, J. *et al.* 1997. Endothelial and epithelial expression of sialyl Lewis(x) and sialyl Lewis(a) in lesions of breast carcinoma. *Int J Cancer* 74 (3), pp. 296-300.
- Retsky, M. *et al.* 2004. Hypothesis: Induced angiogenesis after surgery in premenopausal node-positive breast cancer patients is a major underlying reason why adjuvant chemotherapy works particularly well for those patients. *Breast Cancer Res* 6 (4), pp. R372-374.
- Retsky, M. W. *et al.* 1997. Computer simulation of a breast cancer metastasis model. *Breast Cancer Res Treat* 45 (2), pp. 193-202.
- Reya, T. *et al.* 2001. Stem cells, cancer, and cancer stem cells. *Nature* 414 (6859), pp. 105-111.
- Rintoul, R. C. and Sethi, T. 2002. Extracellular matrix regulation of drug resistance in small-cell lung cancer. *Clin Sci (Lond)* 102 (4), pp. 417-424.

- Risse-Hackl, G. *et al.* 1998. Transition from SCLC to NSCLC phenotype is accompanied by an increased TRE-binding activity and recruitment of specific AP-1 proteins. *Oncogene* 16 (23), pp. 3057-3068.
- Robey, R. W. *et al.* 2001. A functional assay for detection of the mitoxantrone resistance protein, MXR (ABCG2). *Biochim Biophys Acta* 1512 (2), pp. 171-182.
- Robey, R. W. *et al.* 2007. ABCG2: determining its relevance in clinical drug resistance. *Cancer Metastasis Rev* 26 (1), pp. 39-57.
- Robinson, M. D. and Speed, T. P. 2007. A comparison of Affymetrix gene expression arrays. *BMC Bioinformatics* 8, p. 449.
- Robson, E. J. *et al.* 2006. Epithelial-to-mesenchymal transition confers resistance to apoptosis in three murine mammary epithelial cell lines. *Differentiation* 74 (5), pp. 254-264.
- Ross, D. D. and Doyle, L. A. 2004. Mining our ABCs: pharmacogenomic approach for evaluating transporter function in cancer drug resistance. *Cancer Cell* 6 (2), pp. 105-107.
- Rossi, A. *et al.* 2008. New targeted therapies and small-cell lung cancer. *Clin Lung Cancer* 9 (5), pp. 271-279.
- Rosti, G. *et al.* 2006. Chemotherapy advances in small cell lung cancer. *Ann Oncol* 17 Suppl 5, pp. v99-102.
- Rougon, G. *et al.* 1986. A monoclonal antibody against meningococcus group B polysaccharides distinguishes embryonic from adult N-CAM. *J Cell Biol* 103 (6 Pt 1), pp. 2429-2437.
- Rutishauser, U. 2008. Polysialic acid in the plasticity of the developing and adult vertebrate nervous system. *Nat Rev Neurosci* 9 (1), pp. 26-35.
- Rutishauser, U. *et al.* 1988. The neural cell adhesion molecule (NCAM) as a regulator of cell-cell interactions. *Science* 240 (4848), pp. 53-57.
- Rutishauser, U. *et al.* 1976. Mechanisms of adhesion among cells from neural tissues of the chick embryo. *Proc Natl Acad Sci U S A* 73 (2), pp. 577-581.
- Rutishauser, U. *et al.* 1985. Specific alteration of NCAM-mediated cell adhesion by an endoneuraminidase. *J Cell Biol* 101 (5 Pt 1), pp. 1842-1849.
- Saito, Y. *et al.* 2006. Absence of CD9 enhances adhesion-dependent morphologic differentiation, survival, and matrix metalloproteinase-2 production in small cell lung cancer cells. *Cancer Res* 66 (19), pp. 9557-9565.
- Salge, U. *et al.* 2001. Transition from suspension to adherent growth is accompanied by tissue factor expression and matrix metalloproteinase

- secretion in a small cell lung cancer cell line. *J Cancer Res Clin Oncol* 127 (2), pp. 139-141.
- Sattler, M. and Salgia, R. 2003. Molecular and cellular biology of small cell lung cancer. *Semin Oncol* 30 (1), pp. 57-71.
- Sawyers, C. L. 2008. The cancer biomarker problem. *Nature* 452 (7187), pp. 548-552.
- Scharenberg, C. W. *et al.* 2002. The ABCG2 transporter is an efficient Hoechst 33342 efflux pump and is preferentially expressed by immature human hematopoietic progenitors. *Blood* 99 (2), pp. 507-512.
- Schatton, T. *et al.* 2008. Identification of cells initiating human melanomas. *Nature* 451 (7176), pp. 345-349.
- Scheidegger, E. P. *et al.* 1994. In vitro and in vivo growth of clonal sublines of human small cell lung carcinoma is modulated by polysialic acid of the neural cell adhesion molecule. *Lab Invest* 70 (1), pp. 95-106.
- Scheidegger, E. P. *et al.* 1995. A human STX cDNA confers polysialic acid expression in mammalian cells. *J Biol Chem* 270 (39), pp. 22685-22688.
- Schmidmaier, R. and Baumann, P. 2008. ANTI-ADHESION evolves to a promising therapeutic concept in oncology. *Curr Med Chem* 15 (10), pp. 978-990.
- Schmitt, E. *et al.* 2007. Intracellular and extracellular functions of heat shock proteins: repercussions in cancer therapy. *J Leukoc Biol* 81 (1), pp. 15-27.
- Scotto, K. W. 2003. Transcriptional regulation of ABC drug transporters. *Oncogene* 22 (47), pp. 7496-7511.
- Seddon, A. D. *et al.* 1998. Differential expression of cell adhesion molecules in phenotypic variants of the small cell lung carcinoma cell line NCI-H69. *In Vitro Cell Dev Biol Anim* 34 (9), pp. 677-678.
- Seidenfaden, R. *et al.* 2000. Control of NCAM polysialylation by the differential expression of polysialyltransferases ST8SialI and ST8SialIV. *Eur J Cell Biol* 79 (10), pp. 680-688.
- Seidenfaden, R. *et al.* 2003. Polysialic acid directs tumor cell growth by controlling heterophilic neural cell adhesion molecule interactions. *Mol Cell Biol* 23 (16), pp. 5908-5918.
- Sell, S. 1990. Cancer-associated carbohydrates identified by monoclonal antibodies. *Hum Pathol* 21 (10), pp. 1003-1019.
- Seo, D. C. *et al.* 2007. Gene expression profiling of cancer stem cell in human lung adenocarcinoma A549 cells. *Mol Cancer* 6, p. 75.

Seo, J. *et al.* 2004. Interactively optimizing signal-to-noise ratios in expression profiling: project-specific algorithm selection and detection p-value weighting in Affymetrix microarrays. *Bioinformatics* 20 (16), pp. 2534-2544.

Sethi, T. *et al.* 1999. Extracellular matrix proteins protect small cell lung cancer cells against apoptosis: a mechanism for small cell lung cancer growth and drug resistance in vivo. *Nat Med* 5 (6), pp. 662-668.

Setoguchi, T. *et al.* 2004. Cancer stem cells persist in many cancer cell lines. *Cell Cycle* 3 (4), pp. 414-415.

Shah, M. A. and Schwartz, G. K. 2001. Cell cycle-mediated drug resistance: an emerging concept in cancer therapy. *Clin Cancer Res* 7 (8), pp. 2168-2181.

Shevde, L. A. and Welch, D. R. 2003. Metastasis suppressor pathways--an evolving paradigm. *Cancer Lett* 198 (1), pp. 1-20.

Shin, M. S. *et al.* 2001. Mutations of tumor necrosis factor-related apoptosis-inducing ligand receptor 1 (TRAIL-R1) and receptor 2 (TRAIL-R2) genes in metastatic breast cancers. *Cancer Res* 61 (13), pp. 4942-4946.

Shnyder, S. D. *et al.* 2006. Reducing the cost of screening novel agents using the hollow fibre assay. *Anticancer Res* 26 (3A), pp. 2049-2052.

Shnyder, S. D. *et al.* 2005. Development of a modified hollow fibre assay for studying agents targeting the tumour neovasculature. *Anticancer Res* 25 (3B), pp. 1889-1894.

Shriver, Z. *et al.* 2004. Glycomics: a pathway to a class of new and improved therapeutics. *Nat Rev Drug Discov* 3 (10), pp. 863-873.

Shtivelman, E. and Namikawa, R. 1995. Species-specific metastasis of human tumor cells in the severe combined immunodeficiency mouse engrafted with human tissue. *Proc Natl Acad Sci U S A* 92 (10), pp. 4661-4665.

Sieber, O. M. *et al.* 2003. Genomic instability--the engine of tumorigenesis? *Nat Rev Cancer* 3 (9), pp. 701-708.

Skipper, H. E. 1964. Perspectives in Cancer Chemotherapy: Therapeutic Design. *Cancer Res* 24, pp. 1295-1302.

Small, S. J. and Akeson, R. 1990. Expression of the unique NCAM VASE exon is independently regulated in distinct tissues during development. *J Cell Biol* 111 (5 Pt 1), pp. 2089-2096.

Smith, P. J. *et al.* 2000. Characteristics of a novel deep red/infrared fluorescent cell-permeant DNA probe, DRAQ5, in intact human cells analyzed by flow cytometry, confocal and multiphoton microscopy. *Cytometry* 40 (4), pp. 280-291.

- Smith, P. J. *et al.* 2006. Cell Cycle Dynamics and the Challenges for CDK Targeting. In: Smith, P.J. and Yue, E.W. eds. *Inhibitors of Cyclin-Dependent Kinases as Anti-Tumor Agents*. Vol. 2. Boca Raton, FL: CRC Press, Taylor & Francis, p. 448.
- Smith, P. J. *et al.* 2007. Mitotic bypass via an occult cell cycle phase following DNA topoisomerase II inhibition in p53 functional human tumor cells. *Cell Cycle* 6 (16), pp. 2071-2081.
- Smith, P. J. *et al.* 1985. Flow-cytometric detection of changes in the fluorescence emission spectrum of a vital DNA-specific dye in human tumour cells. *Exp Cell Res* 159 (1), pp. 37-46.
- Smith, P. J. *et al.* 2008. Impact of overexpression of metallothionein-1 on cell cycle progression and zinc toxicity. *Am J Physiol Cell Physiol*.
- Soengas, M. S. *et al.* 2001. Inactivation of the apoptosis effector Apaf-1 in malignant melanoma. *Nature* 409 (6817), pp. 207-211.
- Sorensen, M. *et al.* 1995. Characterisation of a human small-cell lung cancer cell line resistant to the DNA topoisomerase I-directed drug topotecan. *Br J Cancer* 72 (2), pp. 399-404.
- Srivastava, V. K. and Nalbantoglu, J. 2008. Flow cytometric characterization of the DAOY medulloblastoma cell line for the cancer stem-like phenotype. *Cytometry A* 73 (10), pp. 940-948.
- Steeg, P. S. 2003. Metastasis suppressors alter the signal transduction of cancer cells. *Nat Rev Cancer* 3 (1), pp. 55-63.
- Steeg, P. S. 2006. Tumor metastasis: mechanistic insights and clinical challenges. *Nat Med* 12 (8), pp. 895-904.
- Stemmler, M. P. 2008. Cadherins in development and cancer. *Mol Biosyst* 4 (8), pp. 835-850.
- Storms, R. W. *et al.* 2000. Hoechst dye efflux reveals a novel CD7(+)CD34(-) lymphoid progenitor in human umbilical cord blood. *Blood* 96 (6), pp. 2125-2133.
- Suggitt, M. *et al.* 2006. The hollow fibre model--facilitating anti-cancer pre-clinical pharmacodynamics and improving animal welfare. *Int J Oncol* 29 (6), pp. 1493-1499.
- Sung, J. M. *et al.* 2008. Characterization of a stem cell population in lung cancer A549 cells. *Biochem Biophys Res Commun* 371 (1), pp. 163-167.
- Suzuki, M. *et al.* 2005. Polysialic acid facilitates tumor invasion by glioma cells. *Glycobiology* 15 (9), pp. 887-894.



- Takahashi, T. *et al.* 1989. Expression and amplification of myc gene family in small cell lung cancer and its relation to biological characteristics. *Cancer Res* 49 (10), pp. 2683-2688.
- Taneja, T. K. and Sharma, S. 2004. Markers of small cell lung cancer. *World J Surg Oncol* 2 (1), p. 10.
- Terasaki, T. *et al.* 1986. Changes in cell characteristics due to culture conditions in cell lines from human small cell lung cancer. *Jpn J Clin Oncol* 16 (3), pp. 203-212.
- Thiery, J. P. *et al.* 1977. Adhesion among neural cells of the chick embryo. II. Purification and characterization of a cell adhesion molecule from neural retina. *J Biol Chem* 252 (19), pp. 6841-6845.
- Thiery, J. P. and Sleeman, J. P. 2006. Complex networks orchestrate epithelial-mesenchymal transitions. *Nat Rev Mol Cell Biol* 7 (2), pp. 131-142.
- Tiseo, M. and Ardizzoni, A. 2007. Current status of second-line treatment and novel therapies for small cell lung cancer. *J Thorac Oncol* 2 (8), pp. 764-772.
- Tomlinson, I. and Bodmer, W. 1999. Selection, the mutation rate and cancer: ensuring that the tail does not wag the dog. *Nat Med* 5 (1), pp. 11-12.
- Townson, J. L. and Chambers, A. F. 2006. Dormancy of solitary metastatic cells. *Cell Cycle* 5 (16), pp. 1744-1750.
- Tsurutani, J. *et al.* 2005. Inhibition of the phosphatidylinositol 3-kinase/Akt/mammalian target of rapamycin pathway but not the MEK/ERK pathway attenuates laminin-mediated small cell lung cancer cellular survival and resistance to imatinib mesylate or chemotherapy. *Cancer Res* 65 (18), pp. 8423-8432.
- Tusher, V. G. *et al.* 2001. Significance analysis of microarrays applied to the ionizing radiation response. *Proc Natl Acad Sci U S A* 98 (9), pp. 5116-5121.
- Twentyman, P. R. *et al.* 1992. Sensitivity to novel platinum compounds of panels of human lung cancer cell lines with acquired and inherent resistance to cisplatin. *Cancer Res* 52 (20), pp. 5674-5680.
- Uhm, J. H. *et al.* 1999. Vitronectin, a glioma-derived extracellular matrix protein, protects tumor cells from apoptotic death. *Clin Cancer Res* 5 (6), pp. 1587-1594.
- Vallee, B. L. 1991. Introduction to metallothionein. *Methods Enzymol* 205, pp. 3-7.
- van 't Veer, L. J. *et al.* 2002. Gene expression profiling predicts clinical outcome of breast cancer. *Nature* 415 (6871), pp. 530-536.

- van der Flier, A. and Sonnenberg, A. 2001. Function and interactions of integrins. *Cell Tissue Res* 305 (3), pp. 285-298.
- Vargas, F. F. *et al.* 1990. Enzymatic lysis of sulfated glycosaminoglycans reduces the electrophoretic mobility of vascular endothelial cells. *Membr Biochem* 9 (2), pp. 83-89.
- Vargas, F. F. *et al.* 1989. Surface charge of endothelial cells estimated from electrophoretic mobility. *Membr Biochem* 8 (4), pp. 221-227.
- Vasiliou, V. *et al.* 2000. Role of aldehyde dehydrogenases in endogenous and xenobiotic metabolism. *Chem Biol Interact* 129 (1-2), pp. 1-19.
- Vaughan, R. B. and Trinkaus, J. P. 1966. Movements of epithelial cell sheets in vitro. *J Cell Sci* 1 (4), pp. 407-413.
- Vezzoni, L. and Parmiani, G. 2008. Limitations of the cancer stem cell theory. *Cytotechnology*.
- Visvader, J. E. and Lindeman, G. J. 2008. Cancer stem cells in solid tumours: accumulating evidence and unresolved questions. *Nat Rev Cancer* 8 (10), pp. 755-768.
- Vivanco, I. and Sawyers, C. L. 2002. The phosphatidylinositol 3-Kinase AKT pathway in human cancer. *Nat Rev Cancer* 2 (7), pp. 489-501.
- Vogelstein, B. and Kinzler, K. W. 2004. Cancer genes and the pathways they control. *Nat Med* 10 (8), pp. 789-799.
- Wagers, A. J. and Weissman, I. L. 2004. Plasticity of adult stem cells. *Cell* 116 (5), pp. 639-648.
- Wallace, S. M. *et al.* 1996. Effect of zinc on metallothionein content of CHO cells transfected with metallothionein gene under the control of a non-inducible promoter. *Biochem Soc Trans* 24 (2), p. 237S.
- Walmod, P. S. *et al.* 2004. Zippers make signals: NCAM-mediated molecular interactions and signal transduction. *Neurochem Res* 29 (11), pp. 2015-2035.
- Wang, C. *et al.* 1994. Requirement of polysialic acid for the migration of the O-2A glial progenitor cell from neurohypophyseal explants. *J Neurosci* 14 (7), pp. 4446-4457.
- Wang, W. *et al.* 2005a. Tumor cells caught in the act of invading: their strategy for enhanced cell motility. *Trends Cell Biol* 15 (3), pp. 138-145.
- Wang, X. *et al.* 2005b. Dysregulation of TGF-beta1 receptor activation leads to abnormal lung development and emphysema-like phenotype in core fucose-deficient mice. *Proc Natl Acad Sci U S A* 102 (44), pp. 15791-15796.

- Wang, Z. *et al.* 2006. Roles for UDP-GlcNAc 2-epimerase/ManNAc 6-kinase outside of sialic acid biosynthesis: modulation of sialyltransferase and BiP expression, GM3 and GD3 biosynthesis, proliferation, and apoptosis, and ERK1/2 phosphorylation. *J Biol Chem* 281 (37), pp. 27016-27028.
- Warren, W. H. and Hammar, S. P. 2006. The dispersed neuroendocrine system, its bronchopulmonary elements, and neuroendocrine tumors presumed to be derived from them: myths, mistaken notions, and misunderstandings. *Semin Thorac Cardiovasc Surg* 18 (3), pp. 178-182.
- Watson, J. V. *et al.* 1985. Flow cytometric fluorescence emission spectrum analysis of Hoechst-33342-stained DNA in chicken thymocytes. *Cytometry* 6 (4), pp. 310-315.
- Wegener, K. L. and Campbell, I. D. 2008. Transmembrane and cytoplasmic domains in integrin activation and protein-protein interactions (review). *Mol Membr Biol* 25 (5), pp. 376-387.
- Weidner, N. 2002. New paradigm for vessel intravasation by tumor cells. *Am J Pathol* 160 (6), pp. 1937-1939.
- Weinhold, B. *et al.* 2005. Genetic ablation of polysialic acid causes severe neurodevelopmental defects rescued by deletion of the neural cell adhesion molecule. *J Biol Chem* 280 (52), pp. 42971-42977.
- Whang-Peng, J. *et al.* 1982. A nonrandom chromosomal abnormality, del 3p(14-23), in human small cell lung cancer (SCLC). *Cancer Genet Cytogenet* 6 (2), pp. 119-134.
- Wiggin, O. *et al.* 2002. Pax3 induces cell aggregation and regulates phenotypic mesenchymal-epithelial interconversion. *J Cell Sci* 115 (Pt 3), pp. 517-529.
- Wilson, C. L. and Miller, C. J. 2005. Simpleaffy: a BioConductor package for Affymetrix Quality Control and data analysis. *Bioinformatics* 21 (18), pp. 3683-3685.
- Wilson, T. R. *et al.* 2006. Chemoresistance in solid tumours. *Ann Oncol* 17 Suppl 10, pp. x315-324.
- Winter, C. *et al.* 2008. Neural cell adhesion molecule (NCAM) isoform expression is associated with neuroblastoma differentiation status. *Pediatr Blood Cancer*.
- Wistuba, II *et al.* 2001. Molecular genetics of small cell lung carcinoma. *Semin Oncol* 28 (2 Suppl 4), pp. 3-13.
- Witz, I. P. 2008. The selectin-selectin ligand axis in tumor progression. *Cancer Metastasis Rev* 27 (1), pp. 19-30.

Wolf, K. and Friedl, P. 2008. Mapping proteolytic cancer cell-extracellular matrix interfaces. *Clin Exp Metastasis*.

Wolf, N. S. *et al.* 1993. In vivo and in vitro characterization of long-term repopulating primitive hematopoietic cells isolated by sequential Hoechst 33342-rhodamine 123 FACS selection. *Exp Hematol* 21 (5), pp. 614-622.

Wong, S. Y. and Hynes, R. O. 2006. Lymphatic or hematogenous dissemination: how does a metastatic tumor cell decide? *Cell Cycle* 5 (8), pp. 812-817.

Wu, C. and Alman, B. A. 2008. Side population cells in human cancers. *Cancer Lett* 268 (1), pp. 1-9.

Wyckoff, J. B. *et al.* 2000. A critical step in metastasis: in vivo analysis of intravasation at the primary tumor. *Cancer Res* 60 (9), pp. 2504-2511.

Yabe, U. *et al.* 2003. Polysialic acid in human milk. CD36 is a new member of mammalian polysialic acid-containing glycoprotein. *J Biol Chem* 278 (16), pp. 13875-13880.

Yaccoby, S. 2005. The phenotypic plasticity of myeloma plasma cells as expressed by dedifferentiation into an immature, resilient, and apoptosis-resistant phenotype. *Clin Cancer Res* 11 (21), pp. 7599-7606.

Yang, M. and Chitambar, C. R. 2008. Role of oxidative stress in the induction of metallothionein-2A and heme oxygenase-1 gene expression by the antineoplastic agent gallium nitrate in human lymphoma cells. *Free Radic Biol Med*.

Yang, M. H. *et al.* 2008. Direct regulation of TWIST by HIF-1alpha promotes metastasis. *Nat Cell Biol* 10 (3), pp. 295-305.

Yang, P. *et al.* 1992. Intercellular space is affected by the polysialic acid content of NCAM. *J Cell Biol* 116 (6), pp. 1487-1496.

Yano, S. *et al.* 2005. Characterization and localization of side population cells in mouse skin. *Stem Cells* 23 (6), pp. 834-841.

Yarema, K. J. and Bertozzi, C. R. 2001. Characterizing glycosylation pathways. *Genome Biol* 2 (5), p. REVIEWS0004.

Yin, C. *et al.* 1997. Bax suppresses tumorigenesis and stimulates apoptosis in vivo. *Nature* 385 (6617), pp. 637-640.

Zhang, W. H. *et al.* 2008. DNA damage-induced S phase arrest in human breast cancer depends on Chk1, but G2 arrest can occur independently of Chk1, Chk2 or MAPKAPK2. *Cell Cycle* 7 (11), pp. 1668-1677.

Zhang, Y. *et al.* 1999. p21Waf1/Cip1 acts in synergy with bcl-2 to confer multidrug resistance in a camptothecin-selected human lung-cancer cell line. *Int J Cancer* 83 (6), pp. 790-797.

Zhao, H. *et al.* 2008. Phosphorylation of p53 on Ser15 during cell cycle caused by Topo I and Topo II inhibitors in relation to ATM and Chk2 activation. *Cell Cycle* 7 (19), pp. 3048-3055.

Zhou, S. *et al.* 2002. Bcrp1 gene expression is required for normal numbers of side population stem cells in mice, and confers relative protection to mitoxantrone in hematopoietic cells in vivo. *Proc Natl Acad Sci U S A* 99 (19), pp. 12339-12344.

Zhou, S. *et al.* 2001. The ABC transporter Bcrp1/ABCG2 is expressed in a wide variety of stem cells and is a molecular determinant of the side-population phenotype. *Nat Med* 7 (9), pp. 1028-1034.

Zuber, C. *et al.* 1992. Polysialic acid is associated with sodium channels and the neural cell adhesion molecule N-CAM in adult rat brain. *J Biol Chem* 267 (14), pp. 9965-9971.